

https://dspace.org/

A probabilistic structural design process for bord and pillar workings in chrome and platinum mines in South Africa

Kersten, Rudiger Welf Olgert

2016

http://hdl.handle.net/10539/22290

Kersten, Rudiger Welf Olgert (2016) A probabilistic structural design process for bord and pillar workings in chrome and platinum mines in South Africa, University of Witwatersrand, Johannesburg, <http://wiredspace.wits.ac.za/handle/10539/22290>

Downloaded from a DSpace repository. https://dspace.org/

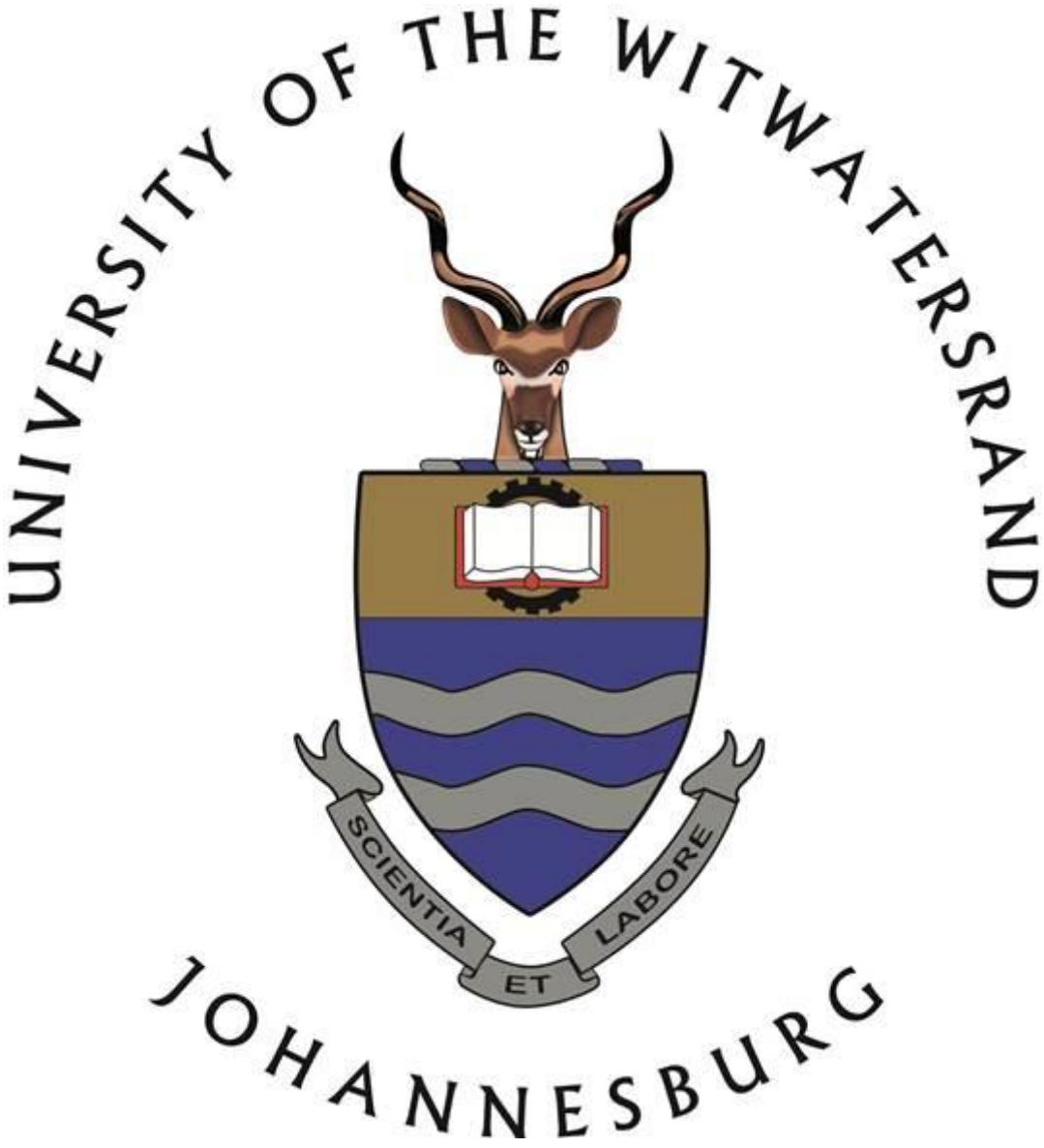
UNIVERSITY OF THE WITWATERSRAND
SCIENTIA
ET
LABORE
JOHANNESBURG

A Probabilistic Structural Design Process for Bord and Pillar Workings in Chrome and Platinum Mines in South Africa

Rudiger Welf Olgert KERSTEN

Student No 7272848

A thesis submitted to the Faculty of Engineering and the Built Environment, University of the Witwatersrand, Johannesburg, in fulfilment of the requirements for the degree of Doctor of Philosophy.

Johannesburg, September 2016

SUMMARY

The design of stable pillars in mining is of fundamental importance not only in the Bushveld mines but in the entire mining industry. Wherever mining occurs, pillars will be formed at some stage, and it is essential to predict their behaviour. It is imperative to know whether they would burst, yield or remain stable. Although of major importance, the design of pillars still suffer from major drawbacks and weaknesses that affect the results in a fundamental manner.

Faced with uncertainty, the designs have, for the most part, been conservative, resulting in the loss of millions of tons of ore by being sterilized and unavailable in the future. The reduction of the life of mines with dire consequences for the long-term life of the mining industry.

With the above in mind the thesis investigated the following:

- The pillar design method currently in use for its strengths and weaknesses
- Alternative methods in use, actual and suggested.
- Proposed an improvedd method for calculating the pillar strength and the loading system.
- Compared the improved method with underground observations.
- Proposed a simplified pillar strength equation based on the improved method.
- Presented main conclusions and recommendations.

Examination of the pillar design method currently in use for its strengths and weaknesses:

Pillar design has been based on the empirical equation on the work done by Salamon and Munro (1967) for coal mines and subsequently modified by Hedley and Grant (1972) at the Elliot Lake uranium mine. By changing the exponents relevant to the hard rock mine, the Hedley-Grant equation was created. It has since become known as the Hedley-Grant strength equation for hard rock pillars.

The weaknesses associated with the empirical method are as follows:

- The method is easy to use but could not be extrapolated beyond the range used for calibration.
- Very few pillar collapses have occurred in Bushveld mines which could possibly be ascribed to over-conservative design or correct design.
- Empirical methods are, by nature, observational and no deep fundamental understanding of the variables is required to derive an answer acceptable in general to the problem of stability.

The pillar strength equation is based on the following:

$$\sigma_{str} = k\, w^{\gamma}\, h^{\alpha}$$

Where k strength factor

w and h width and height of the pillar

γ and α variable exponential “constants”

σ_{str} pillar strength

Except for the width and the height of the pillar, the strength factor and the exponents are based on back-analysis of failed pillar areas. In the absence of failed pillar areas, the strength factor is assumed to be a fraction of the uniaxial compressive strength of the rock mass in the pillar; the value varied from 0.3 to 0.8, which is sometimes increased without sound scientific basis when no pillar failure occurred. This type of approach is not only wasteful but could prove to be dangerous.

The stress imposed on the pillar is determined by using the Tributary Area Theory (TAT) including the percentage extraction, depth below surface and the rock mass density.

One major advantage of the method, Hedley-Grant strength equation and the Tributary Area Theory, is its ease of use; few parameters needed to be defined.

Rock masses are difficult to define as an engineering material. At the time of the research, the average uniaxial compressive strength of five samples for an ore body had been deemed sufficient to design a mine. Detailed analysis of strength values showed that the coefficient of variation (COV) for pyroxenite and chromitite was 0.33 nearly falling outside the region of even statistical predictability.

Variability in the actual pillar dimensions, in plan and section, which differ substantially from design dimensions, adds to the uncertainty of the design.

Using the Monte Carlo simulation method, the influence of the variability of the input parameters for a typical bord and pillar chrome mine, using the Hedley-Grant equation and the tributary area theory showed the following results:

Probability of Failure = 23% at a factor of safety of 1.57.

Accepting that the Hedley-Grant equation is correct and that the Tributary Area Theory is a true reflection of the pillar strength and stress, the design safety factor of 1.57 is acceptable but the probability of failure of 23% due to the variation in input parameters raises the question of whether a factor of safety of 1.57 is sufficient?

The above argument presupposed that the values using Tributary Area Theory and the Hedley-Grant equation provided the correct answer. The fact that the predicted failure did not materialise indicated that the input parameters were overly conservative and/or the pillar equation is suspect.

It should also be noted that the probability of failure related to the probability that any given pillar had a factor of safety < 1.0. Failure of a panel of pillars would only occur if those pillars happened to be in groups.

Investigate alternative methods in use, actual and suggested:

The deficiencies have been identified by other researchers and alternative approaches have been developed addressing some of these deficiencies. The overall conclusions from a literature survey were as follows:

- The influence of the stiffness of the loading system was neglected in the pre-failure region but three methods assessed incorporated the strata stiffness concept in the post-failure regime
- None of the methods considered the interaction between hanging wall and/or footwall and its effect on the pillar strength.
- Composite pillars were generally treated as a uniform entity.
- The variability of the mining dimensions and the rock mass properties were dealt with quantitatively in four methods.
- None proposed a methodology that incorporated a combination of a more realistic strength equation, the system stiffness and the probability approach in design.

Proposal of an improved method for calculating the pillar strength and the loading system.

The proposed alternative approach is based on a semi-analytical strength determination using a two-dimensional mathematical model in conjunction with a failure criterion to calculate the pillar strength.

The selected method is based on the following:-

- Determining the pillar stress using *FLAC2D*,
- Incorporating the modified Hoek-Brown failure criterion.

It is assumed that the pillar/rock mass remained elastic until pillar failure occurred. The interaction between the local mine/pillar stiffness, and an elastic response, determines the loading conditions. The combination of the two concepts, both elastic, was used to determine the factors of safety for the pillar/rock mass.

With further development, the variability of the rock mass properties and mining variations were also incorporated in the proposed methodology.

The *FLAC2D/*Hoek-Brown model could simulate/incorporate the following conditions:-

- The pillar strength for a homogeneous pillar.
- Strength of composite pillars such as found in the chrome mines.
- Incorporation of the effect of planes of weakness.
- Use of known geotechnical parameters.
- Development of a simple equation for a specific set of conditions.

- Although of great importance, the influence of the hanging and /or footwall properties on pillar strength was not considered in the thesis.

Using the *FLAC2D*/Hoek-Brown model the following was observed:-

- The vertical stress was the lowest at the pillar edge at commencement of pillar failure.
- At the average peak pillar stress, the vertical stress at the core of the pillar generally exceeded the uniaxial compressive strength of the rock.
- Pillar failure was seen as a progressive process.
- The volumetric strain increment could be a possible measure of the depth of fracturing in a pillar.

For back analysis, it was obvious that some definitive values had to be used. The required variables were identified as follows:

- The mean uniaxial compressive strength from available samples for the property was used.
- The Geological Strength Index was estimated.
- The m_i value, hence the m_r, was based on the widely used RocLab programme.

Pillar loading is a function of the strata stiffness and the areal extent of the mining geometry while the Tributary Area Theory assumes an infinitely mined area with zero stiffness of the overlying rock mass.

This oversimplification leads to overdesign in most practical mining geometries. It is known that the geological losses in the platinum mines varies between 20% and 30% of the mined area resulting in limited mining spans between the “regional pillars” created by the geological losses.

The influence of the geological losses can be simulated using the concept of the load line of the loading system. The amount of convergence in an elastic medium can be calculated for various spans, different Poisson’s ratios and Young’s Moduli.

The research dealt with the pre-failure portion of the pillar design, therefore, the theory of elasticity could be used to the point of pillar failure allowing accurate calculation of rock mass, pillar stresses and deformations.

Figure 1 is a plot of a pillar strength curve intersecting the system loadline. The system obtains equilibrium at the intersection of the two curves. In this example, the system curve is based on the fact that without any support full elastic convergence would occur. The presence of a support medium, that prevents any convergence, is the product of the area and the vertical primitive stress.

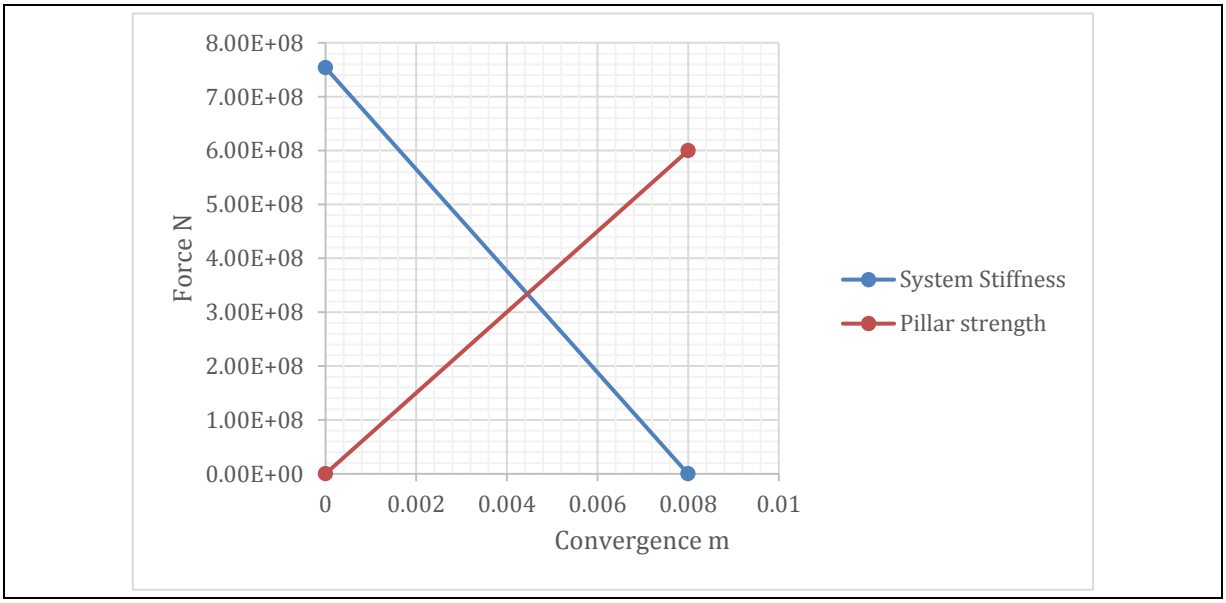

Figure 1. Plot showing pillar resistance and system curve

The pillar resistance curve is based on the stress and convergence obtained using *FLAC2D* and the Hoek-Brown failure criterion, while the system stiffness curve/load line is based on the elastic convergence of a slot in an elastic medium at finite depth. The intersection of the two curves gives the equilibrium condition of a specified geometry.

The combination of the two curves and the intersection point is referred to as the System Pillar Equilibrium Concept, SPEC for short.

The curves in the Figure 1 were obtained by following the process shown in the flow diagram, Figure 2.

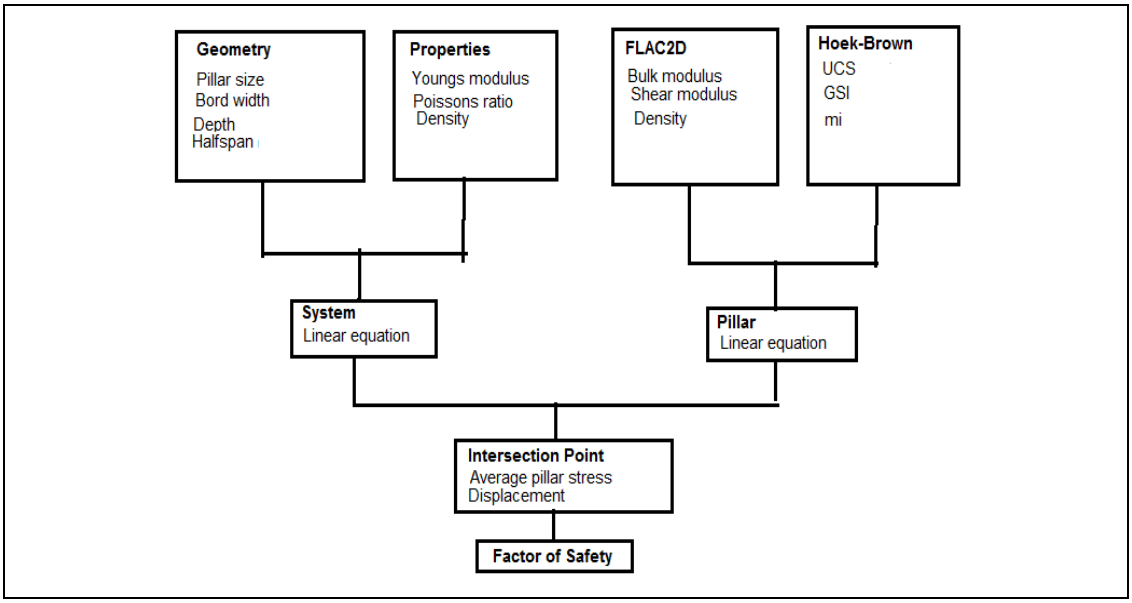

Figure 2. Schematic presentation of the steps involved in the *FLAC2D*/Hoek-Brown and System Pillar Equilibrium/SPEC methodology.

The comparison of the improved method with underground observations:

Two bord and pillar mines in the Bushveld complex were selected for calibration, Two Rivers and Impala Platinum Mines, to test the proposed methodology.

In both cases the extent of pillar failure, as well as the convergence, could be simulated and it was concluded that the method did represent the actual underground conditions better than other current methods.

A propose a simplified pillar strength equation based on the improved method:

One of the main advantage of the Hedley-Grant/Tributary Area Theory is its simplicity in application. In order to achieve a similar ease of modelling, it was attempted to obtain a generic pillar equation that is easy to use.

A simple generic equation was derived, using the Geological Strength Index and the uniaxial compressive strength, based on the detailed back-analysis that could be used for all "normal" situations in the Bushveld mines. It was found that for a specific range of data the equation below can be used:

$$\sigma_{str} = \delta(\frac{w}{h})^{\beta}$$

Where $\delta = de^{fGSI}$

$$\delta = 0.0999e^{0.0704GSI} \quad \text{120 MPa}$$

$$\delta = .1089e^{0.0674GSI} \quad \text{100 MPa}$$

$$\delta = .1675e^{0.06GSI} \quad \text{80 MPa}$$

$$\delta = 0.1652e^{0.0574GSI} \quad \text{60 MPa}$$

$$\beta = TANH\left[\left(\frac{GSI - a}{b}\right)\right]c$$

Where a = 46.866

b = 16.916

C = 1.2906

Where δ and β are both related to the uniaxial compressive strength and the GSI value.

By employing this equation, it was possible to simplify the calculation procedure as well as for use of the Monte Carlo simulation for sensitivity studies.

Present main conclusions and recommendations:

The weaknesses of the current design procedure have all been addressed and it was concluded that the proposed methodology is an improvement on currently available alternative methods of bord and pillar design.

The volumetric strain increment value for failure initiation lay between 1e-2 to 3e-2 for the fracture zone extent for both pyroxenite and chromitite pillars.

From the volumetric strain increment values, it appeared as if the *FLAC2D*/Hoek-Brown model in conjunction with the SPEC method required to calculate the pillar stress and convergence, approximated the real underground situation.

The stage has been reached where the methodology can be used to predict most likely failure of pillars at greater depth and alternative pillar mining methods could be modelled. The concept can also be extended to incorporate the energy balance of the system.

A generic equation based on the *FLAC2D*/Hoek-Brown methodology has been developed for general use in mine design.

Additional research is essential on subsections of the input values to finally establish that the methodology is a representation of underground physical changes.

ACKNOWLEDGEMENTS

Professor Nielen van der Merwe for his persistence and patience in completing this thesis.

Management of Impala Platinum Mine and Two Rivers Platinum Mine Joint venture are thanked for allowing the use their mines as examples as well as the data sets on the rock properties.

DECLARATION

I declare that this thesis is my own, unaided work. It is being submitted for the Degree of Doctor of Philosophy at the University of the Witwatersrand, Johannesburg. It has not been submitted before for any degree or examination in any other University.

_____

R W O Kersten

Student No. 7272848

September 2016

CONTENTS

SUMMARY i
Contents x
List of figures xiv
List of tables xx
LIST OF SYMBOLS xxiii
ABSTRACT xxvi
FOREWORD xxviii
Part I 1
1 Introduction 1
2 Current design methodology 5
2.1 What is wrong with the method? 5
2.1.1 Pillar stresses and the Tributary Area Theory –TAT 5
2.1.2 Pillar strength 6
2.1.3 Factor of Safety 6
2.1.4 The uniaxial compressive strength 7
2.1.5 Determination of the *k*-value 9
2.1.6 Actual pillar dimensions 10
2.1.7 Definition of pillar failure. 11
2.1.8 Interaction between pillar and hanging/footwall 11
2.1.9 Composite pillars 13
2.1.10 Effective width correction 13
2.1.11 Additional pillar design equations 14
2.1.12 Width-to-height ratios investigated 15
2.1.13 The influence of depth on the properties of the specimen collected 15
2.1.14 Pillar stresses and the loading system 18
2.1.15 “Bedding” parallel planes of weakness 18
2.2 Sorting of deficiencies / Classification of the deficiencies 19
2.3 Effect of the variability of the input parameters 19
2.4 What has been done and what needs to be done 22
3 Published alternative design methodologies 22
3.1 Joughin et al (2000) 22
3.2 Esterhuizen (2003) 24
3.3 Barczak et al (2009). 24
3.4 Malan and Napier (2006) 25
3.5 Martin and Maybee (2000) 27
3.6 Godden (2012) 29
3.7 Leach (2008) 30
3.8 Kersten (1992) 32
3.9 Watson (2010). 34
3.10 Ryder and Ozbay (1990). 34

3.11 Roberts (2003) 34
3.12 Summary of Hedley-Grant type of equation. 35
3.13 Scorecard 36
3.14 How to fill the gaps 37
Part II 38
4 Modelling of Pillar Strength 38
4.1 Definition of pillar strength/failure 38
4.2 Pillar models 40
4.3 Three-dimensional or two-dimensional models 46
4.4 *FLAC2D*/Hoek-Brown model used in the investigation 48
4.5 Developing a methodology for determining a simple pillar strength equation 48
4.5.1 Sensitivities 50
4.6 Simple circular pillar with various properties 52
4.7 Planes of weakness/interfaces 56
4.8 Composite pillar 57
4.9 Property variation within the pillar 58
4.10 Calibration: Detail of the stress distribution and volumetric strain increment for simple pillars 60
4.11 Pillar failure mechanism. 64
4.12 The “draping” effect. 65
4.13 Conclusions 66
5 Geotechnical Input Parameters 68
5.1 Input parameters for the Hoek-Brown failure criterion 68
5.1.1 Uniaxial compressive strength 69
5.1.2 Geological Strength Index 76
5.1.3 $\boldsymbol{mi}$ Value 77
5.2 Other relevant rock mass properties: Young’s Modulus and Poisson’s Ratio 85
6 Development of the System pillar equilibrium Concept (SPEC). 89
6.1 Combining pillar behaviour and local mine stiffness and model development 89
6.2 Defining local mine stiffness 91
6.3 Combining pillar and strata/mine stiffness 95
6.4 Comparison with Hedley-Grant/Tributary Area Theory Methodology 101
6.5 Discussion on the equilibrium point 102
6.6 Use of the SPEC Methodology 103
6.7 Pillar stiffness 109
Part III 110
7 Introduction 110
8 General Geological Setting and Mining Method 112
8.1 General geological setting 112
8.2 Mining method 114
9 Impala Platinum Mine 116
9.1 Location, geological setting and mining dimensions 116
9.2 Rock Mass Data 117
9.3 Available data on pillar behaviour 118

9.3.1 Piper and Flanagan (2005) ... 118
9.3.2 Calibration with fracture zone, grid pillars ... 123
9.3.3 Establishing a fracture criterion, grid pillars. ... 125
9.3.4 Fracture zones in barrier pillars ... 130
9.3.5 Piper and Flanagan (2005): Convergence data calibration ... 132
9.3.6 Malan and Napier (2007) ... 134
9.3.7 Grodner and Malan (2006) monitoring at 14 Shaft Pillar Mining Site – Impala Platinum Mine. ... 139
9.3.8 Ryder and Malan (2009) results. ... 142
9.4 Summary of conclusions for Impala Platinum Mine data comparison. ... 143
10 Two Rivers Platinum Mine ... 144
10.1 Geology. ... 144
10.2 Rock mass data ... 145
10.3 Previous work ... 147
10.4 Pillar observations ... 148
10.5 Calibration ... 149
10.6 *FLAC2D* models and simulations ... 151
10.7 Conclusion ... 154
11 General Conclusion from the Calibration. ... 154
Part IV ... 155
12 Deriving A Simple Strength Equation. ... 156
12.1 Derivation of a simple pillar strength equation. ... 156
12.2 Properties of the proposed equation. ... 163
12.3 Comparison with pillar equations derived by Watson (2010) for the Merensky reef. ... 165
12.4 Incremental increase in strength with increase in w/h ratio ... 168
12.5 Summary. ... 169
12.6 Variability of input data and its influence on pillar design ... 170
12.7 Illustrative examples using the SPEC, the generic equation, Hedley-Grant and Tributary Area Theory. ... 172
12.7.1 Hedley-Grant/TAT methodology. ... 173
12.7.2 *FLAC2D*/Hoek-Brown with SPEC methodology. ... 173
12.7.3 Generic equation and Tributary Area Theory. ... 176
12.7.4 Generic and SPEC ... 176
12.7.5 Summary of illustrative examples. ... 177
13 Summary and Conclusions. ... 179
13.1 Brief summary of objective and procedures adopted. ... 179
13.2 Examine the pillar design method currently in use for its strengths and weaknesses. ... 180
13.3 Propose an improved method for calculating the pillar strengths. ... 181
13.4 Re-define pillar loading. ... 182
13.5 Combining the proposed pillar strength and the pillar loading. ... 182
13.6 Compare the improved method with underground observations. ... 183
13.7 Propose a simplified pillar strength equation based on the improved method ... 184
13.8 Incremental increase in strength with increase in w/h ratio ... 185

13.9 Incorporating the variability of the input data. 185
14 Future research. 186
References 188
Appendices 195
Appendix I 195
Report by A. R. Leach on the comparative study between circular and square pillars 195
Appendix II. 1
Appendix III 2
Appendix IV 4
Appendix V 6

LIST OF FIGURES

Figure 1. Plot showing pillar resistance and system curve v

Figure 2. Schematic presentation of the steps involved in the *FLAC2D*/Hoek-Brown and System Pillar Equilibrium/SPEC methodology. v

Figure 2.1.4_1 Variation of UCS values in intersections through the UG2 ore body for five boreholes at Two Rivers Platinum Mine (Coefficient of variation = 0.40, 0.29, 0.17, 0.29, 0.16) 8

Figure 2.1.4_2 Variation of average uniaxial compressive strength in plan between the same boreholes shown in Figure 2.1.4_1 8

Figure 2.1.4_3 Frequency distribution of all UCS values for Two Rivers Platinum Mine, based on 136 values 9

Figure 2.1.6_1 Measured pillar strike and dip width variations in a particular mine section, Two Rivers Platinum Mine (Kersten, 2013) 10

Figure 2.1.8_1 Induced fracturing in the hanging wall of the Merensky Reef 12

Figure 2.1.8_2 Interaction between pillar and hanging wall on the Merensky Reef - Impala Platinum Mine 12

Figure 2.1.910_1 Influence of pillar length on strength ratio of rectangular pillars, width-to-height ratio of 1.0, for strength equations by the authors indicated, Dolinar and Esterhuizen, (2007) 14

Figure 2.1.11_1. Plot of normalised pillar strength for various proposed strength equations, where σc is the uniaxial compressive strength. (Malan, 2011) 15

Figure 2.1.13_1 Core discing of borehole core obtained from above a Pillar - (Watson et al, 2007) 16

Figure 2.1.13_2 Strain differential with increase in axial stress between samples of spotted anorthosite collected at 600 and 1100m below surface - (Watson, 2010) 16

Figure 2.1.13_3 Plot of uniaxial compressive strength vs. depth for pyroxenite samples collected at various depths below surface (Impala data bank, 2012). 17

Figure 2.1.13_4 Plot of uniaxial compressive strength vs. depth of chromitite samples collected at different depths below surface. (Impala data bank, 2012). 17

Figure 2.1.14_1 Stress distribution beneath the steep hillside on one of the UG2 Mines in the Eastern Bushveld 18

Figure 2.3_1 Probability of failure for different variables and coefficients of variation 20

Figure 2.3_2 Frequency distribution of the strength values for chromitite 20

Figure 3.3_1 Ground response and the support response curves - Barczak et al, (2009). 25

Figure 3.4_1 Analytic Finite Equilibrium Model (Malan and Napier 2006) 26

Figure 3.4_2 Comparison between Limit Equilibrium and *FLAC2D* models. 27

Figure 3.5_1 Plot of normalised pillar strength based on the equations in Table 3.5_1 (Martin and Maybee, 2000) 29

Figure3.7_1 Force-based comparison of pillar load-deformation characteristics to stope system support requirement (system stiffness) in terms of the 30 x 30 m tributary area associated with pillars in the planned layout. Leach (2008). 32

Figure 3.8_1 Cumulative frequency distribution of pillars in terms of their safety factors at Black Rock mining Operations. Kersten (2009) 33

Figure 3.8_2 Frequency distribution of pillar strength and pillar stress, Black Rock Mining Operations. (Kersten 2009) 33

Fig 3.8_1 Modelling two rock types (Roberts 2003) 35

Figure 4.1_1 Force/convergence diagram for a square 15 by 15 m for pillar heights of 10, 20 and 30 m (Repeat of figure 3.7_1 for ease of access) (Leach, 2009) 39

Figure 4.1_2 Section across half width showing vertical stress contours, $\boldsymbol{syy}$ across a 2 m high, 8 m wide, pillar at peak average pillar stress. Axis of symmetry at the Left 39

Figure 4.2_1 Basic explicit calculation scheme - *FLAC* Manual, 2012 41

Figure 4.2_2 Influence of the $\boldsymbol{mr}$ value on the pillar strength. 44

Figure 4.2_3 illustrating the effect of Geological Strength Index on the pillar strength for different w/h ratios (HB - Hoek-Brown criterion) 45

Figure 4.3_1 Three Dimensional FLAC model (Leach 2011) 47

Figure 4.3_2 Ratio of difference in strength between 3D square and 2D circular pillars 48

Figure 4.5_1 Basic *FLAC2D* grid for pillar strength calculations 50

Figure 4.5.1_1 Influence of number of elements on output in basic model 51

Figure 4.5.1_2 Influence of loading rate on pillar strength 51

Figure 4.6_1 Strength variation with change in the width-to-height ratio and GSI values for a constant height of 2 m.53

Figure 4.6_2 Influence of variation in GSI, jointing, on pillar strength - all pillars are 2 m high 54

Figure 4.6_3 Increase in pillar strength for variations of $\boldsymbol{mi}$ and a pillar 2 m high, 6 m wide 55

Figure 4.6_4 Strength variation with changes in the residual of the $\boldsymbol{mb}$ values 56

Figure 4.7_1 Influence of frictionless layer at top of pillar as compared with the “standard” model, fixed top and bottom, as well as the Hedley-Grant value 57

Figure 4.8_1 Influence of weak pyroxenite layer in a chromitite pillar on the volumetric strain increment 58

Figure 4.9_1 Increase in pillar strength with increase in friction angle 59

Figure 4.10_1 Vertical stress contours for a 2 m high, 8 m wide pillar at peak average pillar stress 61

Figure 4.10_2 Stress strain diagram for a 4 m radius pillar (The vertical axis is the average pillar stress based on a FISH function) 62

Figure 4.10_3 Volumetric strain increment contours in a pillar 63

Figure 4.10_4 Volumetric strain increment profile across a 4 m radius pillar at mid height showing that at a volumetric strain increment of .01 the fracture zone commences at 0.8 m from the edge (Vertical line intercept}. 63

Figure 4.11_1 Stress deformation of a 1.8 m high and 2.4 m radius pillar, Stress y-axis with deformation on the x-axis. 64

Figure 4.11_2. Average pillar stress vs the percentage intact volume for the pillar 65

Figure 4.12_1. “Draping” as defined by Watson (2010) 66

Figure 5.1.1_1 Variation of the uniaxial compressive strength across an ore body for 5 different boreholes, the left side being the hanging wall and the right hand the footwall side. 69

Figure 5.1.1_2 Rock strength variation below and above the Merensky Reef, Western Bushveld. (After Wilson et al, 2005) 72

Figure 5.1.1_3 Apparent lower strength values for pyroxenite in the deeper mines 73

Figure 5.1.1_4 Calculated normal distributions of some of the values in Table 5.1.1_3 74

Figure 5.1.1_5 Borehole data distribution with the Kriging contours. 75

Figure 5.1.2_1 GSI values for blocky ground (Hoek and Marinos, 2000) 76

Figure 5.1.3_1: Relationship between the $\boldsymbol{mi}$ value and the uniaxial compressive strength of anorthosite 80

Figure 5.1.3_2 Increase in strength with increase in $\boldsymbol{mi}$ value (data from Table 5.1.3_4). 81

Figure 5.1.3_3 Change in pillar strength for different residual $\boldsymbol{mr}$ values 83

Figure 5.1.3_4 Example of fracturing and estimated GSI value of 80 for a pillar at Impala Platinum Mine. 84

Figure 5.2_1 Stress-strain diagram of chromitite from Impala Platinum Mine 86

Figure 5.2_2 Stress-strain diagram for pyroxenite from Impala Platinum Mine 87

Figure 5.2_3 Definition of the tangent and secant modulus 88

Figure 6.1_1 Plot of OSR (Overburden Stability Ratio) and PSF (Pillar Safety Factor) after van der Merwe, 1999 90

Figure 6.1_2 Variation in hanging wall response to different strength springs. (Salamon and Oravecz, 1976) 90

Figure 6.1_3 Modified hanging wall response for different strengths springs for a totally “stiff” hanging wall (top) and a totally “soft” hanging wall system (bottom) 91

Figure 6.2_1 Schematic drawing of a slot mined at h m below surface with a half span of l m 92

Figure 6.2_2 Convergence in a slot at a depth of 650 m for different halfspans. (Poisson’s ratio = 0.28) 93

Figure 6.2_3 Force convergence diagram for a slot 80 m wide for a Young’s modulus of 68 GPa at 650 m below surface 95

Figure 6.2_4 Local mine/strata stiffness for various spans 95

Figure 6.3_1 Pillar resistance curve. 96

Figure 6.3_2 Schematic presentation of the SPEC methodology; calculation of system stiffness and the pillar strength curve. 99

Figure 6.3_3 Local mine /strata stiffness curve with pillar strength curve. 100

Figure 6.4_1 Comparison between Hedley-Grant/TAT and SPEC calculated factors of safety. 101

Figure 6.5_1 Force-convergence equilibrium point curves. 103

Figure 6.6_1 Graphical output for a halfspan of 100 m with a pillar strength calculated using the Hedley Grant equation in conjunction with convergence calculated using the Young's Modulus. 106

Figure 6.6_2 Comparison between Factor of Safety calculated using Hedley-Grant and FLAC2D/Hoek-Brown strength equation 108

Figure 7_1 Process adopted in the back analysis 111

Figure 8.1_1 Overview of mines in the Bushveld sequence (Impala 2012 web site) 112

Figure 8.1_2 Geological column for the lower portion of the Bushveld sequence showing the relative position of the Merensky reef and the UG2 horizon. (Mitchell and Scoon, 2007) 113

Figure 8.1_3 Detail of Merensky reef succession. (Mitchell and Scoon 2007) 113

Figure 8.1_4 Detail of the UG2 Horizon - Godden (2012). 114

Figure 9.1_1 Impala Platinum Mine location (Impala 2012 web site) 116

Figure 9.1_2 Detail of the planned pillar support system in use at 12 Shaft, Malan and Napier, (2007). 117

MPa 118

Figure 9.3.1_1 Planned layout for experimental section showing barrier and grid pillars 119

Figure 9.3.1_2 Actual layout at end of experiment of Piper and Flanagan, 2005. 120

Figure 9.3.1_3 Dog earing in grid pillars - (Piper and Flanagan, 2005 120

Figure 9.3.1_4 Unfractured core width in grid pillars, 6 by 4 m - (Piper and Flanagan, 2005) 121

Figure 9.3.1_5 Convergence in panel 22S vs distance from the face - (Piper and Flanagan, 2005) 122

Figure 9.3.1_6 Average convergence rate/panel on dip, Piper and Flanagan, (2005). 123

Figure 9.3.3_1 Comparison between observed data by Piper and Flanagan (2005) and a superimposed curve representing a constant fracture zone width of 0.5 m either side of the pillar. 126

Figure 9.3.3_2 Plot of solid core for individual pillars widths based on observation as well as the calculated vsi of 1e-2 and 3e-2 for the given pillar width. Note total pillar failure for 1e-2 for the 2 m pillar. 127

Figure 9.3.3_3. Width of zone between commencement of dog-earing and the pillar sidewall. 128

Figure 9.3.3_4 Vertical stress profile across one half of the 4 m width pillar showing the limit of the dog-earing, horizontal axis, and the vertical stress on the vertical axis 128

Figure 9.3.3_5 Volumetric strain increment profile across the 4 m pillar 129

Figure 9.3.4_1 Volumetric strain increment profile for a barrier pillar at 133 MPa for a stope width of 2.5 m, 1e-2 contour extends 0.5 m into the pillar 131

Figure 9.3.4_2 Vertical stress profile for a pillar stress of 133 MPa on the barrier pillar showing 40 and 120 MPa value intersects the x-axis at 5.5 and 6.5 m. 132

Figure 9.3.5_1 Elastic and measured convergence. The elastic convergence was added by the author. 133

Figure 9.3.6_1 Overall geometry of South section indicating area 2 (Experimental site) discussed in the previous section with extended mining thereafter 135

Figure 9.3.6_2 Planned layout beyond the experimental section 2, note the increase in strike length of the pillars from 6 to 12 m 136

Figure 9.3.6_3 Calculated grid pillar stresses along strike for the model geometry, South section, Malan and Napier (2007). 136

Figure 9.3.6_4 Calculated barrier pillar stresses on strike for the model geometry, South section. Malan and Napier (2007). 137

Figure 9.3.7_1 Experimental site at 14 Shaft, Impala Platinum Mine - (Grodner and Malan 2006) 139

Figure 9.3.7_2 Extensometer readings in 3 m long horizontal boreholes in positions shown in Figure 9.3.7_1. (Grodner and Malan, 2006) (EXT04 was not recorded between 15/10/2006 to 11/05/2006) 140

Figure 9.3.7_3 Horizontal displacement profile at a factor of safety of 1.34. 142

Figure 9.3.7_4 Average pillar stress according to Malan and Ryder (2009). 142

Figure 10.1_1 General setting of Two Rivers Platinum Mine in relation to other platinum producers in the eastern Bushveld (Implats Web site 2012) 144

Figure 10.1_2 Geological section through the ore body and the immediate hanging wall (Code of practice, Two Rivers Platinum Mine, 2007) 145

Figure 10.2_1 Borehole data distribution, van der Merwe, (2013) (Repeat of Figure 5.1.1_5 for convenience). 146

Figure 10.4_1 Edge of pillar in 7N panel, slight curvature at top of pillar and initial spalling, note distinct fractures, on sidewall 148

Figure 10.4_2 Face of up dip split before holing showing stress induced curvature over the whole face 149

Figure 10.5_1 Stoping outline of portion of 7N panel 150

Figure 10.5_2 Stress distribution along a section parallel to the main decline on the UG2 reef at Two Rivers Platinum Mine, showing position of 7N panel 151

Figure 10.6_1 Volumetric strain increment contours for a 2.6 high by 6.2 m pillar at a half span of 100 m 154

Figure 12.1_1 Example of pillar strength for GSI values of 60 to 90 and a UCS values of 60, 80 and 100 MPa. 159

Figure 12.1_2. Correlation between the Delta value and GSI. 160

Figure 12.1_3 Beta value curves for GSI values of 60, 70, 80 and 90 for different UCS values. 161

Figure 12.1_4. Beta values using equation 12.11 compared to all beta values obtained from FLAC2D modelling, Appendix VI. 161

Figure 12.1_5 Comparison between the calculated pillar strength *FLAC2D/*Hoek-Brown simulations and the generic equation 12.1. 163

Figure 12.2_1. Various curves for the strength w/h ratios and $\boldsymbol{\beta}$ values. 164

Figure 12.2_2. The Overlap Reduction Equation curves for coal and a low strength hard rock. 165

Figure 12.3_1. Comparison between Hedley-Grant, power equation 5.11 and 5.10 linear equation with the *FLAC2D/*H-B simulations. 167

Figure 12.4_1. Bi-linear strength curve for granite obtained by Mathey (2015) 168

Figure 12.4_2. Possible bi-linear behaviour, Watson (2010) 169

Figure 12.6_1 Sensitivities for the listed input parameters 172

Figure 12.7.2_1. Pillar strength and system stiffness for the 8 by 8 m pillar example design 176

Figure 13.1_1 Generalized grouping of pillar strength with strong, medium and weak geology, after Gale (1999) 179

Figure 13.5_1. Design methodology summary. 183

Figure A_1 Example model geometry 196

Figure A_2 Comparison of compression in model between top and bottom of model (red line) and between footwall and hangingwall of pillar (black line) 197

Figure A_3 Circular pillar, 6 m in diameter 199

Figure A_4 Circular pillar, 4 m in diameter 199

Figure A_5 Circular pillar, 2 m in diameter 200

Figure A_6 Square pillar, 6 x 6 m in size 200

Figure A_7 Square pillar, 4 x 4 m in size 201

Figure A_8 Square pillar, 2 x 2 m in size 201

LIST OF TABLES

Table 2.1.5_1: $\boldsymbol{k}$-Values used on different mines 10

Table 2.1.9_1: Chromitite and pyroxenite properties 13

Table 2.3_1: Assumed values for a typical case 21

Table 3.1_1: Example of input parameters used for a specific area - (Joughin et al, 2000) 23

Table 3.5_1: List of pillar strength equations summarized by Martin and Maybee (2000) 28

Table 3.12_1: Factor of safety using the equations listed in Table 3.5_1 and the strength ratio in Figure 3.5_1 36

Table 3.13_1: Summarised listing of methods and their various attributes 36

Table 4.2_1: Pillar strength with decrease in the $\boldsymbol{mr}$ and $\boldsymbol{sr}$ value, as well as the residual pillar strength 44

Table 4.2_2: Comparison between the FLAC/Hoek-Brown model and Malan and Napier's limit equilibrium model 46

Table 4.3_1: Pillar strengths in the different models 47

Table 4.6_1: Pillar strength for specific sets of values 53

Table 4.6_2: Input parameter and results for variation in GSI values 54

Table 4.6_3: Pillar strengths with variation in $\boldsymbol{mi}$ values for w/h ratio of 3, GSI = 80 and UCS = 131 MPa 55

Table 4.9_1: Average Values for a Variable Strength Chromitite Pillar 60

Table 5.1.1_1: Summary of rock strength, UG2 Horizon, for the Eastern Bushveld (Spencer, 2012) 70

Table 5.1.1_2: Summary of rock strength, UG2 Horizon, for the Western Bushveld (Spencer, 2012) 71

Table 5.1.1_3: Summary of mean UCS data with the standard deviation 73

Table 5.1.3_1.: $\boldsymbol{m\ i}$ Values for sedimentary, metamorphic and igneous rocks as published by Hoek and Marinos, (2000) 77

Table 5.1.3_2: $\boldsymbol{m\ i}$Values for igneous rocks (Qi et al, 2012) 78

Table 5.1.3_3: $\boldsymbol{mi}$ values obtained from tri-axial tests using the RocLab programme 79

Table 5.1.3_4: Influence of the $\boldsymbol{mi}$ value on the pillar strength (GSI=80) 80

Table 5.1.3_5 83

Variation $\boldsymbol{mb}$ and $\boldsymbol{mr}$ values using the equations from Joughin et al (2000) and for a constant $\boldsymbol{mi}$ of 20 83

Table 6.3_1.: SPEC input 100

Table 6.3_2: SPEC output 101

Table 6.6_1.: SPEC Input (Hedley-Grant equation) 105

Table 6.6_2.: SPEC Output / Hedley Grant 105

Table 6.6_3: SPEC Input, using FLAC2D/Hoek-Brown strength and convergence values. 107

Table 6.6_4: SPEC Output. *FLAC2D*/Hoek-Brown. 107

Table 6.6_5: Variation in factor of safety with change in span. 108

Table 6.7_1: Pillar stiffness for a data set obtained using the *FLAC2D*/Hoek-Brown model. 109

Table 9.2_1: Uniaxial Compressive Strength of Pyroxenite, Chromitite and Pegmatoid. (Impala Mine data bank, 2012). 118

Table 9.3.1_1: Extent of fracturing in barrier pillars, 19 by 12 m, width 12m - (Piper and Flanagan, 2005) 121

Table 9.3.1_2: Summary of convergence rates measured by Piper and Flanagan 123

Table 9.3.2_1: Calculated pillar strengths for planned as well as measured pillars. 124

Table 9.3.2_2 SPEC input, grid pillar. 125

Table 9.3.2 _3: SPEC Output for 2.6 m effective radius, halfspan 30 m. 125

Table 9.3.4_1: Reproduced from Table 9.3.1_1 (Piper and Flanagan, 2005) 130

Table 9.3.4_2: Spec Input, barrier pillar 131

Table 9.3.4_3: Spec Output, barrier pillar 131

Table 9.3.6_1: SPEC Input for grid pillars 138

Table 9.3.6_2: SPEC Output 138

Table 9.3.6_3. Comparative pillar stresses for grid and barrier pillars 139

Table 9.3.7_1: SPEC Input 141

Table 9.3.7_2: SPEC Output 141

Table 10.2_1: Variation of rock properties over the width of an intersection of the UG2 (Data base at Two Rivers Platinum Mine) 147

Table 10.6_1: SPEC Input and Output, planned layout. 152

Table 10.6_2. : SPEC input and output for actual geometry. 153

Table 10.6_3: Factor of safety and pillar stresses for various half spans using design parameters for the pillars and bords 153

Table 12.1_1: Properties data set at GSI 80 157

Table12.1_2: Example of selected pillar strength values for different sized pillars at variable GSI and UCS values. Constant pillar height of 2 m. 158

UCS 158

Table 12.1_3 Delta values for a given range of GSI and UCS values. 162

Table 12.1_4 Beta obtained using the equation 12.11. 162

Table 12.3_1. Copy of data input from Watson (2010) Thesis, linear equation 5.10. 166

Table 12.3_2. Copy of data input from Watson (2010) Thesis, power equation 5.11. 166

Table 12.7.1_1: Material properties and geometry of the mining layout. 173

Table 12.7.2_1. Input data required 174

Table 12.7.2_2: Equations and numerical values, *FLAC2D*/Hoek-Brown. 174

Table 12.7.4_1: SPEC Input and Output. 177

Table 12.7.4_2: Comparison of safety factors for the methodologies used 178

LIST OF SYMBOLS

σ = Normal Stress

τ = Shear stress

E = Young‘s modulus

v = Poisson‘s ratio

ρ = Density

g = Gravitational acceleration

l = Halfspan

aps = Average pillar Stress

$paps$ = Peak Average Pillar Stress, Pillar strength,

h = Pillar height

w = Pillar width

w_{eff} = Pillar effective width

FOS = Factor of safety

k = Hedley-Grant/Salamon and Munro strength factor

ε = Strain

UCS = Uniaxial Compressive Strength

σ_{str} = Pillar strength

$sigc$ = Rock mass strength (RocLab)

F_g = System force

m_g= Slope of the ground reaction curve

d_g = system convergence

F_p = Force on pillar

m_p = pillar stiffness

d_p = pillar convergence

c_g= total overburden weight

GSI = Geological Strength Index

δ = Strength factor for the generic equation

β = Exponential factor for generic equation

γ = Exponential for the Hedley-Grant equation

α = Exponential for the Hedley-Grant equation

$a, b, c, d, e\ and\ f$ = Parameters for generic strength equation.

Myself, when young, did eagerly frequent
Doctor and saint, and heard great argument
About it and about: but evermore
Came out by the same door as in I went.
Omar Khayyam

ABSTRACT

The aim of this research was to investigate the bord and pillar design procedure in use at the time on chrome and platinum mines and subject it to a critical appraisal and, if necessary, propose an improved methodology. An analysis of the current method and some of the alternatives proposed in the literature has shown that the methodologies suffer from drawbacks that can be detrimental to the mining industry due to overdesign or rendering an excavation unsafe. The conclusion was that improvement is essential.

The influence of the variability of the rock mass properties input parameters on the factor of safety in the current equation was calculated and the findings were that the value of the factor of safety can vary by up to 30% due to these variation.

The proposed process adopted *FLAC2D* /Hoek-Brown simulations to develop full stress deformation curves for typical pillars. The mine stiffness concept was introduced to determine the pillar load which automatically included the influence of the pillar and strata stiffness, excavation spans, pillar yield and failure.

The factor of safety was obtained by dividing the pillar strength by the stress value of the intersection point of the two linear equations for the stiffness of the system and the pillar respectively.

The proposed methodology was calibrated by applying it to two mines in the Bushveld. The conclusion was that the methodology is a significant improvement over the one in use.

To simplify the procedure, a generic pillar equation, based on the findings of this thesis, was developed which not only facilitated the study of the influence of the variability of the input parameters using the Monte Carlo simulation but also resulted in a simplified pillar strength equation for general use on the platinum mines.

$$\sigma_{str} = \delta(\frac{w}{h})^{\beta}$$

Where $\delta = de^{fGSI}$

$\delta = 0.0999e^{0.0704GSI}$ 120 MPa

$\delta = .1089e^{0.0674GSI}$ 100 MPa

$\delta = .1675e^{0.06GSI}$ 80 MPa

$\delta = 0.1652e^{0.0574GSI}$ 60 MPa

$$\beta = TANH\left[\left(\frac{GSI - a}{b}\right)\right]c$$

Where a = 46.866

b = 16.916

C = 1.2906

It was shown that a combination of the *FLAC2D*/Hoek-Brown and the System Pillar Equilibrium Concept can predict the extent of the fracture zones and, to certain extent, the pillar stresses. The stage has been reached where the methodology can be used to predict the most likely commencement of failure of pillars at greater depth and alternative pillar mining methods can be modelled.

FOREWORD

The thesis is subdivided into five parts:-

In Part I, the currently most favoured method of pillar design is examined. The Hedley-Grant strength equation in conjunction with the Tributary Area Theory is subjected to a critical review and deficiencies as well as possible improvements proposed by various authors are discussed.

Part II deals with an alternative method that established an equilibrium between pillar strength and deformation calculated using *FLAC2D*, using the Hoek-Brown criterion and the elastic deformation of the surrounding rock mass. This equilibrium condition can be used to design pillars with differing geometries and properties.

Part III deals with comparisons between observed and calculated equilibrium conditions between a pillar and the rock mass where it was concluded that the method was better suited for pillar design than the current method.

Part IV discusses the possibility of deriving a generic pillar strength equation for specific mines and the sensitivity of the design to variables is determined using the Monte Carlo simulation. .

Part V is a summary of the conclusions.

PART I

1 INTRODUCTION

The design of stable pillars in mining is of fundamental importance not only in the Bushveld mines but in the entire mining industry. Wherever mining is done, pillars will be formed at some stage and it is essential to predict their behaviour in order to be able to assess whether they would burst, yield or remain stable. Although of such importance, the design of pillars still suffers from major deficiencies, weaknesses that affected the results in a fundamental manner.

Faced with such uncertainty, the designs have for the most part been conservative, resulting in the loss of millions of tons of sterilized ore that would be unavailable in future, reducing the lives of mines with dire consequences to the long-term life of the mining industry.

It was decided that a systematic approach was required and the thesis was structured on the following sequence:

- An examination of the pillar design method currently in use for its strengths and weaknesses.
- Investigation of alternative methods in use, actual and suggested.
- Propose an improvedd method for calculating the pillar strength and the loading system.
- Comparison of the improvedd method with underground observations.
- Propose a simplified pillar strength equation based on the improvedd method.
- Main conclusions and recommendations.

Malan and Napier (2011) provided an excellent overview of some of the difficulties associated with determining the strength of hard rock pillars. The salient points of their paper formed part of the introduction to this document.

Essentially two methods were, and still are, employed; empirical back analysis and numerical modelling with an appropriate failure criterion. The weaknesses associated with the empirical method are as follows:-

- The methods are easy to use but cannot be extrapolated beyond the range investigated.
- The pillar strength equation is based on the work done by Salamon and Munro (1967) for coal mines but modified by Hedley and Grant (1972) at Elliot Lake uranium mine. By changing the exponents relevant to the hard rock mine, the Hedley-Grant equation was created.
- Very few pillar collapses occurred in Bushveld mines which could possibly be ascribed to correct or possibly over-conservative design.
- Empirical methods were by nature observational and no deep fundamental understanding of the variables was required in order to derive an answer acceptable in general to the problem of stability.

Numerical modelling techniques, in conjunction with a failure criterion, can be used but have a number of disadvantages. They rely on empirically determined design parameters for use in

the failure criterion. In addition there is uncertainty about the influence of the stiffness of the loading system in the pre-failure region.

The Hedley-Grant equation is used extensively in the design of bord and pillar workings in the platinum and chrome mines in the Bushveld with the full knowledge that it has certain known weaknesses which have been expanded on and discussed in great detail in this thesis;

The pillar strength equation are based on the following:-

- k, strength factor
- w and h, the width and height of the pillar
- γ and α, variable exponential "constants"

$$\sigma_{str} = k\, w^{\gamma}\, h^{\alpha.} \qquad 1.1$$

Where σ_{str} = pillar strength

The strength factor and the exponents in the original equation are based on back-analysis of failed pillar areas. In the absence of sufficient number of failed pillar areas in the platinum mines, the strength factor is assumed to be a fraction of the uniaxial compressive strength of the rock mass in the pillar. While the exponents of width and height in the original equation varied between 0.33 and 0.8, it is sometimes increased without a sound scientific basis in the absence of pillar failure.

Rock masses at deposition have a highly variable composition, which is further complicated by subsequent tectonic processes, enhancing their unpredictability as an engineering material. At present, the average uniaxial compressive strength of say five samples for an ore body was deemed sufficient to design a mine. Detailed analysis of strength values by the author showed that the coefficient of variation (COV) for pyroxenite and chromitite was of the order of 0.33, nearly outside the region of even statistical predictability.

Not only do the rock mass characteristics vary substantially, but also the actual mine dimensions. The actual pillar dimensions, in plan and section, differed substantially from design dimensions and a future design methodology needs to incorporate this variation. (Kersten, 2009).

To date, most of the design values are based on relatively few uniaxial compressive strength values, percentage extraction, depth below surface and the density of the overburden. Unfortunately, the robustness generally resulted in a higher safety factor than required, especially with width-to-height ratios in excess of 3, with obvious serious economic consequences.

With all its deficiencies, the current method is robust, simple and easily understood by practitioners, management as well as the regulatory authorities. Any alternative methodology would have to attempt to be of a similar nature.

The deficiencies were identified by other authors and a review of published alternative approaches were summarized:

- None of the methods considered the interaction between hanging wall and/or footwall and its effect on the pillar strength.
- Three methods considered composite pillars, Joughin (2000), Godden (2012), Roberts (2003)
- Three methods discussed the strata stiffness concept but did not incorporate it in the pre-failure region. Godden (2012), Leach (2008), Roberts (2003).
- The variability of the mining dimensions and the rock mass properties were dealt with quantitatively in parts by three methods. Esterhuizen (2003), Godden (2008), Kersten (1992).

Part II of the thesis deals with the investigation and proposal of an alternative semi-analytical methodology. It was proposed to use proven analytical models, such as *FLAC2D*, in conjunction with the modified Hoek-Brown failure criterion, the results of which could be summarized in a simple generic pillar strength equation, satisfying the simplicity requirement.

It was assumed that the pillar/rock mass remained elastic until pillar failure occurred. The interaction between the local mine and pillar stiffness, and an elastic response determined the loading conditions. The combination of the two concepts, both elastic, was used to determine the factors of safety for the pillar/rock mass.

The concept could be extended to incorporate the post-failure curves as determined by numerical modelling but would not be pursued since the present study dealt with the design of stable, not yielding, pillars.

The proposed methodology not only facilitated obtaining a more reliable factor of safety but also:

- It was found that a volumetric strain increment could be used to predict the extent of the fracture zone.
- The equilibrium point between the pillar resistance and the system load could be used for determining the factor of safety.
- The overall conclusion is that the combination of the *FLAC2D*/Hoek-Brown model in conjunction with the system-pillar-equilibrium method could be used to calculate the extent of pillar failure zones as well as realistic pillar stresses at various half spans, and for a range of typical situations.

Part III deals with the comparison between predicted pillar response and that observed underground which led to the conclusion that;

- The method gives a better understanding of the process of pillar failure and is predictable.

- The design values and their variability are relatively easy to obtain; uniaxial compressive strength, percentage extraction, depth below surface and the density of the overburden.

- A simplified equation for determining pillar strength was derived for simple designs.

- The proposed methodology is a more reliable form of calculating the factor of safety of bord and pillar workings than the currently used method.

In some cases the same data is given in Tables as well as in Figures because trends are clearer in figures while the detail data is available for reference purposes.

2 CURRENT DESIGN METHODOLOGY

The current design methodology used on all the platinum mines consists of five components (SAIMM workshop, 2011):-

- A detailed description of the geological column in the immediate vicinity of the platinum bearing strata which included planes of weakness such as shear zones, chromitite stringers, igneous layering and isopachs of the thickness of the immediate hanging-wall beam. Geological structures, such as joints and faults, were also identified. Some mines used a rock mass classification system, such as the Q-system, RMR or MRMR methods. With the aid of the above data, ground control districts are defined.
- The Hedley-Grant equation is used to calculate the required pillar strength able to support the overburden. For the strength of the ore body, a fraction of 0.33 to 0.8 of the uniaxial compressive strength is generally used which is sometimes adjusted as mining progressed to a lower or higher value depending on observed pillar behaviour.
- The average stress acting on the pillars is calculated using the Tributary Area Theory.
- The factor of safety is determined by dividing the pillar strength by the average pillar stress; a limiting value of 1.2 to 1.6 is commonly used.
- Pillar monitoring is generally done by visual inspection of smaller pillars in an array of pillars for signs of scaling. In a few instances, boreholes were drilled into the pillar to determine the extent of the stress induced fracturing. The result of this monitoring is then used to adjust the strength factor in the Hedley-Grant equation.

2.1 What is wrong with the method?

The current method is based on two fundamental factors:-

- The Tributary Area Theory to calculate the stress acting on the pillar.
- The pillar strength calculated using the Hedley-Grant equation.

2.1.1 Pillar stresses and the Tributary Area Theory –TAT

The average pillar stress,aps is determined by the vertical stress component and the percentage extraction by the following function:-

$$aps = \sigma_v/(1-e) \qquad 2.1$$

σ_v= Virgin vertical stress

e = extraction ratio

For instance, at a depth of 100 m, σ_v= 2.8 MPa with an average overburden density of 2800 kg/m^3 an extraction ratio of 0.85 the average pillar stress is 2.8/0.15 = 18.7 MPa using a rounded value of 10 m/s^2 for gravitational acceleration.

2.1.2 Pillar strength

The Hedley-Grant equation (1972) for pillar strength is:

$$\sigma_{str} = k(w^{\gamma}/h^{\alpha}) \qquad 2.2$$

w = width of pillar, or effective width, w_{eff} for non-square pillars

h= height of the pillar

k, α, γ = constants

$$w_{eff} = \frac{2(l*w)}{(l+w)} \quad \text{for rectangular pillars} \qquad 2.3$$

l= pillar length

The pillar strength equation was developed by Salamon and Munro (1967) for South African coal mines where α and γ values were 0.46 and 0.66 respectively. Back analysis of collapsed pillars in the Elliot Lake uranium mine by Hedley and Grant (1972) obtained values of 0.5 and 0.75 respectively.

The values of 0.5 and 0.75 for α and γ and a specific k value made it the Hedley-Grant strength equation for hard rock pillars which was in common use on the Bushveld mines.

The k value generally used varies between 0.3 and 0.8 of the uniaxial compressive strength of the pillar material.

2.1.3 Factor of Safety

For non-yield pillar layout, the ratio of pillar strength to applied stress is called the Factor of Safety or FOS

$$FOS = \sigma_{str}/aps. \qquad 2.4$$

aps= average pillar stress

The deficiencies identified of the equations 2.2 to 2.4 were as follows:-

- The equation was based initially on coal mine research and modified by data obtained in one base metal mine (Hedley and Grant, 1972). It is in use in all the non-coal bord and pillar mines in South Africa irrespective of whether it is a copper, nickel, and platinum or manganese mine. The strength factor is only changed based on the uniaxial compressive strength.
- The inherent variability of the rock mass properties is not included in the stability assessment.

- The use of the safety factor as a criterion has to be evaluated.
- The strength differences or similarities between the ore and the hanging- and footwall are disregarded resulting in possible incorrect pillar strength values.
- The presence of different rock type layers in the pillars is generally disregarded. Only in instances where soft layers were encountered in the immediate hanging wall were they considered and that only after major collapses occurred.
- The influence of the stiffness of the loading system was totally ignored leading to inappropriate designs in limited span or thick tabular ore bodies.
- Back analysis was mainly based on pillar width-to-height ratios of < 3.

A combination of all the above factors could result in a gross over- or under-design of an entire mine or mining industry. The resultant sterilization of ore would be greatly felt in the near future, especially as mining increases in depth.

The listed deficiencies are discussed in greater detail below.

2.1.4 The uniaxial compressive strength

In the absence of failed pillar areas for back analysis, the uniaxial compressive strength is the only quantitative value available for determining the pillar strength in mine design at the moment. An average number of three to five samples was deemed sufficient by industry norms. Inspection of available data bases from the mines (Impala and Two Rivers Platinum Mines) showed that there was a large variation in uniaxial compressive strength values over very short distances.

In Figure 2.1.4_1 the uniaxial compressive strength of chromitite, obtained from five boreholes drilled in an area of approximately 500 m^2, is shown. When the average values for each individual borehole (Figure 2.1.4_2) was taken, the average uniaxial compressive strength varied between 120 and 180 MPa.

Figure 2.1.4_3 shows the frequency distribution of uniaxial compressive strength values for the Two Rivers Platinum Mine; again the variation is large.

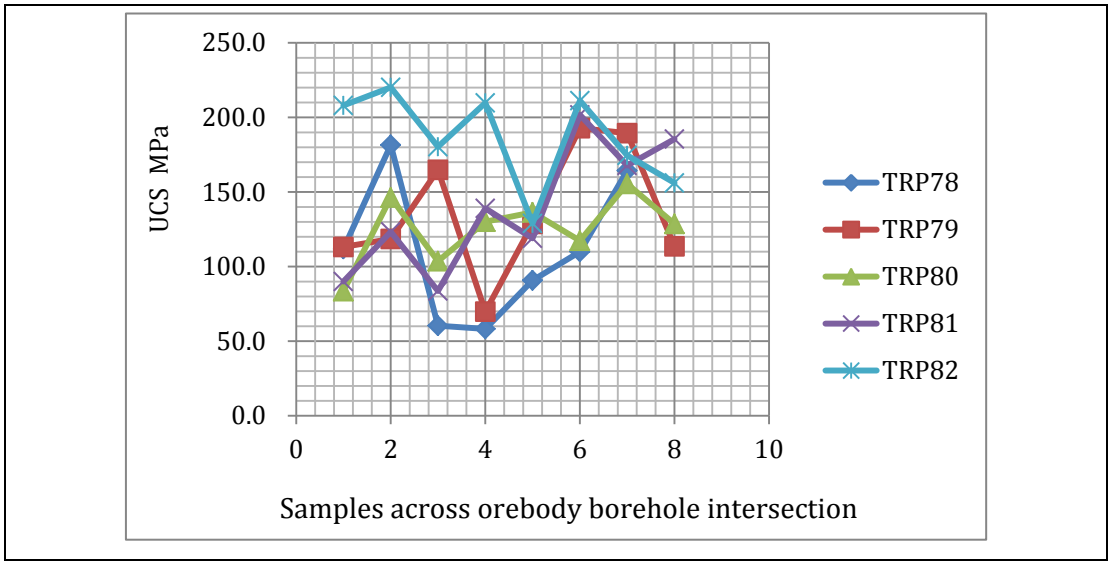

Figure 2.1.4_1 Variation of UCS values in intersections through the UG2 ore body for five boreholes at Two Rivers Platinum Mine (Coefficient of variation = 0.40, 0.29, 0.17, 0.29, 0.16)

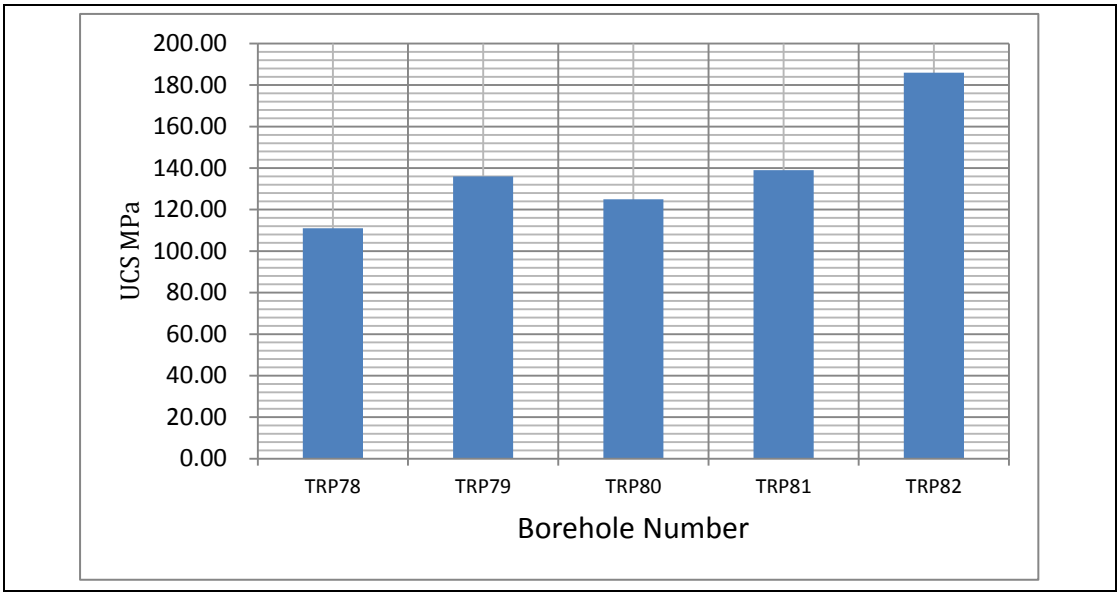

Figure 2.1.4_2 Variation of average uniaxial compressive strength in plan between the same boreholes shown in Figure 2.1.4_1

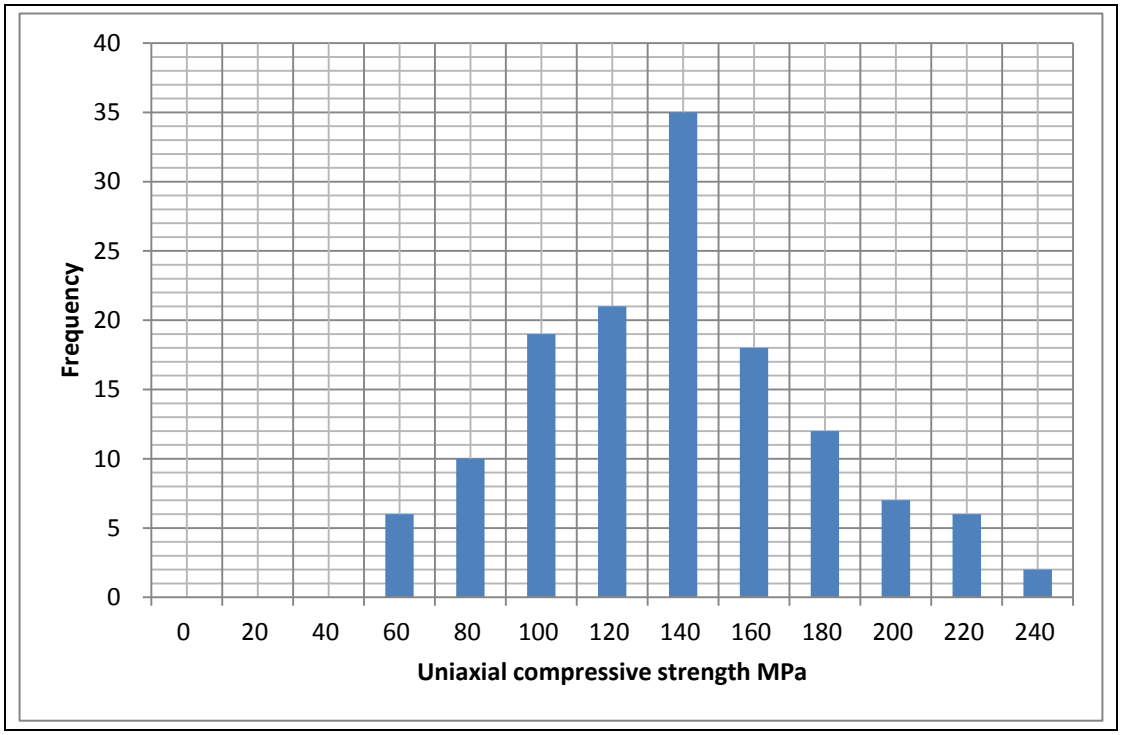

Figure 2.1.4_3 Frequency distribution of all UCS values for Two Rivers Platinum Mine, based on 136 values

2.1.5 Determination of the *k*-value

The k-value in the Hedley-Grant equation as used on the platinum and chrome mines was derived from the average uniaxial compressive strength of the ore body for individual mines, sometimes as few as three values, which was then reduced by a ratio which could vary from 0.33 to 0.8. The value of the ratio was dependent on the mine and its age. The approach in designing a new mine was to commence with a low ratio and, as mining increased and no pillar failure was obvious, the ratio was increased.

To illustrate this point, the variation in *k*-values used in different mines, mining similar ore bodies, is shown in Table 2.1.5_1.

It is clear that, with an incorrect estimate of the uniaxial compressive strength and the selected ratio for$k$, the effect on the pillar strength calculation is compounded.

Table 2.1.5_1: k-Values used on different mines

Mine	Orebody	k-Value
Two Rivers Platinum Mine	UG2	68
Bathopele	UG2	34-44-54
Kroondal	UG2	55
Lannex	LG6	53
Tweefontein	LG6	53
Doornbosch	LG6	31
Lavino	LG6	26-30
Limpopo	UG2	41
Kroondal	LG6	45.6

2.1.6 Actual pillar dimensions

Actual dimensions of pillars cut underground differ significantly from the design dimensions as illustrated in Figure 2.1.6_1. The actual measured pillar dimensions obtained from a 1:500 plan from Two Rivers Platinum Mine differed substantially from the design value of 6 m (dip) and 6 m (strike). (Kersten 2013).

Obviously the factor of safety would be strongly influenced by these actual variations in dimensions.

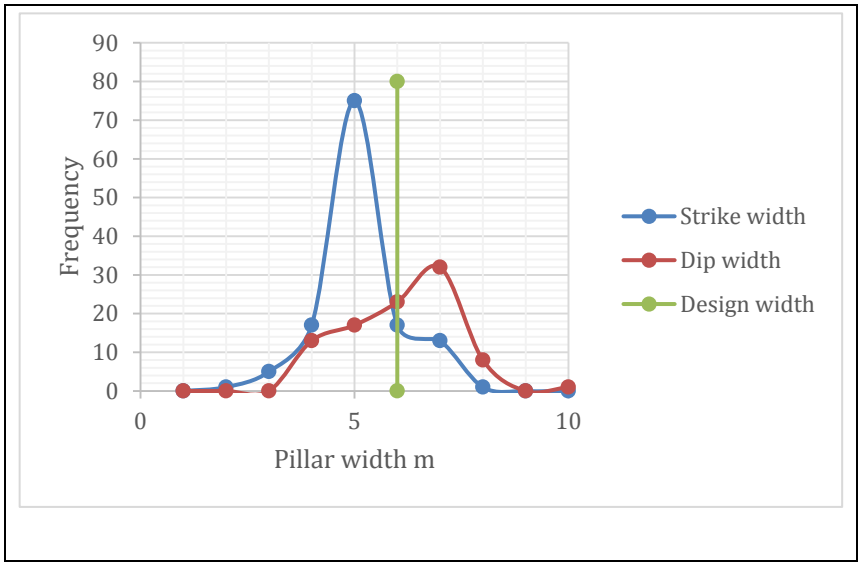

Figure 2.1.6_1 Measured pillar strike and dip width variations in a particular mine section, Two Rivers Platinum Mine (Kersten, 2013)

2.1.7 Definition of pillar failure.

Pillar failure was difficult to define for mainly three reasons:

- As the stress on a pillar increased, sidewall spalling commences and propagates into the pillar. The effect of this fracture propagation creates higher stresses in the remaining central intact portion of the pillar and on the width of the pillar, failure will stop due to the increase in the confining forces acting in the pillar centre. The pillar had not failed.
- In the case of a stiff loading system, the pillar scaling process is governed by the elastic hanging/footwall convergence, and is span dependent. Even though such pillars can apparently be loaded to beyond their strength, the system stiffness prevents the collapse of the pillar and it can then appear to be stronger than it actually is.
- Where the stress exceeds the strength, the material starts to fail and the structure will fail once the induced strain/deformation exceeds the critical strain/deformation.

In summary, pillar spalling/sidewall fracturing is controlled by the elastic hanging wall deformation. It does not define the strength of the pillar. The stress could be anywhere near the peak of the linear pillar strength curve, or already strain softening portion, but will still not lead to a regional collapse.

2.1.8 Interaction between pillar and hanging/footwall

Interaction between the rock above and below the pillar had largely been ignored. Laboratory strength tests on specimens were conducted where the platten strength was far in excess of that of the specimen. Underground observations, however, indicated that there were a variety of interactions between the pillar and the hanging/footwall. In instances where the strength of the pillar material and the hanging wall/footwall are similar, stress fractures will be induced in both. The subsequent effect on the overall pillar behaviour and the hanging wall stability needed to be incorporated as mining increases in depth.

Figure 2.1.8_1 illustrates an example where the pillar induces curved fractures in the hanging wall of the Merensky reef. (Impala Platinum Mine.)

Classification of joints, blast induced fractures and stress induced fractures urgently required definition as stress induced fractures were often referred to as blast induced, which creates major confusion.

It was not the purpose of the researcher to provide an overall definition of the individual sets but, in the context of time period of the research, fractures surrounding the mining excavation that duplicate the excavation shape in detail, are defined as stress induced fractures.



Figure 2.1.8_1 Induced fracturing in the hanging wall of the Merensky Reef

Figure 2.1.8_2 is a close up on the pillars edge of the same phenomena and illustrates that the effect that the pillar had on the bord stability required attention.



Figure 2.1.8_2 Interaction between pillar and hanging wall on the Merensky Reef - Impala Platinum Mine

Alternatively, the opposite effect was that of a clearly defined bedding plane on the hanging wall contact where fractures are not transmitted from the pillar edge into the hanging wall.

The influence of the hanging and footwall on the pillar strength was not pursued further in the thesis as detail of simple pillar behaviour on its own is primarily needed before further complicating factors are introduced.

2.1.9 Composite pillars

The presence and effect of pyroxenite layers in chromitite pillars had, in most instances, been ignored in the design methodology.

In 2005 the author used the *FLAC2D*/Mohr model of pillars containing various combinations of pyroxenite and chromite with properties given in table 2.1.9_1 (Ryder 2005). For a pillar, 1.6 m high and 3 m wide, the strength of the pillar varied from 80 MPa to 350 MPa for the different combinations listed. (Table 2.1.9_1).

Table 2.1.9_1: Chromitite and pyroxenite properties

h=1.6 m	Bulk Modulus-bu GPa	Shear Modulus sh GPa	Cohesion MPa	Angle of friction	UCS MPa
Chromitite 1	41	13.5	20	49	120
Chromitite 2	28	4	8	53	60
Pyroxenite1	70	18	40	35	240
Pyroxenite 2	4.5	0.34	20	35	

Combination	***FLAC2D*/Mohr Strength MPa**
Chr1/Pyx1	242
Chr1/Pyx2	200
Chr2/Pyx1	240
Chr2/Pyx2	180
Chr2 only	350
Chr1 only	350
Pyx1 only	120
Pyx2 only	80

The information above illustrated that layers of different composition play a significant role and required investigation.

2.1.10 Effective width correction

Wagner (1980) developed an equation that included the influence change in relative plan dimensions of rectangular pillars on the strength

$$w_{eff} = 4\,(l * w)/2(l + w) \quad , \qquad 2.5$$

Where w_{eff} = Effective width

l = Pillar length

w = pillar width

Alternative equations had been proposed by several authors, listed in Figure 2.1.10_1, which shows that the strength increase over square pillars as a function of the length to width ratios. The Grobbelaar and Wagner equations, according to Roberts et al. (2005) had not been proven or substantiated. The Wagner curve was used for the Salamon and Munro (1967) equation for pillar strength calculations.

The above would have significant influence on the pillar strength calculated and it was concluded that the definition of effective width needs further investigation for Bushveld rocks and reigning pillar dimensions.

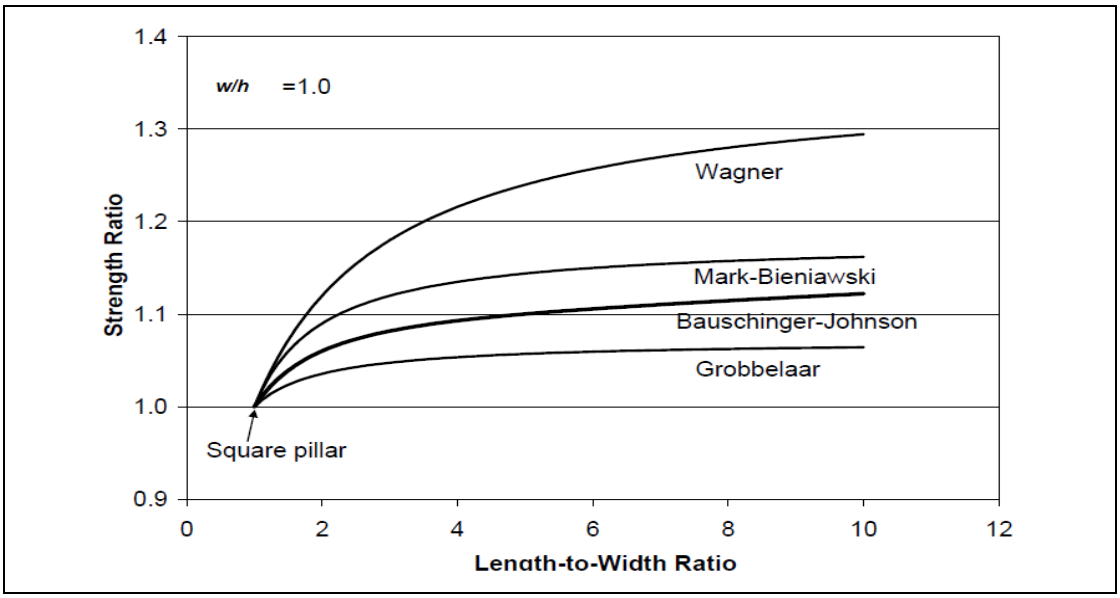

Figure 2.1.910_1 Influence of pillar length on strength ratio of rectangular pillars, width-to-height ratio of 1.0, for strength equations by the authors indicated, Dolinar and Esterhuizen, (2007)

2.1.11 Additional pillar design equations

Additional equations, summarised by Malan (2011), mainly variations on the Hedley-Grant equation have been proposed and used in practical application.

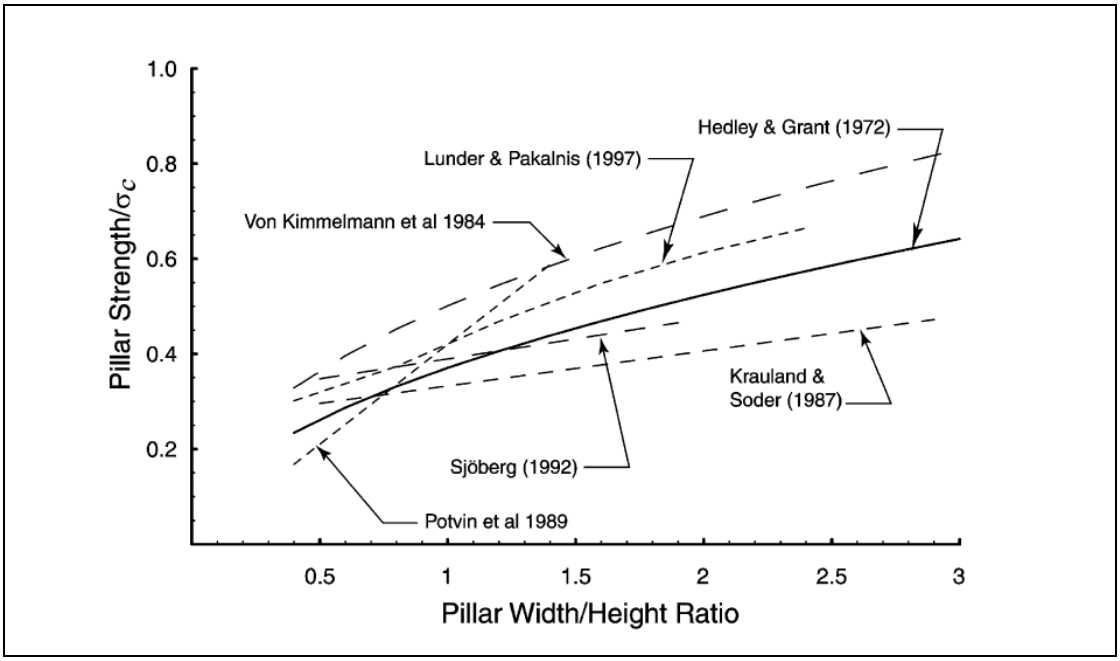

Figure 2.1.11_1. Plot of normalised pillar strength for various proposed strength equations, where σ_c is the uniaxial compressive strength. (Malan, 2011)

The divergence in results using the different equations are substantial and raises the problem of deciding which one is correct.

A common feature of the strength values is that the strength increase decreases with increase in width to height ratio.

2.1.12 Width-to-height ratios investigated

Figure 2.1.11_1 shows that the strength calculations are limited to pillars with a width-to-height ratio below 2.5. Simulations by the author, using *FLAC2D/*Hoek-Brown model, showed that there is an increase in the strength with increase in the width to height ratio beyond a ratio of 2.5. Work by Malan and Napier (2006) using the finite equilibrium model, also shows an increase with increase in the width to height ratio.

This is a significant observation and is dealt with in detail in the thesis.

2.1.13 The influence of depth on the properties of the specimen collected

Watson (2010) described the difference between the uniaxial compressive strength of specimens collected at 600 m and 1100 m below surface (Figure 0_2). He ascribed the differences to the influence of the stress concentrations at the tip of the drill bit, introducing and/or extending micro-cracks.

The common occurrence of discing during drilling (Figure 0_1) operations is also proof that the drill bit stress field plays a major role. The field stress at this position was of the order of

50 MPa when drilled. Incipient discing could be expected at stress levels of approximately 0.5 to 0.3 of the uniaxial compressive strength, Figure 0_2.



Figure 0_1 Core discing of borehole core obtained from above a Pillar - (Watson et al, 2007)

It is here postulated that the properties of the specimen are strongly influenced by the stress level to which the sample was exposed during the drilling process.

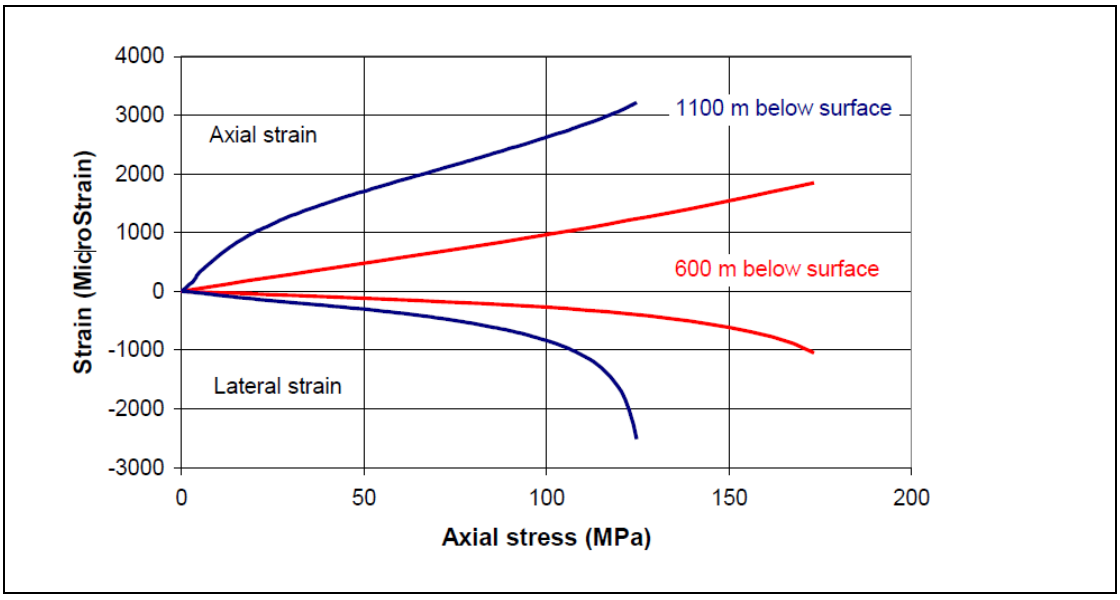

Figure 0_2 Strain differential with increase in axial stress between samples of spotted anorthosite collected at 600 and 1100m below surface - (Watson, 2010)

Figure 0_3 and Figure 2.1.13_4 give the uniaxial compressive strength of rocks collected at different depths in the Western and Eastern portion of the Bushveld mines. There appears to be a tendency for the average values to be lower for specimens collected at greater depth.

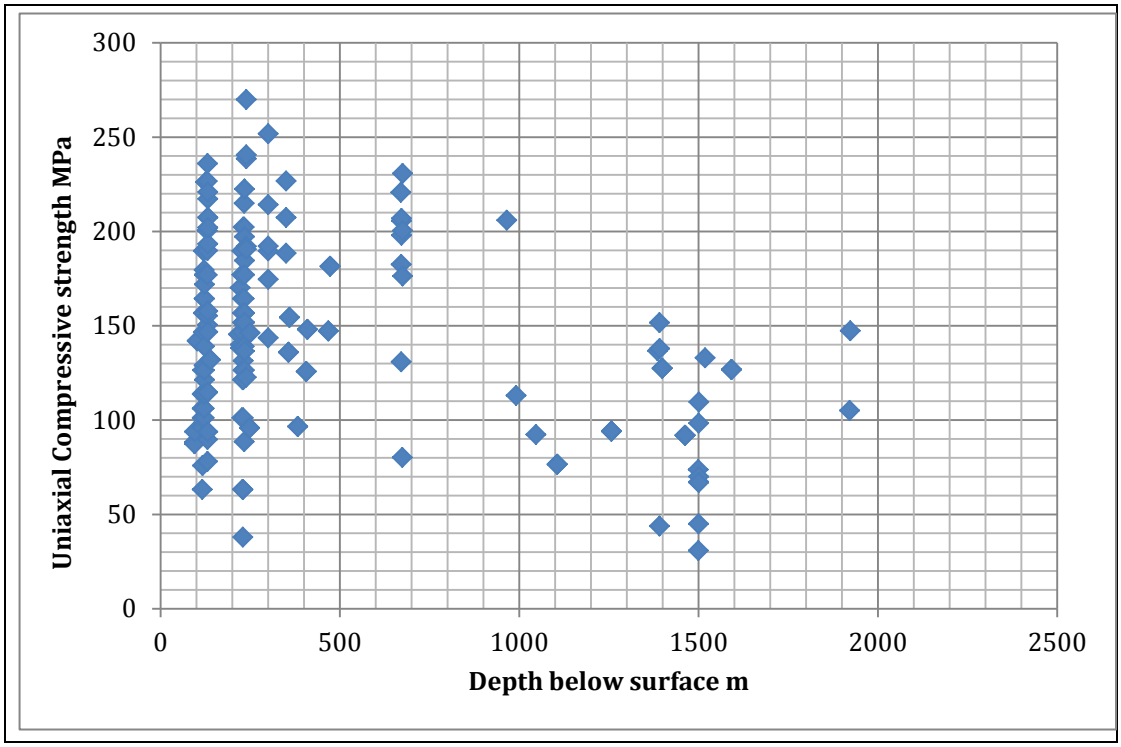

Figure 2.1.13_3 Plot of uniaxial compressive strength vs. depth for pyroxenite samples collected at various depths below surface (Impala data bank, 2012).

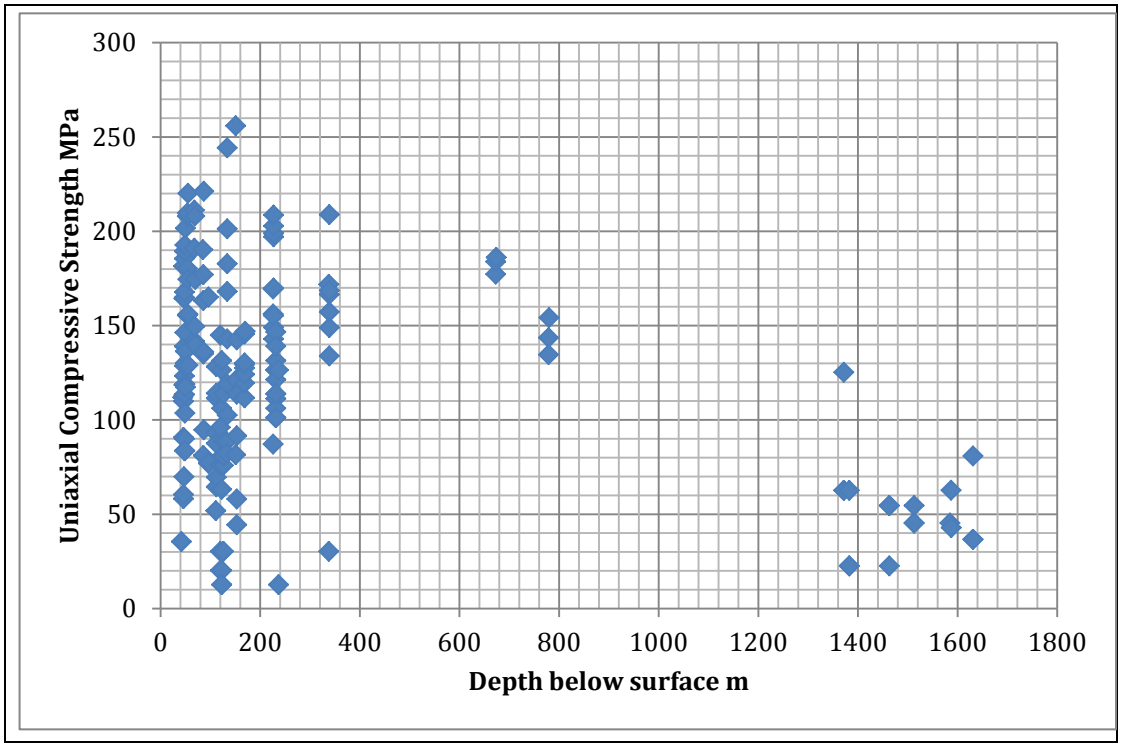

Figure 0_4 Plot of uniaxial compressive strength vs. depth of chromitite samples collected at different depths below surface. (Impala data bank, 2012).

2.1.14 Pillar stresses and the loading system

The Tributary Area Theory used to calculate the pillar stress assumes a loading medium with no shear resistance simulating the worst case scenario and is generally not a true reflection of actual underground conditions. To model the correct average pillar stress MinSim (Watson, et al. 2007), or the Texan code developed by Malan and Napier (2006), could be used.

Geological losses, which create medium to large un-mined areas, consistently about 20 to 30% in the Bushveld mines, are generally not considered in the Tributary Area Theory model.

The influence of topography needs to be incorporated in the stress calculations in the Eastern Bushveld as the UG2 and the Merensky reef horizon usually extended underneath steep mountain sides. (Figure 2.1.14_1).

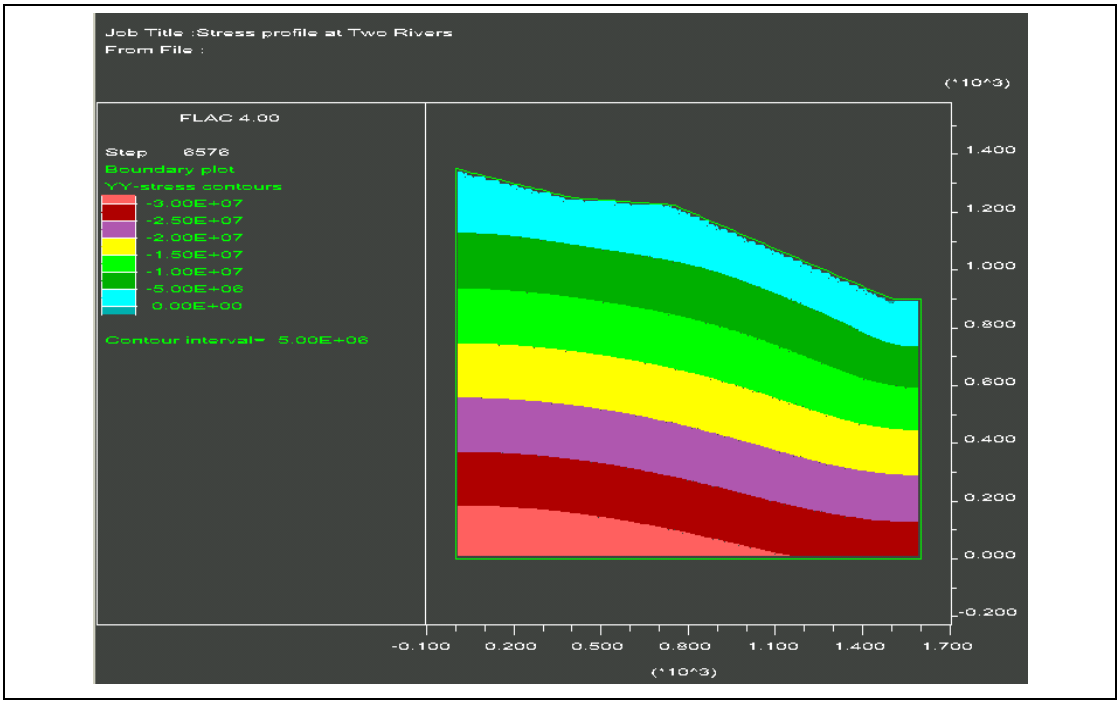

Figure 2.1.14_1 Stress distribution beneath the steep hillside on one of the UG2 Mines in the Eastern Bushveld

The decision to use the average depth would lead to over design in the shallow portions and under design in the deeper areas and subdivision into smaller districts was recommended.

2.1.15 "Bedding" parallel planes of weakness

Planes of weakness in pillars had been the cause of regional pillar failures (Godden, 2012) but this effect had not been analysed in a quantitative manner.

2.2 Sorting of deficiencies / Classification of the deficiencies

The deficiencies could be subdivided into two main groups:-

- Variation and uncertainty in input parameters; and
- Relation to the pillar strength equation.
- Simplistic pillar stress calculations.

The rock mass “constants”, uniaxial compressive strength and mining dimensions were the main variables with the pillar strength equations also needing revision to cater for greater width to height ratios and variable composition. Pillar stresses calculated using the Tributary Area Theory leads to overdesign in most cases.

2.3 Effect of the variability of the input parameters

To determine the effect of the variability of input parameters when using the Tributary Area Theory with the Hedley–Grant equation, a Monte Carlo simulation (van der Merwe 2011) was run for individual variables for a series of coefficients of variation. The input parameters selected were typical of the average Bushveld platinum mine.

- 300 m below surface.
- Density 3000 kg/m^3
- k value 50 MPa.
- Pillar centre spacing 14 m by 14 m.
- Pillar width 6 m by 6 m.
- Pillar height 2 m.

Coefficients of variation were assigned, one at a time, to the above values. For example, to determine the influence of the variation of the k value, the remaining variables were assigned an extremely low coefficient of variation, since the value 0 could not be used in the simulation spreadsheet.

Figure 2.3_1 gives the relative calculated influence of individual parameters on the probability of failure.

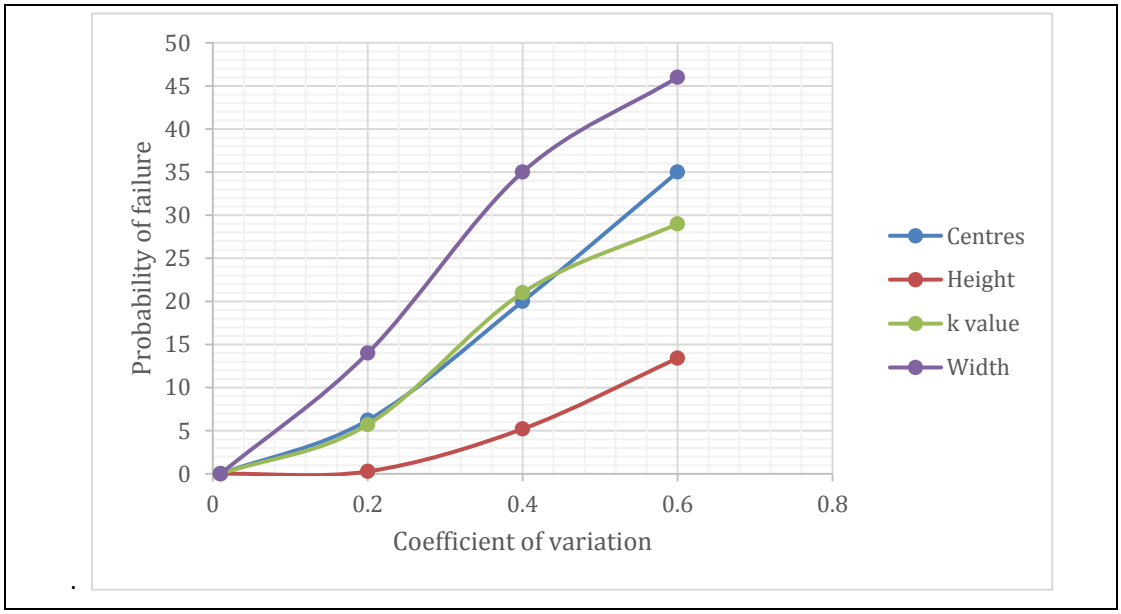

Figure 2.3_1 Probability of failure for different variables and coefficients of variation

Apparently the variation in pillar dimensions had the greatest influence on the probability of failure, with the pillar height the least significant when using the Hedley-Grant equation for strength and the Tributary Area Theory for the loading.

Figure 2.3_2 illustrates the spread of values of the uniaxial compressive strength of chromitite obtained from Impala Platinum Mine database, showing the actual and calculated distribution, coefficient of variation of 0.31.

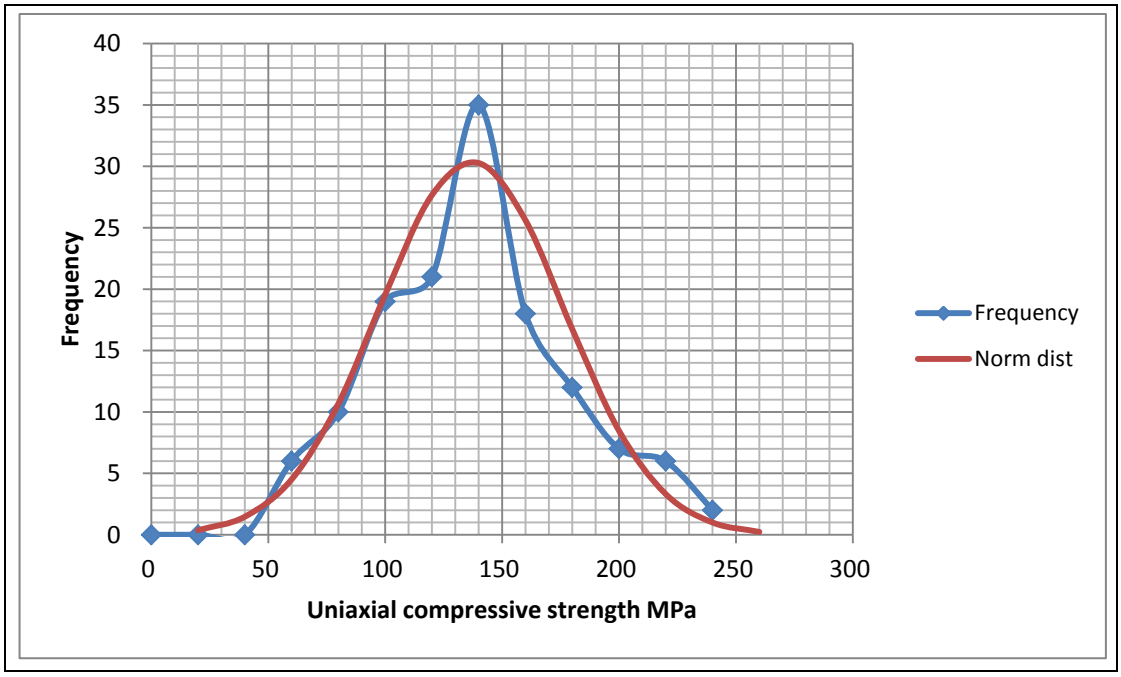

Figure 2.3_2 Frequency distribution of the strength values for chromitite

To further illustrate the combined effect of input variation, a Monte Carlo simulation was run for a typical case with mean values and standard deviations listed in Table 2.3_1.

Table 2.3_1: Assumed values for a typical case

	u mean	*Standard Deviation*	COV
Depth m	250	15	0.06
Density kg/m^3	3000	150	0.05
k	50	15	0.30
Centres m	14	2	0.14
Pillar width m	6	1.2	0.20
Pillar length m	6	1.2	0.20
Pillar height m	2.34	0.74	0.31

The results of the simulation were:-

- Probability of failure =23%
- Factor of safety = 1.57

Accepting that the Hedley-Grant equation was correct and that the Tributary Area Theory was a true reflection of the pillar strength and stress, the above was a typical example of a UG2 mine in the Eastern Bushveld. The design safety factor of 1.57 was entirely acceptable but the probability of failure of 23% due to the variation in input parameters raises the question whether a factor of safety of 1.6 is sufficient. (Because of the lack of an acceptable value of an industry based figure, the probability of failure is used by the author to compare and assess the rate of change of the values.)

The above argument presupposed that the values using Tributary Area Theory and the Hedley-Grant equation provided the correct answer. The fact that the predicted failure did not materialise indicated that the input parameters were overly conservative and/or the pillar equation was suspect.

It should also be noted that the shown probability of failure related to the probability that any given pillar had a factor of safety < 1.0. Failure of a panel of pillars would only occur if those pillars happened to be in groups. This grouping reduced the likelihood of catastrophic failure to less than the number shown.

In the present example, the standard deviation of the depth, density, k-value and height were a function of the ore body geometry and could not be manipulated.

However, by reducing the COV for the centre spacing and pillar size to absolute minimum of say 0.05, the probability of failure was reduced to 14%.

2.4 What has been done and what needs to be done

The deficiencies identified had also been noticed and addressed by other authors such as Malan (2011) and proposals were made that addressed some of the deficiencies listed. A literature survey for pillar design on the Bushveld and other South African mines has been summarised and a score card developed for the different alternatives in terms of their incorporation of variables.

3 PUBLISHED ALTERNATIVE DESIGN METHODOLOGIES

The authors referred to in the following section were all aware of some of the deficiencies listed and had all, in their unique way, attempted to obtain a more reliable answer. Their methods are described briefly highlighting the main problems identified. At the end of the chapter, a scorecard rates these methods according to the problems incorporated in their system as well as on the simplicity and robustness of the methodology.

3.1 Joughin et al (2000)

The risk-based approach was used to incorporate the effect of the variation in rock mass properties as well as pillar dimensions using analytical methods, based on the Hoek-Brown failure criterion to calculate the strength of individual pillars.

Joughin, et al., (2000) used the Point Estimate Method (PEM) to evaluate the influence of variable rock mass conditions and pillar geometries

The mean and standard deviations of the rock mass properties and the pillar dimensions were required:-

- The mean and standard deviation of the results from all permutations of the uniaxial compressive strength, Geological Strength Index and $m_i$values for pyroxenite and chromitite were used.
- Variation in pillar dimensions.
- Span variation of bords.
- Use of composite pillars consisting of chromitite and pyroxenite.

An example of the permutations of the input parameters used in their method is shown in Table 3.1_1.

Table 3.1_1: Example of input parameters used for a specific area - (Joughin et al, 2000)

Term	m_i	UCS	GSI	UCS	m_b	s	m_r	s_r
1	+	+	+	125.8	16.9	0.043	6.2	0.0088
2	+	+	-	125.8	12.7	0.017	3.5	0.0023
3	+	-	+	31.8	16.7	0.043	6.2	0.0088
4	+	-	-	31.8	12.7	0.017	3.5	0.0023
5	-	+	+	125.8	10.0	0.042	3.7	0.0088
6	-	+	-	125.8	7.5	0.017	2.1	0.0023
7	-	-	+	31.8	10.1	0.042	3.7	0.0088
8	-	-	-	31.8	7.5	0.017	2.1	0.0023

Wherem_i, GSI, s values refer to variables used in the Hoek-Brown failure criterion.

An axi-symmetric non-linear finite element model (PHASE 2) was used to calculate the individual pillar strength for all the above mentioned permutations with the output given in terms of:-

- Factor of Safety.
- Probability of failure (POF).
- Reliability.

The method was applied to a collapsed area where the results corresponded reasonably well with the number of collapsed pillars. The method was then used to design a new area to be mined.

Joughin, et al. (2000) addressed the following problems identified earlier in this thesis:-

- Variability of rock mass properties.
- An accepted empirical failure criterion.
- A non-linear finite element program.
- The strength of composite pillars.
- The tributary area theory for calculating the pillar stresses.

It did not include the following aspects:-

- Strata and pillar stiffness.
- Losses of ground.
- Simplicity and robustness.

3.2 Esterhuizen (2003)

Esterhuizen highlighted the degree of uncertainty associated with each design parameter and discussed the influence of the variability of input parameters in the Hedley-Grant equation, specifically the pillar strength factor, k and the width, length and height of a pillar. He ascribed the uncertainty to the inherent variability of the rock material or to a lack of understanding of the way in which rock behaved.

The uncertainty was usually taken into consideration by making use of a factor of safety, which was defined as the ratio between the capacity of a system and the demand on the system.

With mean and standard deviations available for the relevant quantities, he used the point estimate method (PEM) to calculate the mean pillar strength with the standard deviation permutation based on the Hedley-Grant equation.

Subjecting the pillars to a uniform stress, using the Tributary Area Theory, he determined the factor of safety (FOS) as well as the probability of failure of the pillars and expressed it in terms of the reliability of the result;

$$\text{Reliability} = 100(1 - POF) \qquad 3.1$$

A brief sensitivity study showed that for the specific model the reliability did not increase significantly above a FOS of 2.0. Also, increase in depth increased the reliability by decreasing the influence of the pillar dimension variation.

He incorporated yield pillar design for deeper ore bodies where he based the strata stiffness and pillar post failure curves on work done by Ryder and Ozbay (1990).

Esterhuizen addressed the following deficiencies by:-

- Incorporating the variability of the rock mass properties as well as pillar dimensions in the Hedley Grant equation.
- Applying the concept of probability of failure.
- Including the stiffness of the system in the post-failure regime.

These actions did not include the following:-

- A pillar-strength equation that could incorporate variation in composition
- Losses of ground
- The strata stiffness in the elastic regime.

3.3 Barczak et al (2009).

Barczak et al (2009) discussed the concept of a ground response curve and states that it was originally developed for the civil tunnelling industry where the timing and method of ground

support is determined by monitoring the support pressure and excavation convergence during construction obtaining a schematic ground response curve, Figure 3.2_1.

The ground response curve plots the support pressure against the excavation convergence, as shown conceptually in figure 3.3_1. If the excavation boundaries are subject to support pressure equal to the stress in the surrounding rock, no convergence will occur (Point A). As the support pressure is reduced, the excavation boundaries converge and the pressure required to prevent further convergence reduces as arching and the self-supporting capacity of the ground develops. An equilibrium point is reached, point Q, where the support resistance equals the self-supporting capacity and the system comes to rest. The remainder of the curve deals with the non-elastic response and does not impact on the design of pillars with a factor of safety in excess of 1.0.

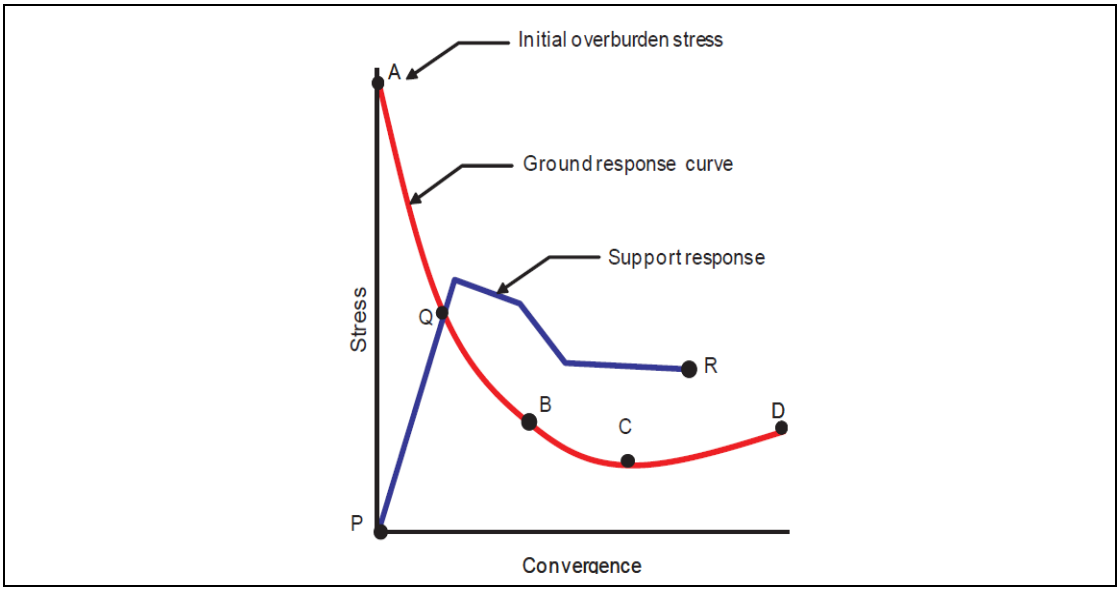

Figure 3.2_1 Ground response and the support response curves - Barczak et al, (2009).

3.4 Malan and Napier (2006)

Malan and Napier (2006 and 2007) proposed a limit equilibrium method for calculating the strength of hard rock pillars.

The limit equilibrium model simulating the progressive fracturing of the pillar sidewall is illustrated in Figure 3.4_1. The fractured slices are restrained by the hanging wall and the footwall parallel stress σ_s and seam normal stress σ_n , as well as by shear traction which was proportional to the seam normal stress σ_n. The relevant equations are listed below and were used to obtain the results shown in Figure 3.4_2.

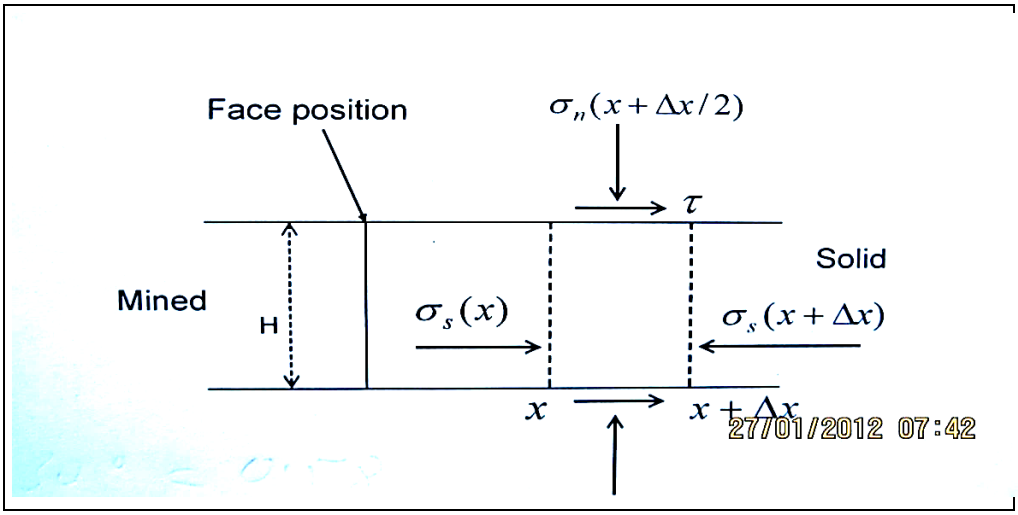

Figure 3.4_1 Analytic Finite Equilibrium Model (Malan and Napier 2006)

$$\mathrm{T} = \sigma_n \tan\theta \qquad 3.1$$

$$= \mu_s \sigma_n$$

Where θ = friction angle between the fractured and intact material

T = shear traction

The incremental change in reef parallel stresses, maintaining equilibrium, is governed by the differential equation

$$\frac{d\sigma s}{dx} = 2\ \mu_s \sigma_n / H \qquad 3.2$$

A further assumption is that the seam normal stress is related to the average seam parallel stress by the "limit equilibrium" relationship:

$$\sigma_n = c + m\,\sigma_s \quad , \qquad 3.3$$

Where c = cohesion of the fractured material and m is an appropriate slope parameter.

The change in seam parallel stress as a function of the distance l from the edge of the seam is obtained by combining equations (3.3) and (3.2):

$$\sigma_s = C\lfloor(exp\ \alpha l) - 1)\rfloor/m \quad , \qquad 3.4$$

Where $\alpha = \mu_s m/H$

A comparison between *FLAC2D*/Hoek-Brown and Limit Equilibrium Model is shown in Figure 3.4_2.

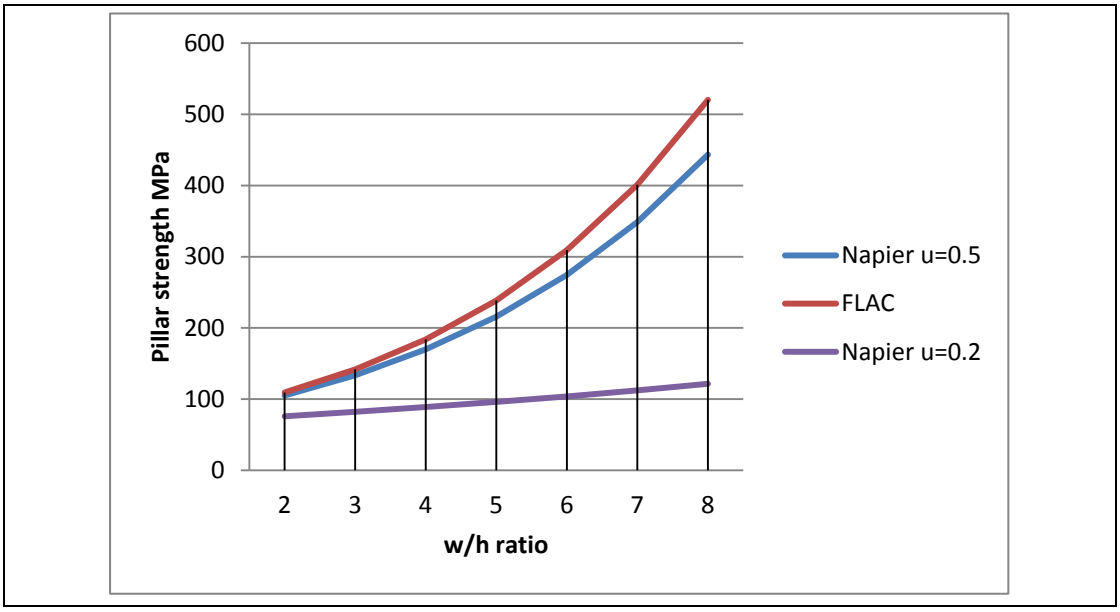

Figure 3.4_2 Comparison between Limit Equilibrium and *FLAC2D* models.

The trend in increase in strength with increase in the width to height ratio is predicted by both the FLAC2D and Limit Equilibrium Method and can be expressed in two similar equations:

Limit Equilibrium Model $\sigma_{str} = 65e^{0.24(\frac{w}{h})}$ 3.5

FLAC2D/Hoek-Brown $\sigma_{str} = 60e^{0.26(\frac{w}{h})}$ 3.6

Where σ_{str} = Pillar strength

The method has the advantage that it proposes a failure mechanism but the disadvantage is that it has not been developed into a simple methodology hence it has not been used widely in actual pillar design.

3.5 Martin and Maybee (2000)

Martin and Maybee (2000) studied the brittle failure of pillars in the Canadian Shield hard rock mines and concluded that the dominant mode of failure was progressive slabbing and spalling. They commenced by investigating the commonly used empirical equations listed in Table 3.5_1. The equations are based on failed pillars confined to w/h ratios less than 2.5.

Table 3.5_1: List of pillar strength equations summarized by Martin and Maybee (2000)

Author	Rock Type	UCS MPa	Equation	k
Hedley and Grant (1972)	Quartzite	230	$133^{w^{0.5}/_{h^{0.75}}}$	133/230 = 0.58
Von Kimmelman (1984)	Metasediments	94	$65^{w^{0.46}/_{h^{0.66}}}$	65/94 = 0.69
Krauland (1987)	Limestone	100	$35.4(0.778 + 0.222\frac{w}{h})$	35.4/100 = .35
Potvin (1989)	Canadian Shield	-	$.42\sigma str(^{w}/_{h})$	
Sjoberg (1992)	Limestone/Skarn	240	$74(0.778 + 0.222\frac{w}{h})$	74/240 = 0.31
Lunder and Pakalnis (1997)	Hard Rocks	-	$0.44\sigma_{str}(0.68 + 0.52)k$	

Where: σ_{str} Uniaxial compressive strength of the rock.

The normalized pillar strength values of the pillars investigated are plotted in Figure 3.5_1, (repeat of Figure 2.1.11_1 for ease of reference) showing the variation in strength for the various rock types. The variation in equations leads one to believe that for the current pillar design methodology, a detailed back analysis of each individual area is required before the pillars can be designed.

This empirical approach is not deemed reliable for the design of bord and pillar operations in a new mining area and highlights the need for a more analytical approach for the determination of the strength of pillars.

Martin and Maybee (2000) therefore followed up by using the Hoek-Brown criterion with different values for the Geological Strength Index (GSI), m_i and m_r values and concluded that for the w/h ratios below 2 the confining forces played little or no role and that the Hoek-Brown criterion should be used with the m_i value equal to 0.

.

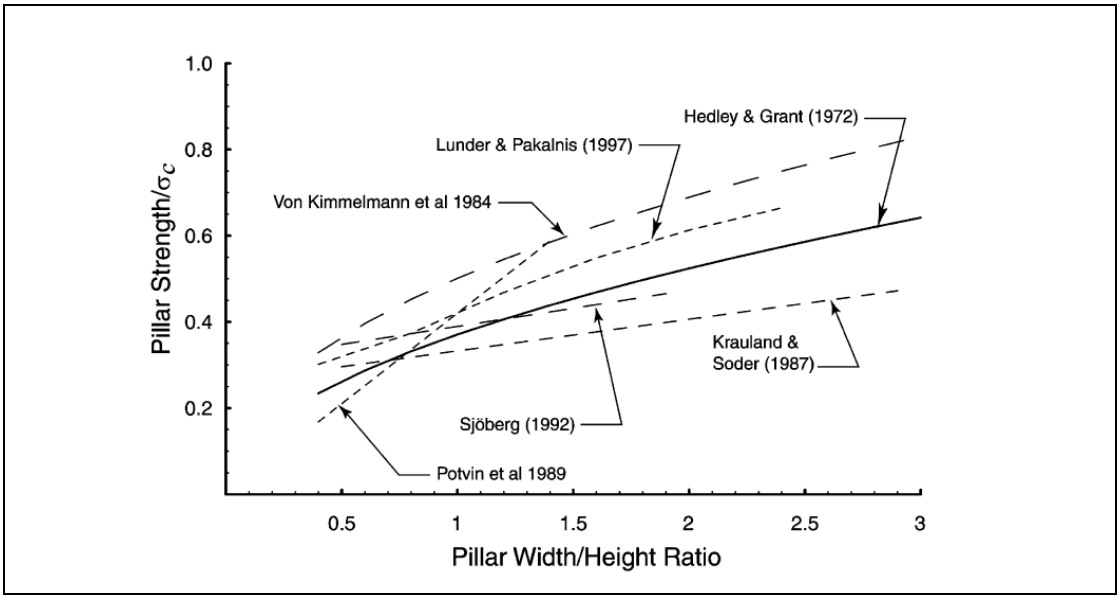

Figure 3.5_1 Plot of normalised pillar strength based on the equations in Table 3.5_1 (Martin and Maybee, 2000)

Martin and Maybee concluded that:-

"*Because at pillar w/h > 2 the confinement at the core of the pillar is increasing significantly the use of Hoek-Brown brittle parameters will be less appropriate. It should be noted that the pillar-failure database shows that there are only a few pillar failures for pillar w/h > 2, hence, the empirical pillar strength equations should be limited to pillar w/h<2".*

The conclusions were based on the limited use of the Hoek-Brown criterion and questionable pillar stress values:-

- The m_i value was acceptable for the calculations at the various GSI values but limiting the m_r value to 1 only limited the range of results that could be obtained.
- The use of either the elastically determined average pillar stress, or the maximum stress at the centre of the pillar could only result in two different sets of values since the maximum centre pillar stress had to be higher than the average pillar stress dependent on the width of the pillar.
- None of the other deficiencies were addressed.

3.6 Godden (2012)

Godden (2012) published an article titled "Pillar Design for Bushveld Mining" in which he discussed and recommended procedures to be used for the design of pillars. The publication is an excellent reference work for rock mechanics practitioners and deals with all the aspects that need to be considered in pillar design. In this discussion, the pillar strength and pillar stresses as he dealt with them would only be referred.

Godden (2012) based his design on an analytic approach generally used in the design of engineering structures. His approach included the following:

- Determination of the behavioural characteristics of the pillar such as width, height, stiffness, frictional properties etc.
- Determination of the input parameters for the pillar forming material such as strength, elastic constants and the influence of discontinuities.
- Selection of an appropriate failure criterion, in this instance the Hoek-Brown method.
- Stepwise assessment of the internal stress distribution of the pillar; the mechanism of the confining effect of the horizontal stress.
- Calibration of the model with actual underground data.

The determination of the input parameters were discussed in detail and cognisance was taken of their variability laterally as well as vertical; mean values for defined areas are recommended.

The failure mechanism of the pillar was discussed and the influence of the horizontal stress at the middle of the pillar was quantified. Using standard values for the Hoek-Brown criterion, the pillar strength was calculated.

The design procedure covered most of the deficiencies listed in the beginning and, overall, is the most realistic pillar design methodology to date.

The influence of the loading system was dealt with extensively but only for the post failure region.

Deficiencies addressed:-

- Variability of input parameters was discussed but only mean values were used.
- System stiffness not considered for the pre-failure regime.

3.7 Leach (2008)

During 2008 the author and Leach conducted a research programme to establish the validity of the Hedley-Grant method for calculating the strength of large pyroxenite pillars at Nkomati mine. During discussions it was decided to investigate the influence of span on pillar loading. On the basis of these discussions Leach prepared a report for Nkomati Mine dealing with pillar strength in thick ore bodies with limited lateral extent using *FLAC3D* to calculate pillar strength and stress distribution for two sets of rock properties.

- RMR 65, UCS 158 MPa, taken from previous work carried out for Nkomati.
- RMR 70, UCS 170 MPa, recently updated average values for the mining area.

To include the effect of the limited span the force convergence curve, the load line of the loading system was incorporated

The resultant force/convergence curves and the load line are shown in Figure 3.7_1. In all cases, the local mine stiffness line crosses the pillar strength lines in the linearly elastic portion of the pillar curve, well before peak strength is reached.

The local mine stiffness was determined initially by applying an equivalent force to the hanging wall preventing any deformation. This force was reduced in steps until it reached zero. As the force was reduced, the convergence increased and the resultant local mine stiffness curve was drawn.

The curves in Figure 3.7_1 are indicative of a very stable pillar system. In the hypothetical situation, if the local mine stiffness had intersected the pillar strength lines close to or beyond the peak pillar strength position it would have been strongly indicative of a risk of pillar failure with different scenarios:-

- The 10 m high pillar would show incrementally lower strength increase and no pillar collapse would occur.
- The 20 m high pillar would yield with a reduction in strength and pillar failure would result. With the post-failure slope of the pillar steeper than the local mine stiffness curve, yielding would occur in a “stable” manner.
- The 30 m high pillar would fail and with a post peak slope apparently steeper than the local mine stiffness, failure would be “unstable” with a release of energy.

  Note: The ore body at Nkomati mine consisted of disseminated sulphides in a pyroxenite matrix with orebody thickness/widths of up to 30 m in places.

The following deficiencies were addressed:-

- Limited spans because of limited ore body size.
- Strata stiffness
- Full pillar strength curves based on Hoek-Brown failure criterion.
- *FLAC3D* for calculating pillar stresses.

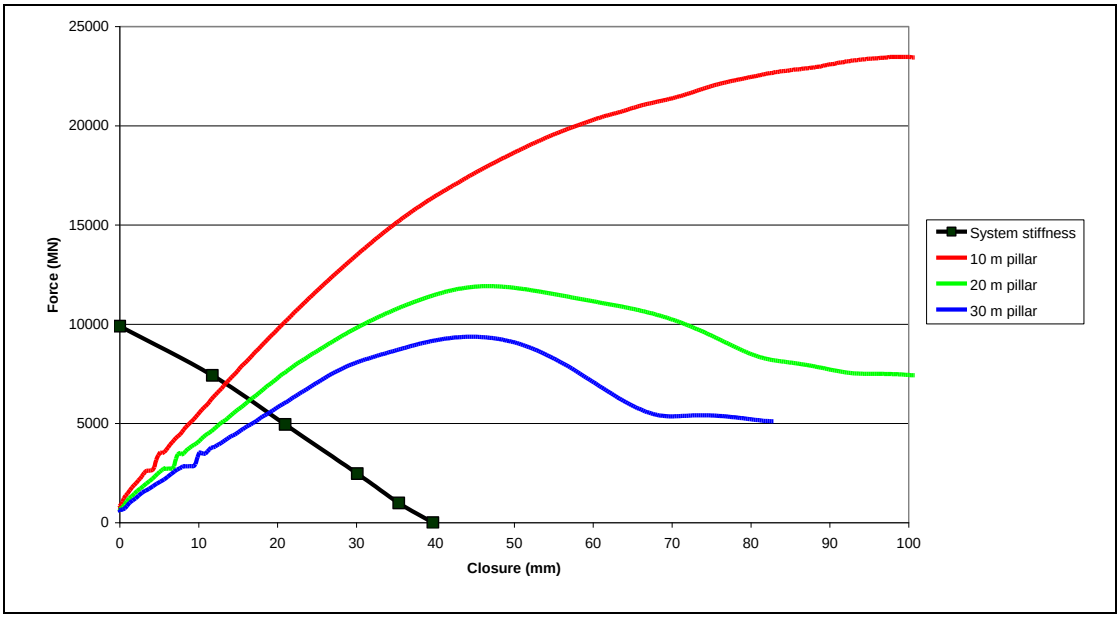

Figure3.7_1 Force-based comparison of pillar load-deformation characteristics to stope system support requirement (system stiffness) in terms of the 30 x 30 m tributary area associated with pillars in the planned layout. Leach (2008).

3.8 Kersten (1992)

Kersten (1992) proposed a modified Hedley-Grant/Tributary Area Theory for back analysis of chromitite pillars at Lavino Chrome Mine. The width, breadth and height of individual pillars were measured and listed in spread sheet form.

The pillar stresses were calculated as per standard Tributary Area Theory; dividing the entire area, assuming constant pillar centre spacing, by the number of pillars to obtain the tributary area for each pillar.

The force over the average tributary area was then divided by the area of the individual pillar giving the resultant individual pillar stresses.

Using the standard Hedley-Grant equation, the strength of each pillar was calculated, based on the individual pillar dimensions and the safety factor of each pillar. The safety factor for all the pillars was then presented in a cumulative frequency distribution. (Figure 3.8_1).

The individual strength and stress values for individual pillars with their varying dimensions can also be expressed in frequency distributions, shown in Figure 3.8_2.for a set of pillars at Black Rock Mining Operations.

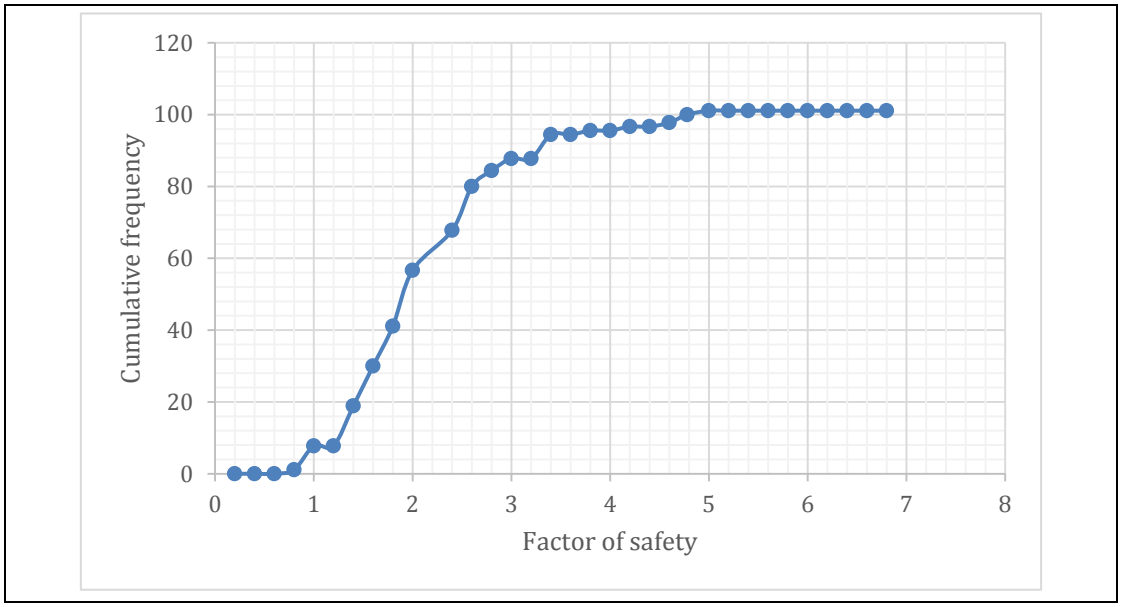

Figure 3.8_1 Cumulative frequency distribution of pillars in terms of their safety factors at Black Rock mining Operations. Kersten (2009)

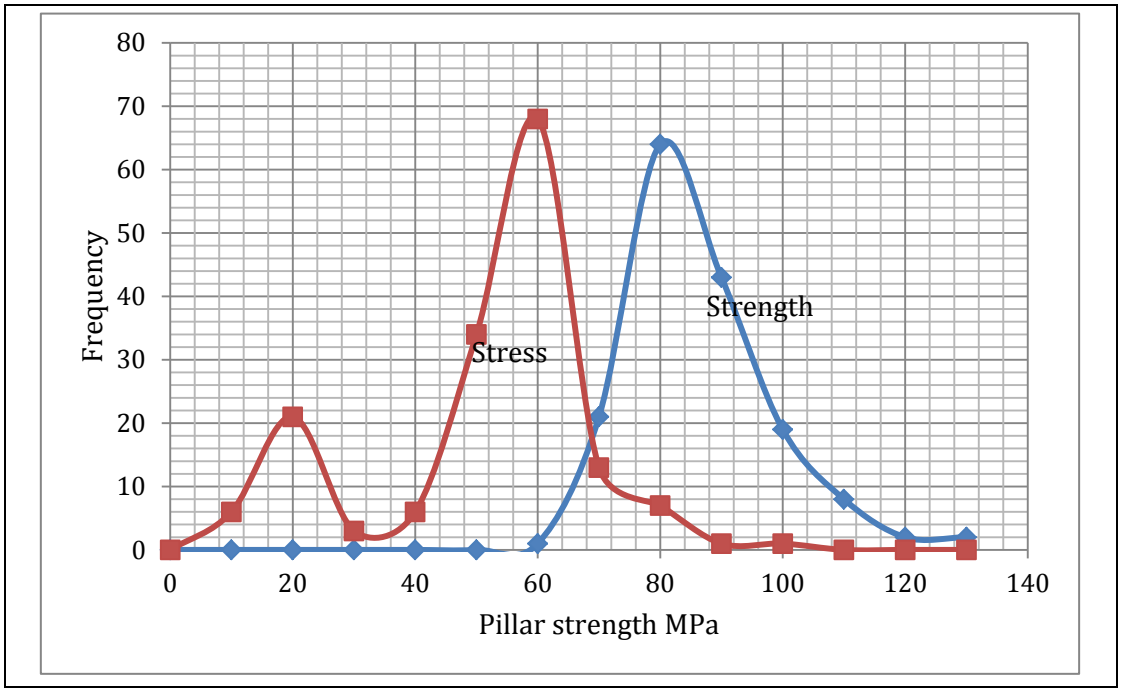

Figure 3.8_2 Frequency distribution of pillar strength and pillar stress, Black Rock Mining Operations. (Kersten 2009)

The method was also used to back analyse a collapsed pillar area at Kamoto Mine, (Kersten 2009), in order to determine the design values for pillars strength on a copper mine.

Deficiencies that were addressed are the variability of mine dimensions and the use of individual pillar strength values.

Deficiencies that were not addressed were limited spans, strata stiffness, still using the Hedley-Grant equation and variation in the UCS value due to the dearth of strength tests.

3.9 Watson (2010).

Watson (2010) proposed a method for designing yield pillars in the platinum mines, using underground observations and measurements to calibrate the Hedley-Grant as well as the linear Ryder equation.

The pillar behaviour on three mines on the Merensky Reef were investigated where it was stated that the relationship between pillar strength and width-to-height ratio follows a curvilinear as well as a linear pattern.

It was also concluded that for the range of pillars investigated, the pillar strength is to a certain extent based on the interaction between the pillar and the country rock for the high stress levels acting on the yield pillar situated in areas with 90 % extraction.

It was concluded that pillar strength on the Merensky Reef can be calculated using the power formula developed by Salamon and Munro (1967) using 0.76 and -0.36 for γ andα.

$$\sigma_{str} = k(w^{\gamma}/h^{\alpha}) \qquad 3.7$$

3.10 Ryder and Ozbay (1990).

Bieniawski and van Heerden (1975) developed a linear formula for the prediction of coal pillar strength which was subsequently modified by Ryder and Ozbay (2005) to include the strengthening effect on pillars which are longer than they are wide.

$$\sigma_{str=k\left[b+(1-b)\frac{w}{h}\right]} \qquad 3.8$$

Where b = linear $^{w}/_{h}$ parameter

k = Strength factor

Watson (2010) used equation 3.8 in his back analysis of pillar strength.

3.11 Roberts (2003)

Work done by Roberts (2003) for Impala Platinum Mine included the effect of two rock types on the pillar strength, hanging wall pyroxene and footwall anorthosite. (The influence of the chromitite marker was ignored). (Figure 3.11_1).

2D finite element modelling, using the Mohr-Coulomb model with strain softening, as well as 3D modelling using a homogeneous medium gave average pillar stress values and the safety factor was calculated for various geometries.

Reference was made to the effect a pillar had on the hanging wall rock but was not discussed.

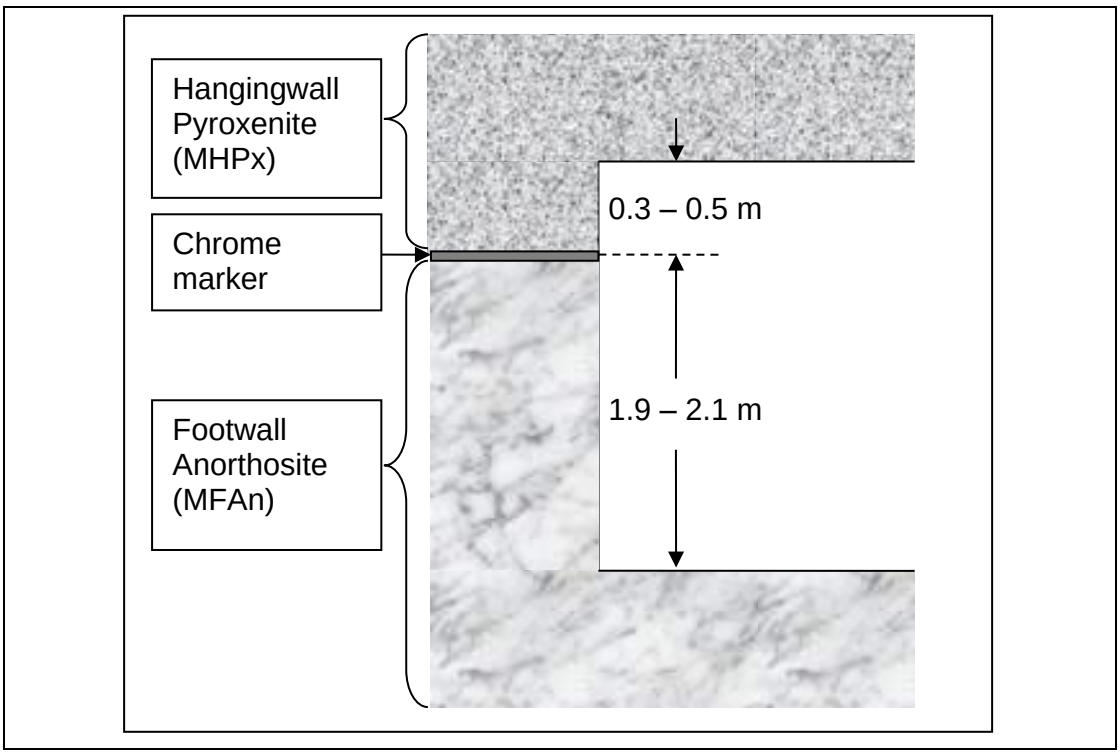

Fig 3.8_1 Modelling two rock types (Roberts 2003)

The following deficiencies were considered: composite pillars, influence of hanging and footwall mentioned, use of a failure criterion and 2D finite element modelling.

3.12 Summary of Hedley-Grant type of equation.

Table 3.12_1 is a summary of the published strength equations used to calculate the pillar strength and the resultant factors of safety for a typical situation:-

- Pillar centre spacing = 10 m.
- Bord width = 5 m.
- Pillar size = 5 by 5 m.
- Depth below surface = 300 m.
- Pillar height = 2.5 m.
- Uniaxial compressive strength = 75 MPa.
- Strength factor k= 35 MPa
- Vertical virgin stress component = 7.8 MPa.
- Average pillar stress = 31.2 MPa.

Table 3.12_1: Factor of safety using the equations listed in Table 3.5_1 and the strength ratio in Figure 3.5_1

	Pillar stress MPa	Pillar strength MPa	Factor of safety
Hedley-Grant	31.2	39	1.25
Von Kimmelman	31.2	53	1.68
Krauland	31.2	29	0.91
Potvin	31.2	60	1.92
Sjoberg	31.2	35	1.11
Lunde + Pakalnis	31.2	44	1.39

The factor of safety varies from over design for normal purposes, 1.92 to probable instability at 0.91 for accepted equations.

3.13 Scorecard

Table 3.13_1 is a summary of the methodologies discussed briefly with their advantages and disadvantages.

- None of the methods considered the interaction between hanging wall and/or footwall and its effect on the pillar strength.
- Three methods considered composite pillars
- Three methods discussed the strata stiffness concept but did not incorporate it in the pre-failure region.
- The variability of the mining dimensions and the rock mass properties were dealt with quantitatively in parts by 4 methods.

Table 3.13_1: Summarised listing of methods and their various attributes

Method	Pillar Strength	H/W Pillar	Composite Pillar	w_{eff}	Size Effect	System stiffness	Pillar var Dimensions	UCS var	E var	μ var	GSI var
H-G	Yes	No	No	Yes	Yes	No	No	No			
Joughin	Yes	No	Yes	Yes		No	No	Yes			
Esterhuizen	Yes					No	Yes	Yes			
Watson	Yes		No	Yes		No	No	No			
Malan and Napier	Yes	No	No	No		No					
Martin and Maybee	Yes	No				No	No				
Godden	Yes	No	Yes	Yes		Yes	Yes	No	Yes	Yes	
Kersten	Yes	No	No	Yes		No	Yes	No			
Leach	Yes	no		Yes		Yes	No	No			
Roberts	Mentioned	Yes	Yes	Yes		Yes		No	No	No	

3.14 How to fill the gaps

The main deficiencies of the different approaches are as follows;

- Empirical methodology needed to be replaced by analytical procedures.
- The influence of the variation in input parameters have to be incorporated.
- For rectangular pillars, the definition of effective width required refinement.
- Strata stiffness should be incorporated in stable pillar design.
- Pillar/hanging wall/footwall interaction to be quantified.

All the above components, except for the hanging and footwall interaction, would be addressed and incorporated in the proposed design methodology.

PART II

4 MODELLING OF PILLAR STRENGTH

4.1 Definition of pillar strength/failure

Failure: The breakdown of a mechanism, or ceasing of a part of a structure to function. (Oxford Dictionary, 1994).

Pillar failure can be in the form of strain softening, yielding or pillar “bursting”. In the present context the pillar behaviour is limited to the point of “failure” where pillar failure is defined when the factor of safety is equal to or less than 1.0.

Pillar failure on the platinum mines, especially bursting, has been mainly confined to the “longwall” mining method where strike pillars are left spaced approximately 30 m apart on dip. Failure of bord and pillar workings have been recorded where weaker layers occur in the reef plane. To the knowledge of the author, no report on this type of regional bord and pillar failure has been published.

Pillar failure leading to “system failure” in two bord and pillar mines has occurred at Lavino and in 1973 at Winterveld chrome mines, but no published report is available on these events. (The Winterveld event date obtained from personal notes.)

The behaviour of the post failure curve of the pillar could still support the mine structure in yielding without the structure losing its function. For instance, pillar scaling is not a sign of the pillar losing its supporting function; the pillar edge starts to fail before the peak strength is reached, while still maintaining the overall stability.

Since the proposed design methodology dealt with the design of stable pillars the analysis was restricted to where the slope of the force deformation curve remained positive.

Figure 3.7_1 is an example, discussed earlier in Part I, Section 3.7, of the force-convergence curves for a 15 by 15 m pillar, 10 m high, remaining positive while for the higher pillars of 20 to 30 m, with the same plan dimensions with the force-convergence curves changed gradually from elastic linear to non-elastic flatter slope, referred here to as strain softening.

Pillar failure as generally accepted requires a negative stress-strain/ force-convergence curve. Figure 4.1_1 shows that the 10 m high pillar would never “fail” in the sense that the structure will become unstable.

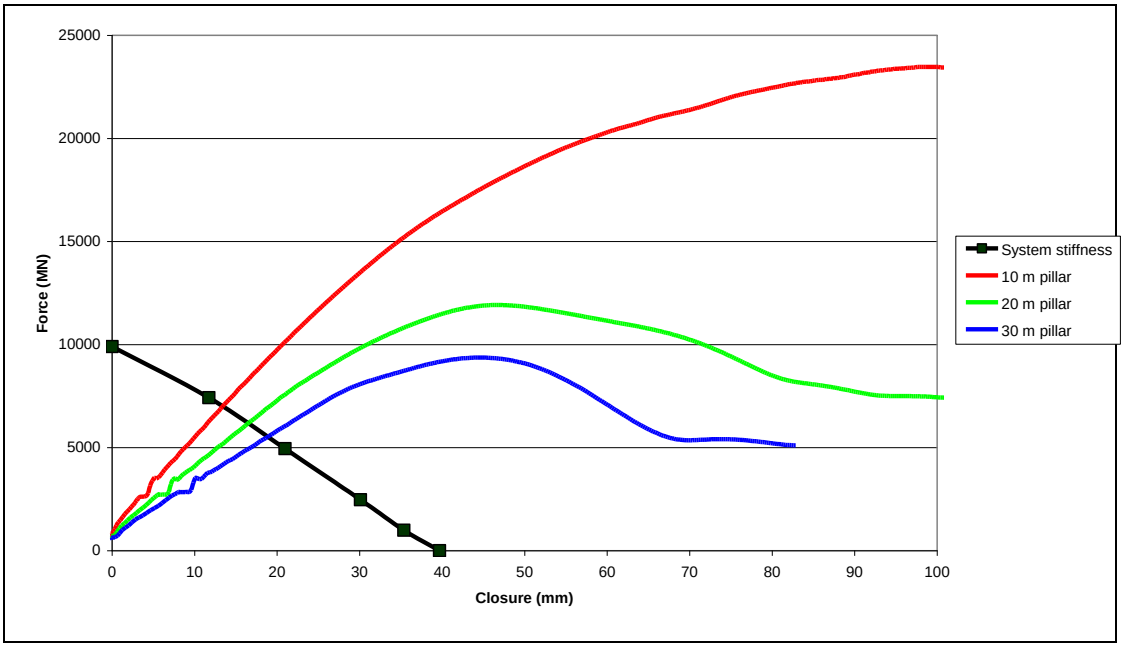

Figure 4.1_1 Force/convergence diagram for a square 15 by 15 m for pillar heights of 10, 20 and 30 m (Repeat of figure 3.7_1 for ease of access) (Leach, 2009)

To further illustrate the complexity of defining pillar failure, using numerical modelling, Figure 4.1_2 represents a section through a 2 m high and 4 m radius pillar with an average pillar stress of 300 MPa. The vertical stress component changes from 800 MPa at the centre to 0 MPa on the pillar edge due to failure on the circumference of the pillar with the inner core remaining intact. (The hanging and footwall contact was fixed for this simulation.)

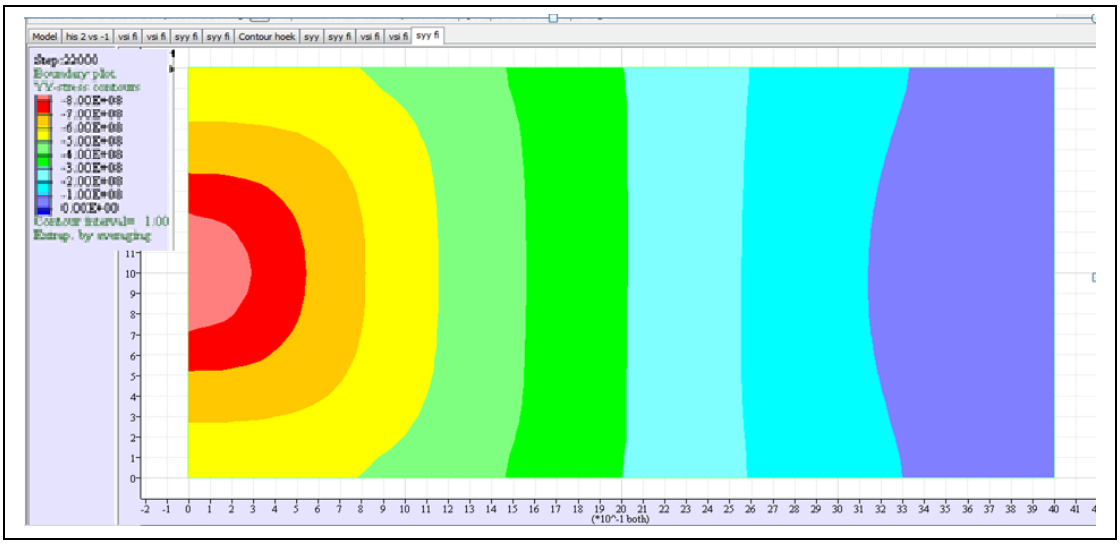

Figure 4.1_2 Section across half width showing vertical stress contours, S_{yy} across a 2 m high, 8 m wide, pillar at peak average pillar stress. Axis of symmetry at the Left

Another method for determining the pillar strength (Malan 2006) by back-analysis consisted of determining the stress levels of smaller individual pillars in a general layout of bigger pillars

and observe whether spalling and fracturing of the pillar sidewalls occurs. If so, it was concluded that the pillar strength was being reached or exceeded.

This was not a definitive sign that the failure strength of the pillar had been reached, only that the uniaxial strength of the rock at the pillar edge had been exceeded, hence the value obtained could be misleading since the slope of the force deformation curve could still be positive. It could be used to correlate the measured with the predicted fracture zone if a reliable analytical model was available using a proven failure criterion.

In section 4.11 the pillar failure mechanism is dealt with in greater detail.

4.2 Pillar models

An alternative pillar strength model should address all or most of the deficiencies listed that are associated with the current Hedley-Grant equation. Ideally, it should have the following properties:-

- The ability to incorporate the variability of the input parameters.
- The input variables should consist of commonly accepted properties such as the uniaxial compressive strength (UCS), Geological Strength Index (GSI), m_i values or other quantifiable rock mass properties.
- If possible, it should result in a simple set of equations for general use by practitioners and that could be incorporated in a Monte Carlo simulation.
- The ability to cater for multilayer pillars as well as planes of weakness.
- Simulation of the interaction between the pillars and the hanging/footwall.
- Clear distinction between pillar failure and pillar spalling.
- The ability to model 3-dimensional geometries such as rectangular pillars.
- The production of results that could be used to calibrate the model results with underground observations such as fracture zones, convergences and stress variations within the pillar.

Numerical models that would satisfy the above conditions in all or most of the requirements were as follows:-

- *FLAC2D.*
- *UDEC.*
- *FLAC3D.*
- Rock-science programmes.

UDEC satisfies the condition of a jointed medium but introduces input parameters poorly known or understood. It fails the simplicity test. It is also a programme not in general use locally and expensive to purchase.

FLAC3D is an excellent programme but fails the simplicity test. In addition, it is expensive.

FLAC2D satisfies a limited set of requirements when the axisymmetric function could be used to simulate three-dimensional problems. It is also reasonably simple to use and interpret. It has the most commonly used failure criteria, (*FLAC3D* as well) incorporated in the system.

The author's experience in using *FLAC2D* in a consulting capacity over several decades had found that the programme generally predicted actual underground conditions (Kersten 1996, 2001 and 2002) and that it was flexible enough to simulate practical mining conditions.

The following description of the basic *FLAC2D* program is found in the manual accompanying the *FLAC2D,* version 7, program, 2012.

FLAC2D is an "explicit, finite difference program" that performs a "Lagrangian analysis," terms that need to be described and their relevance to the process of numerical modelling, with a detailed description form the ITASCA on-line manual, 2012:

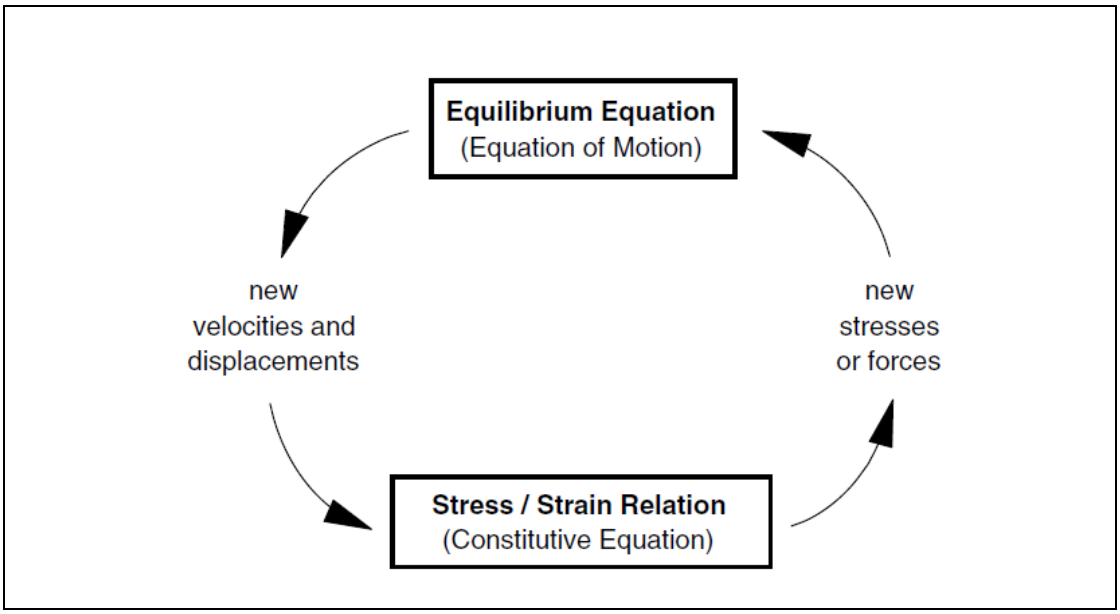

Figure 4.2_1 Basic explicit calculation scheme - *FLAC* Manual, 2012

"The general calculation sequence embodied in FLAC is illustrated in Figure 4.2_*1. The procedure first invokes the equations of motion to derive new velocities and convergences from stresses and forces. Then, strain rates are derived from velocities, and new stresses from strain rates taking one time-step for every cycle around the loop. The important thing is that each box in Figure 4.2_1 updates all of its grid variables from known values that remain fixed while control is within the box. For example, the lower box takes the set of velocities already calculated and, for each element, computes new stresses. The velocities are assumed to be frozen for the operation of the box (i.e., the newly calculated stresses do not affect the velocities*).

This may seem unreasonable because it is known that if a stress changes somewhere, it will influence its neighbours and change their velocities. However, a small enough time-step is chosen so that information cannot physically pass from one element to another in that interval. (All materials have some maximum speed at which information can propagate.) Since one

loop of the cycle occupies one time-step, the assumption of "frozen" velocities is justified – neighbouring elements really cannot affect one another during the period of calculation. Of course, after several cycles of the loop, disturbances can propagate across several elements, just as they would propagate physically".

"The central concept is that the calculational "wave speed" always keeps ahead of the physical wave speed, so that the equations always operate on known values that are fixed for the duration of the calculation. There are several distinct advantages to this (and at least one big disadvantage!). The most important advantage is that no iteration process is necessary when computing stresses from strains in an element, even if the constitutive law is wildly nonlinear. In an implicit method (which is commonly used in finite element programs), every element communicates with every other element during one solution step: several cycles of iteration are necessary before compatibility and equilibrium are obtained. The disadvantage of the explicit method is seen to be the small time-step, which means that large numbers of steps must be taken. Overall, explicit methods are best for ill-behaved systems (e.g., nonlinear, large-strain, physical instability); they are not efficient for modelling linear, small-strain problems".

"*Since it is not necessary to form a global stiffness matrix, it is a trivial matter to update coordinates at each time-step in large-strain mode. The incremental convergences are added to the coordinates so that the grid moves and deforms with the material it represents. This is termed a Lagrangian formulation, in contrast to an Eulerian formulation, in which the material moves and deforms relative to a fixed grid. The constitutive equation at each step is a small-strain one, but is equivalent to a large-strain formulation over many steps*".

Three basic *FLAC2D* models with incorporated relevant failure criteria are available:-

- *FLAC2D*/Mohr-Coulomb.
- *FLAC2D*/Hoek-Brown.
- *FLAC2D*/Strain softening.

The Mohr-Coulomb model is based on the coefficient of friction and the cohesion of the intact rock but has the disadvantage that the post failure load/deformation remains plastic. By introducing residual cohesion and strain values, strain softening can be simulated.

Kersten (1996) used the strain softening model to predict the failure and deformation of rocks at an equivalent depth of 3000 m with great success. The current study deals with the elastic portion of the rock mass behaviour for which the prediction of onset of non-linear behaviour is required more so than the post failure regime as in the rock mass behaviour at great depth.

The strain softening model is based on laboratory results of the post failure properties. The standard deviation of rock mass properties is generally high, as discussed earlier, and the number of samples required for a representative value is about 20. Strain softening parameters for such a number of samples were not available for the present study.

The Hoek-Brown failure criterion is based on empirical/analytical method and readily obtainable parameters.

- The uniaxial compressive strength.

- The Geological Strength Index, GSI.
- The m_i value, a constant for a specific rock type.

The empirical components are the equations for calculating the values of s, s_r and m_r values (discussed in detail, section 5.1) are based on the Geological Strength Index value using empirically derived equations.

For simulating the strain softening behaviour with the standard Hoek-Brown model, the residual values of m_r and s_r are reduced to below the value of m_b and s.

This reduction in m_b and s values is based on empirical relationships (Hoek et al, 2002):

$$m_b = m_i e^{((GSI-100)/28)} \quad 4.1$$

$$m_r = m_i e^{(\frac{GSI-100}{14})} \quad 4.2$$

$$s = e^{(\frac{GSI-100}{9})} \quad 4.3$$

$$s_r = e^{(\frac{GSI-100}{6})} \quad 4.4$$

Where m_i= material constant related to the frictional properties of the rock.

m_r= material constant in the post-failure regime related to the frictional properties of the rock.

s = dimensionless constant analogous to the cohesive strength of the rock.

s_r= residual dimensionless constant

The reduction in m_b and s values is due to the decrease in the Geological Strength Index due to progressive failure of the pillar.

The reduction in strength with increase in strain is simulated by the progressive iteration of failing and stable elements in the *FLAC2D* mode, Table 4.2_1 and Figure 4.2_2; it reduces the strength of the overall model progressively and results in a lower pillar strength for a decrease in the m_r and s_r values. (Hart, 2012).

The influence is significant and determination of mainly the m_r value is an essential function. Note that the brittle reaction sets in at a m_r value of below 4, where the post pillar strength is below the peak average pillar stress.

The Hoek-Brown failure criterion is in common use and, with the correct input parameters, simulates the failure process realistically.

Table 4.2_1: Pillar strength with decrease in the m_r and s_r value, as well as the residual pillar strength

m_i	s	m_r	s_r	Pillar strength MPa	Post peak pillar strength MPa
11	0.1084	11	0.1084	339	339
		7	0.0700	220	220
		5	0.0400	159	159
		3	0.0200	105	98
		1	0.0090	56	37

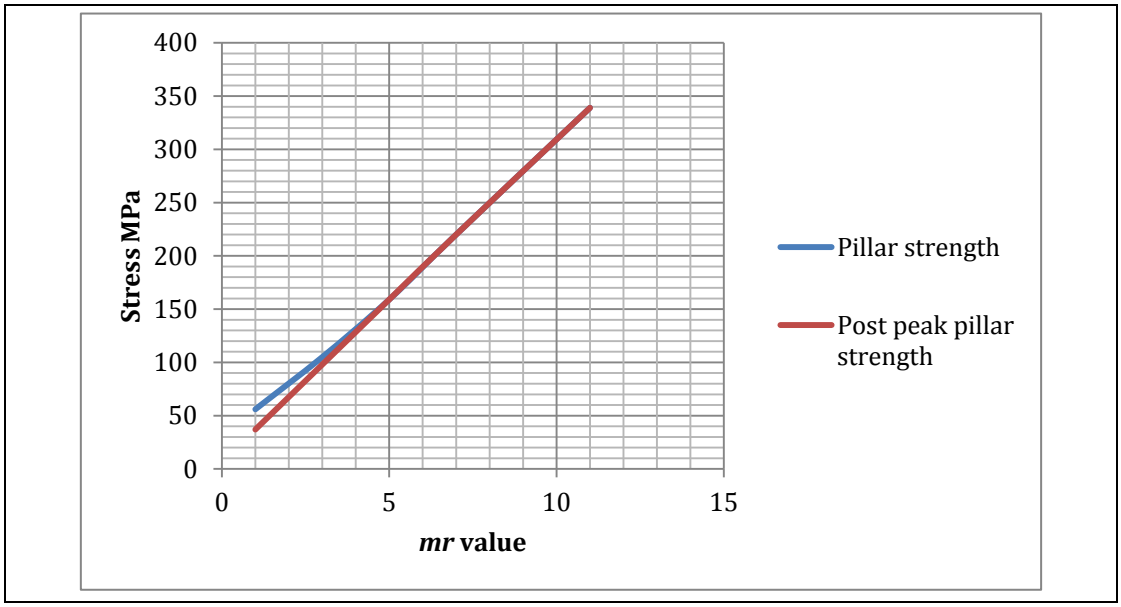

Figure 4.2_2 Influence of the m_r value on the pillar strength.

Since the *FLAC*2D/Hoek-Brown model simulates strain softening by adjusting the residual m_r value, as well as using a commonly accepted failure criterion, it was selected as the most appropriate for the present investigation. More detailed work on specific mines could consider using the *FLAC2D*//Strain Softening model if sufficient laboratory results could be made available.

Figure 4.2_3 illustrates that the *FLAC2D*/Hoek-Brown model combination modelling various geological conditions.

On the basis of the facts listed above, the FLAC2D/H-B methodology was selected for the present study:

- Commonly available quantitative rock mass description.
- The availability of strain softening mechanism.
- The research deals with the pre-failure, elastic portion of the pillar, but also contains the strain softening beyond the elastic portion.

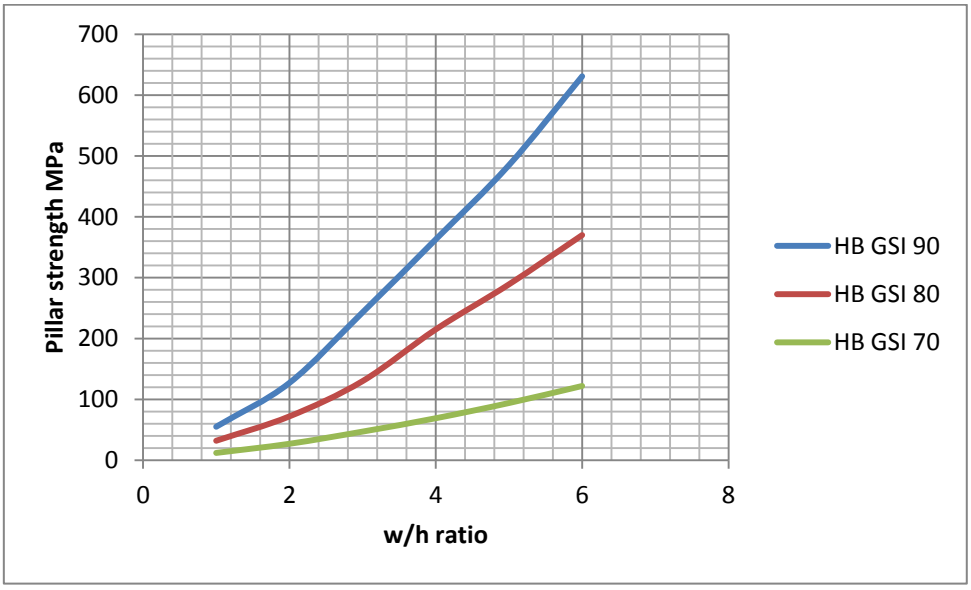

Figure 4.2_3 illustrating the effect of Geological Strength Index on the pillar strength for different w/h ratios (HB - Hoek-Brown criterion)

The Mohr Coulomb criterion was used to model a set of heterogeneous models such as encountered in nature and discussed in the section on variation in rock mass properties. The reason was that the model is relatively easy to construct with a minimum of variables and yet the interaction between layers could be quantified.

The Malan-Napier (2006) Limit Equilibrium method, section 3.4, is also based on a failure mechanism with Table 4.2_2 below giving a measure of how it compares with *FLAC2D*/Hoek-Brown.

The main disadvantage of the Malan and Napier (2006) Limit Equilibrium model, while it has considerable promise, is that it had not been developed into a practical design tool and was still in the research stage. The *FLAC2D* /Hoek-Brown model was well founded and practical in a production environment.

FLAC2D is an extremely useful tool and can model complex models. These complex models obviously require a similar number of variables, all of which are not generally known. The author found that for practical applications a simple model with the minimum number of variables are required before the more complex models are introduced. It is for this reason that the present thesis concentrates on a simple model for calibration, the more complex model can follow once it is found reliable.

An additional argument is that for the creation of a simple generally applicable pillar design equation the number of variables need to be kept to a minimum and the abnormal situation cannot be solved by using the "simple generally applicable "pillar equation l, Table 4.2_2: Comparison between the FLAC/Hoek-Brown model and Malan and Napier's limit equilibrium model

Requirement	*FLAC*2D/ Hoek-Brown	Malan and Napier(2006)
Commonly used parameters e.g. GSI, *m* etc.	Yes	Yes
Simple Equation	Yes	Yes
Multilayer system	Yes	No
Pillar-H/W F/W interaction	Yes	Yes
Pillar failure process	Yes	Yes
Planes of weakness	Yes	No/Yes
Loading system stiffness	Yes	No
Fully developed procedure	Yes	No
Calibration, fracturing, convergences	Yes	No

4.3 Three-dimensional or two-dimensional models

One of the main aims of the proposed methodology was to keep it as simple as possible without losing essential accuracy. The *FLAC2D* model is simple to construct and could be run using the *FLAC2D,* version 7, and demonstration model.

The *FLAC3D*, on the other hand, was not as simple to construct and to achieve the objective of relative simplicity, it was decided to use the freely available *FLAC2D* demonstration model.

The axial symmetry function of *FLAC2D* could be used to simulate a three-dimensional circular model of pillars and would have been ideal if it could be proven that the circular pillar replicated a square pillar by giving similar answers.

In order to investigate this possibility, the author initiated a comparative study between square pillar and circular pillars using *FLAC3D* by Leach (2011). Details of the model are given in a report by Leach (2011) in Appendix 1.

Figure 4.3_1 represents the *FLAC3D* model.

Details of the rock mass properties of the pillar are given in Appendix 1 with the hangingwall and footwall modelled as an elastic medium.

The essential findings are shown in Table 4.3_1 where the results are compared between the three-dimensional square and circular pillars as well as the equivalent two-dimensional circular pillar obtained using *FLAC2D* axial model.

Table 4.3_1: Pillar strengths in the different models

Pillar size Diameter m	3D Circular pillar – strength MPa	3D Square pillar – strength MPa	*FLAC 2D* Ax Symmetry strength MPa	Ratio 2D/3D Square
6	150.3	149.9	143	0.95
4	98.1	98.7	88	0.89
2	61.7	56.1	43	0.77

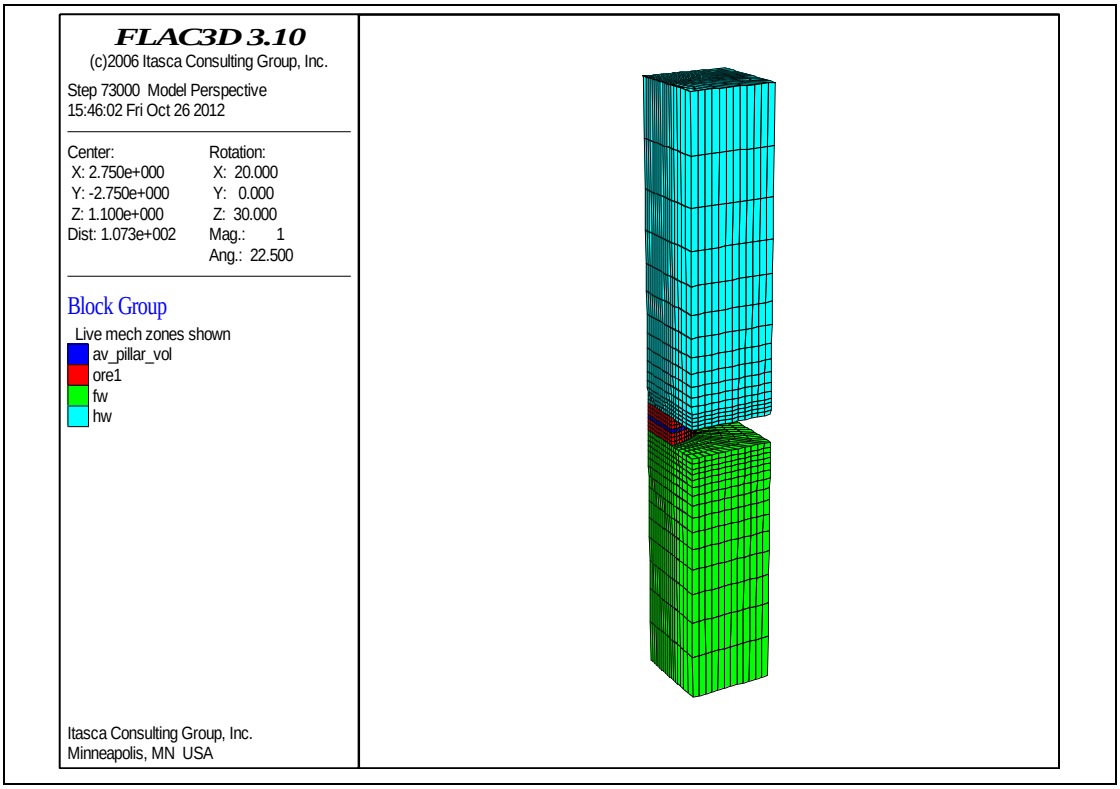

Figure 4.3_1 Three Dimensional FLAC model (Leach 2011)

The strength values for the *FLAC3D* circular and square pillars were calculated by Leach (2011) and the values for the *FLAC2D* axial symmetry from the programme discussed in Section 4.2.

There appears to be a gradual change in values and the ratios are plotted in Figure 4.3_2 illustrating that the difference in result decreases with increase in diameter. For diameters in excess of 4 m, which was the case in all instances on the mines in question, this error is deemed acceptable in the thesis but should not be ignored. As the three dimensional strength in all cases exceeded the two dimensional strength by less than 10% the approach of using the two dimensional strength is conservative.

The similarity between the square and circular pillar in the *FLAC3D* model was explained by the fact that failure started at the corners of the square pillar, reducing the pillar to an equivalent circular geometry. The lower average pillar stress of the *FLAC2D* simulation for the same geometry was deemed acceptable for the current study

Based on these findings the remainder of the thesis uses the *FLAC2D* axial model.

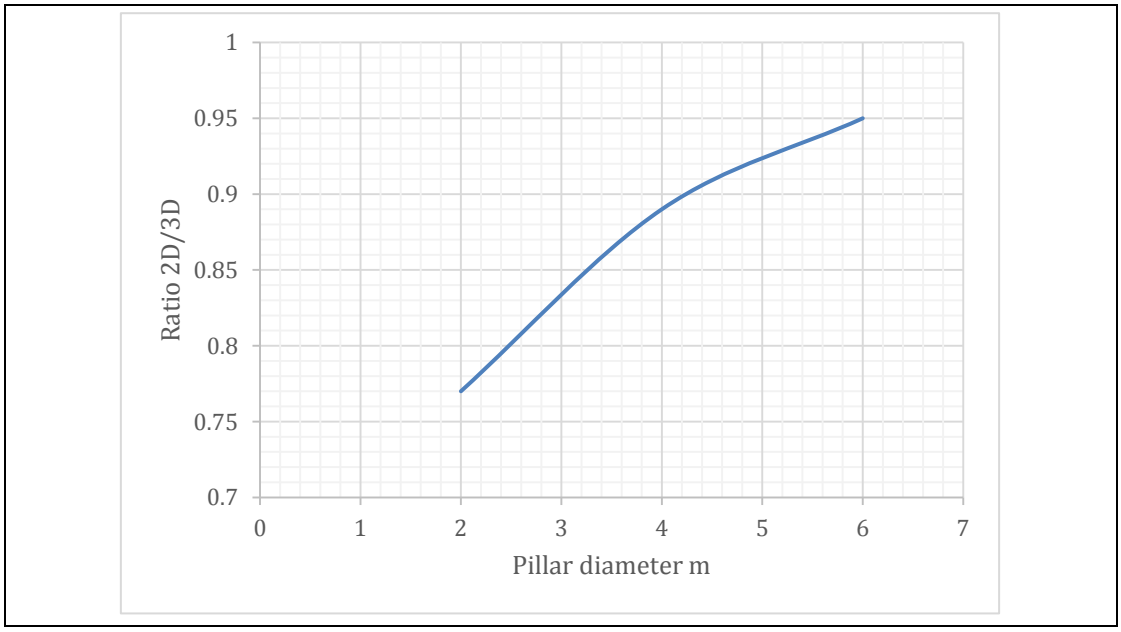

Figure 4.3_2 Ratio of difference in strength between 3D square and 2D circular pillars

4.4 *FLAC2D*/Hoek-Brown model used in the investigation

The model incorporates quantitatively the following states:-

- Calculation of the peak average pillar stress, pillar strength, for a homogeneous pillar.
- Simulation of a composite pillar such as found in the chrome mines.
- Incorporation of the effect of planes of weakness.
- Utilization of commonly used geotechnical parameters.
- Inclusion of property variation.

4.5 Developing a methodology for determining a simple pillar strength equation

The strength of a pillar could be calculated using the *FLAC2D* code by:-

- Developing or using a proven failure criterion.
- Using commonly used rock mass parameters to input in the *FLAC2D* model.

To achieve the objective of obtaining a simple equation from a more complex method such as *FLAC2D*/Hoek-Brown model, the latter needed to be proven as applicable to solving the pillar design objectives set.

The proposed design methodology was based on the average pillar strength, the peak of the stress strain curve, or where there is a distinctive reduction in stress with an increase in deformation, the result of strain softening.

*FLAC2D/*Hoek-Brown input files are listed in the Appendices where critical pillar models were considered and can be used by the reader by simply copying the file to notepad and then submit it directly to *FLAC2D*. An example of a simple *FLAC 2D* model for a homogeneous pillar, written in standard *FLAC2D* input format contains the following 4 sections. (Appendix):

- The first part is the identification and geometry of the grid and the model.
    - The type of model, e.g. Hoek-Brown model.
    - Axial configuration simulating a circular pillar.
    - A grid of 24 by 20.
    - Pillar dimensions, 2 m high with 6 m radius
- The second part deals with the rock mass properties.
    - Properties of chromitite
    - Hoek-Brown parameters.
    - Hoek-Brown failure criterion, hoek2.fis
- Thirdly, a function which calculates the average pillar stress in the pillar.
    - A function for calculating the average pillar stress over the entire pillar for each programme step.
- The last part imposes the boundary conditions and the load application.
    - A velocity applied to the top boundary simulating a strain controlled loading system.
    - The hanging wall and footwall were fixed in both the x and y direction with the y axis a line of symmetry.
    - Alternatively, the effect of frictionless hanging wall and or footwall contact could be simulated by fixing y only on the hangingwall and/or footwall.
    - The number of steps that the programme has to run.

The programme was used in all the simulations of homogeneous pillars throughout the thesis.

The model geometry shown in Figure 4.5_1 represents a circular pillar with a radius of 6 m and a height of 2 m.

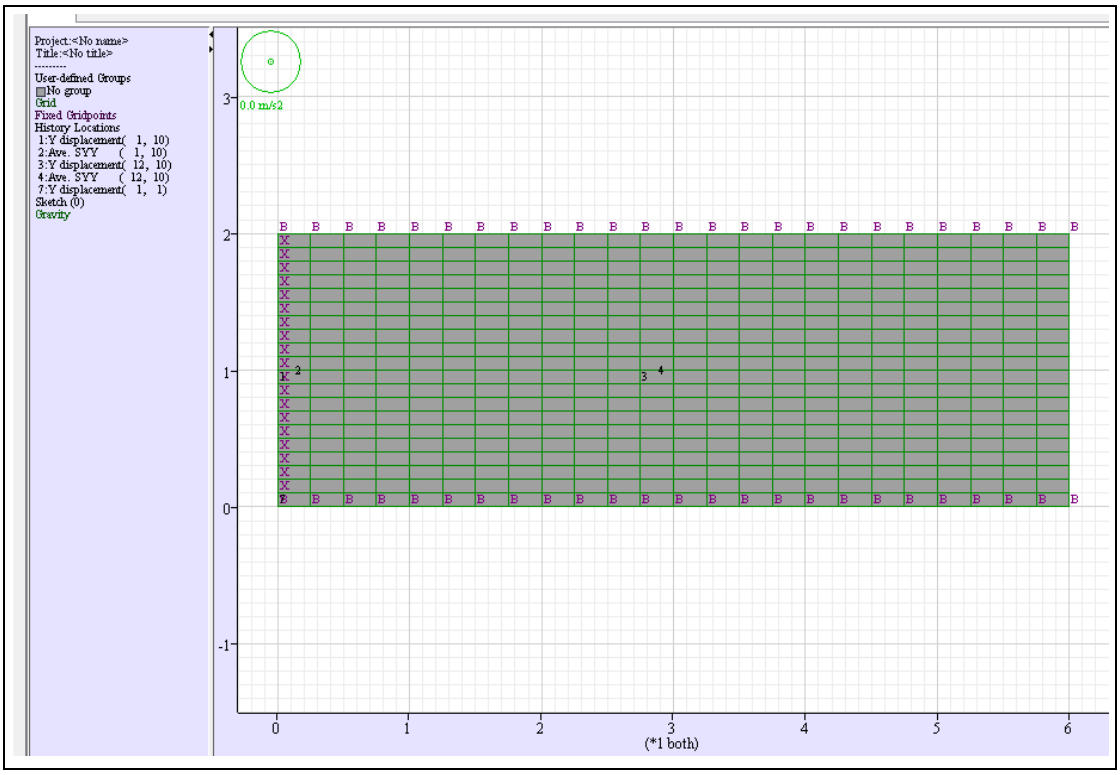

Figure 4.5_1 Basic *FLAC2D* grid for pillar strength calculations

It should be noted that the same model can be used for different pillars simply by changing the geometry, material properties and the Hoe-Brown parameters

4.5.1 Sensitivities

FLAC2D model results are sensitive to the number of zones and a series of simulations were required to determine where this influence was reduced to an acceptable limit. According to the results shown in Figure 4.5.1_1, 200 elements would be acceptable. Using a 24 by 20 grid, containing 480 elements, provided excellent resolution to the contour diagrams without unduly extending run times.

The loading rate of the pillars affected the results in a similar way to those in the laboratory; the higher the rate of loading, the higher the strength of the specimen.

Figure 4.5.1_2 shows that at a loading rates below 1e-6 m/sec, the effect becomes on the pillar strength becomes negligible.

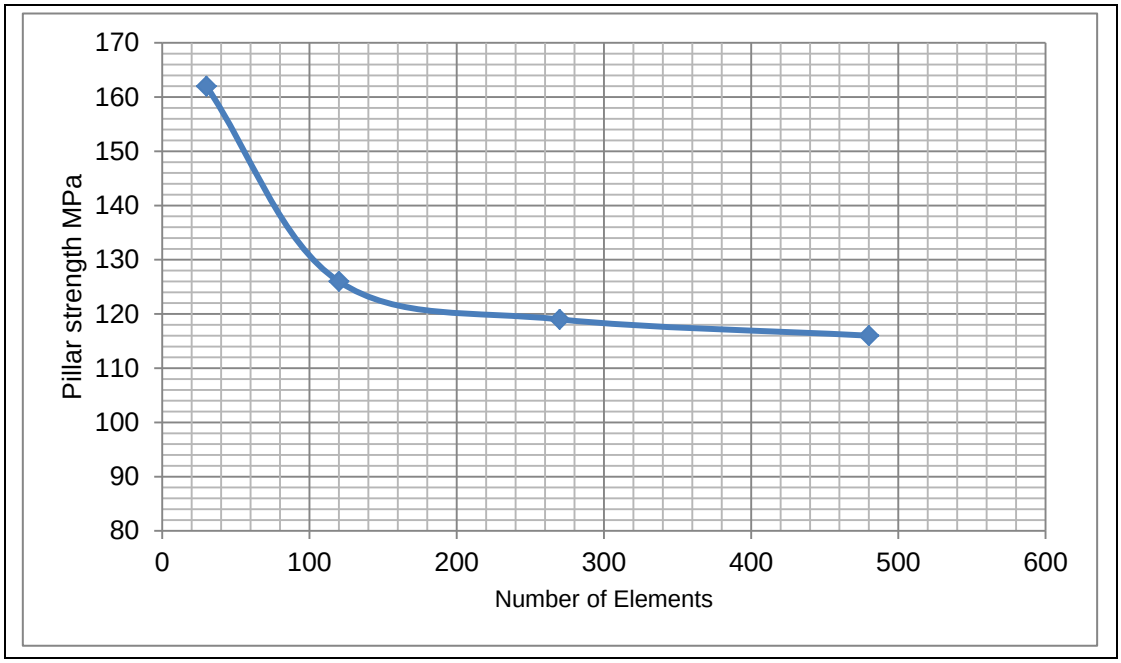

Figure 4.5.1_1 Influence of number of elements on output in basic model

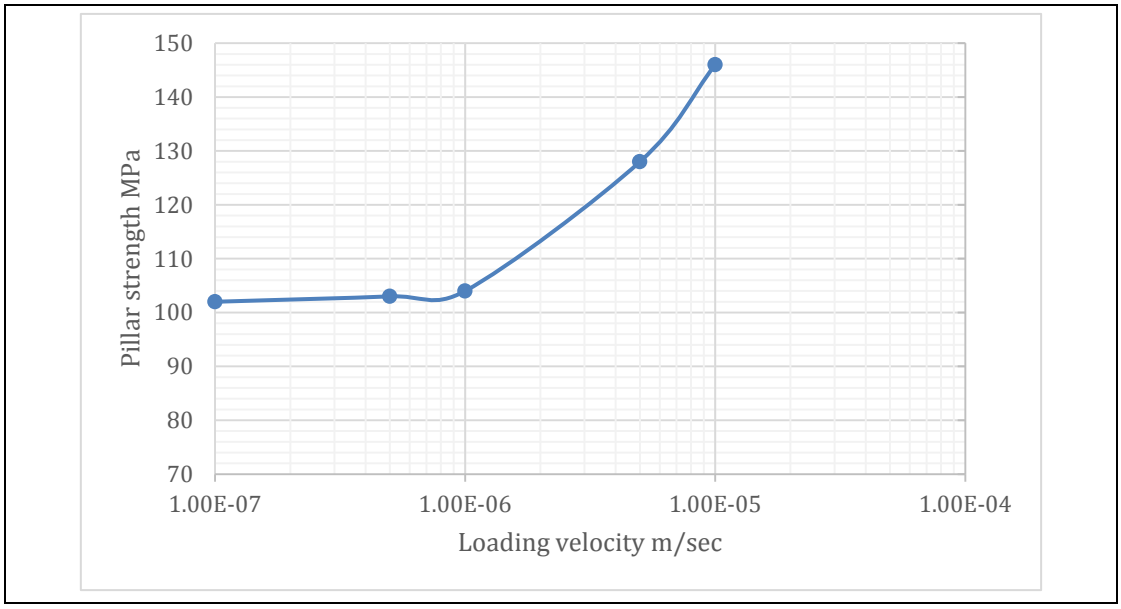

Figure 4.5.1_2 Influence of loading rate on pillar strength

More complex models were required to satisfy the conditions generally encountered in the mines such as the following:-

- Composite pillars, consisting of two different rock types such as chromitite and pyroxenite.
- Pillars with a plane of weakness such as a thrust plane within or close to the pillar in the hanging wall or footwall.
- Pillar consisting of the same rock type but with differing properties.
- Pillar footwall/hanging wall interaction.

The requirements can be incorporated in the *FLAC2D* model using axial symmetry; simulating a three-dimensional situation in conjunction with the Hoek-Brown failure criterion.

The interaction between the hangingwall and footwall with the pillar is important but the objective is to initially simulate a relatively simple model for comparative purposes and if deemed representative of underground observation, extend the process further in future to simulate ever more complex models.

4.6 Simple circular pillar with various properties

The input parameters in the Hoek-Brown failure criterion are based on the Geological Strength Index (GSI), the Uniaxial Compressive Strength (UCS) and the m_i value. To illustrate the use of the criterion an example is given below which is based on the average properties of a pyroxenite specimens from a platinum mine in the western Bushveld.

- Uniaxial Compressive Strength 131 MPa.
- Geological Strength Index 90.
- m_i Value 20
- Bulk modulus = 54 GPa
- Shear Modulus = 27 GPa

The widely used and readily available RocLab programme (Rocscience) was used to determine the effect of a Geological Strength Index value of 90 on the required input parameters.

- m_b= 14
- m_r = 7.
- s = 0.3292.

  s_r = 0.166.
- $sigc$= 75e6 Pa.

(The m_r and s_r values are taken as 50% of m_b and$s$)

Note: The m values are discussed in greater detail in section 5.1.

For calibration purposes, the initial simulation was done for a standard circular intact specimen 10 cm diameter by 20 cm high, m_i = 20, s = 1 and GSI = 100. The calculated specimen, strength value obtained was 136 MPa, comparing well with the uniaxial compressive strength of 131 MPa obtained in the laboratory.

To show the effect of a reduction in the GSI value, the strength of pillars was calculated for GSI values of 90, Table 4.6_1.

Table 4.6_1: Pillar strength for specific sets of values

Pillar height m	Pillar width m	Pillar strength MPa
2	2	72
2	4	153
2	6	252
2	8	363

The data in Table 4.6_1 is shown in the top curve in Figure 4.6_1, while for a GSI of 80, the drop in strength is clearly illustrated.

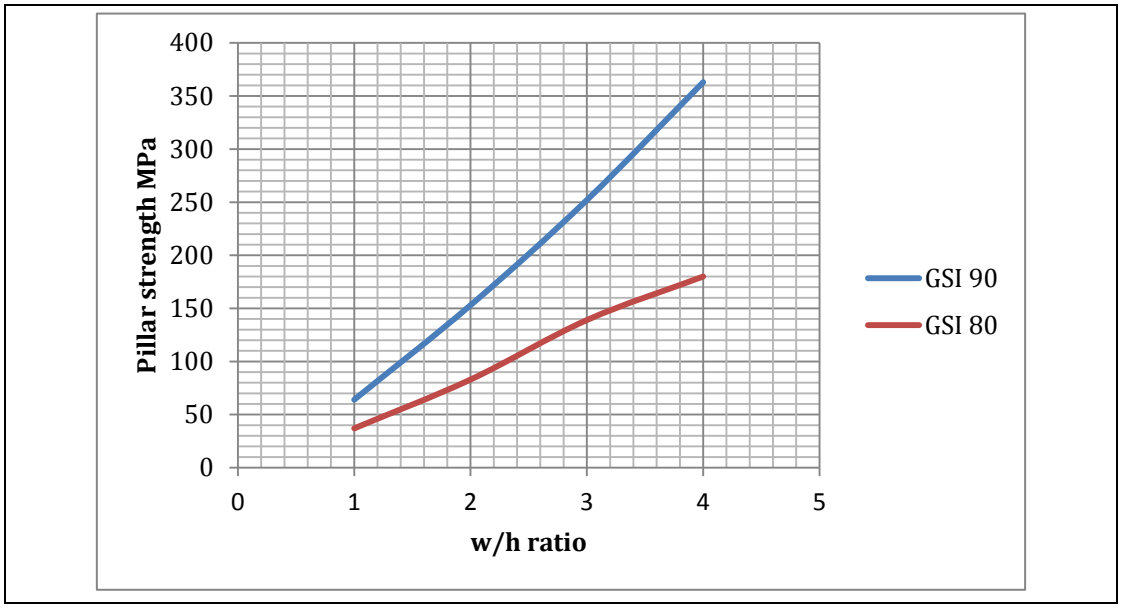

Figure 4.6_1 Strength variation with change in the width-to-height ratio and GSI values for a constant height of 2 m.

The influence of the change in the value of the Geological Strength Index on the pillar strength is further illustrated for input parameters given in Table 4.6_2.

Table 4.6_2: Input parameter and results for variation in GSI values

GSI	w/h ratio	Strength MPa
90	2	141
	3	255
	4	360
	5	502
80	2	64
	3	105
	4	152
	5	206
70	2	23
	3	39
	4	58
	5	80

Figure 4.6_2 illustrates the effect graphically of jointing; reduction in the GSI value. The strength differences are substantial and indicate the variation in pillar strength that can occur due to jointing.

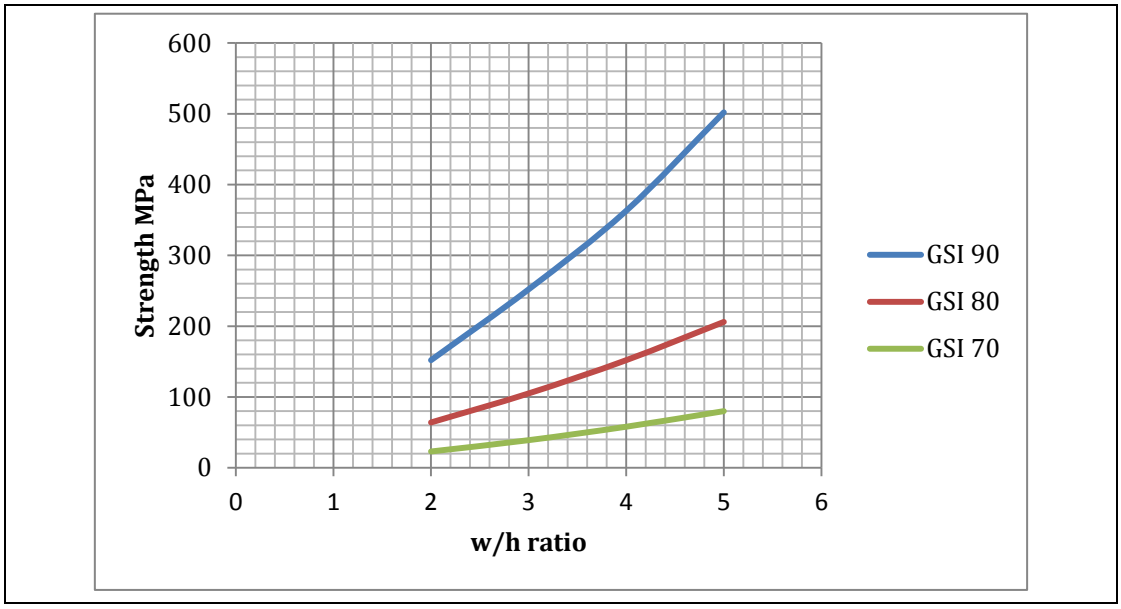

Figure 4.6_2 Influence of variation in GSI, jointing, on pillar strength - all pillars are 2 m high

The m_b and m_r values are a function of the m_i value and vary in their values for different GSI values as illustrated in the following example.

Table 4.6_3: Pillar strengths with variation in m_i values for w/h ratio of 3, GSI = 80 and UCS = 131 MPa

m_i	m_b	m_r	s	s_r	σ_{str} MPa
5	2.45	1.23	0.1084	0.054	36
10	4.9	2.45	0.1084	0.054	54
15	7.34	3.7	0.1084	0.054	75
20	9.8	4.9	0.1084	0.054	96

In the above simulation, the value of m_r was assumed to be 50% of the m_b value but it was found that the pillar strength was heavily dependent on a change in the m_r value as Figure 4.6_4 illustrates. The figure shows that the peak average pillar stress, for the same GSI value and m_i value, changes from 30 MPa to 150 MPa for a GSI value of 80 and a width-to-height ratio of 3.

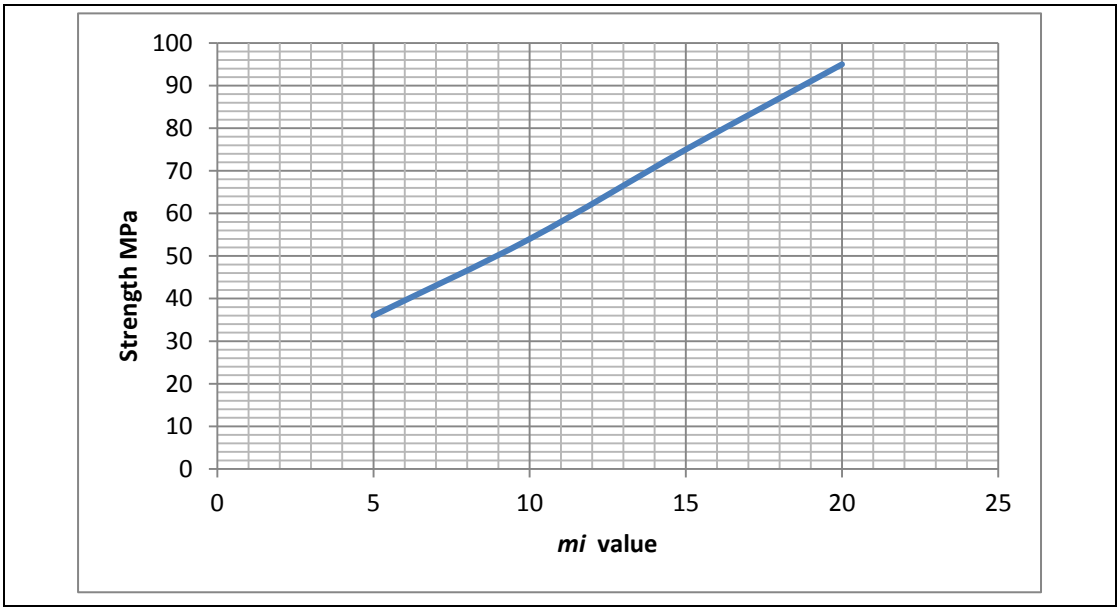

Figure 4.6_3 Increase in pillar strength for variations of m_i and a pillar 2 m high, 6 m wide

Similarly, the peak average pillar stresses were strongly influenced by the m_r values, Figure 4.6_4, which shows the effect of a change in the m_r values. The lack of definitive data and the results obtained by Joughin et al (2000) with m_r estimated at 50% of m_b it was decided that for the present thesis to use this value.

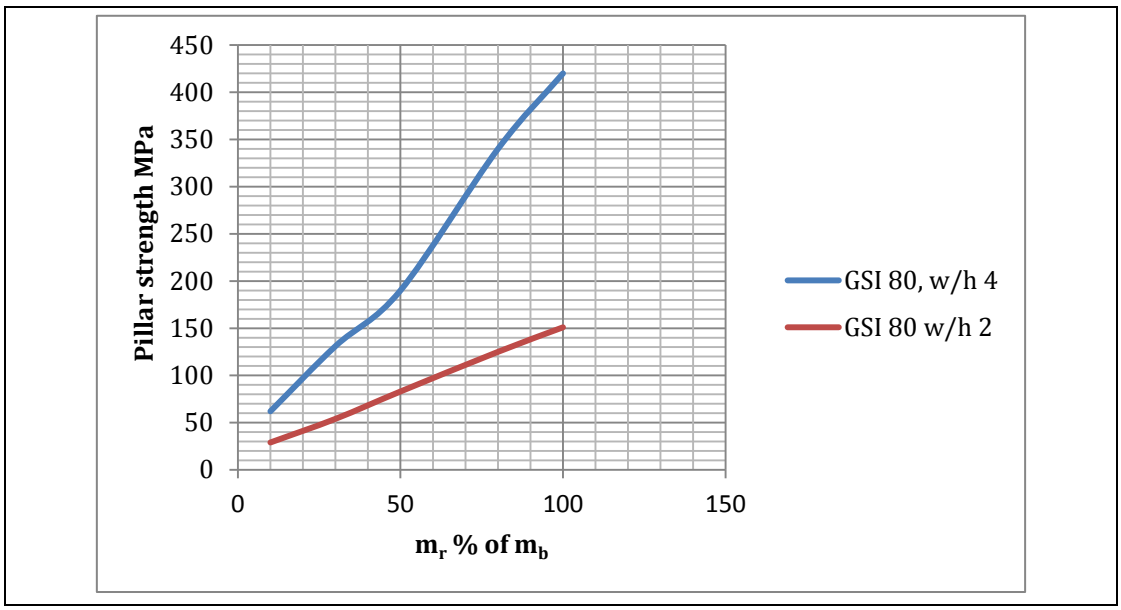

Figure 4.6_4 Strength variation with changes in the residual of the m_b values

4.7 Planes of weakness/interfaces

The effect of a smooth plane on the contact between the pillar and the hanging wall was illustrated by using the simple model in Section 4.6, Appendix IV, with UCS = 91 MPa, GSI = 90, m_i= 16 and m_r= 5, but not fixing the x axis in the *FLAC2D* model, simulating a frictionless contact between the pillar and the loading surfaces. Figure 4.7_1 is a plot for a varying width-to-height ratio for such a condition.

Also plotted in Figure 4.7_1 are the pillar strength value obtained with fixed, "free" contact as well as the strength obtained using the Hedley-Grant equation. The effect of frictionless loading surfaces, (free contact) simulating planes of weakness results in a significant reduction in pillar strength.

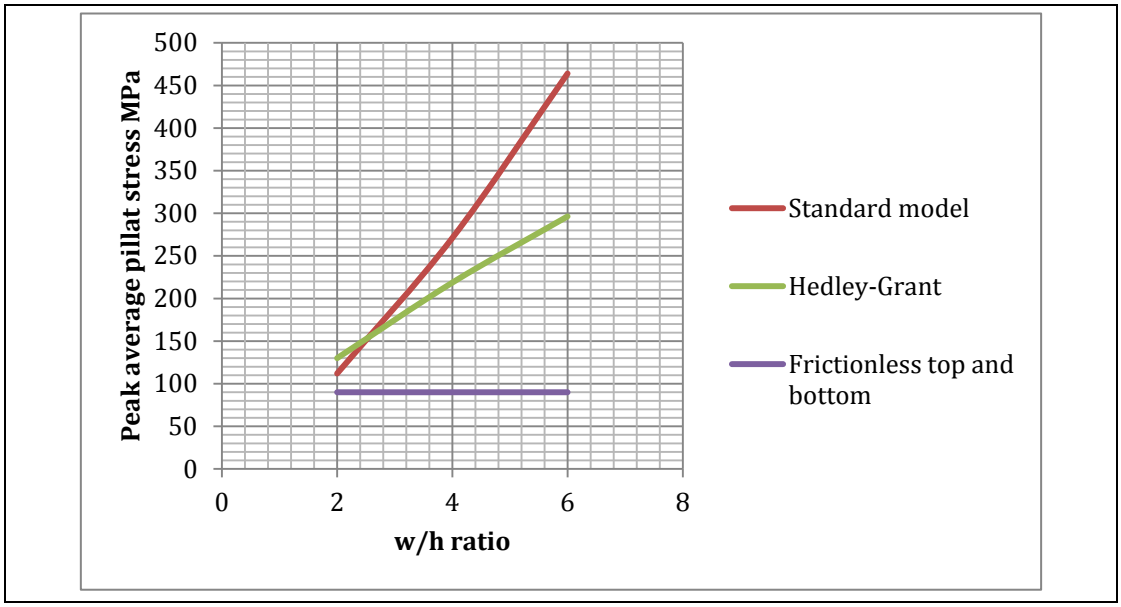

Figure 4.7_1 Influence of frictionless layer at top of pillar as compared with the "standard" model, fixed top and bottom, as well as the Hedley-Grant value

Having a frictionless surface at the hangingwall as well as footwall contact results in a pillar strength equal to the UCS value, 90 MPa.

The current thesis concentrates on establishing a new methodology based on simple models which can later be extended to more complex forms if it is found that the simple models are correct.

For the current investigation the hangingwall and footwall contacts were fixed.

4.8 Composite pillar

Composite pillars are common especially in the chrome seams but also on the Merensky reef where thin chromitite layers are present which influences the peak average pillar strength. As an example, the influence a chromitite pillar including a very weak pyroxenite layer near the top is illustrated with detail of the *FLAC2D*/H-B two layer model is given in Appendix II.

The pillar strength without the "soft" layer is 92 MPa. By reducing the GSI value of the pyroxenite to 40 and the bulk and shear moduli to 3.3 GPa and 1.5 GPa respectively, the pillar strength reduces to 6 MPa. (Disp=0.37e-3 m).

Figure 4.8_1 is a plot of the volumetric strain increment showing the compression of the weak pyroxenite layer and the expansion on the interface.

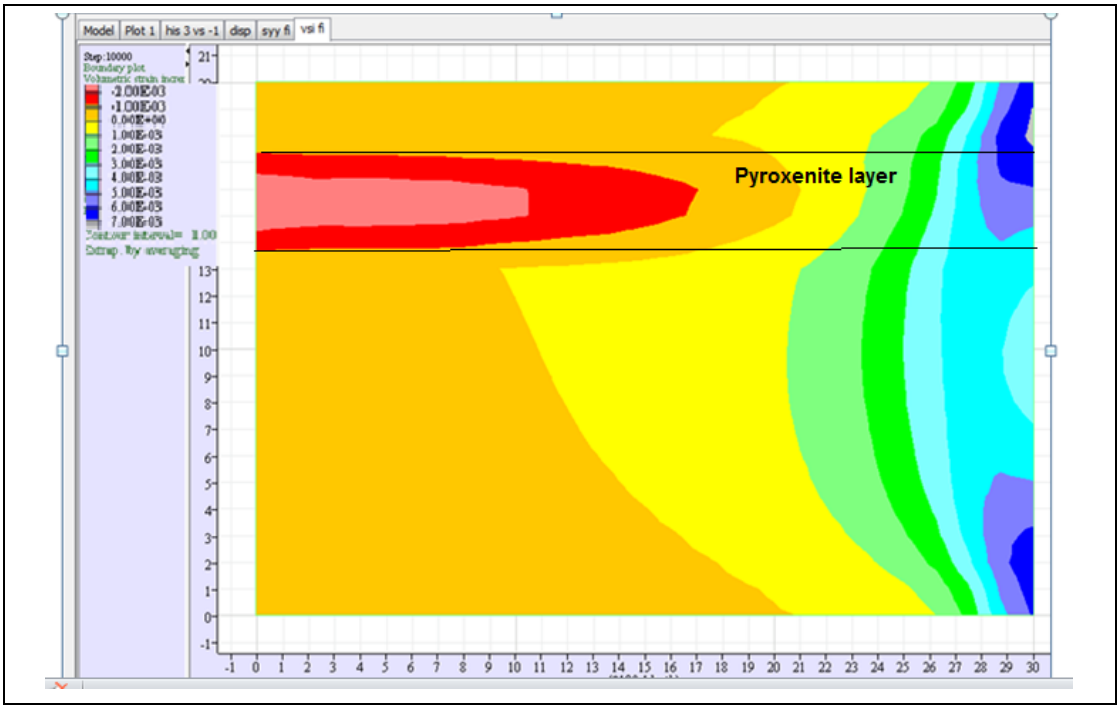

Figure 4.8_1 Influence of weak pyroxenite layer in a chromitite pillar on the volumetric strain increment

The weak layer has caused a drastic reduction in the pillar strength, from 92 MPa to a negligible 6 MPa. Figure 4.8_1 shows that the presence of "soft" layers with a low Young's modulus or a shear zone cannot be ignored in the design of bord and pillar workings.

4.9 Property variation within the pillar

To simulate the strength variation in a chromitite pillar the Mohr-Coulomb model was used since this model is less complex to model than a *FLAC2D/*Hoek-Brown for a multi-layer medium, while adjusting the values obtained from the Roclab model as explained by Hart (2012)

"*In order to fit a linear Mohr-Coulomb failure surface to the nonlinear Hoek-Brown failure surface, it is necessary to vary friction and cohesion as a function of*σ_3*. If only one value for cohesion and friction is used, then it is necessary to fit the Mohr-Coulomb surface over the range of* σ_3 *as close as possible. In the simple model, mc_vs_hb.dat, the Mohr-Coulomb failure surface is a rough fit to the Hoek-Brown failure surface, plotted in shear stress-normal stress space, for Hoek-Brown material with* m_b *= 7.8, s = 0.1084 and s* $_{ci}$*= 5.69e7 Pa. A Mohr-Coulomb failure surface is approximately fitted to the Hoek-Brown surface. A value of coh=34 MPa and friction=17 degrees roughly fits the Hoek-Brown surface The resulting average peak stress for the Mohr-Coulomb model 218 MPa, is within 5% of the value for the Hoek-Brown model (227 MPa)"*

The standard Mohr-Coulomb model calculates the strength for a model where the m_r value is equal to the m_b value. If the m_r value is less than the m_b value, the strength is reduced and

to simulate this effect, the friction angle in the Mohr-Coulomb has to be reduced by incorporating its residual value.

The reduction of m_b is equivalent to imposing strain softening in the Hoek-Brown model. To illustrate the effect using the Mohr-Coulomb model without "strain softening", the strength results obtained are shown in Figure 4.9_1. Watson (2010) used a strain softening Mohr-Coulomb model by introducing a residual cohesion. In the present Mohr-Coulomb model, the friction angle was reduced artificially to "simulate" strain softening.

For example, taking the model used previously:-

UCS=131 MPa

GSI=80

m_i=20

The values obtained from the Roclab programme are:-

Coh=12.94

Friction=45.26^0

w/h ratio=4 (w=8, h=2)

Inserting the values in a Mohr model in *FLAC2D* results in pillar strength in excess of 9 000 MPa.

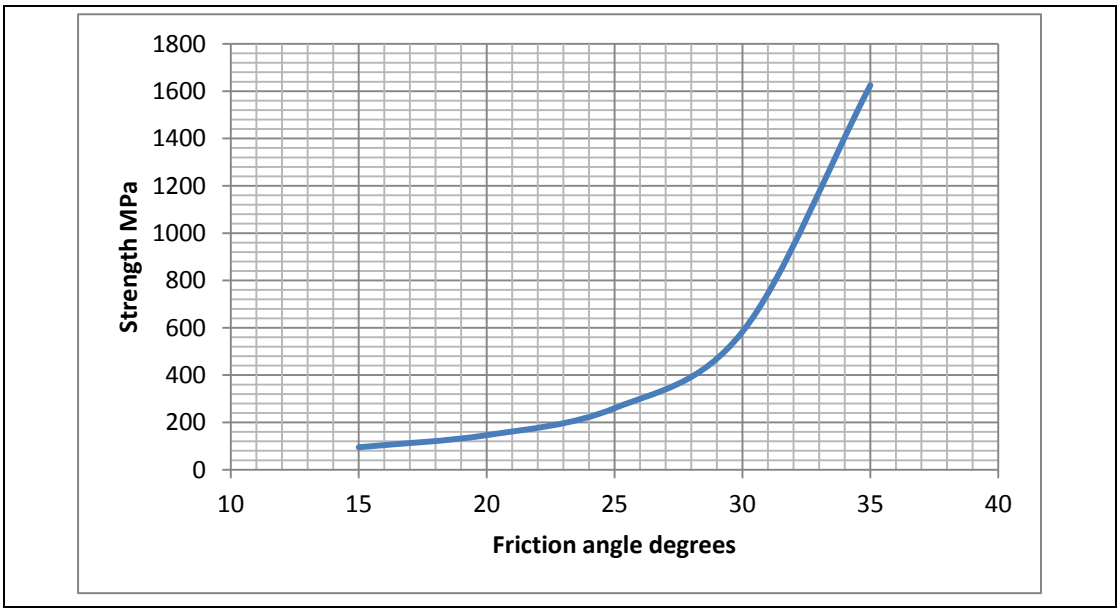

Figure 4.9_1 Increase in pillar strength with increase in friction angle

The pillar strength obtained from the *FLAC2D*/Hoek-Brown model for the same parameters and a m_r value of 50% of m_b is 180 MPa; a value equivalent to a friction angle of 22^0 instead of 45^0 derived from the Roclab programme.

Similar sets of comparisons were done and the average reduction required is of the order of 60% of the Roclab friction angle value, maintaining the cohesion value as given by the Roclab programme.

The conclusion is that the friction value from the Roclab programme needs to be reduced to provide similar answers as the Hoek-Brown/*FLAC2D* model. The friction values obtained by the RocLab programme in the model in Appendix III were therefore multiplied by a factor of 0.4.

Due to the rapid changes in the strength of individual chromitite layers, Figure 2.1.4_1, it was decided to establish the effect by modelling the individual layers as against using an average of these values for the pillar.

For the reasons discussed above, the *FLAC2D*/Mohr-Coulomb model rather than the FLAC2D/H-B model was used, Appendix III, where it was found that pillar strength for the multi-layer model is 214 MPa.

To compare the effect of using an average instead of the individual layers, Table 4.9_1 gives the average from the individual layer model.

Table 4.9_1: Average Values for a Variable Strength Chromitite Pillar

bu	***Sh***	**coh**	**Friction**
7.9e10	4.2e10	13.0e6	18.3

For a Mohr-Coulomb model using the average values given in Table 4.9_1, the pillar strength is 226 MPa, within 5% of the value using the individual layers.

It was concluded that the average of a set of values can be used as a single value in a Mohr-Coulomb *FLAC2D* model without loss of reasonable accuracy.

A number of questions have arisen while investigating the *FLAC2D*/Hoek-Brown and Mohr models that need to be addressed in another forum:-

- The influence of the residual m_r values is high and requires closer study. In the thesis a value of 50% of the m_b value was used.
- The difference between the *FLAC2D*/Hoek-Brown and the Mohr-Coulomb model when using the Roclab data requires further research.

4.10 Calibration: Detail of the stress distribution and volumetric strain increment for simple pillars.

In this section, a pillar only was considered. The interaction between the hanging and footwall can be varied by fixing/freeing the upper and/or lower elements.

The vertical stress contours (s_{yy}) across a section of a pillar shown in Figure 4.10_1 vary from 800 MPa in the centre to zero values at the pillar edge. The magnitude of the stress at the pillar centre is a function of the failure state of the pillar, where it is found that even after the peak pillar strength has been reached and plastic flow results, a high stress still acts at the pillar centre. (The absolute value is obviously a function of the pillar width, the greater the width, the greater the central stress magnitude.)

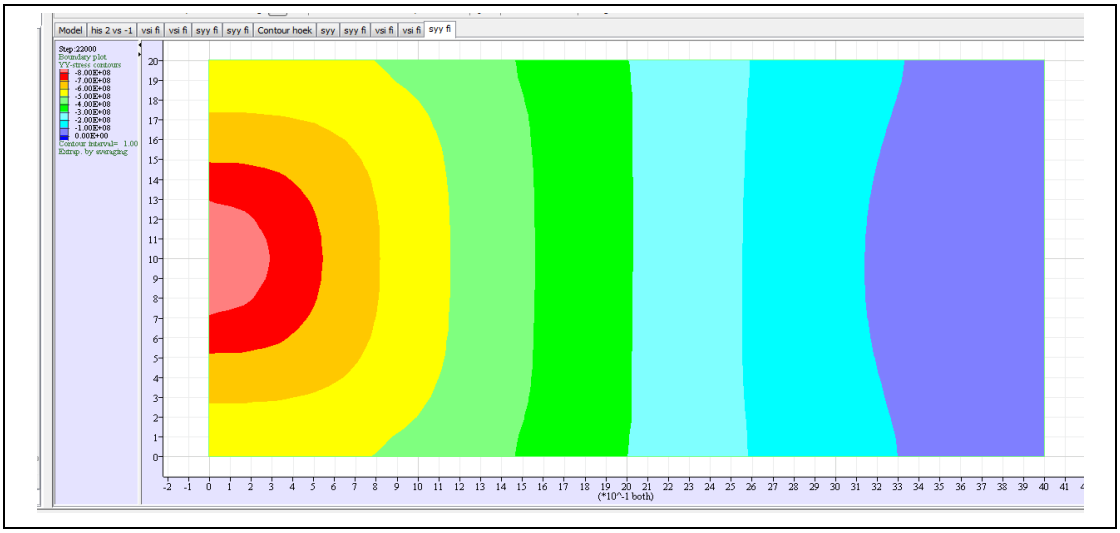

Figure 4.10_1 Vertical stress contours for a 2 m high, 8 m wide pillar at peak average pillar stress

From personal experience, the Hoek-Brown criterion does not predict the actual fracture zones around excavations well. The use of the plastic strain, e-plastic, in the strain softening model and the volumetric strain increment,vsi in the *FLAC2D* model, once calibrated, predicted the underground fracture zone accurately. (Kersten and Leach, 1996).

Strain rates are based on grid point velocities and the current coordinates. “Strain increments” are computed with the same equations, but with convergences substituted for velocities

vsi is the volumetric strain increment:

$$vsi = \varepsilon_{xx} + \varepsilon_{yy} + \varepsilon_{zz} \qquad 4.6$$

The value is computed using incremental convergences:

$$vsi = \frac{\Delta u_x}{\Delta x} + \frac{\Delta u_y}{\Delta y} + \frac{\Delta u_z}{\Delta z} \qquad 4.7$$

Where $\Delta x \Delta y \; and \; \Delta z$ are incremental convergences on the x, y and z axis.

The calculated value of vsi is the volumetric strain increment since convergences were reset to zero.

$vsi\ (i, j)$ volumetric strain increment, equation 4.6.

Figure 4.10_2 is a plot of the stress-strain diagram for a 4 m radius pillar with a pillar strength of 149 MPa with a gradual change in slope of the curve. The curve equals that of the stress-strain curves observed in rock strength tests to be discussed in section 5 where the geotechnical properties are defined and discussed in detail.

Figure 4.10_3 is a plot of the cumulative volumetric strain increment contours at the average peak pillar stress, which appears to resemble the fracturing in a pillar sidewall, and could possibly define the extent of the fracture zone in a pillar at different stages of the average pillar stress. The contours have the distinct curved shape identical to the induced fracture surfaces in the pillars.

A profile of the cumulative volumetric strain increment through the pillar at mid height is shown in Figure 4.10_4.

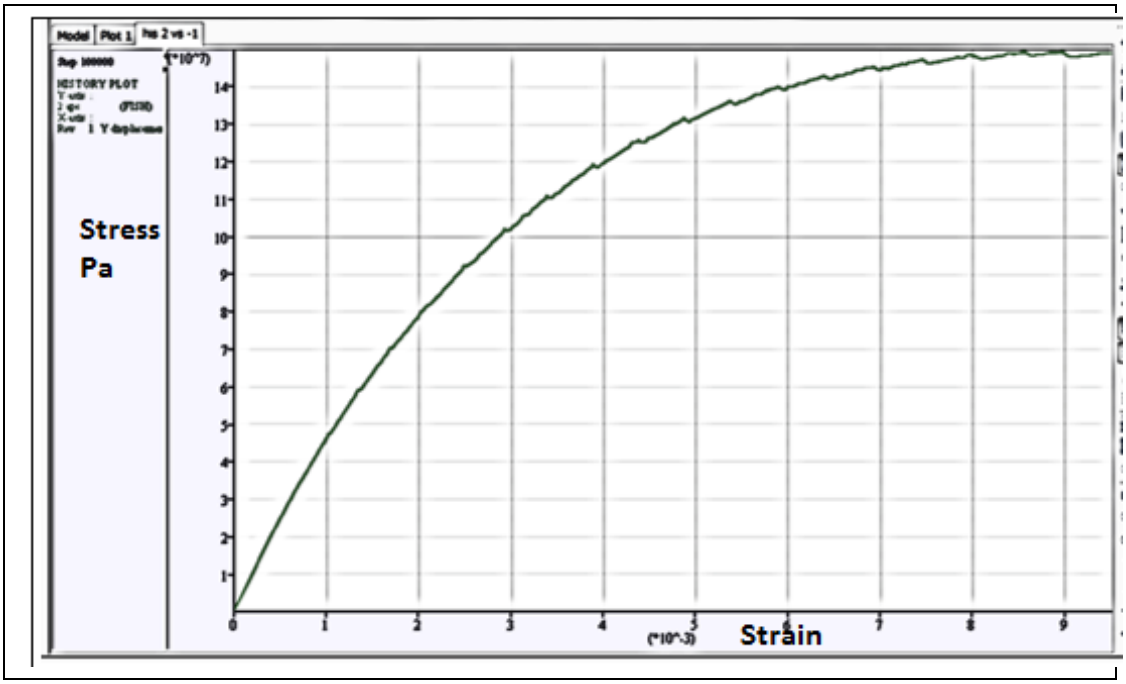

Figure 4.10_2 Stress strain diagram for a 4 m radius pillar (The vertical axis is the average pillar stress based on a FISH function)

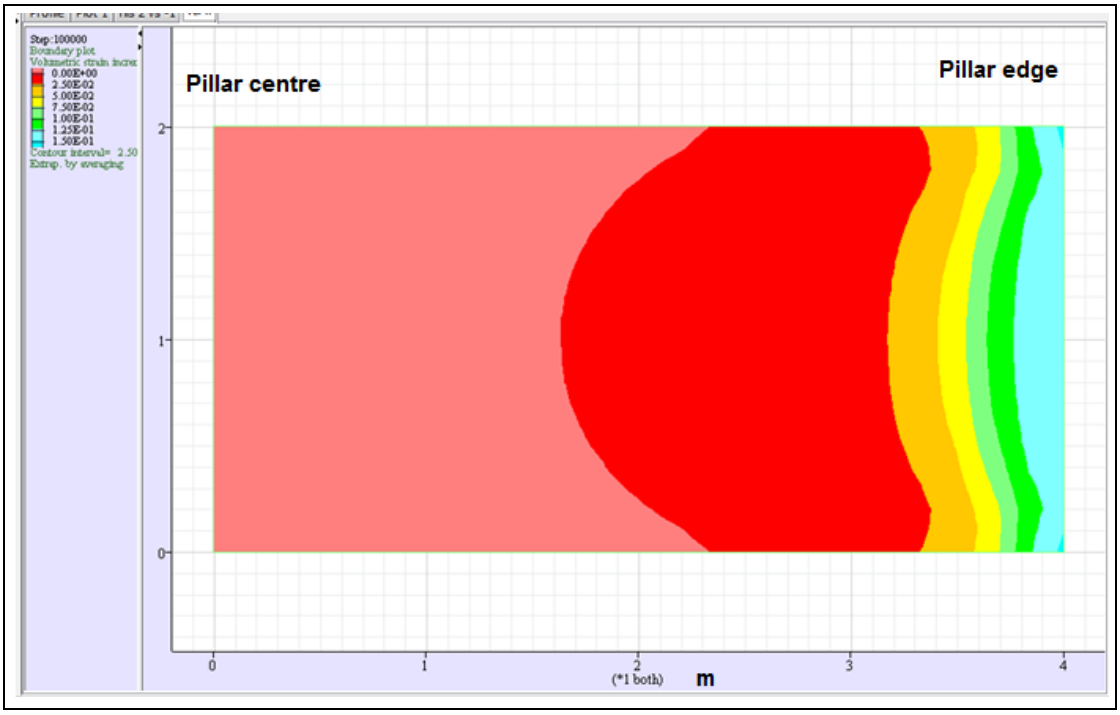

Figure 4.10_3 Volumetric strain increment contours in a pillar

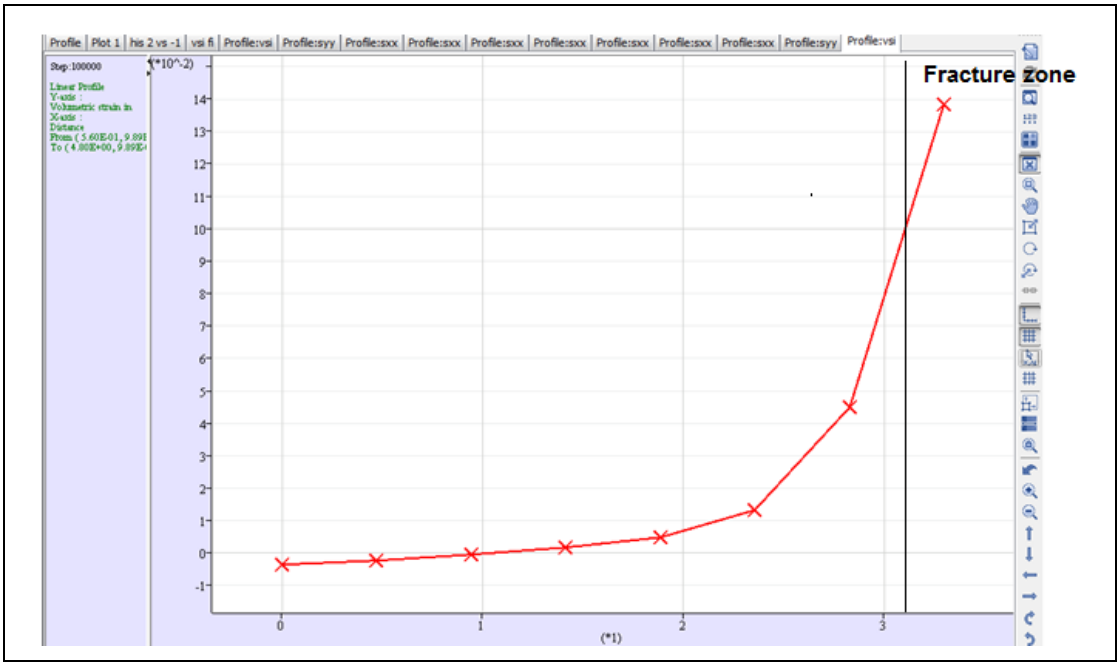

Figure 4.10_4 Volumetric strain increment profile across a 4 m radius pillar at mid height showing that at a volumetric strain increment of .01 the fracture zone commences at 0.8 m from the edge (Vertical line intercept}.

The volumetric strain increment is zero to negative at the pillar centre, a volume reduction, which changes to a volume increase as it approaches the pillar edges. The volume

reduction/increase boundary is a function of the stress level imposed on the pillar and changes as the stress field increases.

The rapid change in the volumetric strain increment could be ascribed to a non-elastic response, simulated by a “Poisson’s ratio’ of greater than 0.5.

The assumption was that the rate of increase in the volumetric strain increment could be a measure of the fracture zone. For instance, if a value for the volumetric strain increment of 1e-2 was assumed to define the onset of fracturing, the width of the fracture zone in an 8 m pillar was 80 cm, Figure 4.10_4. This concept is subject to detailed investigation in the calibration section.

4.11 Pillar failure mechanism.

The strength of a pillar can be defined by the change in the slope of the stress strain curve, such as shown in Figure 4.11_1. It shows the stress/convergence graph for a 1.8 m high and 2.4 m radius pillar behaving in an apparent plastic manner.

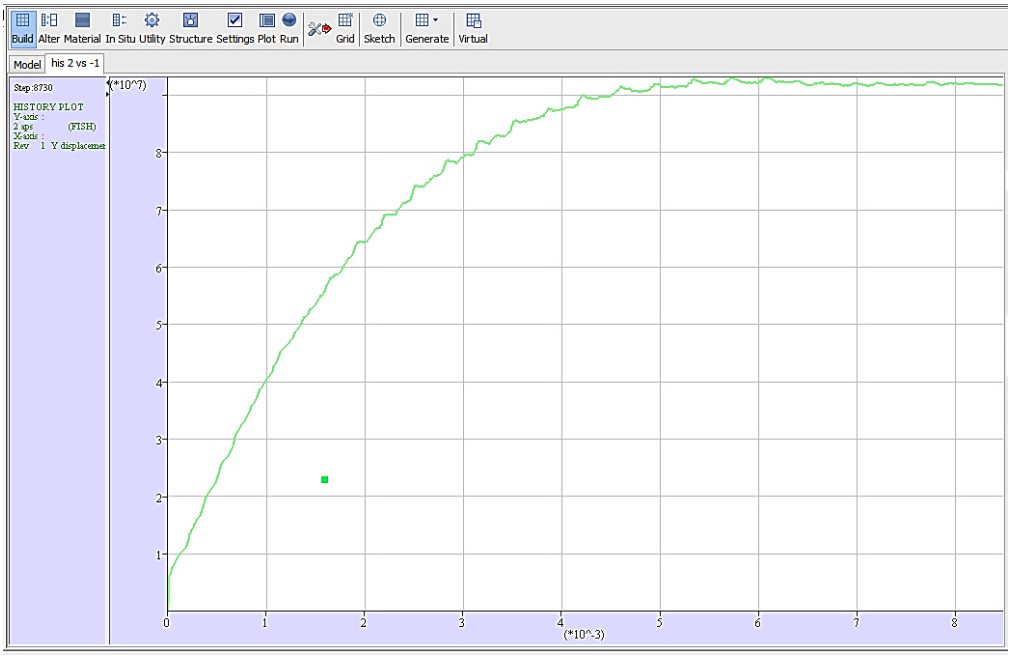

Figure 4.11_1 Stress deformation of a 1.8 m high and 2.4 m radius pillar, Stress y-axis with deformation on the x-axis.

It is difficult to determine the absolute value of the pillar strength due to the gradual change of the curve. An alternative method needs to be found to define the pillar strength accurately.

An attempt was made to define the pillar strength in a more rigorous manner by plotting the solid core of the pillar, assuming a certain value of the volumetric strain increment, say 1e-2, as defining onset of fracturing.

By plotting the extent of the volumetric strain increment in excess of 1e-2 at different stress levels, the intact core, or volume of the intact core can be determined.

The sudden decrease of the remaining solid core indicates that the entire pillar has fractured at an average pillar stress of 95 MPa, Figure 4.11_2, defining the pillar strength. (It incidentally also shows that the volumetric strain increment of 1e-2 is valid for this pillar as is discussed in the Sections 9, 10 and 11.)

In the remainder of the thesis the pillar strength was determined by estimating the maximum slope where it was found that the influence on the strength estimate is small, of the order of 5%, while more sensitive to convergence values, of the order of 10% .

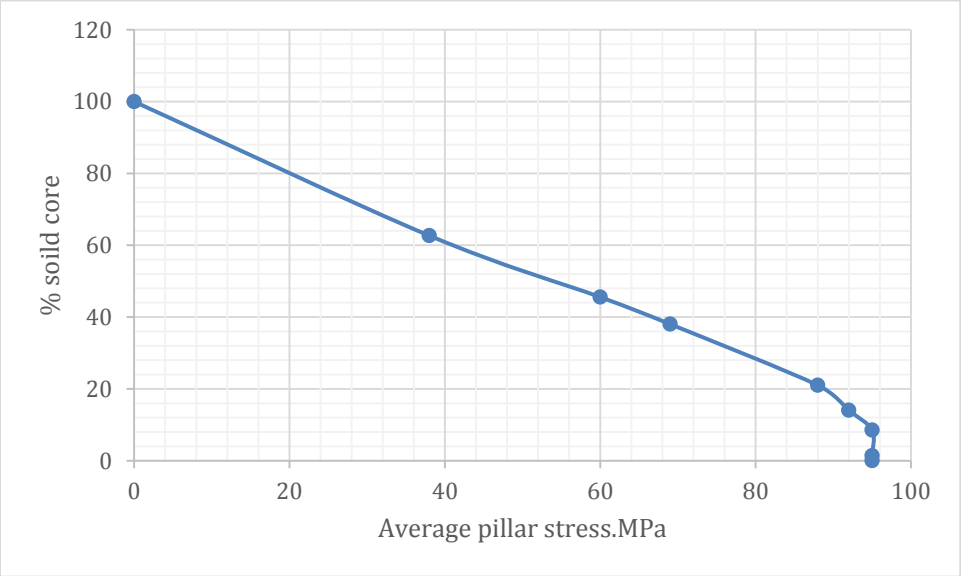

Figure 4.11_2. Average pillar stress vs the percentage intact volume for the pillar

Figure 4.11_2 illustrates that the failure of a pillar is progressive, fractures moving towards the centre of the pillar. During this process the average pillar stress keeps increasing, albeit at a reducing rate until the two fracture zones coalesce in the pillar centre. The stress on the pillar edges decreases progressively while at the pillar centre, the stresses increase maintaining a relative high average pillar stress, until such stage that the two fracture zones interact.

4.12 The “draping” effect.

Watson (2010) discusses “draping” of the hanging/footwall over the pillar edge with Figure 4.12_1 illustrating the mechanism. The capacity of the interface to transfer lateral/horizontal stress from the foundation to the pillar results in the inner core of the pillar being confined and thus strengthened

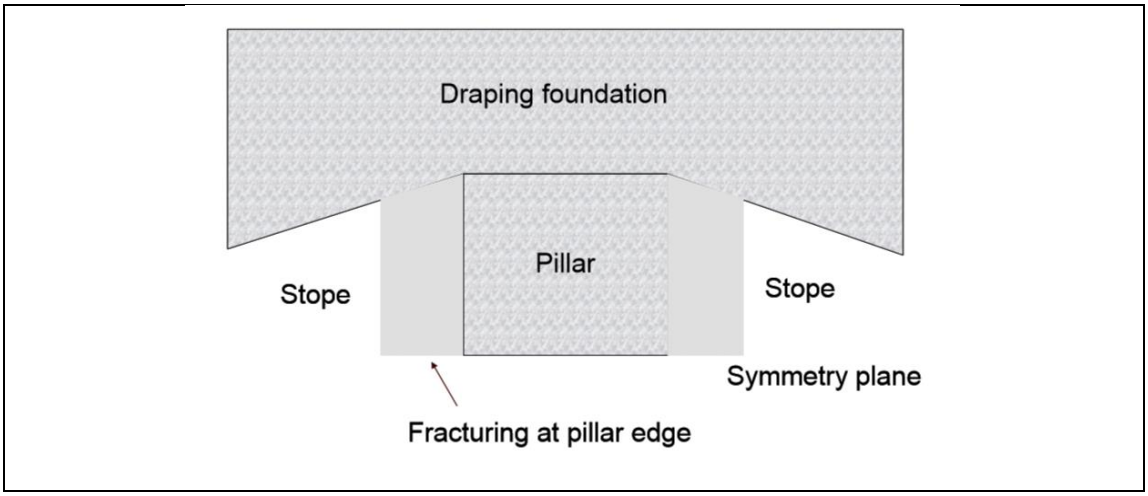

Figure 4.12_1. "Draping" as defined by Watson (2010)

Watson (2010) further states that in reality, the extent of mining around underground pillars determines the amount of hanging- and footwall drape and hence the severity of this influence.

Watson investigated the strength of strike pillars spaced at 30 m and found, using *FLAC* modelling, that for a pillar/hangingwall "frozen" interface, the average pillar strength is less in the case of "draping" when compared to a pillar loaded by solid platen. The detailed explanation for this process is given in the quote below (Watson)

"The draping effect of the hangingwall over the pillar results in high peak stresses at the edge of the pillar before failure. Therefore, early failure initiates on the edge and progresses towards the centre. The capacity of the interface to transfer lateral/horizontal stress from the foundation to the pillar results in the inner core of the pillar being confined and thus strengthened. ……The stope pillar is initially stiffer and subsequently more ductile than either of the other loading environments, again resulting from an early peak stress at the edge of the pillar and the progression of failure towards its centre. Note that the highest peak occurs after pillar failure'.

The pillar behaviour modelled by Watson (2010) without hangingwall and footwall draping, but with elastic loading foundations, without an interface between the pillar and the foundation, gives a similar progression of failure and load shedding, but resulting in a higher average pillar stress than the one with "draping". Fixing the hangingwall and footwall of the pillar has the same effect by confining, hence strengthening the pillar, as mentioned by Watson above.

Considering that the current thesis deals with bord and pillar geometries with limited bord width, the effect of draping is not considered a major factor and has not been included.

4.13 Conclusions

FLAC2D/Hoek-Brown model can be used to realistically simulate most pillar geometries encountered in the mining industry. Some common observations were the following:

- The vertical stress is the lowest at the pillar edge at failure.

- At the average peak pillar stress, the vertical stress at the core of the pillar generally exceeded the uniaxial strength of the rock.
- Pillar failure was simulated as a progressive process.
- The cumulative volumetric strain increment could be a possible measure of the depth of fracturing in a pillar.
- The percentage solid in the pillar is a reliable measure of pillar strength for plastic and strain hardening rock types.

The model was based on the following restrictions and conditions which in the author's opinion and experience are valid:

- The model simulates a condition of a frozen contact between hangingwall/footwall with the pillar by fixing the boundaries of the model, in this instance x and y for the two contact zones.
- The influence of draping for pillar at shorter spans in bord and pillar workings is deemed to be less and fixing x and y has a similar "clamping" effect as "draping".
- Loading velocity over the pillar width were held constant simulating a very stiff hangingwall.
- According to Watson (2010) foundation failure occurs above an average pillar stress of 250 MPa. It was found that in the pillar geometries investigated, bord and pillar workings, this stress level was not reached and was not taken into consideration. Also, the simple model used assumes infinitely strong loading surfaces.
- It was shown that the presence of shear planes, low friction contacts and weak layers affects the pillar strength to a degree that cannot be ignored and neither is it deemed possible to create a generic pillar strength equation for such deviations from a homogeneous pillar.
- In the presence of strength variations in the pillar or pillar contact zones, full use must be made of the options available in *FLAC2D* or similar analytical programs, to create a pillar strength for the specific site incorporating estimates for the situation at hand.
- Verbal information from colleagues confirms that at Kroondal, Henry Gould, Zimplats and Everest mines, planes of weakness were responsible for regional pillar collapses. Their design was based on the standard Hedley-Grant equation.
- To be able to obtain a simple generic equation for pillar strength, the simplest model was selected as a starting point which can incorporate known geotechnical parameters.
- The introduction of the hangingwall and or the footwall in the model is the next obvious step in expanding the approach followed in the thesis.

5 GEOTECHNICAL INPUT PARAMETERS

5.1 Input parameters for the Hoek-Brown failure criterion

Hoek (1983) and Hoek and Marinos (2000) developed the Hoek-Brown failure criterion used in this research.

The basic equation for the Hoek-Brown failure criterion is (Hoek and Marinos, 2000):-

$$\sigma_{str} = \sigma_3 + \sigma_c\{m_b\,(\frac{\sigma_3}{\sigma_c}) + s\}a \qquad 5.1$$

$$m_b = m_i e^{(GSI-100)/(28-14D)} \qquad 5.2$$

$$s = e^{(GSI-100)/(9-3D)} \qquad 5.3$$

$$a = \frac{1}{2} + \frac{1}{6}(e^{\left(-\frac{GSI}{15}\right)} - e^{\left(-\frac{20}{3}\right)}) \qquad 5.4$$

$$\sigma_{ci} = \sigma_c.sa \qquad \sigma_3 = 0 \qquad 5.5$$

$$m_i = \sigma_c/\sigma_t \qquad 5.6$$

Where σ_3 = minimum principal stress

m_b = Reduced value for material constant m_i

σ_c = Uniaxial compressive strength

s = Material constant

a = Derivative, equation 5.4

D = Rock mass disturbance by blasting and/or stress induced fracturing.

σ_{ci} = Global strength

GSI = Geological Strength Index.

σ_t = Tensile strength

The criterion is governed by the following:

- The uniaxial compressive strength.
- The GSI, Geological Strength Index.
- The m_i value.
- Tensile strength (According to Hoek, 2012).

Failure is deemed to occur when the maximum principal stress exceeded the value of σ_{str} in equation 5.1

5.1.1 Uniaxial compressive strength

The uniaxial compressive strength is the rock mass property most commonly available and was discussed in some detail in Part I indicating that a coefficient of variation of 0.3 is common within a data set from a population in a limited area.

Of the three variables used in common strength equations, the uniaxial compressive strength is the only variable that could be obtained by controlled means in the laboratory. It has been used in an adjusted form as the main component in the pillar strength equations.

A possible method of establishing a reliable mean uniaxial compressive strength value was to obtain a complete intersection of the ore body in at least two boreholes, additional samples dependent on the coefficient of variation, or complete underground sampling sections. Figure 5.1.1_1 (Repeat from Section 2.14) is an example of strength variations across a chromitite seam for five sections.

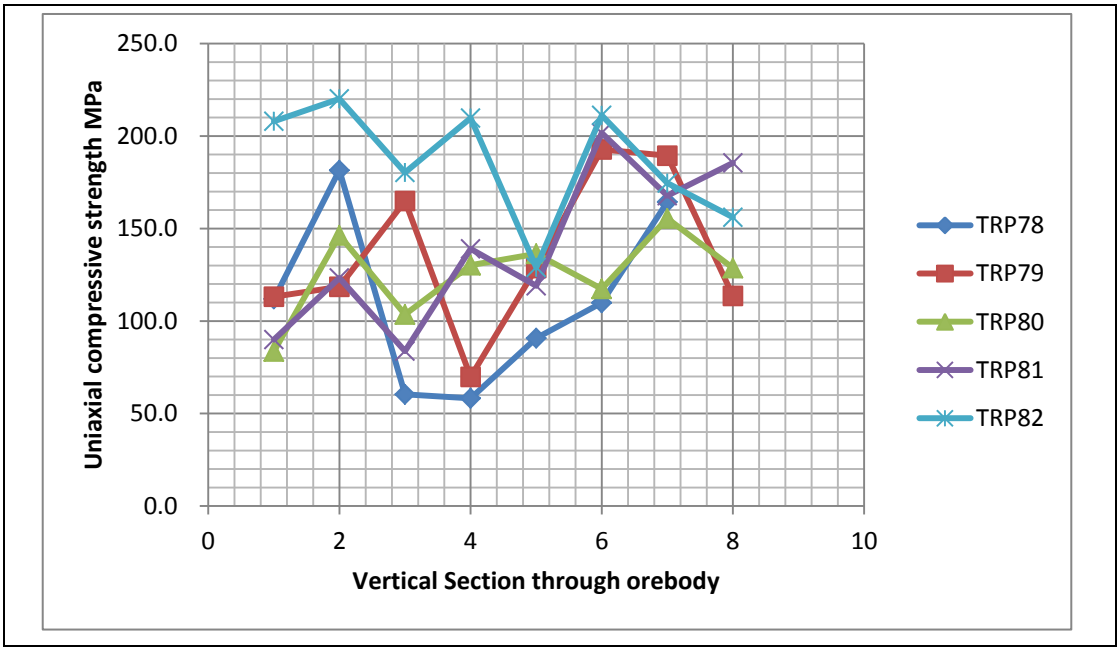

Figure 5.1.1_1 Variation of the uniaxial compressive strength across an ore body for 5 different boreholes, the left side being the hanging wall and the right hand the footwall side.

It appears that selecting a number of individual samples from different boreholes or sites would not be representative of the mean value of the ore body and misleading results could result.

Strength determinations were also obtained for different mines and relevant rock types which are summarised by Spencer (2012) for the Eastern and Western portions of the Bushveld, Tables 5.1.1_1 and 5.1.1_2.

Table 5.1.1_1: Summary of rock strength, UG2 Horizon, for the Eastern Bushveld (Spencer, 2012)

Rock Type.		Density. (kg/m^3).	UCS. (MPa).	Poisson's Ratio	Young's Modulus. (Gpa).
UG2 Hangingwall Pyroxenite.	**Average:**	**3221,8**	**142,7**	**0,279**	**114,5**
	Standard Deviation:	**27,50**	**16,21**	**0,073**	**22,98**
	Maximum:	**3280**	**172,7**	**0,440**	**151,0**
	Minimum:	**3170**	**110,7**	**0,202**	**89,2**
	Coefficient of variation	0,01	0,11	0,26	0,20
UG2 Chromitite.	**Average:**	**3960,0**	**87,2**	**0,440**	**91,8**
	Standard Deviation:	**181,00**	**28,67**	**0,194**	**40,52**
	Maximum:	**4540**	**133,2**	**1,027**	**203**
	Minimum:	**3770**	**35,5**	**0,267**	**30,7**
	Coeficient of variation	0,05	0,33	0,44	0,44
UG2 Footwall Pegmatoid.	**Average:**	**3191,1**	**112,0**	**0,336**	**88,1**
	Standard Deviation:	**92,26**	**31,51**	**0,139**	**22,28**
	Maximum:	**3300**	**183,6**	**0,538**	**126,0**
	Minimum:	**3010**	**81**	**0,159**	**62,1**
	Coeficient of variation	0,03	0,28	0,41	0,25
UG2 Footwall Norite.	**Average:**	**2852,0**	**223,7**	**0,347**	**97,6**
	Standard Deviation:	**127,95**	**42,56**	**0,112**	**15,32**
	Maximum:	**3000**	**259,7**	**0,507**	**114,6**
	Minimum:	**2730**	**158,8**	**0,240**	**82,5**
	Coeficient of variation	0,04	0,19	0,32	0,16
UG2 Footwall Spotted Anorthosite.	**Average:**	**2836,0**	**202,1**	**0,395**	**78,6**
	Standard Deviation:	**17,13**	**19,61**	**0,042**	**7,19**
	Maximum:	**2870**	**224,0**	**0,442**	**87,6**
	Minimum:	**2810**	**170,3**	**0,338**	**70,2**
	Coeficient of variation	0,01	0,10	0,11	0,09
UG2 Footwall Norite - Drive Elevation.	**Average:**	**2876,0**	**180,9**	**0,385**	**72,0**
	Standard Deviation:	**47,22**	**29,42**	**0,075**	**1,68**
	Maximum:	**2940**	**202,1**	**0,463**	**74,7**
	Minimum:	**2810**	**129,9**	**0,271**	**70,2**
	Coeficient of variation	0,02	0,16	0,19	0,02

Table 5.1.1_2: Summary of rock strength, UG2 Horizon, for the Western Bushveld (Spencer, 2012)

Rock Type.		Density. (kg/m^3).	UCS. (MPa).	Poisson's Ratio	Young's Modulus. (Gpa).
UG2 Hangingwall Pyroxenite.	Average:	3219,5	128,4	0,2	129,0
	Standard Deviation:	56,35	36,58	0,04	16,42
	Maximum:	3300	207,4	0,272	157
	Minimum:	3080	89	0,178	107,5
	Coeficient of variation	0,02	0,28	0,15	0,13
UG2 Chromitite.	Average:	3981,4	98,4	0,280	129,7
	Standard Deviation:	182,47	33,70	0,094	35,16
	Maximum:	4250	162,4	0,452	160,9
	Minimum:	3640	25,7	0,111	53,6
	Coeficient of variation	0,05	0,34	0,33	0,27
UG2 Footwall Pegmatoid.	Average:	3223,3	112,2	0,262	92,2
	Standard Deviation:	118,46	25,54	0,038	34,49
	Maximum:	3360	139,7	0,297	131,7
	Minimum:	3150	89,2	0,222	68,2
	Coeficient of variation	0,04	0,23	0,14	0,37
UG2 Footwall Norite.	Average:	2986,7	118,0		
	Standard Deviation:	102,11	22,70		
	Maximum:	3140	144,8	0,000	0,0
	Minimum:	2850	90,6	0,000	0,0
	Coeficient of variation	0,03	0,19	#DIV/0!	#DIV/0!
UG2 Footwall Pyroxenite.	Average:	3100,0	194,1	0,3	120,3
	Standard Deviation:	115,07	75,07	0,02	15,06
	Maximum:	3270	277,2	0,285	142
	Minimum:	2970	99,2	0,235	108
	Coeficient of variation	0,04	0,39	0,09	0,13

A general assumption in the platinum mines was that the strength of the Merensky reef horizon is a function of the mineralogy and that the relative proportions of feldspar and pyroxene are the governing factor, with the popular opinion that the higher the feldspar content, the greater the strength. Wilson et al. (2005) did an extensive study to explain the variation in rock strength of the Merensky reef at Impala Platinum Mine. The apparent correlation was put to the test and the results are summarized in Figure 5.1.1_2.

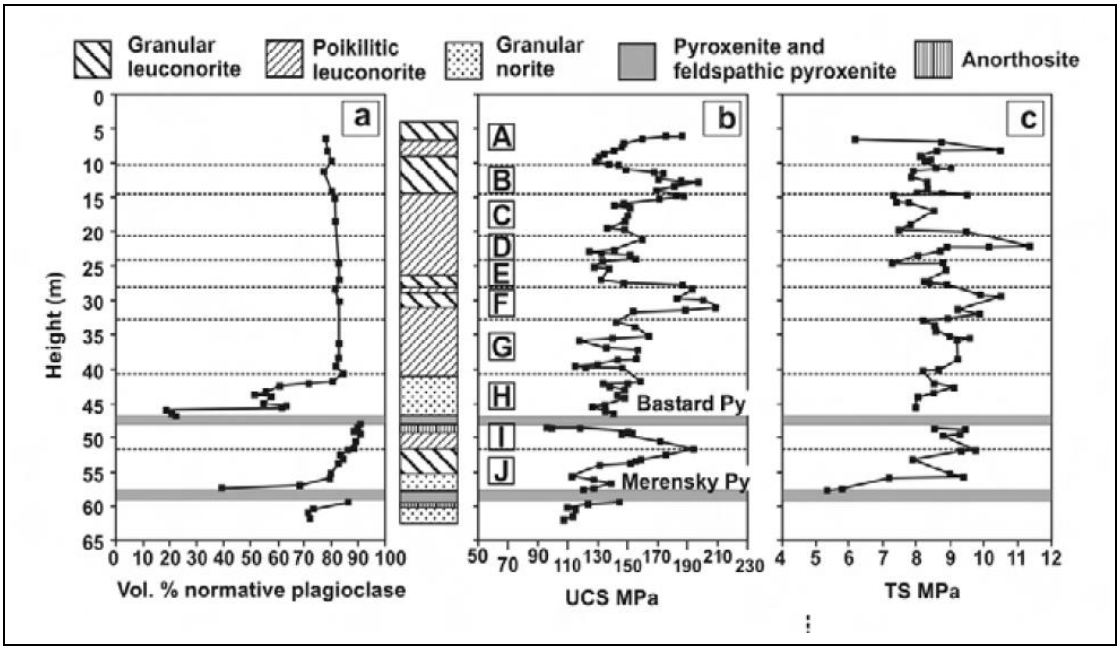

Figure 5.1.1_2 Rock strength variation below and above the Merensky Reef, Western Bushveld. (After Wilson et al, 2005)

Quotation from Wilson, et al. (2005).

"In conclusion, rock strengths of the norites in the environment of the Merensky reef exhibit considerable variation which is dependent on a number of controls. These include bulk rock composition, textural relations and mineral associations, the nature and amount of cementing medium, fabric and the stress history of the rock from early stage compaction to late-stage cooling. The relative roles of these controls are a fertile area for applied research and should be investigated further."

Figure 5.1.1_3, repeat of Figure 2.1.13_3 for ease of reference, illustrates the possible effect that the depth of sampling can have on the rock strength. Watson (2010) referred to the possible degradation of rock strength since high stresses are active during drilling which cause an increase in the number of micro cracks. The discing of core is proof that micro to macro-fracturing is induced during the drilling process.

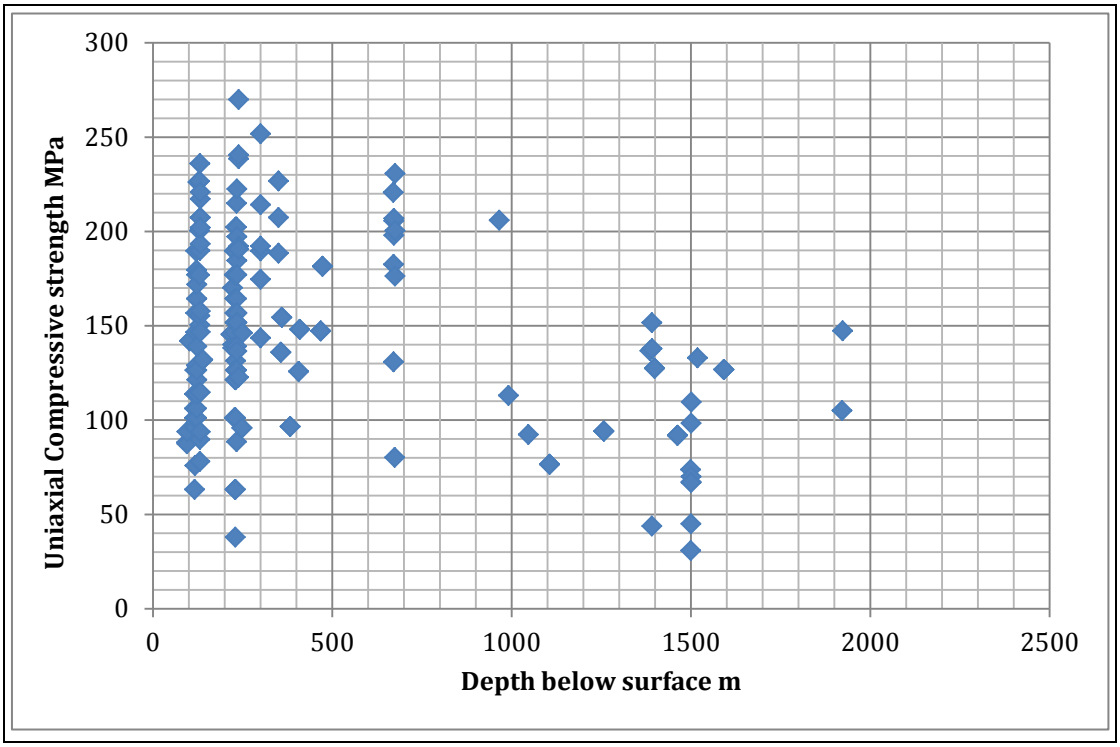

Figure 5.1.1_3 apparent lower strength values for pyroxenite in the deeper mines

Table 5.1.1_3: Summary of mean UCS data with the standard deviation

		Eastern Bushveld			Western Bushveld		
	Rock Type	**UCS MPa**	**St Dev**	**COV**	**UCS MPa**	**St Dev**	**COV**
Spencer	Pyroxenite	128	37	0.29	142	16.21	0.11
	UG2	98	34	0.35	87.2	28.67	0.33
	F/W Pyroxenite	112	26	0.23	NA		
	F/W Norite	118	23	0.19	N/A		
	F/W Pegmatoid	194	76	0.39	112	31.51	0.28
	Spotted Anorthosite				202	20	0.10
	F/W Norite				181	29	0.16
Two Rivers	UG2	111	45	0.41			
	UG2	136	40	0.29			
	UG2	125	22	0.18			
	UG2	139	41	0.29			
	UG2	186	30	0.16			

Figure 5.1.1_4 is a plot of the calculated normal distributions for some of the values in Table 5.1.1_3. Note the overlap in values of distinctly different rock types.

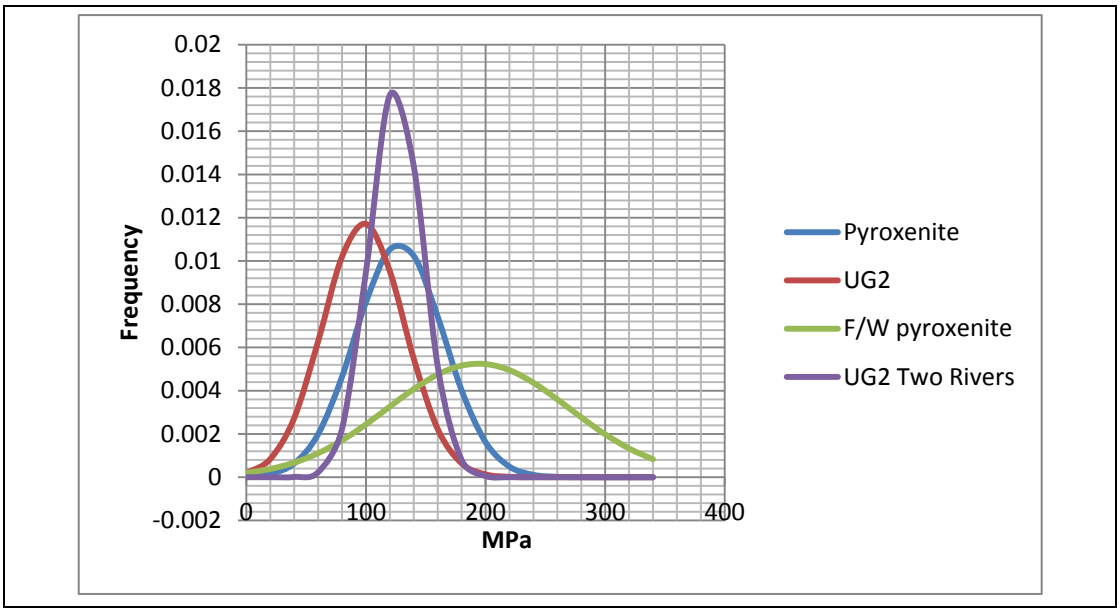

Figure 5.1.1_4 Calculated normal distributions of some of the values in Table 5.1.1_3

Based on the evidence presented, it would appear that an inordinate number of samples are required, in excess of what had been used previously, to determine the effect of the sample collection, for example, the effect of depth. A possible solution would be to use the Kriging method that is used to determine the mean grade values of an ore body.

Figure 5.1.1_5 shows the outcome of an attempt using the Kriging method for the data from Two Rivers Platinum Mine for the UG2 horizon. (Van der Merwe, P. 2013)

A certain trend could be discerned and boreholes TRP 81, 80, 79 and 78 fell within the range 100 to 120 MPa that could be used for mine planning. Unfortunately, the values covered a small portion of the mine only and this example was used simply to illustrate the possibilities inherent in the Kriging method.

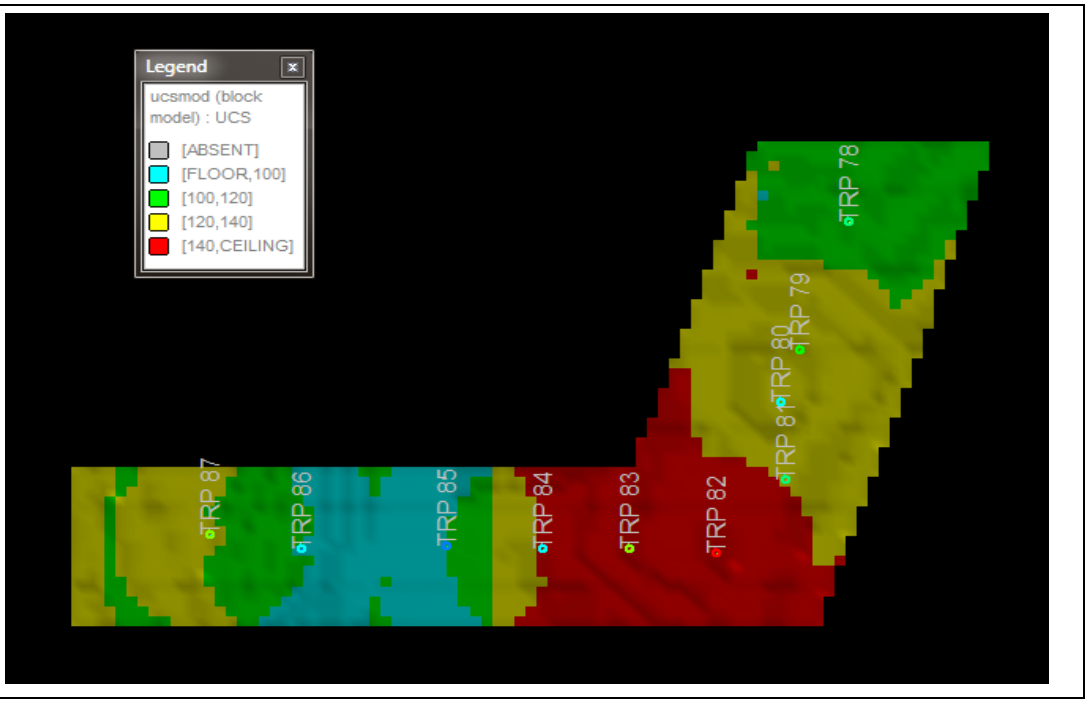

Figure 5.1.1_5 Borehole data distribution with the Kriging contours.

The following conclusions were drawn:

- The value of the uniaxial compressive strength has a coefficient of variation between 0.11 and 0.33.
- Spot samples from individual boreholes could lead to misleading mean values.
- Samples were most likely degraded if obtained from boreholes at great depth or in the immediate vicinity of highly stressed pillars.
- A greater number of samples is required for individual mines to obtain a reliable mean value.
- Samples taken in the vicinity of shear zones where the tectonic process degraded/ disturbed areas resulted in degraded strength values. An example was the presence of thrust faults in the immediate vicinity of the UG2. The thrusting observed in some chrome mines would most likely have degraded the *in situ* chrome and would explain the general instability of the mines under these conditions.
- In this research, all the available values from a specific mine were used to obtain some mean value.
- Shortcomings could be overcome by incorporating the variability in statistical models to determine ranges of safety factors rather than single numbers.

5.1.2 Geological Strength Index

The Geological Strength Index is a function of the frequency and orientation of fractures in the rock mass as well as the number of different fracture systems and their different orientations.

Hoek and Marinos, 2000, give the generalised value for GSI for ophiolites in Figure 5.1.2_1 (Ophiolites were chosen because they were the closest relation to the ultrabasic rock suite in the Bushveld sequence).

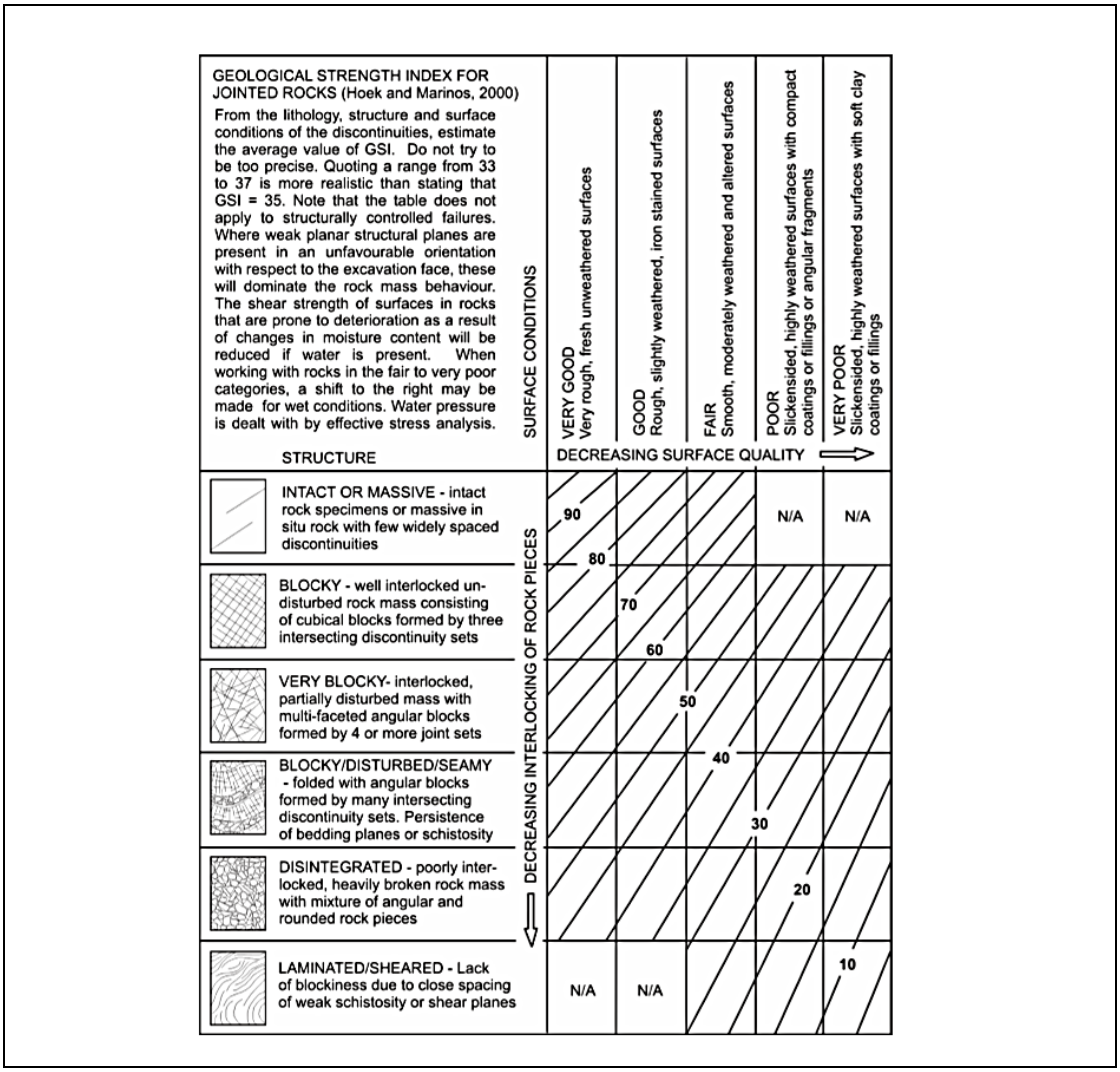

Figure 5.1.2_1 GSI values for blocky ground (Hoek and Marinos, 2000)

GSI values for the Bushveld rocks generally fell within the 70 to 90% region but needed to be determined individually for every site.

Equations 5.2, 5.3 and 5 .4 are all a function of the Geological Strength Index value. An incorrect assessment influenced the entire Hoek-Brown criterion. A reduction of 10, say from 90 to 80, reduced the pillar strength to approximately 0.2 of the “competent” rock mass. This effect is illustrated in the *FLAC2D* model development section.

5.1.3 m_i Value

The m_i value has a strong influence on the results obtained using the Hoek-Brown failure criterion. A simple method of determining the value is to use the tabulation given in Table 5.1.3_1, (Hoek and Marinos 2000).

Table 5.1.3_1.: m_i Values for sedimentary, metamorphic and igneous rocks as published by Hoek and Marinos, (2000)

	Rock type	Class	Group	Texture			
				Coarse	Medium	Fine	Very fine
SEDIMENTARY		Clastic		Conglomerates * Breccias *	Sandstones 17 ± 4	Siltstones 7 ± 2 Greywackes (18 ± 3)	Claystones 4 ± 2 Shales (6 ± 2) Marls (7 ± 2)
		Non-Clastic	Carbonates	Crystalline Limestone (12 ± 3)	Sparitic Limestones (10 ± 2)	Micritic Limestones (9 ± 2)	Dolomites (9 ± 3)
			Evaporites		Gypsum 8 ± 2	Anhydrite 12 ± 2	
			Organic				Chalk 7 ± 2
METAMORPHIC		Non Foliated		Marble 9 ± 3	Hornfels (19 ± 4) Metasandstone (19 ± 3)	Quartzites 20 ± 3	
		Slightly foliated		Migmatite (29 ± 3)	Amphibolites 26 ± 6	Gneiss 28 ± 5	
		Foliated**			Schists 12 ± 3	Phyllites (7 ± 3)	Slates 7 ± 4
IGNEOUS		Plutonic	Light	Granite 32 ± 3 Granodiorite (29 ± 3)	Diorite 25 ± 5		
			Dark	Gabbro 27 ± 3 Norite 20 ± 5	Dolerite (16 ± 5)		
		Hypabyssal		Porphyries (20 ± 5)		Diabase (15 ± 5)	Peridotite (25 ± 5)
		Volcanic	Lava		Rhyolite (25 ± 5) Andesite 25 ± 5	Dacite (25 ± 3) Basalt (25 ± 5)	
			Pyroclastic	Agglomerate (19 ± 3)	Breccia (19 ± 5)	Tuff (13 ± 5)	

Qi, et al. (2012), in an excellent summary of the current state of knowledge on the m_i value, stated that the strength parameter m_i was dependent on the minerals in the intact rock and that there were mainly two methods for determining m_i.

- Based on statistical data.
- Based on experiments.

The statistically determined values determined by Hoek and Marinos (2000) are summarised in Table 5.1.3_1 which for igneous rocks covers a range between 20 and 35.

In addition to the above, Table 5.1.3_ 2 is a summary of m_i values published by Qi et al, (2012) all falling within the range given above.

Table 5.1.3_2: m_i Values for igneous rocks (Qi et al, 2012)

Rock type	m_i Mean	Std Dev.
Norite	20	5
Peridotite	25	5
Gabbro	27	3
Diabase	15	5
Granite	32	3
Diorite	25	5

The m_i values for the Bushveld rocks obtained using the RocLab programme differed significantly from those listed in the table 5.1.3_2, with the average and standard deviation given at the bottom of the Table 5.1.3_3 (Impala Mine data base.)

Note that the highest value for m_i calculated by the RocLab programme, as well as the modification of m_i to m_b, was limited to a value of 50. (The reason and logic behind this falls outside the scope of the research but needs investigation.)

A plot of the m_i value against the uniaxial compressive strength of anorthosite is shown in Figure 5.1.3_1. (Impala data bank, 2012). It appears that there is a negative correlation between the uniaxial compressive strength and the m_i value; the higher the uniaxial compressive strength the lower the m_i value. This is an indication only since the correlation is very low.

The influence of variation in m_i values on the pillar strength, consisting of a rock mass having a uniaxial compressive strength of 130 MPa and GSI = 90, was provided by the average pillar stress at failure, Table 5.1.3_4 and Figure 5.1.3_2.

m_i values vary between 10 and 50 (chromitite) in Table 5.1.3_3. The values in Table 5.1.3_4 illustrate the effect of variation of m_i on the pillar strength. The difference in the average pillar stress at failure between two m_i values say 30 and 50 is 20 MPa, a 30 % difference, was big enough to make a material difference in the required stable pillar size.

Table 5.1.3_3: m_i values obtained from tri-axial tests using the RocLab programme

	Anorthosite		Pyroxenite		Norite		Pegmatoid		Chromitite	
	UCS MPa	m_i	UCS MPa	m_i	UCS MPa	m_i	UCS MPa	m_i	UCS MPa	m_i
	70	50	162	8.1	180	19	104	18	87	50
	147	50	196	3.1	123	50	67	15	44	50
	157	50	104	40	228	27	158	13	45	50
	165	40	107	34	170	32	150	9.5	108	30
	165	39	139	29	153	26	164	29.5		
	176	50	156	8.5	143	24	98	7.5		
	177	50	141	22						
	178	40	155	18						
	185	34	59	31						
	192	48	130	18						
	193	50	132	24						
	194	50	110	19						
	218	16	174	10						
	222	35	45	35						
	223	24								
	225	42								
	229	11								
	248	29								
Average	187	**39**	129	**21**	166	**30**	124	**15**	71	**45**
Standard Deviation	39	**12**	40	**11**						

No standard deviation is given where less than 10 values are available.

Hoek (2012) stated that the most probable cause for the high m_i values listed could be due to one or more of the following:

- Lack of triaxial equipment capable of applying confining pressures of up to 50% of the UCS of the samples,
- No attempt to determine or estimate the tensile strength of the intact rock samples,
- Poor maintenance of laboratory equipment including lack of regular calibration which could result in incorrect results,
- Poor specimen selection and preparation resulting in premature or atypical failure,
- Insufficient number of tests on any one rock type.

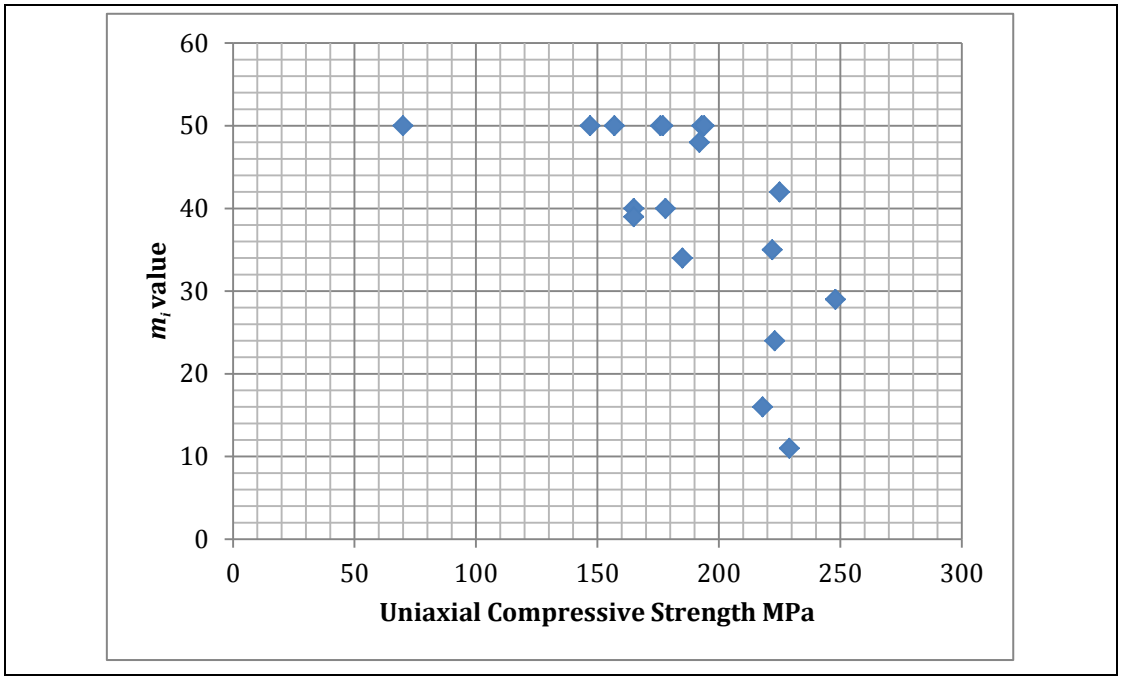

Figure 5.1.3_1: Relationship between the m_i value and the uniaxial compressive strength of anorthosite

Table 5.1.3_4: Influence of the m_i value on the pillar strength (GSI=80)

m_i	m_b	*pillar strength* MPa
10	7	47
20	14	58
30	21	65
40	28	73
50	35	77
60	42	84
70	49	88
80	56	91

An analysis of the data obtained using the RocLab programme giving m_i values of approximately 50 generally indicated that one or more of these problems could be present and that the results were questionable. (Hoek, 2012)

In conclusion, Hoek (2012) stated that the uniaxial strength divided by the tensile strength should be used for obtaining the value of m_i.

,

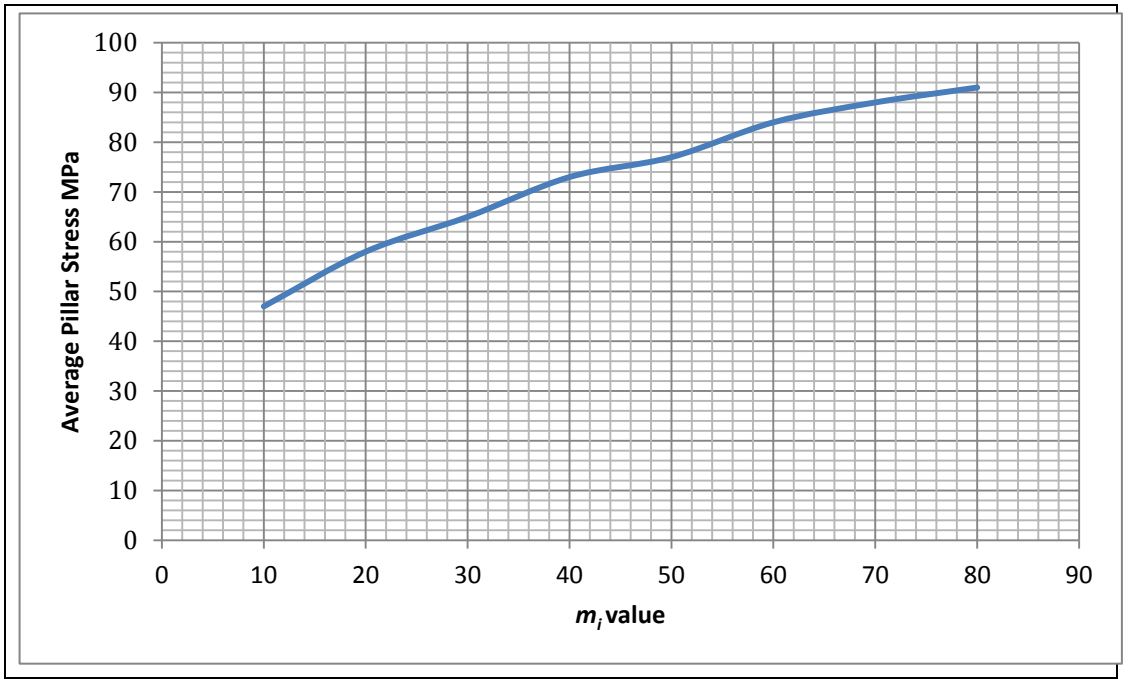

Figure 5.1.3_2 Increase in strength with increase in m_i value (data from Table 5.1.3_4).

Qi et al (2012) investigated the m_i value in detail by modelling and stated that:-

"*Apart from the conceptual starting point provided by the Griffith theory, there are no fundamental relationships between the empirical constant* m_i *included in the strength criterion and any physical characteristic of the intact rock"*

Previous studies as well as experimental results are summarized in the equations 5.7 to 5.11, (Qi et al, 2012):-

$$m_i = (\sigma_1 - \sigma_3)^2 - {\sigma_c}^2/\sigma_c\sigma_3 \qquad 5.7$$

$$m_i = \frac{\sigma t}{\sigma_c} - \frac{\sigma_c}{\sigma_t} \qquad 5.8$$

$$m_i = \frac{16\sigma_{tb}}{\sigma_c} - \frac{\sigma_c}{\sigma_{tb}} \qquad 5.9$$

$$m_i = 4\sin\theta/[(1-\sin\theta)(1+2\sin\theta)]^{0.5} \qquad 5.10$$

$$m_i = \frac{4\sigma_c}{[6\sin^2\theta + 11\sin\theta + 5 - \sigma_3]\left[\frac{3c}{\sin\theta}\right]} \qquad 5.11$$

Where

θ Instantaneous friction angle at zero normal stress.

σ_1 Maximum principal stress

σ_c Compressive strength

σ_{tb} Indirect Tensile strength

σ_t Direct tensile strength

m_i Values from statistical data are summarized in Table 5.1.3_1.

According to Qi, et al. (2012) the results from a particle flow model indicated that the grain size played an insignificant part but that the contact model as well as the normal to shear strength ratio had the main effect on the m_i value.

Based on all the above observations, it is concluded that the m_i value needs to be investigated in greater detail. Because of the absence of sufficient tensile strength test values, the present study used values are based on empirical mean values, Table 5.1.3_1.

The m_b value is obtained from the m_i value and is a function of the GSI value, equation 5.2. As pillar failure occurs, the m_b value changes and becomes the residual m_r value. The residual m_r value creates a similar problem. Figure 5.1.3_3 is a plot of the average pillar stress for three values ofm_r, m_b constant, for the same basic data set for three different sized pillars.

Note for example for a 6 m pillar the difference for m_r of 2 gave a pillar strength of 73 MPa and at a m_r value of 7.5, 203 MPa - a significant difference. More research would be required to determine correct values for the residual m_r value.

The m_r value could also be determined by estimating the GSI value of a failed pillar. The pillar in Figure 5.1.3_4 shows a cross section exposed by a cutting through a pillar which shows failure planes pervading the whole width. The estimated GSI value lies between 60 and 45, say 50. Hence the m_b value would be 3.354, and the m_r value 0.562, Table 5.1.3_5.

An alternative approach was that given by Joughin et al (2000) where the $m_r$and s_r values were calculated using the equations given 5.12 to 5.15.

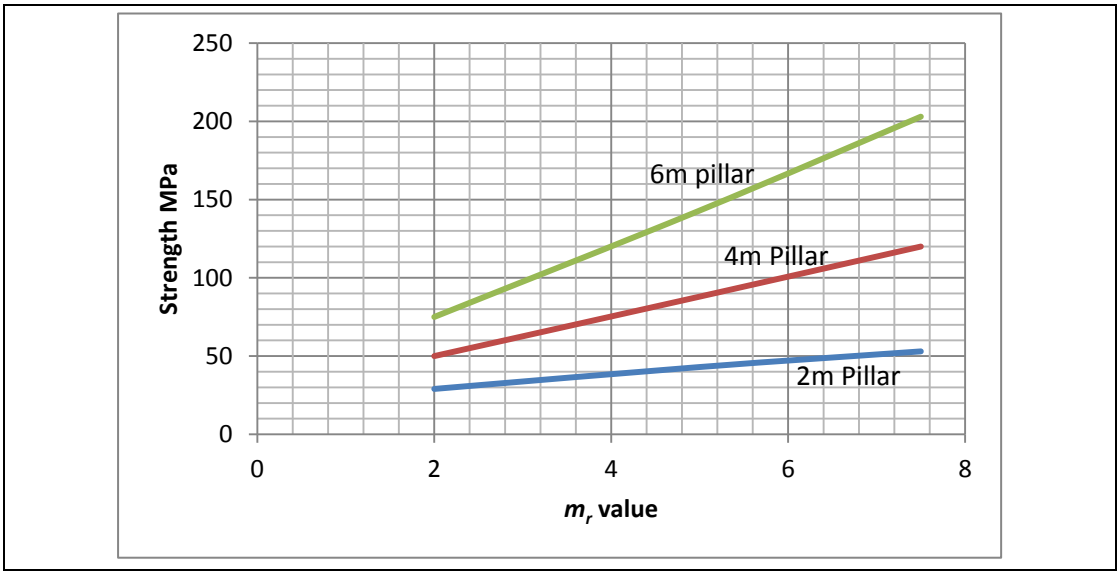

Figure 5.1.3_3 Change in pillar strength for different residual m_r values

$$m_b = m_i \, e^{(GSI-\left(\frac{100}{28}\right))} \qquad 5.12$$

$$m_r = m_i e^{(GSI-\left(\frac{100}{14}\right))} \qquad 5.13$$

$$s = e^{(GSI-\left(\frac{100}{9}\right))} \qquad 5.14$$

$$s_r = e^{\left(GSI-\left(\frac{100}{6}\right)\right)} \qquad 5.15$$

Table 5.1.3_5

Variation m_b and m_r values using the equations from Joughin et al (2000) and for a constant m_i of 20

GSI	m_b	s	m_r	s_r
100	20.000	1.0000	20.000	1.0000
90	13.993	0.3292	9.791	0.1889
80	9.791	0.1084	4.793	0.0357
70	6.850	0.0357	2.346	0.0067
60	4.793	0.0117	1.149	0.0013
50	3.354	0.0039	0.562	0.0002
40	2.346	0.0013	0.275	0.0000



Figure 5.1.3_4 Example of fracturing and estimated GSI value of 80 for a pillar at Impala Platinum Mine.

Summary

The definition of rock mass properties used in the Hoek-Brown criterion requires serious attention.

For the back analysis described in Sections 9 and 10, it was obvious that some definitive values had to be used. The principles adopted here were as follows:

- The mean uniaxial compressive strength from available samples for the property were used.
- The Geological Strength Index could be estimated.
- The m_i value, hence the m_b and m_r value as well, posed the greatest problem. For the lack of any definitive data, the value used was based on the value for igneous rocks in Table 5.1.3_1, the Roclab programme and the m_r = 0.5(m_b).

5.2 Other relevant rock mass properties: Young's Modulus and Poisson's Ratio

FLAC2D modelling not only requires the Hoek-Brown parameters but the bulk and shear moduli of the various rock types which were derived from the Young's modulus and the Poisson's ratio.

Figure 5.2_1 and Figure 5.2 _2 are two examples of the stress-strain diagrams of chromitite and pyroxenite. The examples were chosen to illustrate the effect of the non-linearity for both the axial and lateral strain variations on the value of the two "constants".

This difference is a common feature of the rocks tested and the problem of non-linearity is usually dealt with by using either the secant or tangent values of the graphs definition given in Figure 5.2 _3.

Inspection of the stress-strain graphs for chromitite and pyroxenite showed a significant difference in the value of the secant and tangent moduli for various positions on the graph. The tangent modulus was usually reported for 50 or 70% deformation.

160 experimentally determined values of the tangent and secant modulus for the Bushveld rocks were examined and the summarized results showed that for the relevant Bushveld rocks, 75% of the specimens tested reached a Poisson's ratio of 0.5 before achieving peak strength, appendix II. This was an indication that the specimen tested exhibited non elastic behaviour (fractured) before reaching peak strength. The non-linear behaviour was evident over the full cycle of the laboratory test which could indicate a very early onset of micro to macro- fracturing

The effect of the variation of the Young's modulus would be accommodated by selecting the stress range under which a specific model was analysed and, accordingly, the relevant modulus selected. For instance, at a low stress level, the tangent modulus would be used while at high stress levels close to the failure point, the secant modulus would give the appropriate deformation values. The answer would, obviously, not be absolutely correct, but, at the time, no other approach had come to the attention of the author.

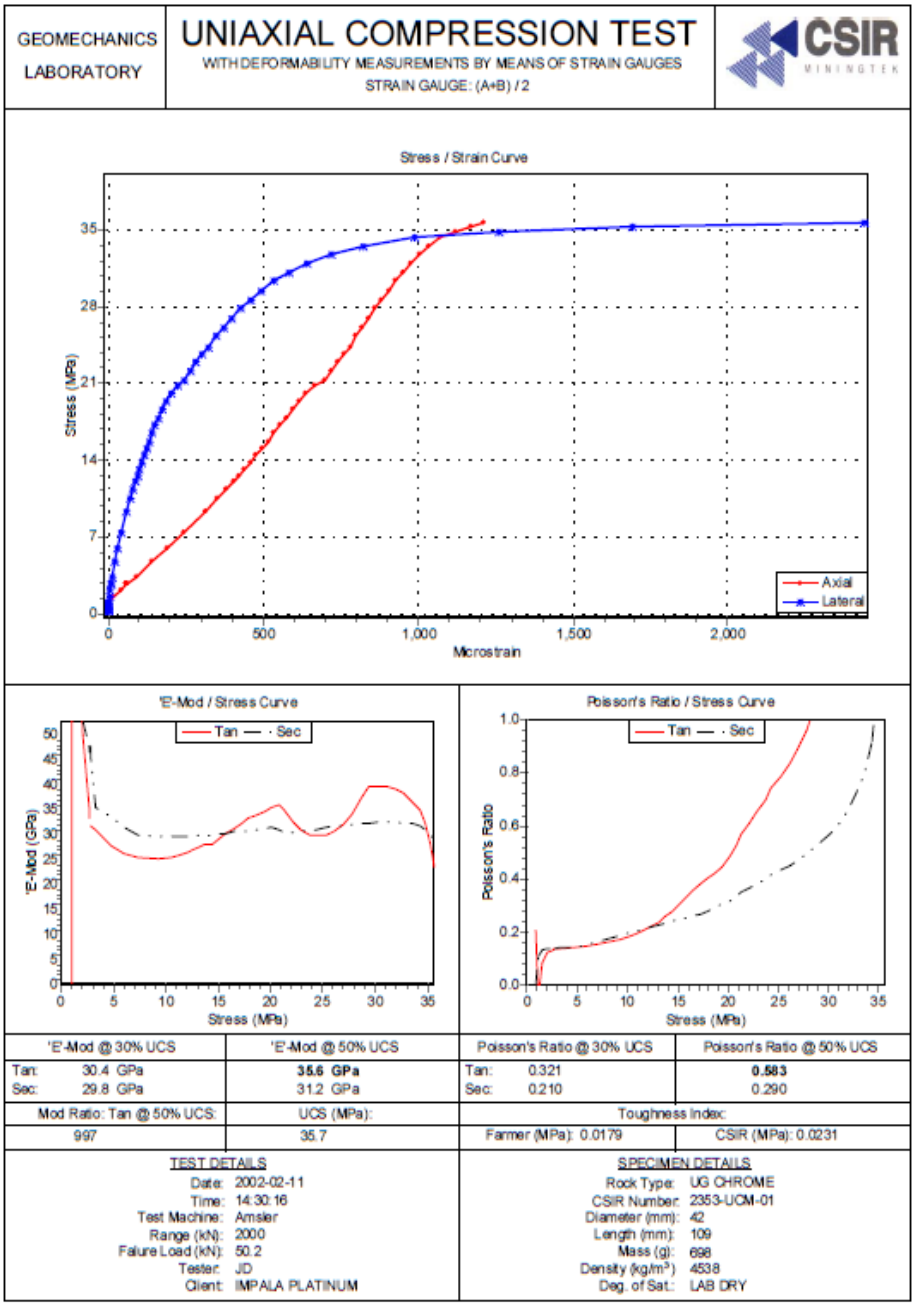

Figure 5.2_1 Stress-strain diagram of chromitite from Impala Platinum Mine

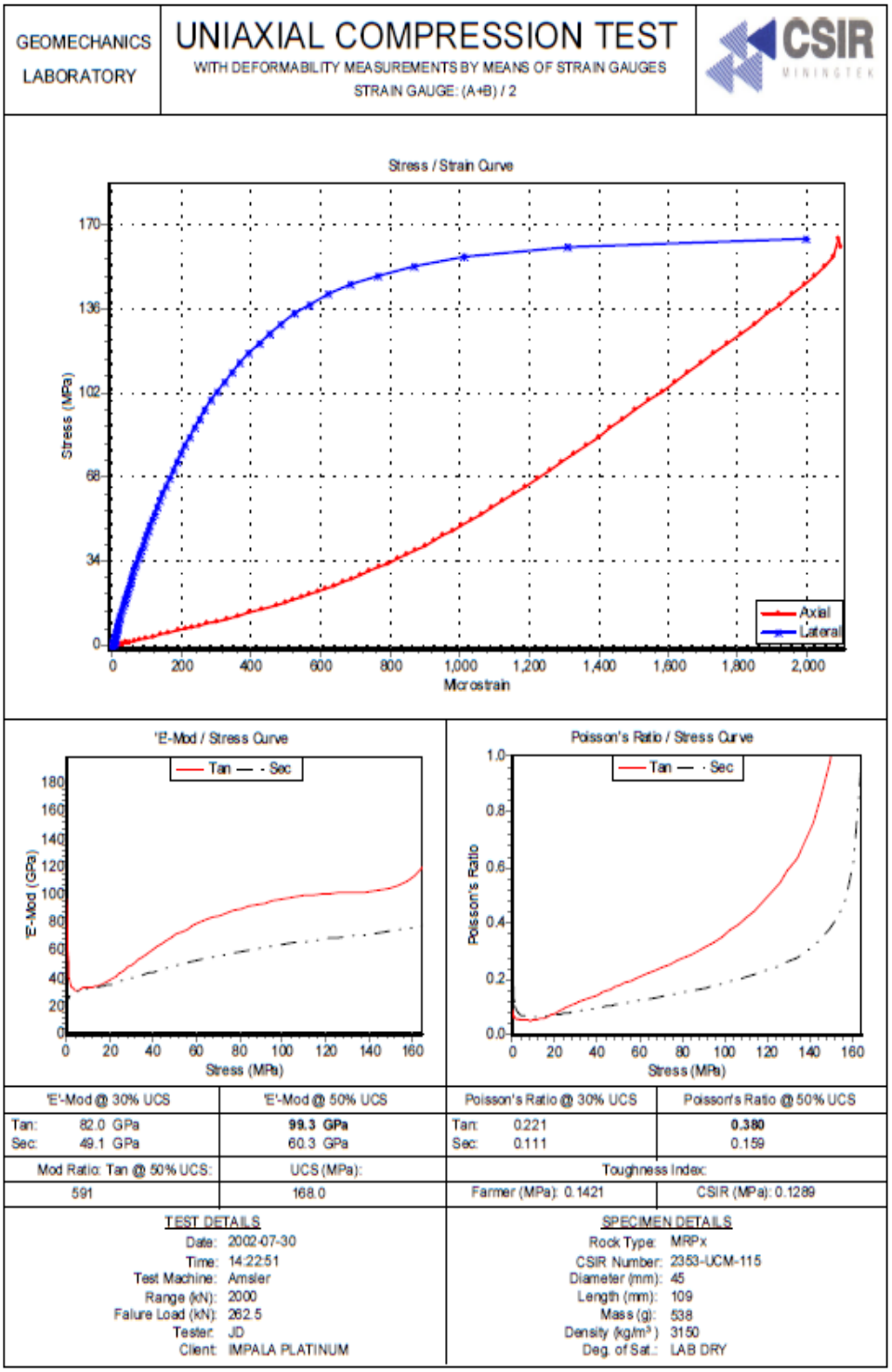

Figure 5.2_2 Stress-strain diagram for pyroxenite from Impala Platinum Mine

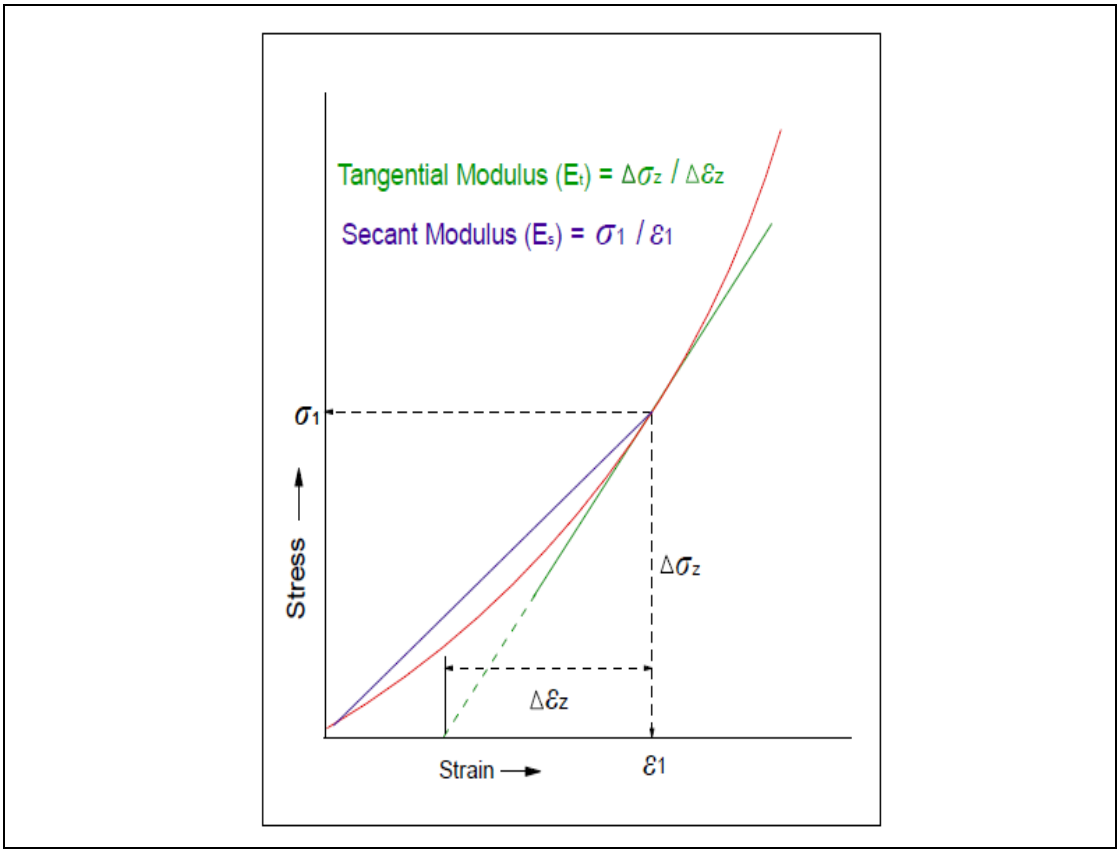

Figure 5.2_3 Definition of the tangent and secant modulus

6 DEVELOPMENT OF THE SYSTEM PILLAR EQUILIBRIUM CONCEPT (SPEC).

6.1 Combining pillar behaviour and local mine stiffness and model development

The current standard procedure for calculating the average pillar stress used the Tributary Area Theory which states that the average pillar stress is a function of the pillar area and the weight of the overburden.

The average pillar stress is obtained by dividing the vertical force by the tributary area of the remaining pillars. It is valid for situations when the mined out span is greater than the depth of mining.

The method is a gross over-simplification as the effective “stiffness” of the hanging-wall rock mass and the pillar deformation was ignored therefore it tends to over-estimate the real load on pillars.

Pillar and strata stiffness has been discussed by Ryder and Ozbay (1990) in the design of stable, post-failure pillars at shallow depth. The proposed method was not generally adopted mainly due to its apparent complexity. Other authors (Zipf, 1998) also used the concept to construct a post-failure stability criterion in pillar design similar to the concept proposed by Ryder and Ozbay (1990).

Van der Merwe (1999) published a conceptual diagram that delineated various stability scenarios in coal mines. According to him, for pillar failure to occur, the following two requirements had to be satisfied:

- The pillar had to be loaded to beyond its load-bearing capacity,
- The overburden had to deflect sufficiently to totally deform the pillars.

The first requirement received almost all of the attention but only scant attention was paid to the stiffness and strength of the overburden.

Two essential stability parameters, the Pillar Safety Factor (PSF) and the Overburden Stability Ratio (OSR) were introduced by van der Merwe (1999) shown in Figure 6.1_1.

The four quadrants are:-

- I where both the OSR and PSF have a value in excess of 1.0, reacting elastically.
- II where the PSF is in excess of 1, hence stable, but the strata is in a state of failure.
- III both the pillar and the strata are in a state of failure
- IV where pillar is in the failed state but the hanging wall in the elastic state.

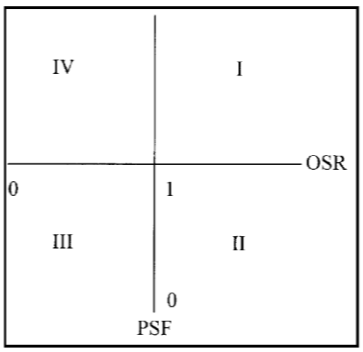

Figure 6.1_1 Plot of OSR (Overburden Stability Ratio) and PSF (Pillar Safety Factor) after van der Merwe, 1999

The current research confined itself to the area I where both the pillar and the strata in the hanging wall remained in the elastic state. Although the proposed concept was limited to the pre-failure part of pillar design, it does not exclude its extension into the post-failure regime.

The principle of strata/pillar "stiffness" interaction is illustrated in Figure 6.1_2 where equally spaced springs, with similar moduli, support a beam; resulting in an even convergence. If, however, the springs had different stiffness's, the hanging wall/loading beam would deform. However, the amount of the deformation would depend on the strata stiffness as well as the variation in spring/pillar stiffness.

The concept could be extended to the extreme case where the loading strata stiffness was reduced to a very low value, the deformation for different spring resistances is illustrated in Figure 6.1_3.

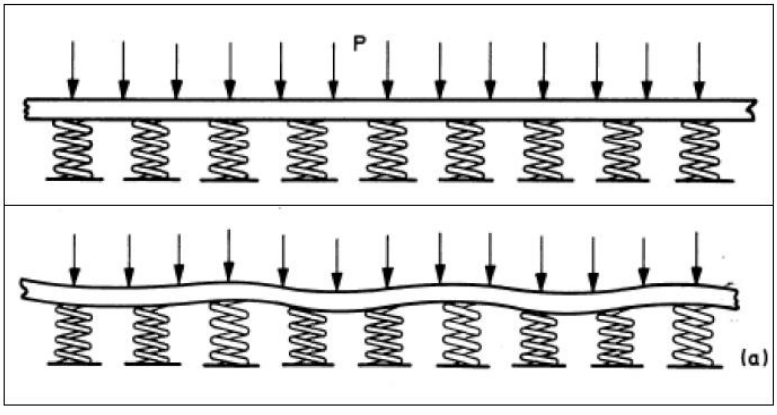

Figure 6.1_2 Variation in hanging wall response to different strength springs. (Salamon and Oravecz, 1976)

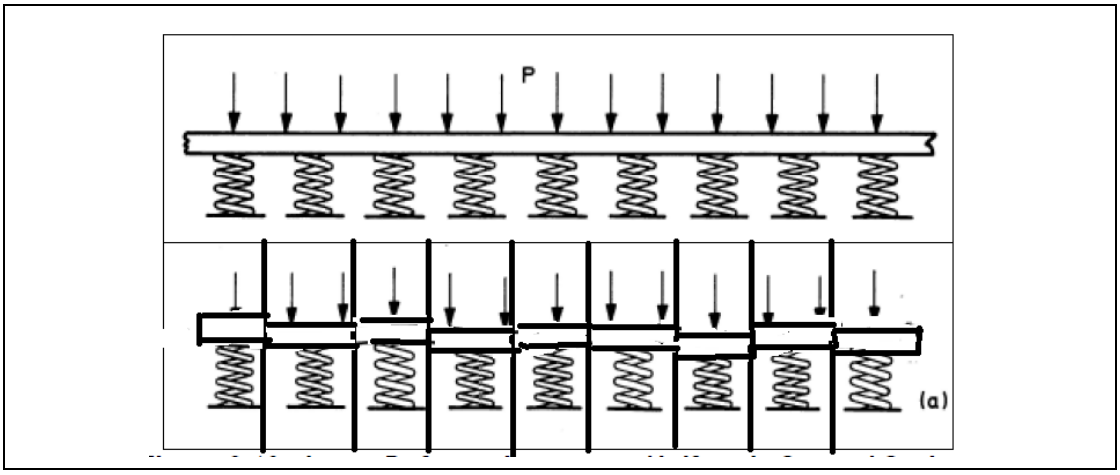

Figure 6.1_3 Modified hanging wall response for different strengths springs for a totally "stiff" hanging wall (top) and a totally "soft" hanging wall system (bottom)

The two systems depicted in Figure 6.1_2 and Figure 6.1_3 illustrate the difference between a very stiff hanging wall and a very soft hanging wall. The first can be seen as a rigid steel platten supported by different strength springs. The load on the springs would be controlled by the deformation of the whole platten and the resultant reaction force of the springs would be a function of the sum of the spring stiffness, each one would have the same convergence but with different resistive force.

In the case of the very soft strata/hanging wall system, each spring would carry the total overburden load of the strip (area) assigned to it. This corresponds to the concept used in the Tributary Area Theory.

The actual condition experienced underground is a system in equilibrium consisting of pillars with different stiffness as well as variation in the strata stiffness; both resulting from a variations in geometry of the pillar and the overall extent of the excavation.

6.2 Defining local mine stiffness

The equilibrium concept can be quantified using the theory of elasticity. Rock masses in the Bushveld mines deform in an elastic manner as determined by Lougher and Ozbay (1995) at Impala Platinum Mine. Therefore, the deformation and stresses in the pre-failure region are predictable.

The local mine stiffness/strata stiffness is also referred to as the "Ground Reaction Curve" (GRC). The relationship between the ground convergence and the tunnel support pressure is based on an infinite plane strain model with the excavation sequence simulated by "unloading" of the tunnel boundary. The simplest such model assumes a circular tunnel and an initial homogeneous hydrostatic stress field in the plane, as was described by Detournay and Fairhurst (1982.) The concept has been extended to analyse unstable failure of pillars by Ryder and Ozbay (1990) and it is here further extended by including the pre-failure region.

The current research dealt with the pre-failure portion of the pillar design hence the theory of elasticity could be used to the point of pillar failure which allowed for the calculation of

accurate rock mass and pillar stresses and deformations. The only requirement is a knowledge of the Young's modulus, the Poisson's ratio of the rock mass and that of the pillar, if different.

Figure 6.2_1 is a schematic drawing of an infinitely long slot in the third dimension cut at a depth of h m below surface having a half span of l m.

The maximum elastic convergence of a tabular excavation at infinite depth can be calculated as follows, Budavari (1983).

$$d_i = 2\frac{[\sigma_y(1-v)l]}{G} \quad , \qquad 6.1$$

Where d_i= vertical or y-convergence, convergence.

l = Halfspan m

σ_y = Vertical primitive stress component

v = Poisson's ratio

G = Shear modulus of the rock

$$G = E/2(1+v) \qquad 6.2$$

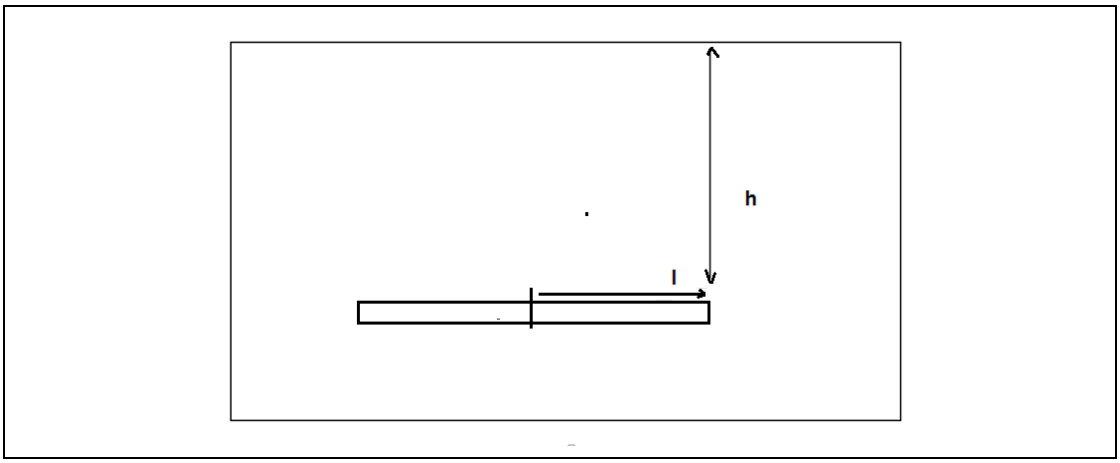

Figure 6.2_1 Schematic drawing of a slot mined at h m below surface with a half span of l m

The convergence of a tabular excavation at finite depth is given by Yilmaz, (2012):

$$d_i = \left(\frac{2(1-v)\sigma_y l}{G}\right) f(\alpha) \qquad 6.3$$

$$f(\alpha) = 1 + 0.41\alpha + 0.149\alpha^2 + 0.008\alpha^3,$$

Where $\alpha = 2l/h$

Equation 6.3 is valid for all geometries and will be used in the development of the system response.

The Young's modulus of the rock mass, as determined by Lougher and Ozbay (1995), is 68 GPa for a typical Bushveld mine on the Merensky reef.

The convergence at the slot centre can be calculated for any depth and span. For a value of the Young's modulus of 68 and 90 GPa, Poisson's ratio of 0.28, Figure 6.2_2 gives the centre convergence for an infinitely long slot at a depth of 650 m below surface.

The difference in convergence is a measure of the stiffness. The higher the Young's modulus, the stiffer the local mine system will be.

To prevent any vertical convergence, the total reacting force required had to be equal to the negative value of the product of the vertical primitive stress and the mined out area. Applying the same force, area times the vertical primitive stress, in the centre of the excavation would have the same effect, or alternatively, could consist of distinct individual units such as pillars of which the sum of the individual forces was equal to the total required resisting force.

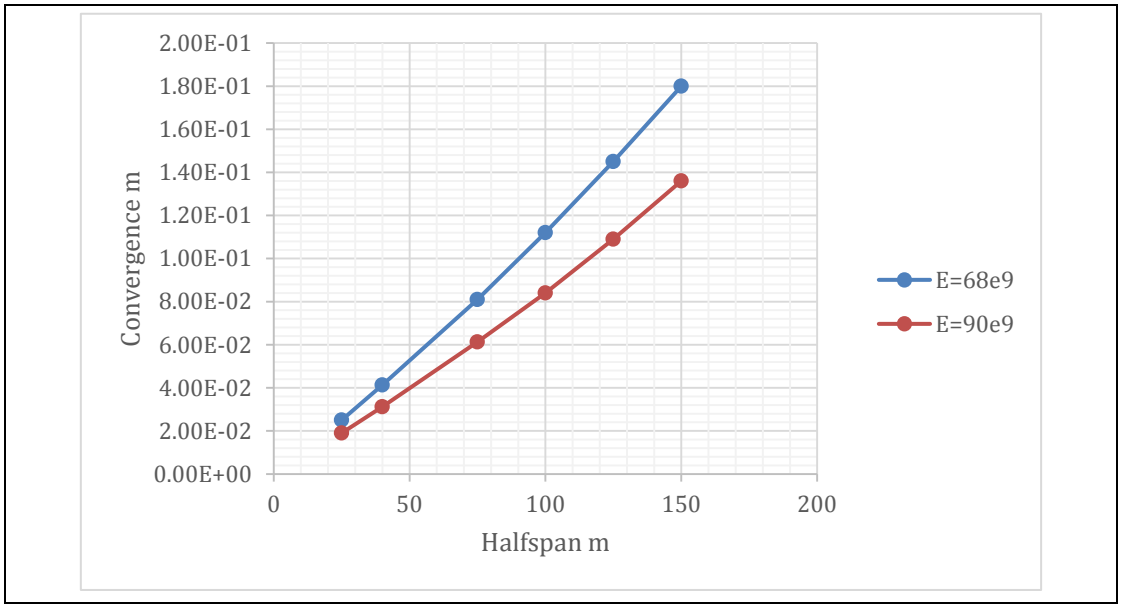

Figure 6.2_2 Convergence in a slot at a depth of 650 m for different halfspans. (Poisson's ratio = 0.28)

The above can be illustrated by assuming the following two extreme limiting conditions:

- If the resistive force was equal to the initial force acting over the projected mined area, the convergence would be zero.
- If the resistive force was zero, then the convergence would be as calculated by equation 6.3.

- Connecting these two points in a force/convergence graph gives a linear load line.
- Work done by Barczac et al (2009) shows that the load line is nonlinear with decreasing slope as the support resistance decreases, implying that increases in support capacity from low capacity to higher capacity, can produce significant reductions in convergence.
- The work done by Leach (2008) also shows a distinct curvature of the load line obtained from detail three-dimensional modelling.
- For the purpose of the current investigation, a simplified linear trend is adopted and to be accurate, detail unloading curves need to be modelled.

In the above example:-

For a depth of 650 m below surface and a mined out span of 80 m, equation 6.3 resulted in the convergence at the centre of 0.042 m for a Young's modulus of 68 GPa and a Poisons ratio of 0.28 in the absence of support.

At the other extreme, for the convergence to be zero, the resisting force had to be equal to the force which is:

$\sigma_v = 650 * .0029*10$ 6.4

$= 18.85$ MPa.

With a strip of 80 m by 1m wide mined, the required force would be:-

Force $=18.85*80*1$ 6.5

$= 1456$ MN

Assuming for simplicity that the overburden response is linear, the force-convergence curve will be as shown in Figure 6.2_3.

The curve in Figure 6.2_3 is referred to as the local mine stiffness which is measured in MN/m, force per unit of convergence. Alternatively, it is also referred to as strata stiffness (Ryder and Ozbay, 1990) which is nominally a property of the strata alone and directly proportional to the Young's modulus and Poisson's ratio of the strata but also influenced by the mining geometry as well as local structural disturbances.

Note: The convergence values calculated throughout the research would be for an infinitely long slit in the third dimension, not that of the plan dimension on the mine. The result of this assumption was that the convergence would be a maximum value. By introducing the third dimension, the convergence would be less than that assumed in the research with the effect of decreasing the slope of the system curve, resulting in a "stiffer" system.

Figure 6.2_4 was drawn for 4 different spans. The slope would remain the same for the same Young's modulus and Poisson's ratio. Changing the Young's modulus or the Poisson's ratio would either "soften" or "stiffen" the system.

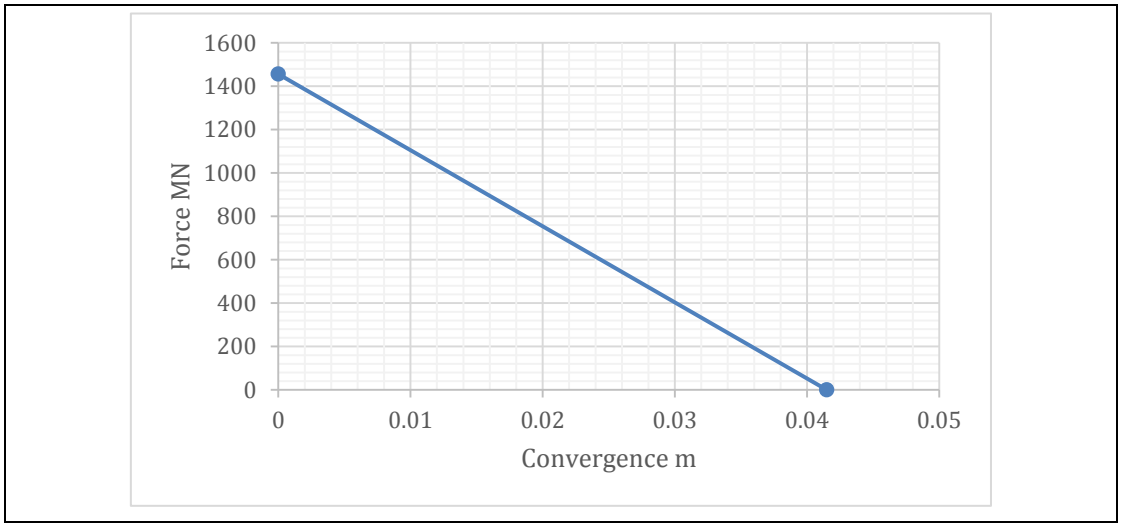

Figure 6.2_3 Force convergence diagram for a slot 80 m wide for a Young's modulus of 68 GPa at 650 m below surface

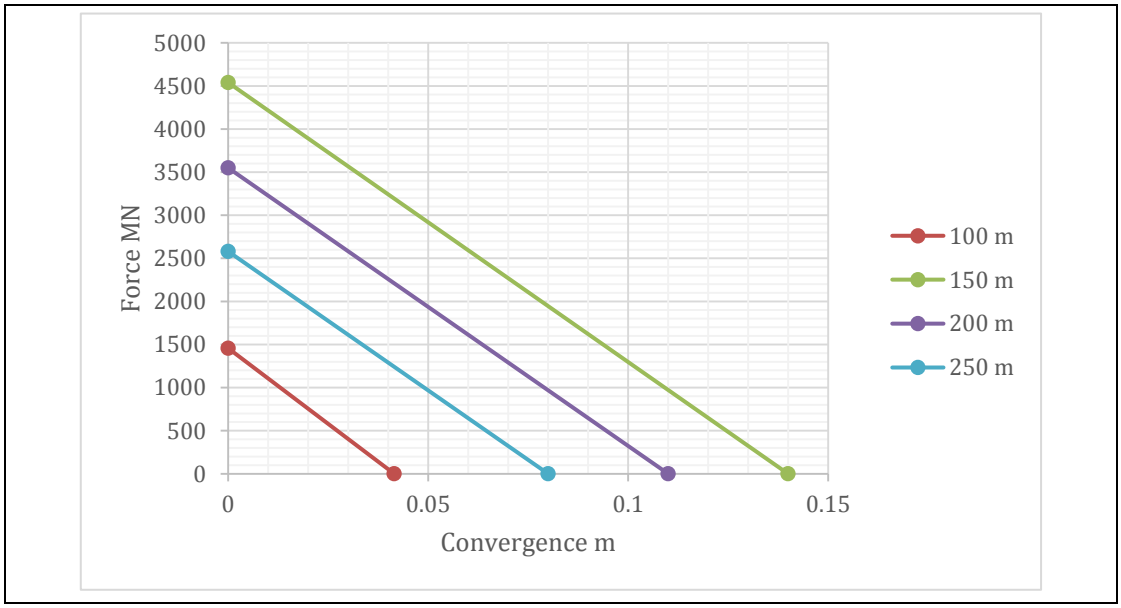

Figure 6.2_4 Local mine/strata stiffness for various spans

To reiterate, all the above was based on the theory of elasticity and is essentially correct for the intact rock mass.

6.3 Combining pillar and strata/mine stiffness

The support resistance is the sum of the pillar/pillars resistance left in place. The support/pillar resistance curve could be drawn by using the Young's modulus of the pillar material, the pillar area and height for the different convergence values. Figure 6.3_1 is a plot of a pillar strength curve intersecting the system stiffness curve. The system is in equilibrium

at the intersection of the two curves. In this example, the pillar would be loaded to 410 MN at a convergence of 0.0037 m.

The pillar/strata system equilibrium point can be determined by the intersection point of two equations assuming the load lines to be linear.

The ground reaction curve given by:

$$F_g = m_g d_g + c_g \qquad 6.6$$

The pillar resistance curve for one or more pillars:

$$F_p = m_p d_p + c_p \qquad 6.7$$

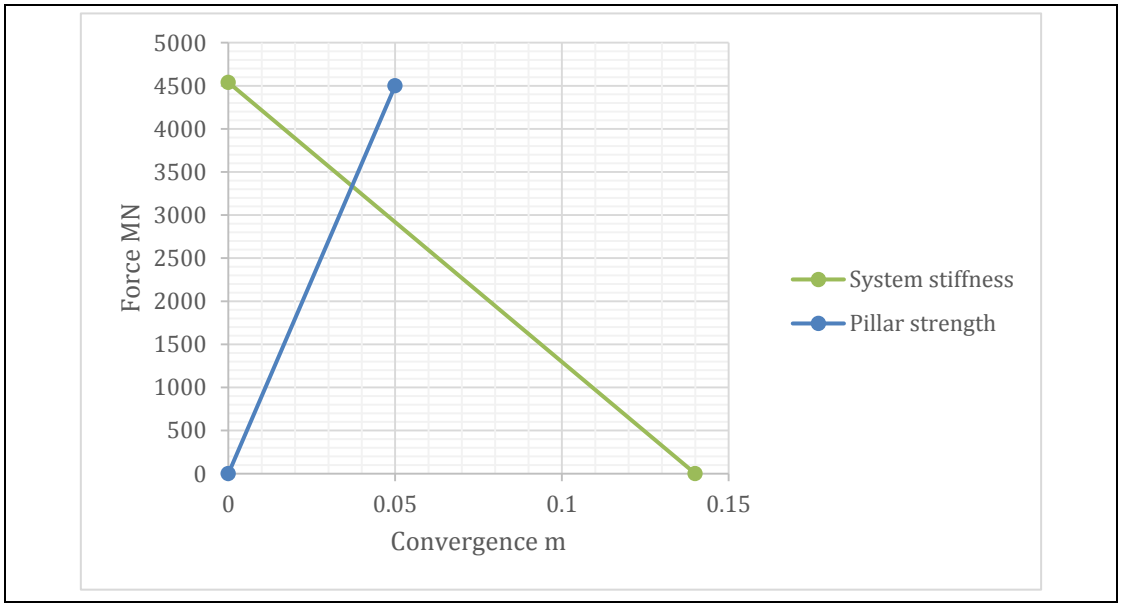

Figure 6.3_1 Pillar resistance curve.

Where F_g = System force

m_g = Slope of the ground reaction curve

d_g = system convergence

F_p = Force on pillar

m_p = pillar stiffness

d_p = pillar convergence

c_g= total overburden weight

The intersection point of the two curves represented by equations 6.6 and 6.7 represent the point where the system is in equilibrium; where the system load equals the pillar load, and the convergences are equal. The equilibrium force F, can then be described by:

$$F = \frac{C_g\, m_p}{m_p - m_g} \qquad 6.8$$

Since c_g has been shown to be the overburden total load over the mined out area,A_m it can be expressed as:

$$c_g = \sigma_v A_m \qquad 6.9$$

The slope of the ground reaction curve m_g, is:

$$m_g = -\frac{c_g}{d_i} \qquad 6.10$$

Where d_i is the maximum deflection of the opening as calculated by equation 6.3, equation 6.8 can be extended to:

$$F = \sigma_v A_m m_p / \left(m_p + \frac{\sigma_v A_m}{d_i}\right) \qquad 6.11$$

In practice, there would be a regular lay-out of approximately equally sized and spaced pillars. If the pillar centre distance is C, a strip with width, equal to C, can be created over a longer distance with span L.

The maximum deflection in the absence of pillars would be given by equation 6.3. The resistance required to prevent any deflection is the weight of the strip of width X over the panel length L.

The intercept of the system load/deflection curve C_g, is:

$$C_g = XLg\rho H \qquad 6.12$$

The slope of the ground reaction curve is then:

$$m_g = C_g / d_i \qquad 6.13$$

The pillars would still have individual convergence response. If the maximum pillar stress at failure is σ_{pm}, the pillar convergence at the point of failure is:

$$d_p = \frac{\sigma_{pm}}{E}.h \qquad 6.14$$

Where h is the stoping width.

The pillar load at failure is:

$$F_p = \sigma_{pm}.w^2 \qquad 6.15$$

Where w is the pillar width.

As there is a system of pillars, the total number of pillars across the panel contained in the width X, is $\frac{L}{X}$, then the total pillar resistance for the system is:

$$F_{pt} = F_p L/X \qquad 6.16$$

The slope of the pillar resistance curve is:

$$m_p = F_{pt}/d_p \qquad 6.17$$

The equilibrium force, F, is obtained by substituting the values of C_g, m_g and m_p in equation 6.8. The factor of safety is then:

$$\text{FOS}=F_{pt}/F \qquad 6.18$$

Equations 6.8 to 6.18 were incorporated in an Excel spreadsheet to facilitate calculating the average pillar stresses and convergences at the equilibrium point as well as the factor of safety.

The flow chart, Figure 6.3.2, is a schematic presentation of the steps involved in the *FLAC2D*/Hoek-Brown and the System-Pillar-Equilibrium-Concept (SPEC) methodology.

The factor of safety is determined by dividing the stress value of the pillar strength by the stress value of the intersection point of the system and pillar lines.

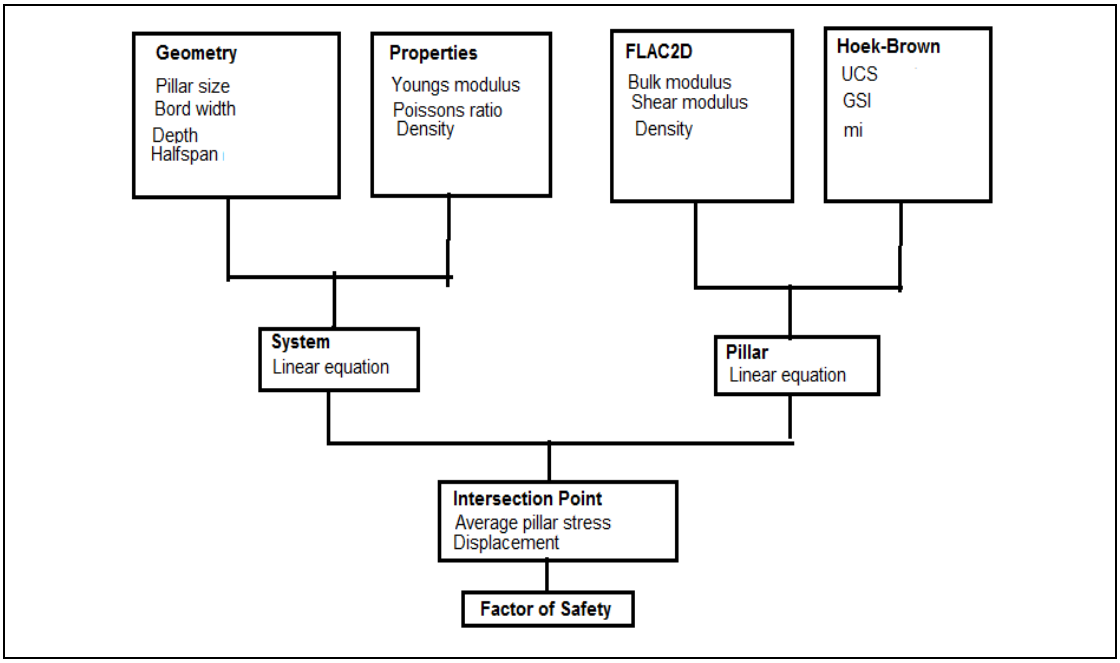

Figure 6.3_2 Schematic presentation of the SPEC methodology; calculation of system stiffness and the pillar strength curve.

Included in the formulation was the force imposed on the pillar before it was cut. The pillar was subjected to a virgin stress with a resultant y-convergence. For practical calibration reasons, the virgin component of the stress was included in the formulation but the y-convergence was taken as zero as all underground measurements commence with zero.

The pillar strength and rock mass deformation consisting of the two linear equations 6.6 and 6.7 were incorporated in the spreadsheet where the respective curves could be generated for a pillar system. (Figure 6.3_3)

Input data required for determining the factor of safety for pillar systems:

- Pillar strength.
- Pillar y-convergence/convergence at failure.
- System stiffness curve
- Depth below surface
- Percentage extraction

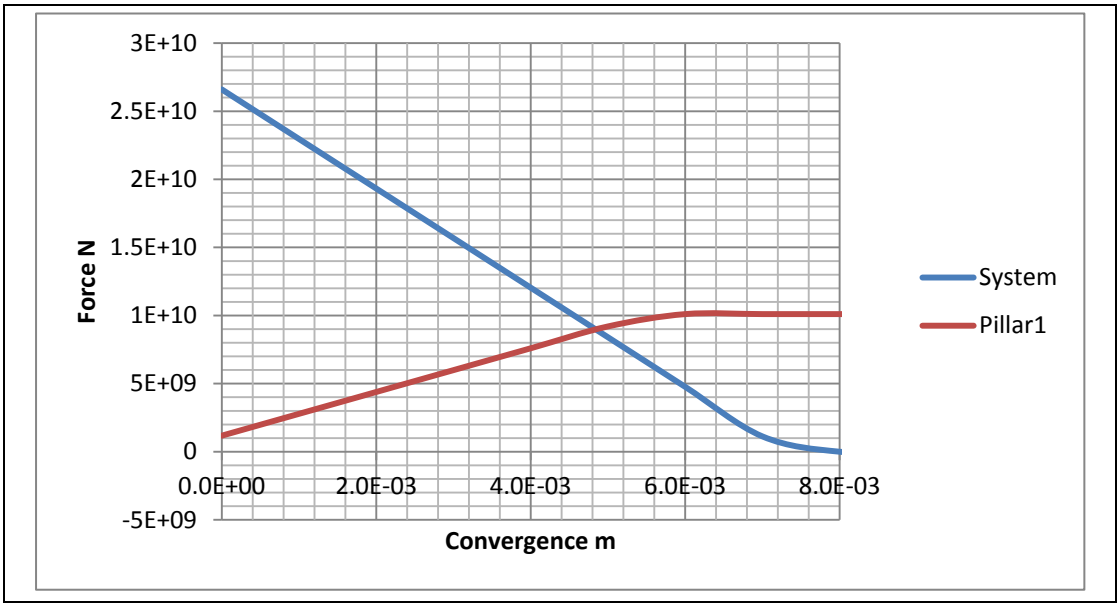

Figure 6.3_3 Local mine /strata stiffness curve with pillar strength curve.

Table 6.3_1 is a detailed listing of the required input data, they consist of geometrical as well as properties of the rock mass and pillar. The pillar strength and convergence were obtained using the *FLAC2D*/Hoek-Brown method.

Table 6.3_1.: SPEC input

Properties	Young's Modulus GPa	68
	Poisons ratio	0.29
	Density kg/m^3	2800
Geometry	**Pillar** Strike m	7
	Dip m	7
	Bord Strike m	15
	Dip m	15
	% Extraction	89,9
	Half Span m	50
	Stope width m	1,5
	Overburden m	500
Pillar	Pillar strength MPa	156
	Convergence m	6,9E-03
Hedley-Grant	k	80e6

The output is given in terms of the safety factor at the intersection point for the specific pillar and half span. To determine the load at the intersection point, the pillar resistance is the sum of the resistances of the pillar conforming to the lay-out for pillar width of 7 by 7 m and a bord width of 15 m. For comparison, the Hedley-Grant factor of safety, based on a k value of 80 MPa, is also shown.

Table 6.3_2: SPEC output

	Pillar
Average Pillar Stress MPa	130
Disp m	5,15E-03
FOS SPEC	1,20 at 100 m span
FOS Hedley-Grant	1,13

The difference between the SPEC result and the Hedley Grant equation is discussed in the following section.

6.4 Comparison with Hedley-Grant/Tributary Area Theory Methodology

The effect that the system geometry/stiffness/span interaction has on the factor of safety is shown by a comparison with the Hedley-Grant/Tributary Area Theory in Figure 6.4_1 illustrating the influence of the increase in span for a certain set of input parameters. The values for the factor of safety converge at great spans.

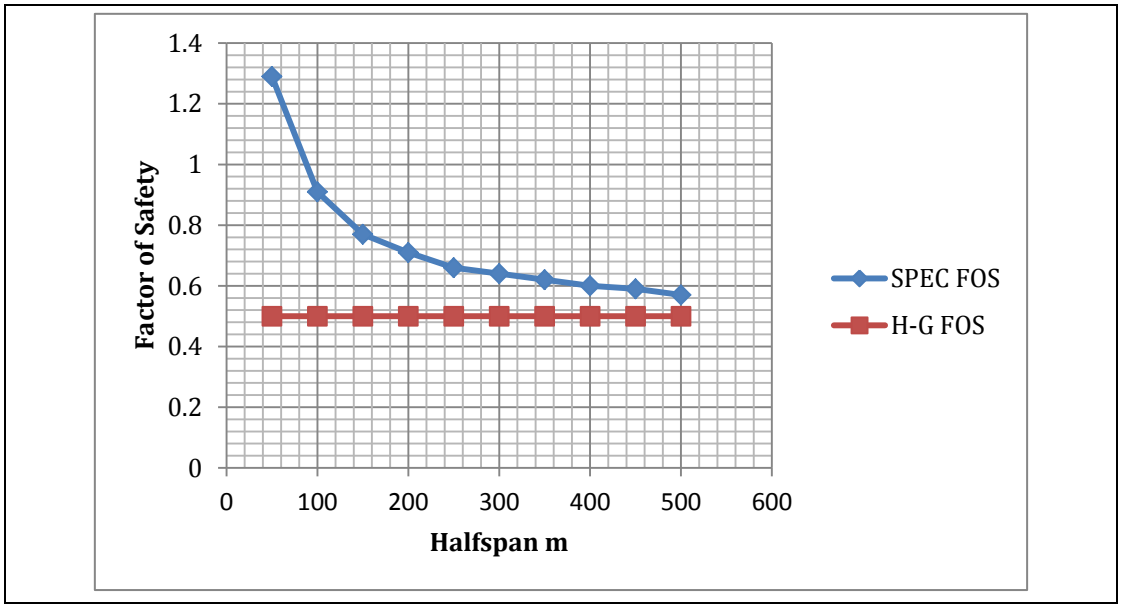

Figure 6.4_1 Comparison between Hedley-Grant/TAT and SPEC calculated factors of safety.

The SPEC method will be extremely useful in the base metal mining branch where the spans of mining areas are mostly limited to a few hundred meters in one of the mining directions or even less in limited span ore deposits.

The system/pillar stiffness methodology could also be used with the Hedley-Grant strength equation. Using the Young's modulus in conjunction with pillar strength determined by the Hedley-Grant equation, the convergence is obtained. The intersection point with the mine stiffness would determine a safety factor closer to reality than the standard procedure.

The influence of the pillar dimensions and stiffness on the pillar stress and convergence are automatically incorporated. The *FLAC2D/*Hoek-Brown simulation provides the pillar strength as well as the convergence of the specific pillar giving a "pillar modulus" which differs substantially with change in properties, dimensions as well as the position of the intersection point on the same stiffness curve.

6.5 Discussion on the equilibrium point

The equilibrium point has certain definite properties which can be used to analyse the development of a pillar area. There are three scenarios, Figure 6.5_1:-

- For a factor of safety greater than 1, the pillar is stable. The effect on the equilibrium point is that the convergence remains constant at the vertical convergence of the pillar at the forces exerted. For instance, for a pillar stress of 50 MPa, a factor of safety equal to 1.5, the y-convergence is 5e-3 m. The latter remains the same irrespective of the extent of mining. Only the overall force would increase. The force over the entire area would increase as the area expands, but so would the number of pillars creating the resisting force.
- For a safety factor of less than 1, the force will remain the same as mining expands, but the convergence will increase until the elastic convergence is limited due to "barrier pillars" or large abutments. This scenario is subject to the condition that the post-failure curve of the pillar has a flatter curve than the strata stiffness curve.
- If the negative pillar curve is steeper than the system curve, energy will become available and bursting conditions will be created. If the pillar line is flatter than the system curve, the pillar will fail in a stable manner; absorbing energy in the process.

Figure 6.5_1 summarises the conditions discussed above.

To summarise, for a factor of safety greater than 1, the force-convergence equilibrium point will increase on the force axis with the convergence constant, for a factor of safety equal to or smaller than 1.0, the force would remain constant and the convergence would increase.

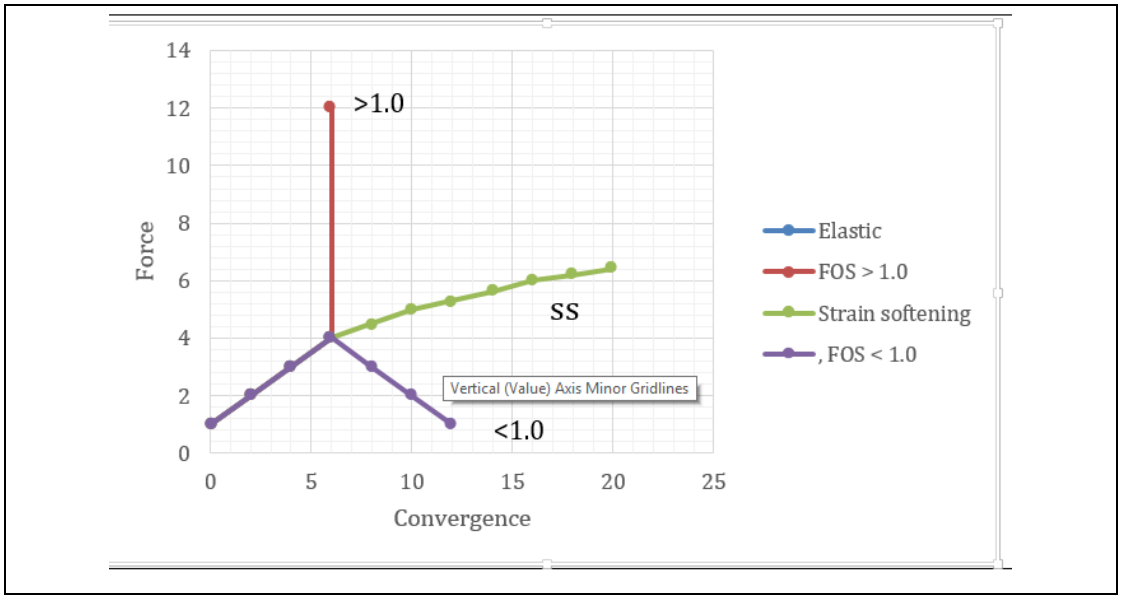

Figure 6.5_1 Force-convergence equilibrium point curves.

6.6 Use of the SPEC Methodology

The exercise illustrates the use of the SPEC method using the Hedley-Grant as well as the *FLAC2D*/Hoek-Brown pillar strength for a pillar and comparison of the resultant factor of safety for the two methods.

Using Hedley-Grant strength equation and TAT.

To use the SPEC methodology, the convergence of the pillar at the pillar strength was calculated using the Hedley-Grant strength equation, the Young's modulus and the pillar height to obtain the pillar convergence at peak stress.

Input data:-

Country rock and pillar Young's modulus = 68 GPa,

Depth below surface = 250 m

Density = 2800 kg/m^3

UCS = 130 MPa

k = 65 MPa

Pillar size = 6 by 6 m,

Pillar height = 2 m

Tributary area = 16*12 m.

Pillar strength = 95 MPa (Hedley-Grant equation)

Vertical convergence at failure for a 2 m high pillar:

$$\Delta l = (\sigma/E) * h \qquad 6.19$$

= (95e6/68e9)*2

= 2.72e-3 m

The vertical primitive stress is 7 MPa and at 91% extraction the average pillar stress is 77.8 MPa.

The standard Hedley Grant/tributary area theory factor of safety for the grid pillars is:

FOS= 95/77.8

= 1.22

Using the Hedley-Grant strength in the SPEC methodology.

Alternatively, the Hedley-Grant strength value could be used in the SPEC method with the input data shown in Table 6.6_1 and output in Table 6.6_2.

Conclusions from using the **Hedley-Grant strength** values and the overall rock mass Young's modulus were as follows:

- The SPEC system could be used as an adjunct to the current Hedley-Grant/TAT design methodology resulting in more realistic values than the original tributary area approach.
- The advantage of using the SPEC methodology was that the influence of geological losses and limited span, can be incorporated in the design.
- The safety factors will differ when using *FLAC2D/*Hoek-Brown calculated strength and convergence values for the pillar. The pillar stiffness differs for individual sized pillars

The output is shown in table 6.6_2 for a half span of 100 m. The convergence was calculated using the Young's modulus and the average pillar stress obtained from the SPEC method.

Table 6.6_1.: SPEC Input (Hedley-Grant equation)

Properties	Young's Modulus GPa		68
	Poisson's Ratio		0.29
	Density kg/m^3		2800
Geometry	Pillar	Strike m	6
		Dip m	6
		Height m	2
	Bord	Strike m	16
		Dip m	12
	Halfspan m		100
	% Extraction		90.9
	Overburden m		250
Pillar Stress and convergence	Strength MPa		95
	Convergence m		2.72e-3

Table 6.6_2.: SPEC Output / Hedley Grant

Hedley Grant	
k value	65
Pillar Strength MPa	95
Average pillar stress MPa	74
Factor of safety	1.28

Figure 6.6_1 illustrates the two curves.

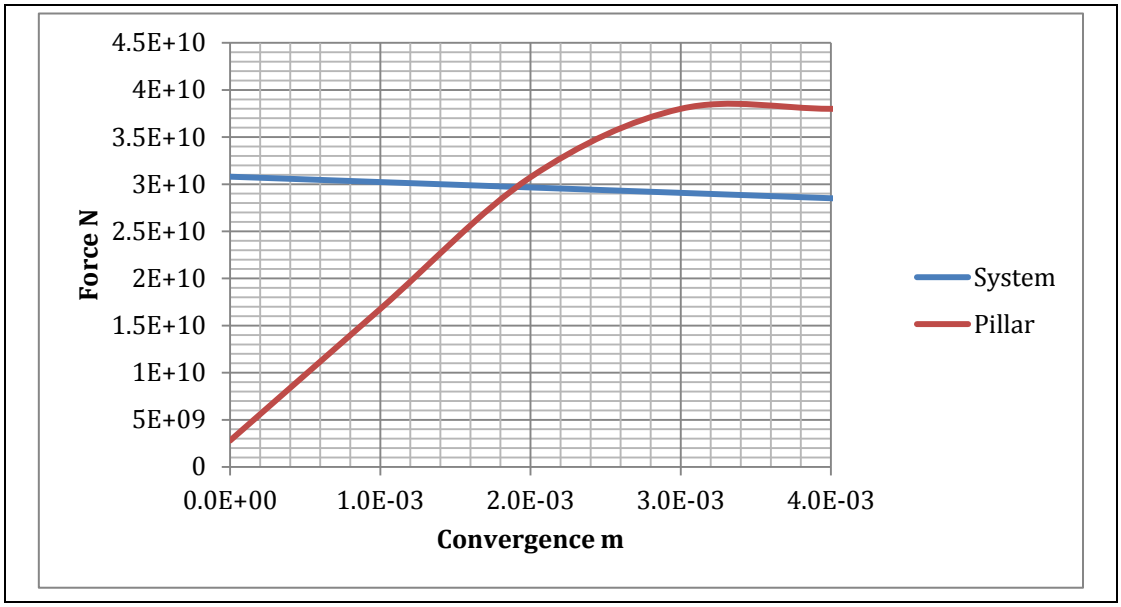

Figure 6.6_1 Graphical output for a halfspan of 100 m with a pillar strength calculated using the Hedley Grant equation in conjunction with convergence calculated using the Young's Modulus.

FLAC2D/Hoek-Brown strength value for pillars.

To improve on the methodology, the pillar strength needed to be determined analytically using the Hoek Brown criterion in conjunction with *FLAC2D*.

The standard *FLAC2D* programme instructions used for all the calibration runs is given in Appendix IV for pillar dimensions of 2 m high and a radius of 3 m.

The calculated pillar strength and y-convergence for the pillar dimensions and properties are given in Table 6.6_3.

Table 6.6_5 is a summary of the factors of safety for the three methods discussed:

- The standard Hedley-Grant/TAT method, 1.22.
- The Hedley-Grant/convergence SPEC method, 1.28.
- *FLAC2D*/Hoek-Brown SPEC method, 1.50.

Table 6.6_3: SPEC Input, using FLAC2D/Hoek-Brown strength and convergence values.

Properties	Young's Modulus GPa		68
	Poisson's Ratio		0.29
	Density kg/m^3		2800
Geometry	Pillar	Strike m	6
		Dip m	6
	Bord	Strike m	16
		Dip m	12
	Halfspan m		100
	% Extraction		90.9
	Overburden m		250
Pillar Stress and convergence	Strength MPa		107
	Convergence m		6.6e-3

The SPEC output gives a factor of safety of 1.50 for a halfspan of 100 m, Table 6.6_4.

Table 6.6_4: SPEC Output. *FLAC2D*/Hoek-Brown.

Average Pillar Stress MPa	71
Convergence m	3.97e-3
Factor of Safety	**1.50**

Table 6.6_5: Variation in factor of safety with change in span.

Halfspan m	*FLAC2D*/Hoek-Brown	Hedley-Grant/SPEC	Standard H-G and TAT
10	2.78	1,84	1.22
25	1.95	1,47	1.22
50	1.65	1,34	1.22
75	1.55	1,30	1.22
100	1.50	1,28	1.22

Figure 6.6_2 illustrates the factors of safety for the *FLAC2D*/Hoek-Brown and the Hedley-Grant/SPEC model including the standard Hedley-Grant/TAT value.

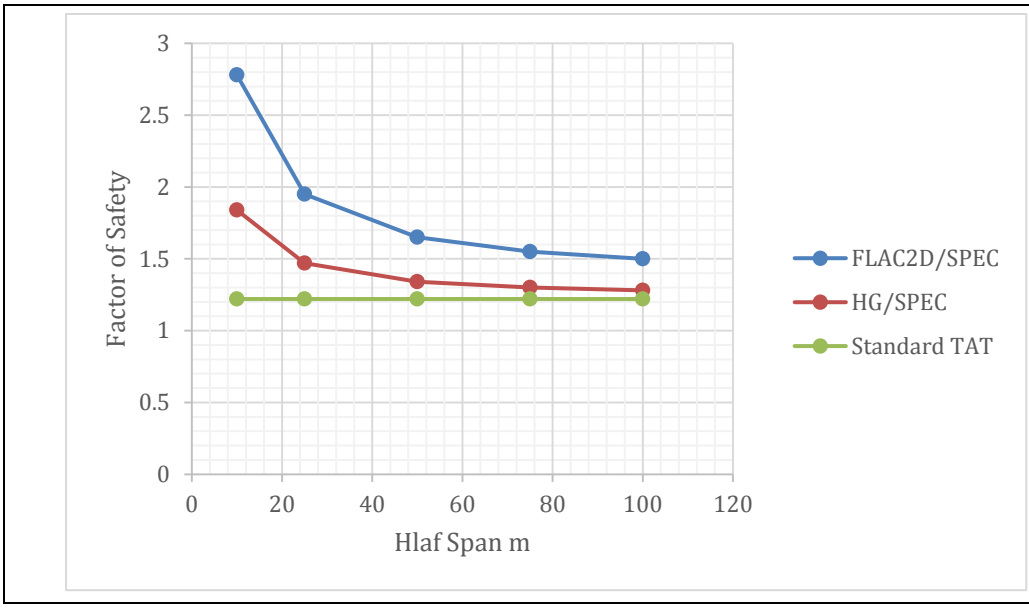

Figure 6.6_2 Comparison between Factor of Safety calculated using Hedley-Grant and FLAC2D/Hoek-Brown strength equation

The curves in Figure 6.6_2 illustrate that:

- The SPEC method can be used with strength/convergence data obtained by any method deemed reliable to the designer.
- For spans less than 150 m, half span of 75 m, there is a distinct possibility of increasing the percentage extraction.
- Extrapolating the curves in Figure 6.6_2, for spans in excess of 150 m the difference between the various methods is marginal.

6.7 Pillar stiffness

The concepts of pillar stiffness plays a significant part in the determination of the factor of safety using the SPEC method. The flatter the pillar stress/convergence curve, the lower the intersection point for the same loading system.

Pillar stiffness is defined by:

$$E_p = (\frac{load}{displacement})$$

$$E_p = \sigma A/di \quad , \qquad 6.20$$

Where σ = pillar stress

A = Pillar area

di = pillar shortening, convergence

Table 6.7_1: Pillar stiffness for a data set obtained using the *FLAC2D*/Hoek-Brown model.

Width m w	Height m h	w/h	Pillar strength MPa	Force MN	Disp e-3 m	Pillar Stiffness GN/m
2	2	1	44	176	2.41	73
3	2	1.5	68	612	4.35	139
5	2	2.5	130	3250	7.33	426
6	2	3	160	5760	10.24	562

The pillar stiffness increases with the width-to-height ratio and has an increasingly steeper slope shown in Table 6.7_1.

PART III

7 INTRODUCTION

Part III describes the calibration of *FLAC2D*/Hoek-Brown and the SPEC models developed in Part II. The procedure adopted in the calibration process consisted of the following:

- Selection of bord and pillar mines in the Bushveld where quantitative data was available that can be used for the calibration of the theoretical model.
- A brief description of the overall geological setting as well as detail for every mine, mining dimensions and origin of data for the mines selected.
- Description of relevant previous work done.
- Detail description of the underground site where the data was collected.
- Determination of the input parameters for the *FLAC2D*/Hoek-Brown model.
- Detail mining dimensions in the specific area.
- Creation of the theoretical SPEC model using the specific values that had been measured.
- Comparison of the two sets of values, observed and calculated, and drawing conclusions on the reliability of the theoretical model.

The general geological setting of the Eastern and Western Bushveld is discussed briefly detailing the geological column in the immediate vicinity of the Merensky and UG2 reefs.

The methodology used for the calibration consisted of three essential components that need to be calibrated:

- The *FLAC2D* axial symmetry model,
- Hoek-Brown failure criterion,
- The SPEC model

The *FLAC2D* model has the capability to calculate the stress distribution in an elastic medium and was shown to be reliable and consistent (*FLAC* manual).

The Hoek-Brown criterion depends on three main input parameters which can vary significantly. In addition, the essential rock mass properties were discussed in detail to obtain mean values and standard deviations. The predicted fracture zone using the *FLAC2D*/Hoek-Brown model in conjunction with the SPEC model was compared to available fracture measurements under known stress conditions.

Note that there was an interactive process between the two models. The *FLAC2D*/Hoek-Brown model provided the pillar strength and convergence for the SPEC model which then supplied the stress level on the individual pillars which was used to predict the extent of the

fracture zone. The *FLAC2D/*Hoek-Brown model was again used to determine the associated stresses and convergences in the pillar at the equilibrium point.

Figure 7_1 describes the process adopted process in the back analysis:-

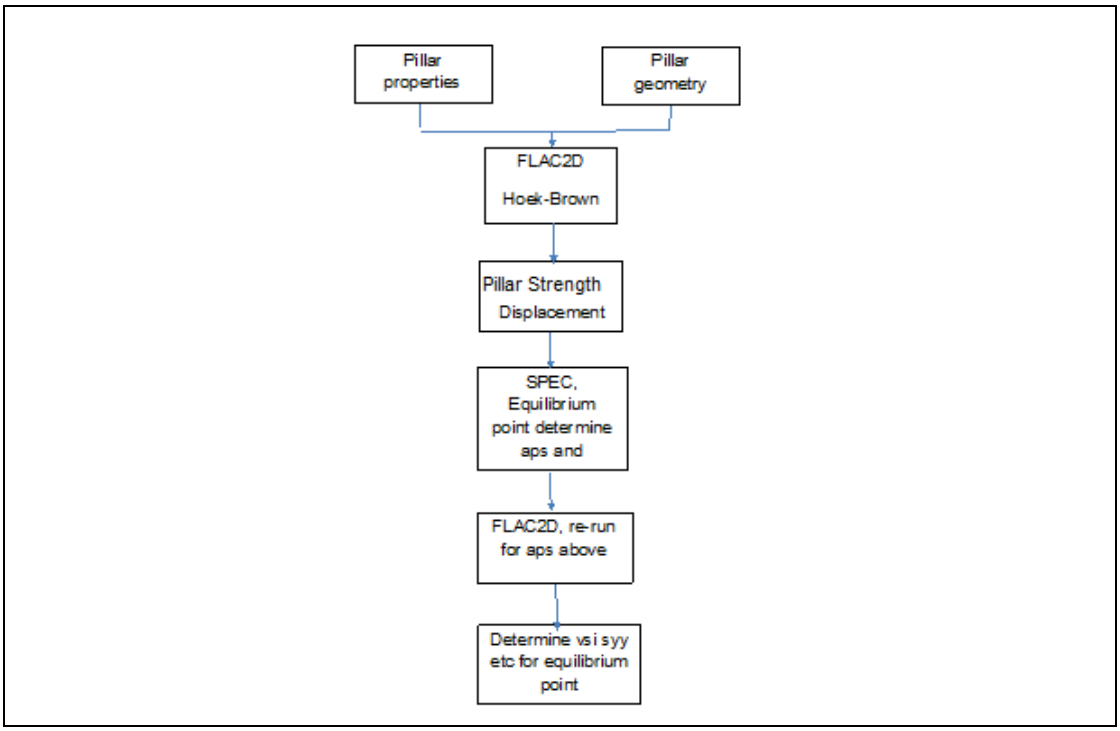

Figure 7_1 Process adopted in the back analysis

8 GENERAL GEOLOGICAL SETTING AND MINING METHOD

8.1 General geological setting

Mechanised bord and pillar workings are situated in the Western as well as Eastern portion of the Bushveld sequence. Figure 8.1_1 shows the locality of all of the mines. However, not all used bord and pillar lay-outs.

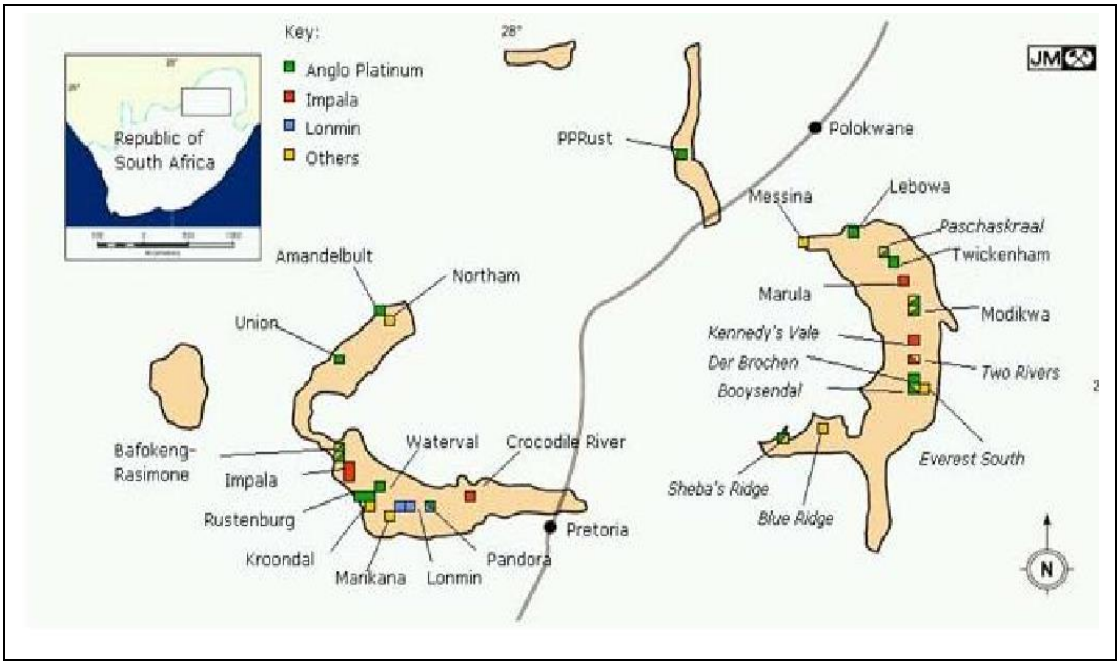

Figure 8.1_1 Overview of mines in the Bushveld sequence (Impala 2012 web site)

The Bushveld Complex (Wilson, et al., 2005):-

"The Bushveld Complex is the largest mafic-ultramafic layered intrusion on Earth covering an area of approximately 67 000 km^2 and has a broadly oval shape extending some 375 km in an east-west direction and 300 km in a north-south direction. The intrusion comprises four lobes which dip inward towards each other forming an elongated deep basin structure reflecting its emplacement into the Transvaal Supergroup sedimentary basin at 2058.9 ± 0.8 Ma (Buick et al, 2001). The mafic and ultramafic rocks of the Bushveld Complex (Rustenburg Layered Suite) form a succession more than 10 000 m thick which is made up of four major stratigraphic components, these being from the base upwards: the Lower Zone, Critical Zone, Main Zone and Upper Zone. The Critical Zone is economically the most important and also represents the transition from ultramafic rocks (harzburgites and pyroxenites) to mafic rocks (norites and gabbronorites). The Merensky reef, one of several major economic horizons in the Bushveld Complex mined for the platinum group elements (PGE) and base metals, is part of a series of cyclic units located close to the Critical Zone – Main Zone boundary."

A general geological sequence for the Merensky reef and the chromitite horizons is shown in Figure 8.1_2, Figure 8.1_3 and Figure 8.1_4.

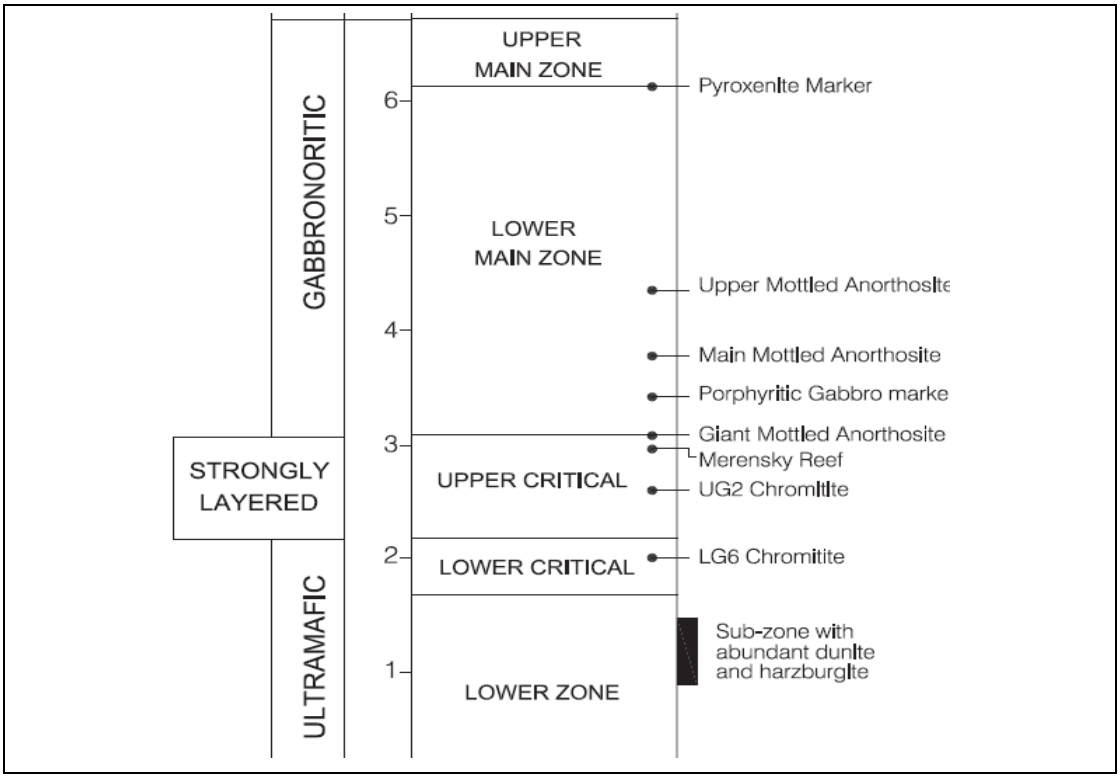

Figure 8.1_2 Geological column for the lower portion of the Bushveld sequence showing the relative position of the Merensky reef and the UG2 horizon. (Mitchell and Scoon, 2007)

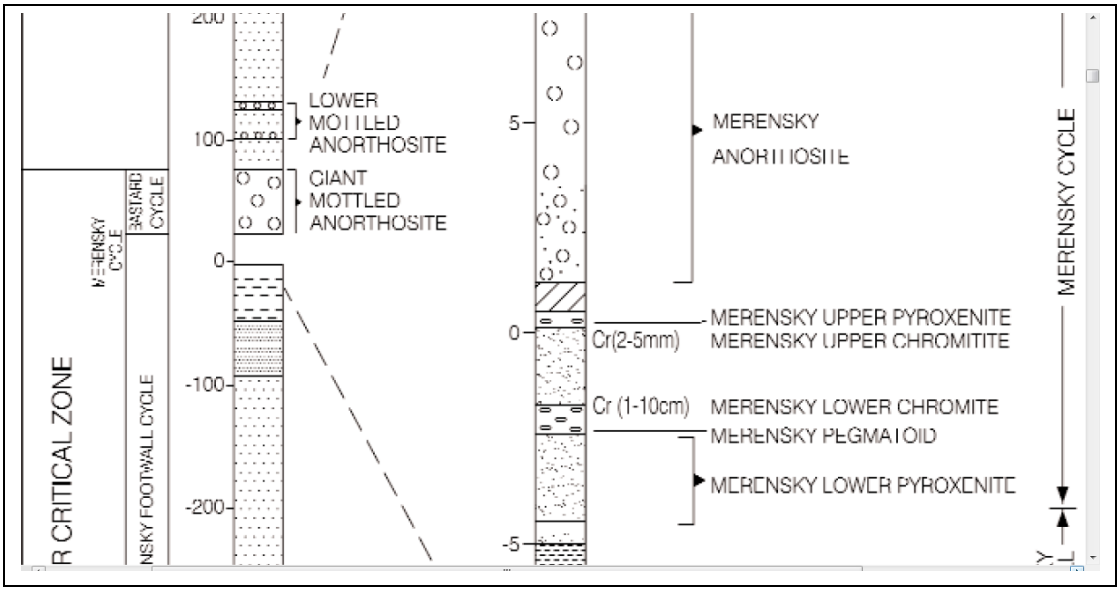

Figure 8.1_3 Detail of Merensky reef succession. (Mitchell and Scoon 2007)

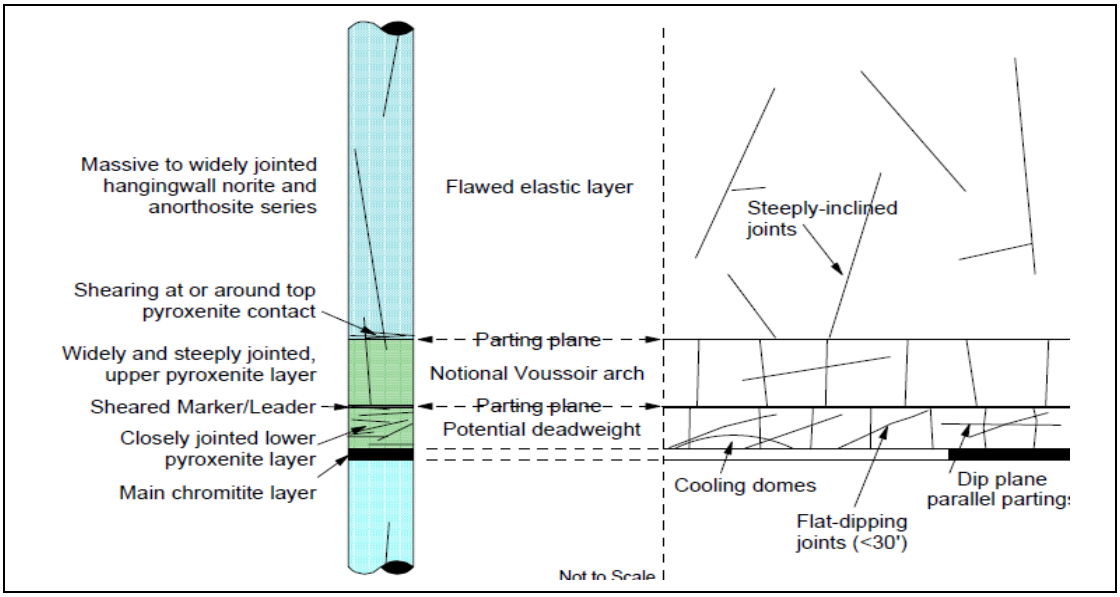

Figure 8.1_4 Detail of the UG2 Horizon - Godden (2012).

The bord and pillar workings are situated in the lower section of the critical and main zone strata with the UG2 chromitite seam and Merensky reef of main interest. The country rock in the immediate vicinity (200 m) consists of rock with a varying content of feldspar, pyroxene and small amounts of olivine.

No distinct bedding planes occur in the sequence except where post-depositional deformation has concentrated convergences on strength boundaries such as between the chromitite layers and the pyroxenitic country rock; bedding plane parallel shear zone dominate in this section of the succession. The presence of bedding planes, parallel shear planes in pillars, or in its immediate vicinity, are important and need close attention as it can reduce the pillar strength and lead to pillar failures below the accepted norm.

The rock strength values have been discussed in detail in Part II, Section 5.1.1 and the values for specific mines will be used in the calibration process.

The Geological Strength Index was discussed in the geotechnical data section and is a property of individual mines or sections of a mine and a measure of all the discontinuities present and, therefore, a measure of the destabilising effect that the discontinuities had.

The primitive stress field in the Bushveld relevant to the current study is limited to the vertical overburden component. The assumption is that the presence of tectonic horizontal stresses did not influence the pillar strength and is, therefore, ignored.

8.2 Mining method

The selection of a mining method mainly depends on the following aspects:

- Ore body geometry
- Depth of mining

- Surrounding rock mass
- Financial consideration

The mostly flat dipping, medium thickness reef geometry of the Bushveld mines lends itself to some form of bord and pillar mining. Basically methods, bord and pillar workings and panel stoping with strike pillars, stable or yielding, are employed.

Of the two methods, panel mining is more labour intensive. Preference is given to mechanized bord and pillar mining which required a minimum ore body thickness of 1.8 to 2 m, limiting the areas that could be mined with this method. This limitation is primarily due to equipment restrictions.

The depth below surface, rock mass properties and geological losses are influencing the bord width and pillar sizes. The latter is not only of financial interest, but also determined the stability of the entire mine and sections of a mine. The smaller the pillars and wider the bords, the greater the percentage extraction which result in a longer life of mine. The purpose of any bord and pillar mine design is to minimise the sizes of stable pillars and maximising percentage extraction.

The design of bord and pillar workings is currently based on the Hedley-Grant equation and the Tributary Area Theory.

The number of variations for the k value in the Hedley-Grant equations used in the various mines differ substantially, but the α and γ constants (Hedley-Grant) are generally kept at 0.5 and 0.75.

No specific government regulation exists for pillar dimensions. The onus is on the mine to determine the percentage extraction and to maintain stable pillars which have to be detailed in the Mine Code of Practice. The dimensions have to be defined in the Standard Operating Procedures which are legally binding to the mine.

9 IMPALA PLATINUM MINE

9.1 Location, geological setting and mining dimensions

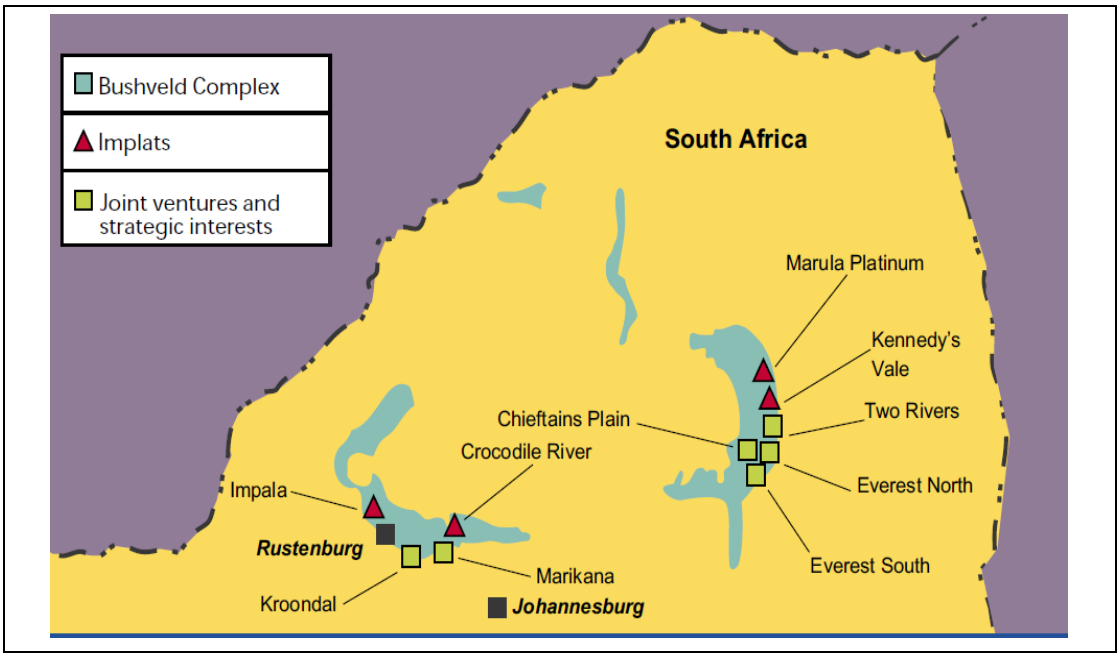

Figure 9.1_1 Impala Platinum Mine location (Impala 2012 web site)

Impala Platinum Mine is situated in the western Bushveld as shown in Figure 9.1_1, and mines the Merensky reef. The details of the succession in the immediate vicinity of the reef is the same as shown in Figure 8.1_3.

Fully mechanised mining is practised at 12 Shaft at a depth 820 m below surface with Figure 9.1_2 showing an example of the mining geometry as described in the Standard Operating Procedure document for the area.

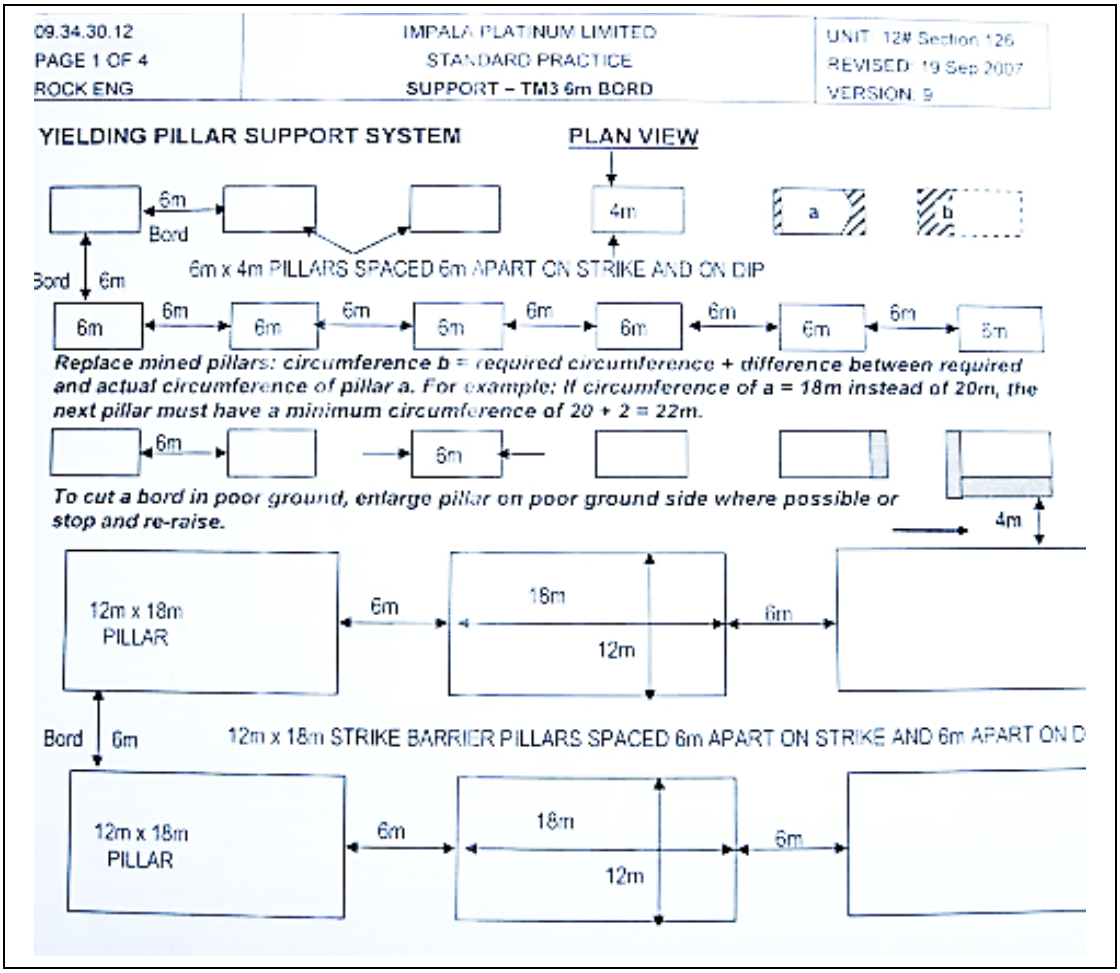

Figure 9.1_2 Detail of the planned pillar support system in use at 12 Shaft, Malan and Napier, (2007).

9.2 Rock Mass Data

A large number of tests have been performed on rock specimens at Impala Platinum Mine with samples collected at five different shafts, along approximately 15 km of strike length. The data was obtained from Impala Platinum Mine which having a uniquely extensive data bank for the area of interest.

From table 9.2_1, the mean uniaxial compressive strength for the Merensky is 122 MPa. Additional information from various sets of triaxial data, from the same data bank, were added giving a mean value of 130 MPa for the Merensky reef.

The calculated m_i value was obtained by dividing the mean uniaxial compressive strength by the tensile strength estimated to be 5.6 MPa, giving a value of 23. (Hoek, 2012).

The Geological Strength Index of 80% was an estimate made during an underground visit to the 12 Shaft experimental area.

Table 9.2_1: Uniaxial Compressive Strength of Pyroxenite, Chromitite and Pegmatoid. (Impala Mine data bank, 2012).

Lithology	Number of samples	Mean	Std Dev MPa	Min MPa	Max MPa
Merensky reef	8	121.6	43.91	60.0	174.4
Chromitite	4	153.2		115.8	198.3
Pegmatoid	3	81.8		65.8	104.4

Note: The standard deviations were calculated for values based on more than five samples only.

9.3 Available data on pillar behaviour

For Impala Platinum Mine, the following three possible sets of data, extent of pillar fracturing, were available for calibration purposes:

- Canbulat, et al. (2006)
- Data collected by Piper and Flanagan (2005)
- Malan and Napier (2006)

The data compiled by Canbulat, et al. (2006), however, was not used for calibration as the definition of the pillar fracture extent included dog-earing observed in the drill hole while it was deemed here that the boundary between the high stress and the fracture zone lies on the boundary between the dog earing and the fracture zone; dog earing defines the area that is still subjected to high stress.

The data collected by Piper and Flanagan (2005) consists of convergence measurements and fracture zone observations in grid as well as barrier pillars which are ideal for calibration purposes.

The data set by Malan and Napier (2006) consists of pillar stress calculations based on actual mining geometries and can be used to compare elastic solutions for the stress levels on individual pillar systems.

9.3.1 Piper and Flanagan (2005)

The calibration process was subdivided into the following three sections:-

- The data as collected is presented with the conclusions drawn by the authors.

- The same data was then compared with results obtained using the *FLAC2D*/Hoek-Brown and the SPEC methodology.
- Conclusions were drawn from the comparison.

Data presentation:-

The paper by Piper and Flanagan (2005) presents the results of a six-month monitoring programme at 12 Shaft, Impala Platinum Mine which was conducted to quantify the *in-situ* performance of yielding grid pillars by means of rock mass measurements and monitoring. The two parameters relevant to the present discussion were the relationship between pillar size and extent of fracturing and convergence measurements in individual panels as the span increased.

The site selected was a mechanised section at 12 Shaft, Impala Platinum Mine. The planned layout is shown in Figure 9.3.1_1.

The layout in Figure 9.3.1_1 differs from that published in the Code of Practice generally used on the mine and is specific to the 12 shaft area.

Generally, there was a difference between the planned and actual dimensions, Figure 9.3.1_2 shows the actual geometry at the end of the monitoring programme. Also shown in the figure are the convergence monitoring sites and the location of the monitoring holes drilled into various pillars.

The actual geometry differed substantially from the planned and this variation had to be incorporated in the final stages of the back analysis. The main change was the inconsistent increase in the strike length of the grid pillars to 12 m.

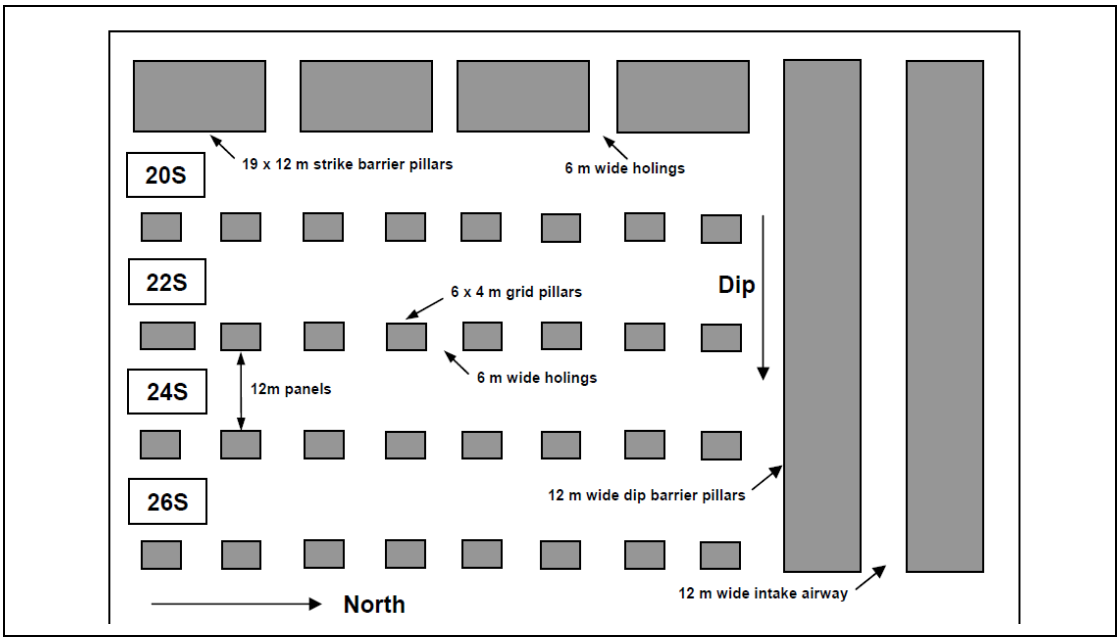

Figure 9.3.1_1 Planned layout for experimental section showing barrier and grid pillars

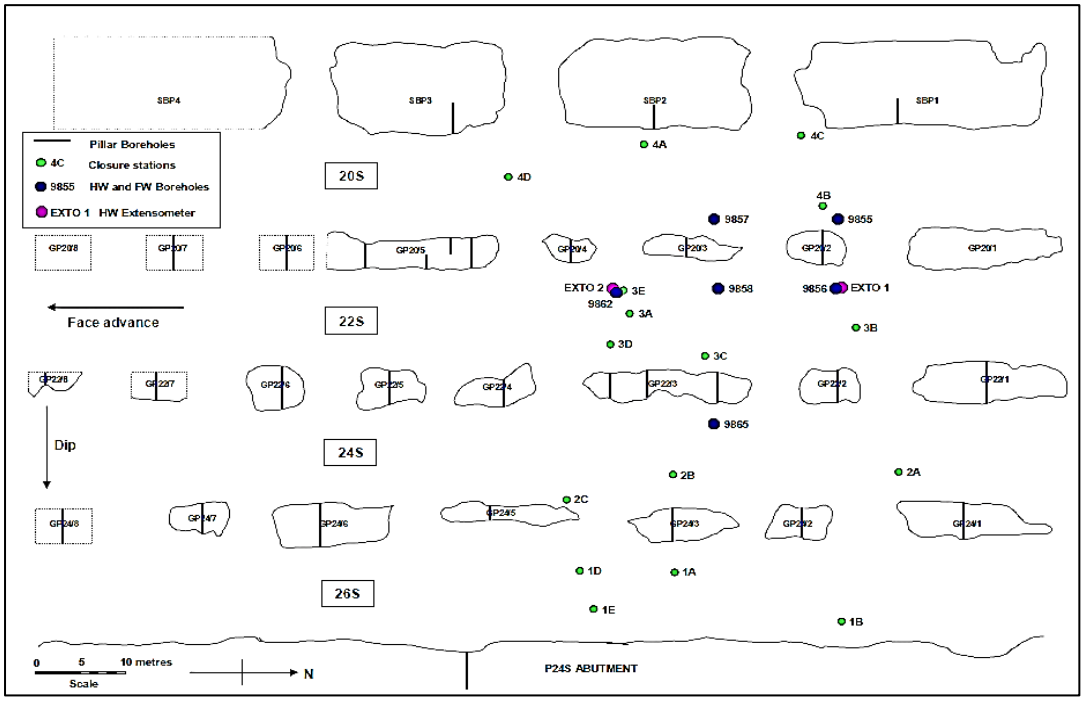

Figure 9.3.1_2 Actual layout at end of experiment of Piper and Flanagan, 2005.

Figures 9.3.1_3 and 9.3.1_4 shows the observed dog-earing and the unfractured core width.

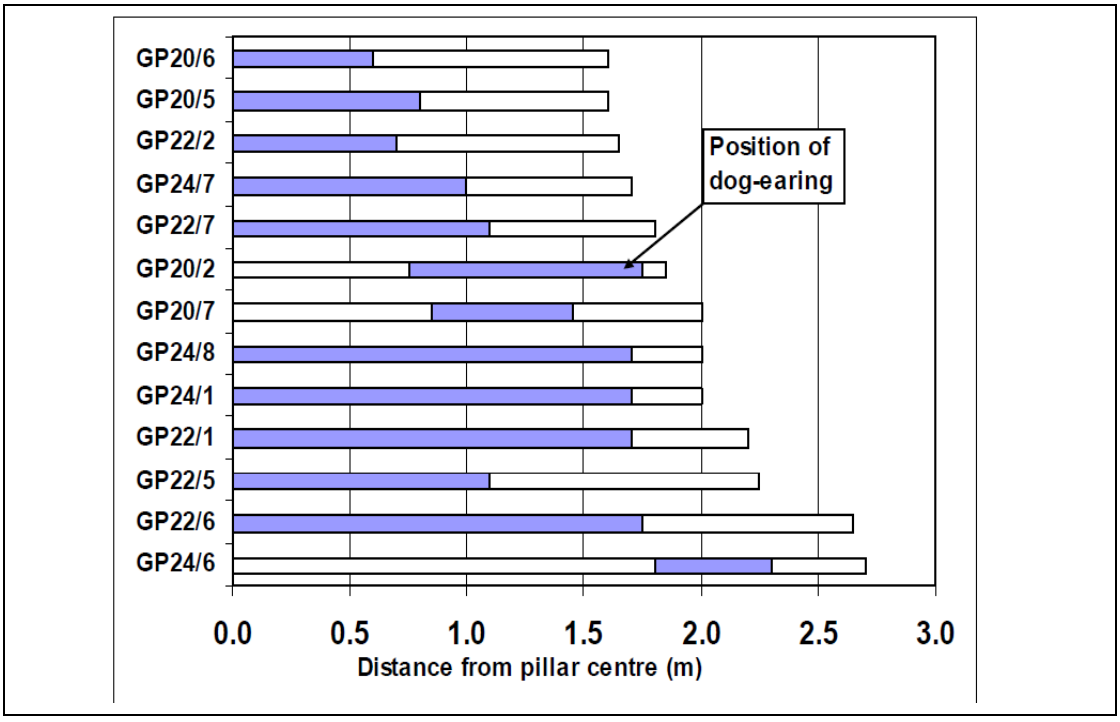

Figure 9.3.1_3 Dog earing in grid pillars - (Piper and Flanagan, 2005

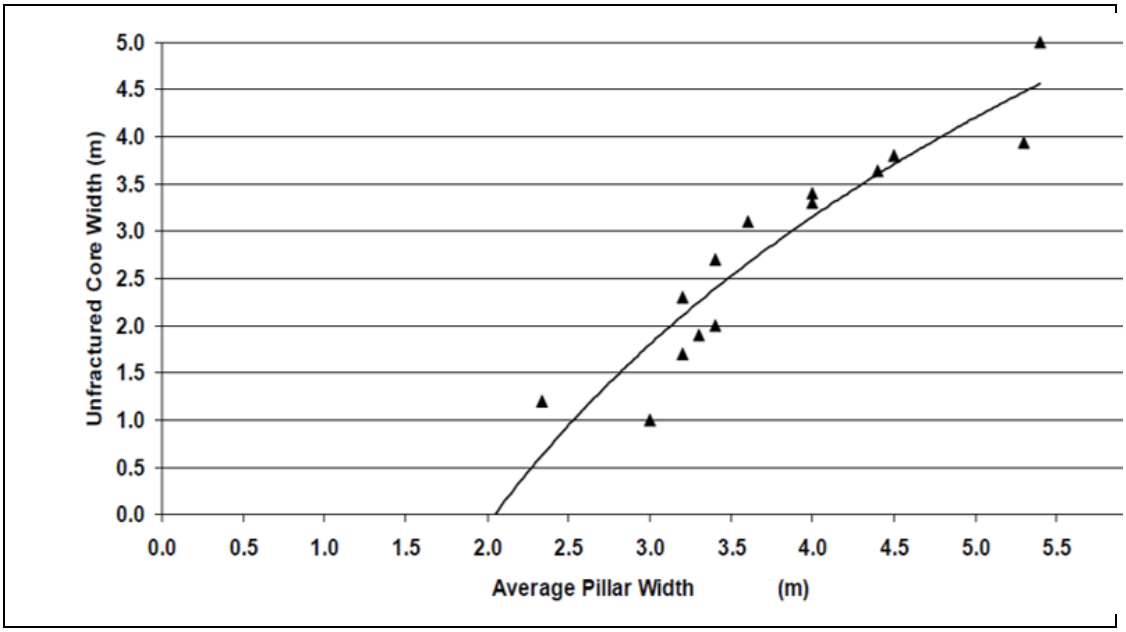

Figure 9.3.1_4 Unfractured core width in grid pillars, 6 by 4 m - (Piper and Flanagan, 2005)

The depth of fracturing was obtained by subtracting the pillar width from the un-fractured (solid) core width. For instance, for a 4 m pillar with a solid core of 3 m, the remainder is fractured, 0.5 m either side. The data was provided by Piper and Flanagan in terms of the half-width times 2, while the un-fractured core width was given as two times the depth measured from one side of the pillar. The results showed that a pillar with a width of 3.5 m would have an un-fractured core of 2.5 m resulting in a fracture zone of 0.50 m either side, Figure 9.3.1_4.

Holes were also drilled into three strike barrier pillars (19 x 12 m), on the up-dip (west) side of the monitoring area, and a further borehole was drilled into the abutment on the down-dip (east) side. The results are summarised in Table 9.3.1_1.

Table 9.3.1_1: Extent of fracturing in barrier pillars, 19 by 12 m, width 12m - (Piper and Flanagan, 2005)

Borehole Number	Pillar Height m	Depth of Fracturing m	Start of Dog-earing m	End of Dog-earing m
SBP1	2.6	0.22	0.2	
SBP2	2.4	0.10	None	None
SBP3	2.1	0.35	None	None
ABUT1	1.6	0.10	None	None

Findings by Piper and Flanagan on the fracture zone, quote:-

"*The most significant finding from the monitoring programme is the relationship between pillar width-to-height ratio and the extent of fracturing. The results show that a pillar with a width-to-height ratio of 1.3 is not completely fractured even far from the face. This suggests that either:-*

- *The full hanging-wall load is not being transferred to the grid pillars, due to the limited dip span of 60m between the strike barrier pillars and the down-dip abutment,*
- *The hanging-wall strata is very stiff and the load is being carried primarily by the strike barrier pillars and the abutment or the pillars are able to absorb the loading without fracturing."*

Convergence between the footwall and hanging wall was measured from initiation of pillar cutting to a distance of 60 to 80 m from the measuring sites 3A, 3B, 3C and 3D. The results are shown in Figure 9.3.1_5.

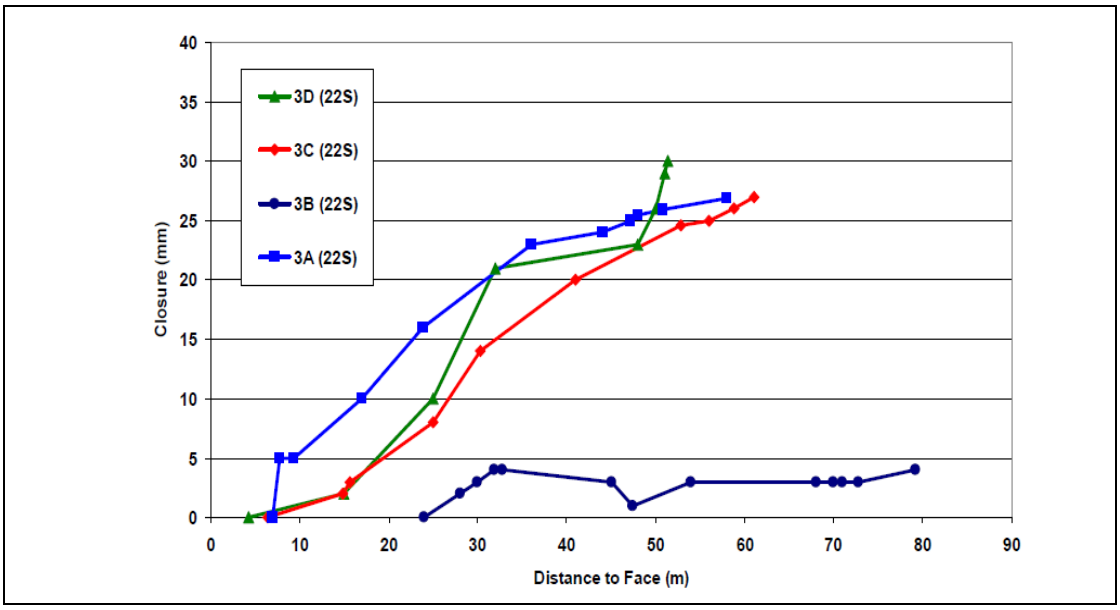

Figure 9.3.1_5 Convergence in panel 22S vs distance from the face - (Piper and Flanagan, 2005)

Conclusion drawn by Piper and Flanagan (2005):-

The rate of convergence was only slightly higher closer to the face than it was when the convergence station was more than 30 metres from the face, which could indicate that the major component of the convergence was an inelastic, not elastic, convergence. However, it was not possible to quantity the elastic component of convergence from these convergence measurements.

On average, the convergence rates were higher in the centre two panels than they were for Panels 20S and 26S which were closest to the strike barrier pillars and the abutment,

respectively. This suggested that the barrier pillars and abutment were providing the necessary hanging-wall support and reducing convergence. (Figure 9.3.1_6).

Table 9.3.1_2: Summary of convergence rates measured by Piper and Flanagan

Panel	Maximum Convergence	Convergence rate, mm/m from face
20S	33	0.47
22S	30	0.43
24S	25	0.35
26S	12	0.20
ALL	33	0.38

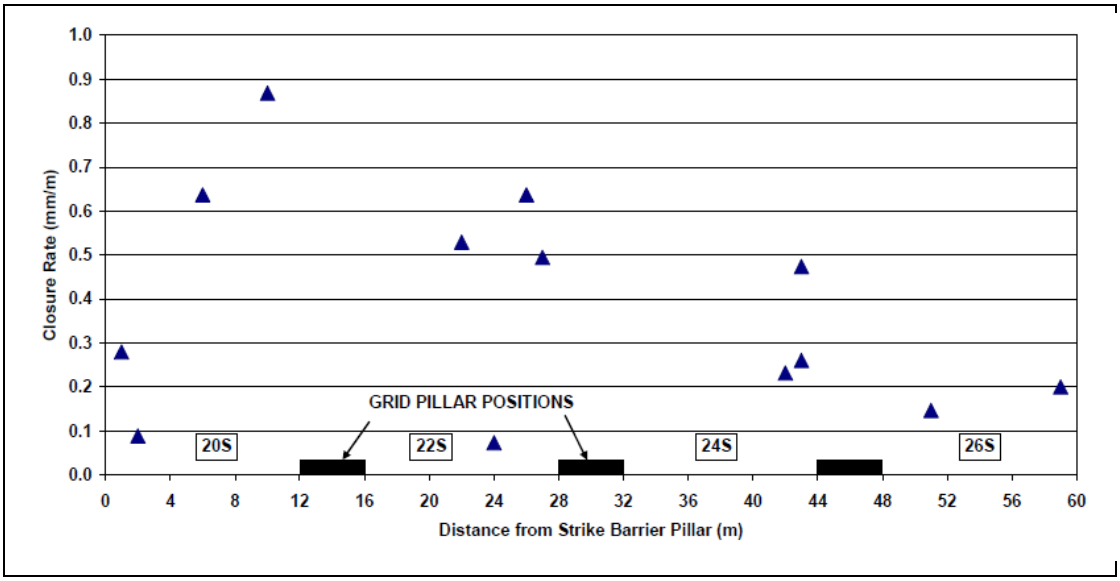

Figure 9.3.1_6 Average convergence rate/panel on dip, Piper and Flanagan, (2005).

The above is a summary of the relevant findings and conclusions as per Piper and Flanagan (2005).

9.3.2 Calibration with fracture zone, grid pillars

Rock mass properties were discussed in 9.2 with a summary given below:-

UCS=130 MPa

GSI = 80%

m_i = 23

m_b = 11.2, m_r= 5.5, s =0.1084, s_r = 0.054, $sigc$ = 42.7 MPa

For calibration purposes the actual, not planned, geometry was used and the dimensions of the grid pillars were determined from the plan shown in Figure 9.3.1_2 which dimensions are summarised in Table 9.3.2_1.

The average stope width was, according to Piper and Flanagan (2005), on average 1.8 m. Underground inspection, confirmed this assumption.

In the absence of an overall pillar height is not mentioned stope width of 2.5 m was modelled as travelling and transport is situated adjacent to the barrier pillars.

Step 1; Used *FLAC2D*/Hoek-Brown model to calculate the pillar strength with the associated convergence for the grid as well as barrier pillars for the dimensions given in Table 9.3.2_1.

Table 9.3.2_1: Calculated pillar strengths for planned as well as measured pillars.

	Barrier Pillar m	Pillar strength MPa	Grid m	Pillar strength MPa	Bord m	% Extrac
Planned	19x12	261	6x4	104	6x12	88
Actual	18.6x11.3	267	10.1x3.5	118	4.7x10.8	83

Step 2: The pillar dimensions of Table 9.3.2_1 and the peak average pillar strength and convergences for both the grid and the barrier pillars were incorporated in the SPEC input below. (Table 9.3.2_2).

The output provided the average pillar stress and the convergence for the intersection point of the system and the support curve and the associated factor of safety, Table 9.3.2_3.

The factor of safety is 0.97 for the average dimensions in Table 9.3.2_1.

Table 9.3.2_2 SPEC input, grid pillar.

	Properties	Young's Modulus GPa		68
		Poisson's Ratio		0.29
		Density kg/m^3		2800
	Geometry	Pillar	Strike m	10.1
			Dip m	3.5
		Bord	Strike m	4.7
			Dip m	10.8
		Halfspan m		30
		% Extraction		83.3
		Overburden m		822
	Pillar Stress and convergence	Strength MPa		115
		Convergence m		6.8e-3

Table 9.3.2 _3: SPEC Output for 2.6 m effective radius, halfspan 30 m.

	Average Pillar Stress MPa	118
	Convergence m	5.6e-3
	Factor of Safety	**0.97**

9.3.3 Establishing a fracture criterion, grid pillars.

Previous studies, Kersten (1996), and detailed discussion in Section 4.11, Part II, showed that the volumetric strain increment is a possible measure of the extent of the fracture zone around excavations and is used here for comparative analysis.

Piper and Flanagan (2005) observed the depth of fracturing and expressed the data in two forms.

- The width of the solid core of individual pillars, Figure 9.3.1_4,
- The extent of dog earing from Figure 9.3.1_3.

Figure 9.3.1_4 creates the impression of an increase in the width of the fracture zone with an increase in the pillar width, but what it shows is that the width of the fracture zone remains roughly the same, 0.5 m, irrespective of the w/h ratio for the equilibrium condition at the site.

Superimposing a constant 0.5 m width of fracturing on either side of the pillar results in a linear plot shown in Figure 9.3.3_1. A linear equation was fitted to the data which correlates well with the theoretical constant width fracture zone, irrespective of the pillar width.

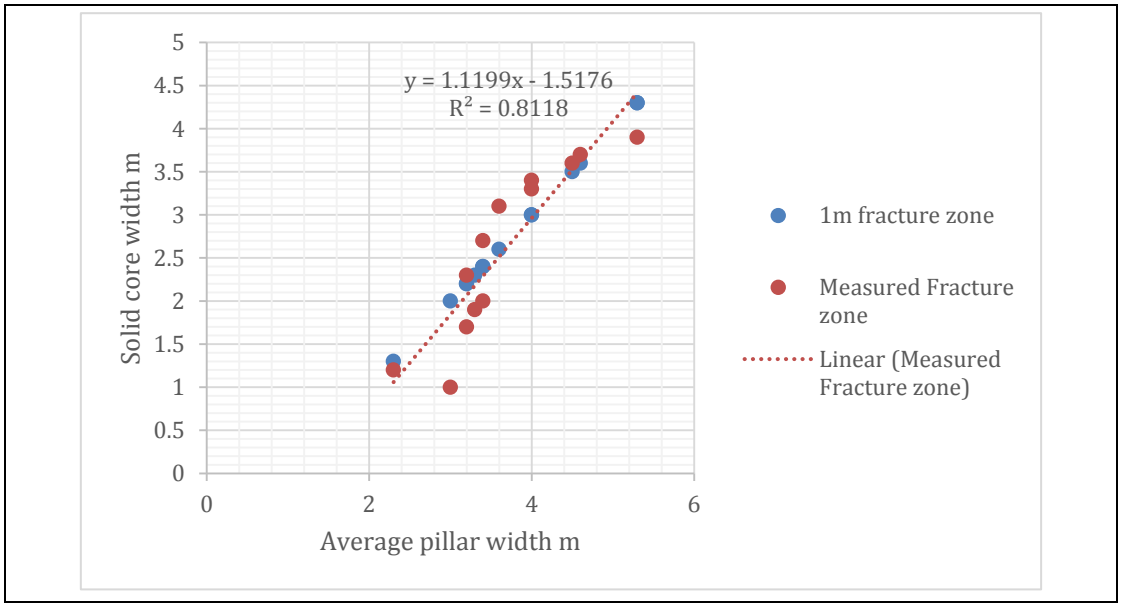

Figure 9.3.3_1 Comparison between observed data by Piper and Flanagan (2005) and a superimposed curve representing a constant fracture zone width of 0.5 m either side of the pillar.

Data from Figure 9.3.1_3 and the mine plan in Figure 9.3.1_2 was combined to create a table of individual strike and dip widths of the individual pillars. The effective widths were then calculated and the strength and extent of the fracture zone predicted using the vsi contours are plotted in Figure 9.3.3_2. Also included in the graph is the constant 0.5 m wide fracture zone for the pillars.

The observed solid core width lies between the vsi curves for 1e-2 to 3e-2.

For the current set of conditions, geometry, depth and rock mass properties the fracture zone width appears to be a constant value irrespective of the pillar width; implying a limit equilibrium control as envisaged by Malan and Napier (2006).

In their publication, Piper and Flanagan (2005) stipulate "*that the pillars will be entirely fractured only if their width is less than 2 m"* which tends to support the finding in Figure 9.3.3_2 where the 1e-2 vsi curve intersects the horizontal axis.

Conclusion:-

The range of volumetric strain increment value of 1e-2 to 3e-2 define the failure zone under current set of conditions and the fracture zone depth is apparently not a function of the pillar widths for the current set of data.

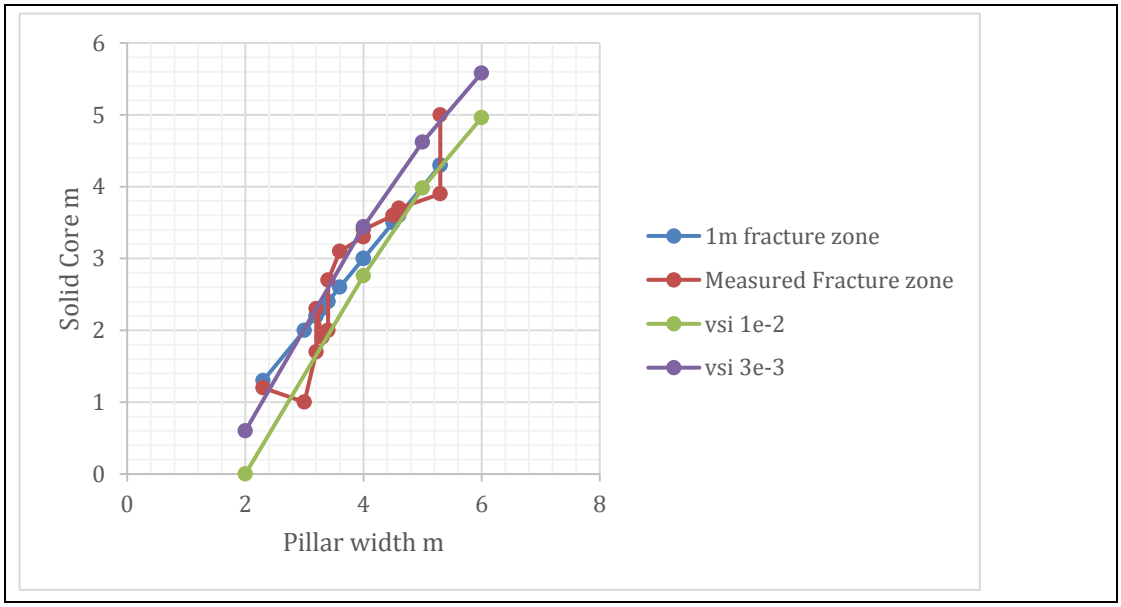

Figure 9.3.3_2 Plot of solid core for individual pillars widths based on observation as well as the calculated vsi of 1e-2 and 3e-2 for the given pillar width. Note total pillar failure for 1e-2 for the 2 m pillar.

Calibration based on the extent of dog-earing.

An alternative calibration approach was to use the position of dog-earing data from Piper and Flanagan (2005) shown in Figure 9.3.1_3. If it is assumed that the dog-earing is the boundary between the fractured and intact rock and the commencement of dog-earing defines the width of the fracture zone, Figure 9.3.3_3, showing a wide scatter.

FLAC2D/Hoek-Brown models were run for a pillar width of 4 m with profiles drawn for the vertical stress and the volumetric strain increment.

Figure 9.3.3_4 shows the vertical stress component in the pillar, along a horizontal profile drawn from the pillar centre towards the sidewall at mid height for the 4 m width pillar.

The fracture zone width in Figure 9.3.3_3 varies between 0.2 m and 1.0 m with a mean value of approximately 0.6 m. Drawing the 0.2 m and the 1 m fracture zone extent on the pillar width/vertical stress graph in Figure 9.3.3_4 the vertical stress values range from 20 to 120 MPa, with the mean value of 55 MPa.

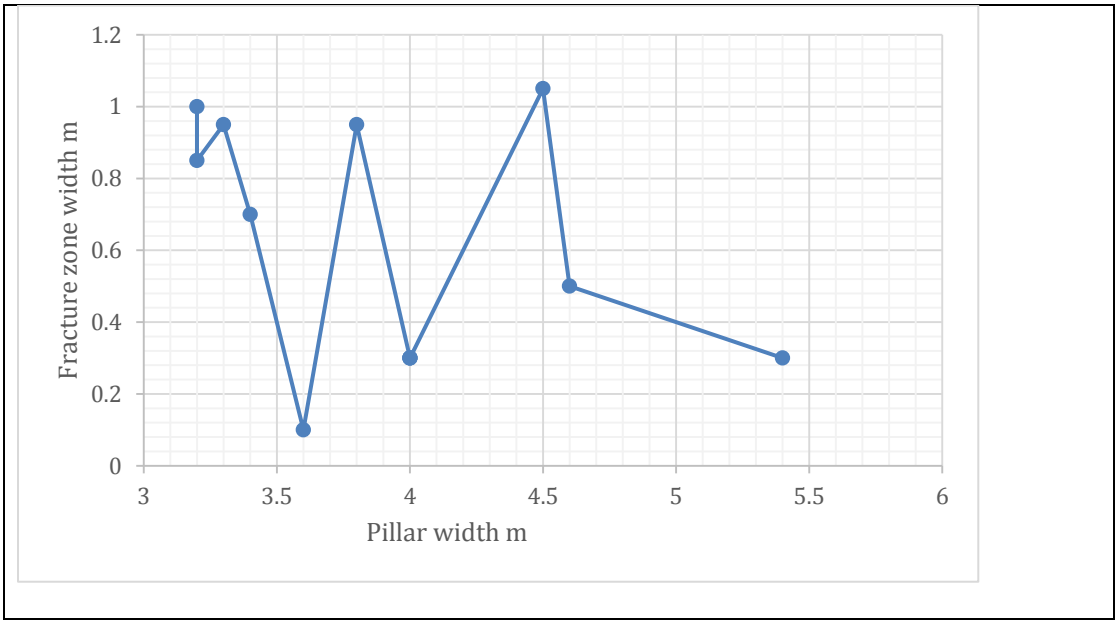

Figure 9.3.3_3. Width of zone between commencement of dog-earing and the pillar sidewall.

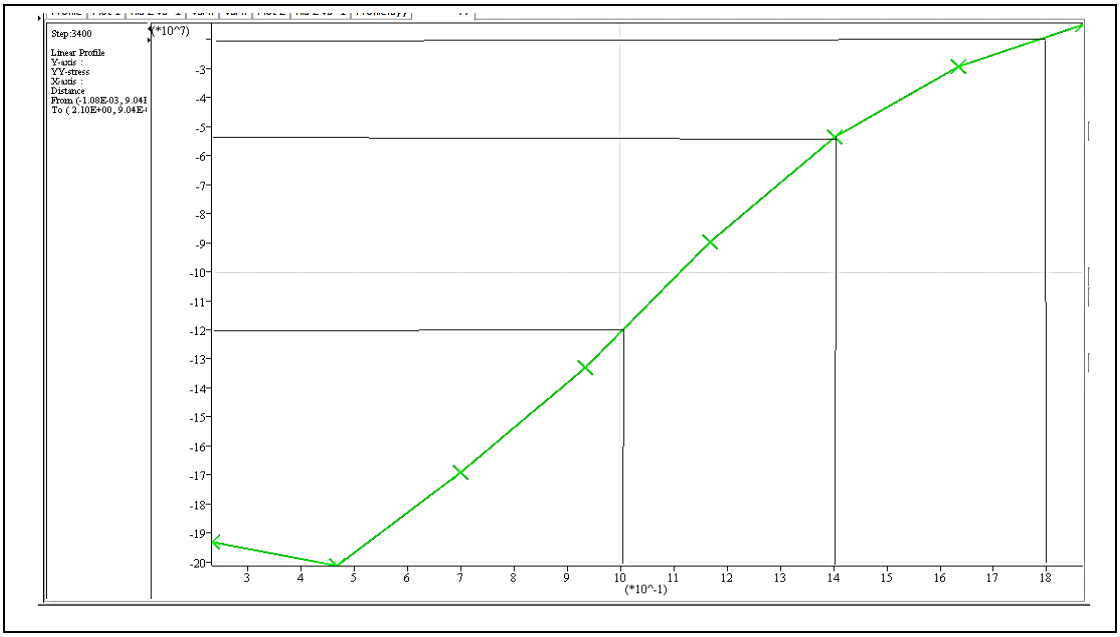

Figure 9.3.3_4 Vertical stress profile across one half of the 4 m width pillar showing the limit of the dog-earing, horizontal axis, and the vertical stress on the vertical axis

Quote from the paper by Piper and Flanagan (2005):-

"The uniaxial compressive strength of Merensky Reef is between 110 and 130 MPa, accordingly, observations on the location and extent of dog-earing in the pillar boreholes can be used to estimate locations within the pillar where the vertical or sub-vertical stress exceeds approximately 40 MPa."

The width of the fracture zone in Figure 9.3.3_3 varies between 0.2 and 1.0 m which intersects the stress axis on 20 and 120 MPa, Figure 9.3.3_4.

Figure 9.3.3_5 is for the same pillar but, in this instance, the profile drawn was for the volumetric strain increment.

According to Figure 9.3.3_5, the volumetric strain increment at which failure occurs is at 0.2e-2 and 1.9e-2 with a mean value of 0.7e-2 for a fracture zone of 0.6 m.

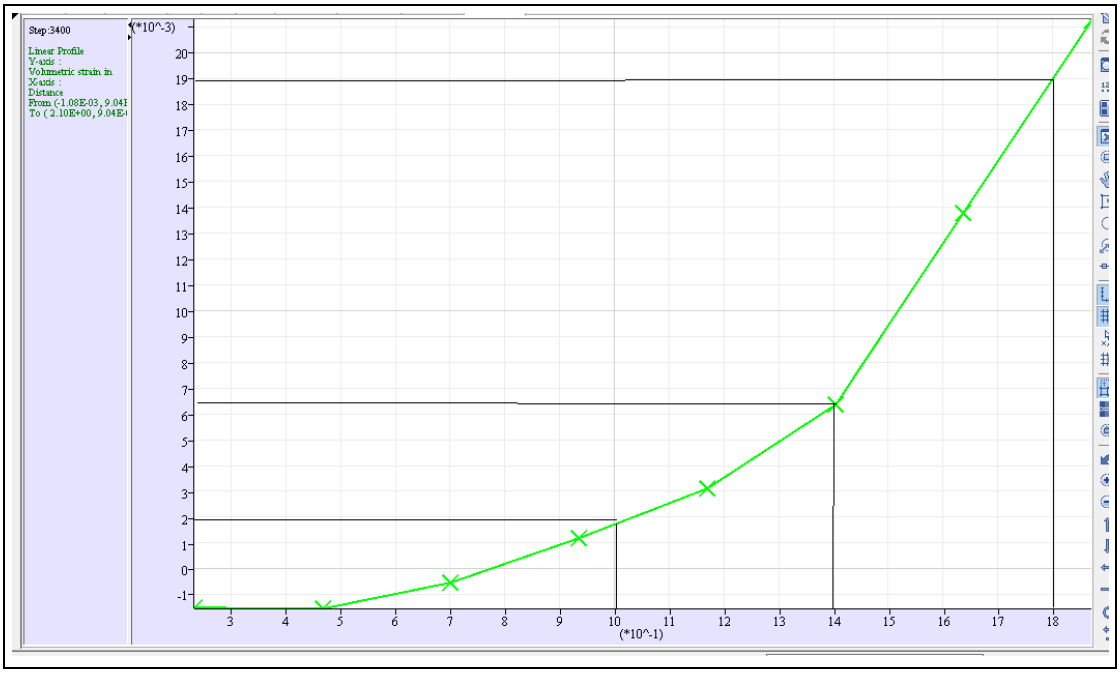

Figure 9.3.3_5 Volumetric strain increment profile across the 4 m pillar

Summary and conclusions.

After obtaining the reigning stress level on the pillars using the SPEC method and the Hoek-Brown criterion, it was concluded that:

- The volumetric strain increment value for failure initiation lay between 1e-2 to 3e-2 for the fracture zone extent.
- The stress at failure at the boundary between the dog-earing and fractured zone varied from 20 to 120 MPa.
- From the above, it appeared that the *FLAC2D*/Hoek-Brown model in conjunction with the SPEC method indicated that the volumetric strain increment was approximating that of the real underground situation better than the stress value obtained using the dog-earing criterion.

9.3.4 Fracture zones in barrier pillars

The depth of fracturing on the barrier pillars as measured by Piper and Flanagan (2005) is given in Table 9.3.4_1.

Table 9.3.4_1: Reproduced from Table 9.3.1_1 (Piper and Flanagan, 2005)

Borehole Number	Pillar Height m	Depth of Fracturing m	Start of Dog-earing	End of Dog-earing m
SBP1	2.6	0.22	0.2	0.6
SBP2	2.4	0.10	None	None
SBP3	2.1	0.35	None	None
ABUT1	1.6	0.10	None	None

The depth of fracturing ranged from 0.1 to 0.35 m, mainly confined to the skin of the pillar, and appeared to increase with pillar height. To reproduce the actual stress condition, the assumption was made that the average pillar stress on the barrier pillar assumed that the effect of the grid pillars was negligible; the model was assumed to contain no grid pillars.

Based on this assumption, it was found that the average pillar stress acting on the barrier pillar and its associated convergence at the equilibrium stress was found to be 133 MPa at a convergence of 10.4e-3, Table 9.3.4_3,

The volumetric strain increment contours in the barrier pillar for the above equilibrium condition were calculated following the standard procedure as previously described in section 9.3.3. An average pillar height of 2.5 m was used and the effective width for the pillar was 14.6 m, Table 9.3.4_2 with output in Table 9.3.4-3.

The volumetric strain increment contours of the barrier pillar is shown in Figure 9.3.4_1 for an average barrier pillar stress of 133 MPa at a convergence of 10.4e-3 m. The volumetric strain increment of 1e-2 intersects the effective radius curve at 6.3 m and the 3e-2 at 6.8 m. With the total effective radius of 7.3 m, the predicted failed zone would be 1 and 0.5 m wide, which is in excess of the measured range of 0.1 to 0.35 m shown in Table 9.3.4_1.

Table 9.3.4_2: Spec Input, barrier pillar

Properties	Young's Modulus GPa		68
	Poisson's Ratio		0.29
	Density kg/m^3		2800
Geometry	Pillar	Strike m	19
		Dip m	12
	Bord	Strike m	6
		Dip m	60
	Halfspan m		30
	% Extraction		87.3
	Overburden m		822
Pillar Stress and convergence	Strength MPa		267
	Convergence m		25.34e-3

Table 9.3.4_3: Spec Output, barrier pillar

Average Pillar Stress MPa	133	
Convergence m	10.4e-3	
Factor of Safety	**2.01**	

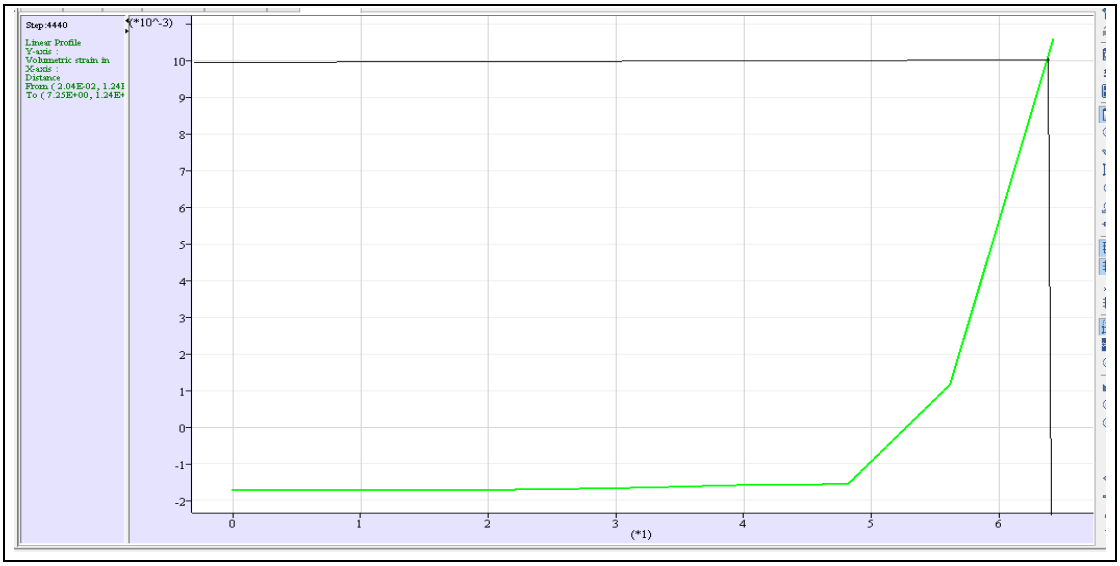

Figure 9.3.4_1 Volumetric strain increment profile for a barrier pillar at 133 MPa for a stope width of 2.5 m, 1e-2 contour extends 0.5 m into the pillar

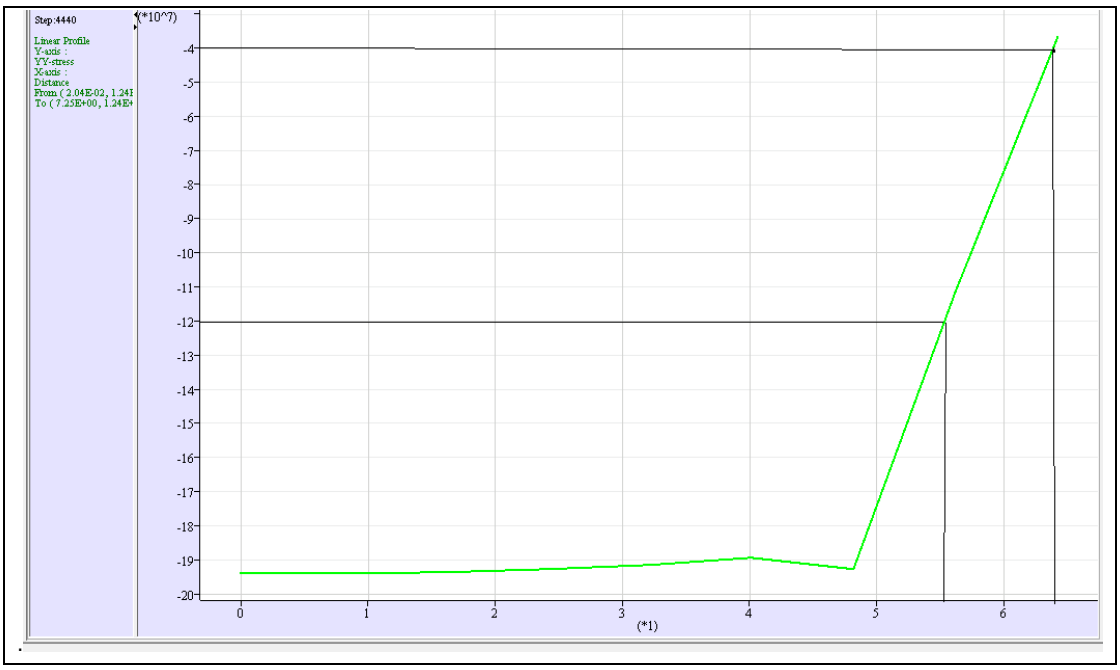

Figure 9.3.4_2 Vertical stress profile for a pillar stress of 133 MPa on the barrier pillar showing 40 and 120 MPa value intersects the x-axis at 5.5 and 6.5 m.

The volumetric strain increment curve shows that the 1e-3 volumetric strain increment intersects the horizontal axis at 0.5 m, with the 2 and 3e-3 not reached. This implies that the theoretical fracture zone in the grid pillar is < 0.5 m, closely related to the measured values shown in Table 9.3.4_1. Rapid changes in the extent of the fracture zone could be expected due to steepness of the curves in Figure 9.3.3_4 and Figure 9.3.3_5 which could explain the variations in Table 9.3.4_1.

Using dog-earing criterion ranging from 40 to 120 MPa, different from the previous observation, Figure 9.3.3_5, the distance from the edge of the pillar where failure should end was at 6.5 m, Figure 9.3.4_2, predicting failure to extend to a depth of the order of 1.5 m for the 120 MPa limit and 0.5 m for the 40 MPa limit.

The conclusion was as follows:

- The volumetric strain increment failure criterion of 1e-2 to 3e-2 appeared to be applicable.
- The range of results obtained from dog-earing is too wide for practical purposes.

9.3.5 Piper and Flanagan (2005): Convergence data calibration

Convergence data could not be used for calibration purposes since the SPEC method confined itself to the elastic convergences of the pillar only. Some comments, however, are required.

At a half span of 30 m, the calculated elastic vertical hanging-wall convergence for the given depth and elastic constants was 40 mm with no grid pillars in place, equation 6.3. The convergence measured by Piper and Flanagan ranges between 23 and 30 mm between grid pillars.

$$S_{z=\frac{2(1-v)q}{G}}\left(\left(l^2-x^2\right)^{0.5}\right)f(\alpha) \qquad 6.3$$

Where x = Distance from stope centreline

The total calculated convergence including the grid pillars consists of:

- The height reduction of the barrier pillar, 10.4 mm, Table 9.3.4_3.
- The height reduction of the grid pillar, 5.6 mm, Table 9.3.2_4.
- Inelastic convergence,

Three of the above values have been obtained in the modelling process and add up to a total of 16 mm; close to the actual measured values.

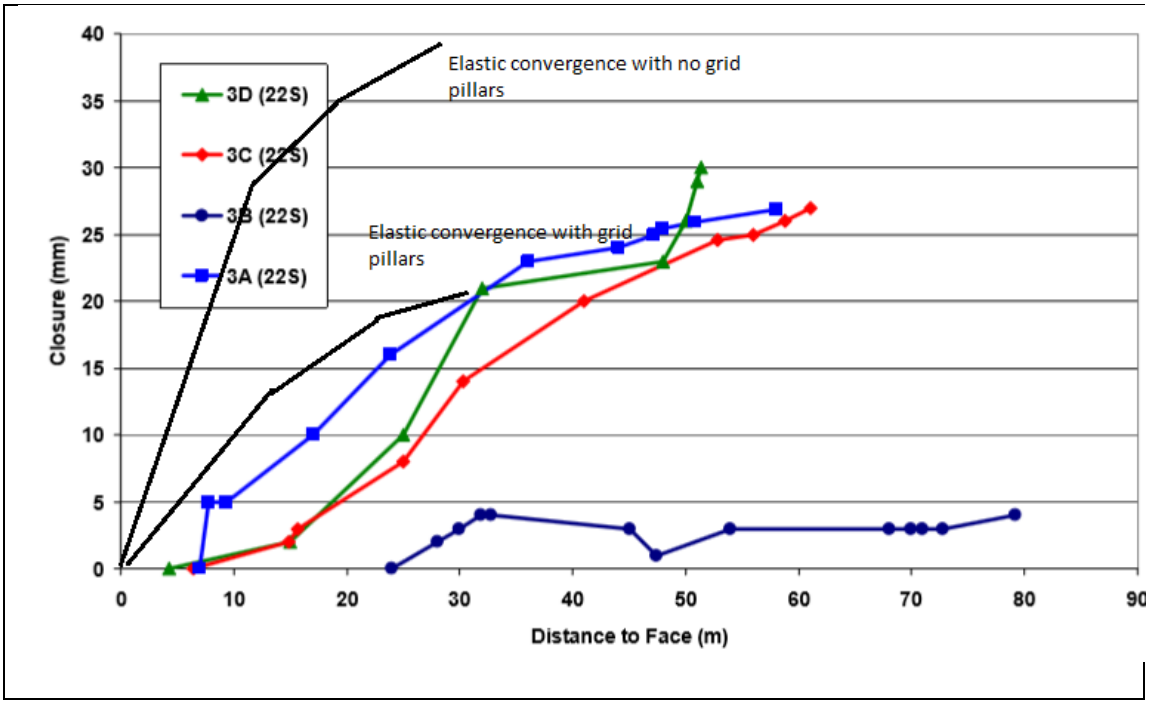

Figure 9.3.5_1 Elastic and measured convergence. The elastic convergence was added by the author.

Figure 9.3.5_1 shows the elastic convergence with no grid pillars as well as the calculated sum of elastic convergence including that of the pillars as well as the elastic convergence between the grid pillars.

The elastic convergence agrees well with the measured convergence at 3A and less so with 3D and 3C. 3A is situated furthest from the dip barrier pillar while the remainder have a minimum span of less than 30 m.

The rate of convergence listed in Table 9.3.1_2 for 22S is given as 0.43 mm/m for 60 m span. Considering the 30 m span only, the measured convergence rate for 3A is 20/30 = 0.63 mm/m, Figure 9.3.5_1, Using the elastic convergence including the grid pillars, 19/30 = 0.69 mm/m is nearly identical to the measured rate for the first 30 m.

(The convergence rates shown in Figure 9.3.1_6 for the different panels shows the average rate for 22S discussed above as well as the rates in 20S, 24S and 26S. There is a general reduction in the convergence rate as the mining approaches the solid abutment, non-mined area down-dip from 26S, while the convergence in 20S is strongly influenced by the extensive mining up-dip from 20S.)

The above tends to support the results obtained using the *FLAC2D*/Hoek-Brown and SPEC method for limited spans.

The method can be extended to incorporate the in-elastic convergence but it is not deemed part of this thesis.

9.3.6 Malan and Napier (2007)

Malan and Napier (2007) conducted research in the same area as Piper and Flanagan (2005) 12 shaft area, Impala Platinum Mine, after additional mining had been done.

The key objectives of the project were the following: -

- An investigation of the layout design to examine if further improvements could be made.
- A comparison between actual convergences measured underground and simulated values.
- Simulation pillar stresses for the actual layout with the irregularly shaped pillars.

The relevant portion of their work was the average pillar stresses which were obtained using the Texan code. The objective of the current investigation was to determine whether the average pillar stresses calculated by the SPEC methodology were similar to those obtained by Malan and Napier.

TEXAN was developed by Malan and Napier with the key attributes of this code being as follows: (From Malan and Napier, 2007)

1. Inclusion of a finite depth solver: A more accurate method to represent the free surface was to use the special boundary element influence functions that automatically met the prescribed boundary conditions along the surface.

2. Flexible element geometries: Element shapes could be triangles or convex quadrilaterals (square elements could be used if required).

3. Higher order convergence discontinuity elements: The traditional convergence discontinuity programs used in the mining industry employed the so- called “constant strength” elements with one collocation point in the centre.

4. In the TEXAN code, each element could have one or more internal collocation points giving constant or higher order discontinuity variations. Triangular elements could be defined to have 1, 10 or 15 internal collocation points.

The result obtained was a better representation of the average pillar stress than the conventional displacement discontinuity codes developed for the gold mines.

Figure 9.3.6_1 shows the extent of mining in the South mechanised section with the experimental site discussed by Piper and Flanagan (2005) shown in the top right hand corner. Obviously extensive mining had occurred since the site was instrumented for the Piper and Flanagan (2005) experiment. Also, the planned mining geometry was changed to that shown in Figure 9.3.6_2.

The differences were important to note since the Piper and Flanagan (2005) results could not be incorporated in the Malan and Napier (2007) analysis.

Texan and SPEC pillar stresses.

Malan and Napier calculated the average pillar stresses for the model geometry as well as the actual geometry. In this research, one set of data for the model geometry only was used for calibration. The average pillar stress using the Tributary Area Theory for the grid pillars was found to be 185 MPa (Malan and Napier 2007).

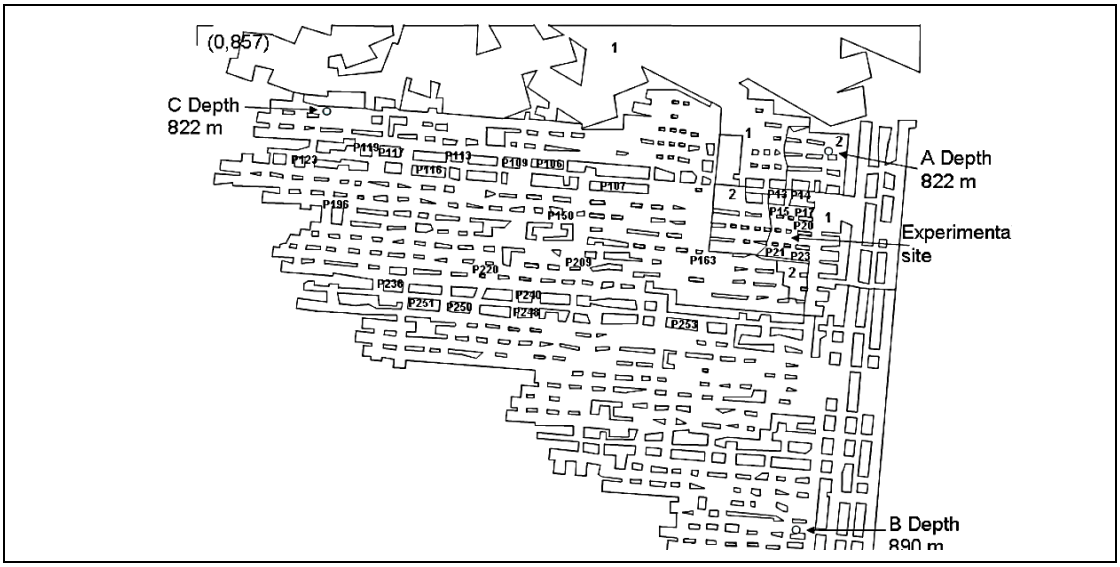

Figure 9.3.6_1 Overall geometry of South section indicating area 2 (Experimental site) discussed in the previous section with extended mining thereafter

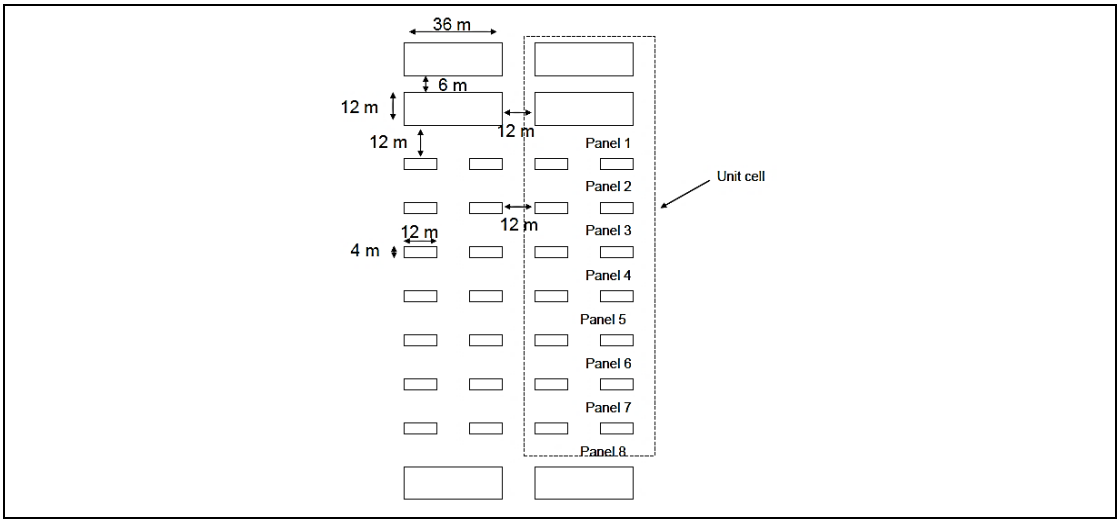

Figure 9.3.6_2 Planned layout beyond the experimental section 2, note the increase in strike length of the pillars from 6 to 12 m

Figure 9.3.6_3 and Figure 9.3.6_4 are reproduced from the work by Malan and Napier (2007) showing the average pillar stresses for grid and barrier pillars using the Texan code on the ideal geometry.

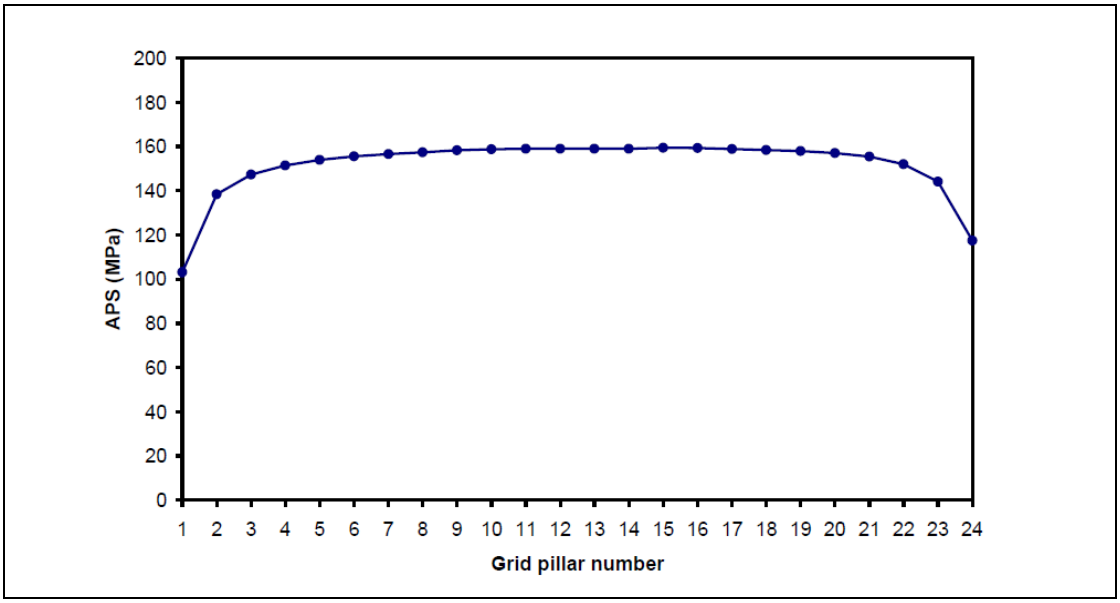

Figure 9.3.6_3 Calculated grid pillar stresses along strike for the model geometry, South section, Malan and Napier (2007).

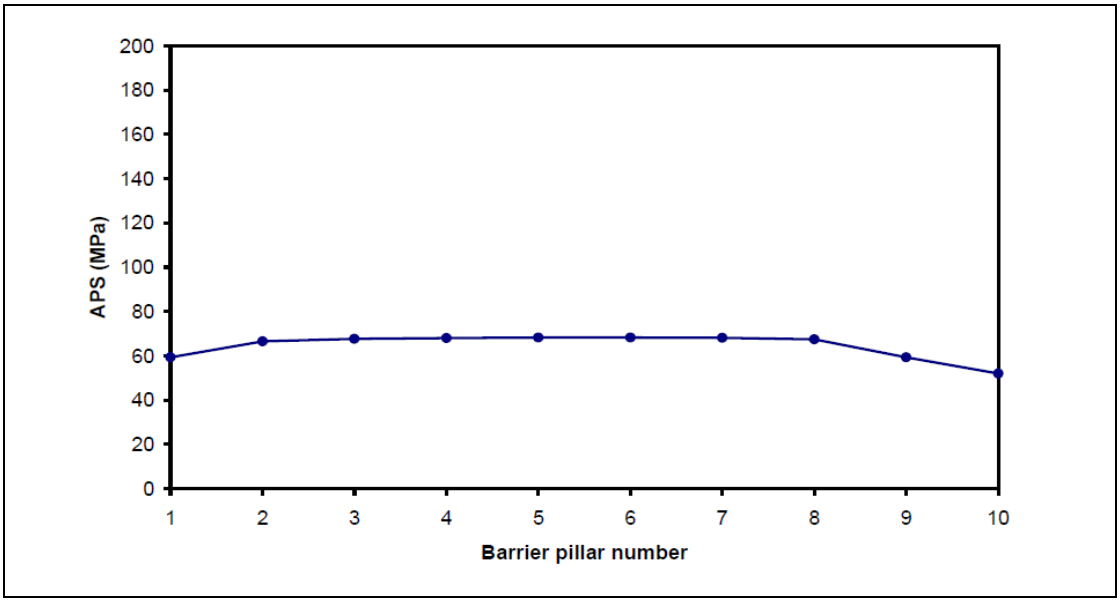

Figure 9.3.6_4 Calculated barrier pillar stresses on strike for the model geometry, South section. Malan and Napier (2007).

To compare the results with the SPEC methodology the following steps were taken:

Step 1: Calculation of the stress/convergence curves for the planned grid pillars of 4 by 12 m, the result obtained is a strength of 129 MPa and a convergence of 6.9e-3 m.

Step 2: Introduction of the pillar and bord dimensions and the peak average pillar stresses of the grid pillars in the SPEC model for a half span of 60 m, the half span between the barrier pillars, Tables 9.3.6_1 and 9.6.3_2.

Step 3: Comparison of the Texan calculated stress levels with those obtained using the SPEC method.

Note: The average pillar stress obtained by the SPEC method for the above configuration is 165 MPa if no pillar failure occurred. (The fact that the factor of safety is less than 1 does not affect the value since the analysis deals with the elastic range only.)

The Texan and SPEC results were very similar and supported each other's findings.

Following the same procedure for the barrier pillars, the average pillar stress obtained with SPEC was 59 MPa while Texan was 63 MPa, input and output in Tables 9.3.6_1 and 9.3.6_2.

Table 9.3.6_1: SPEC Input for grid pillars

Properties	Young's Modulus GPa		68
	Poisson's Ratio		0.29
	Density kg/m^3		2800
Geometry	Pillar	Strike m	12
		Dip m	4
	Bord	Strike m	12
		Dip m	12
	Halfspan m		60
	% Extraction		87.5
	Overburden m		822
Pillar Stress and convergence	Strength MPa		129
	Convergence m		6.9e-3

Table 9.3.6_2: SPEC Output

	FLAC2D/H-B	
	Average Pillar Stress MPa	165
	Convergence m	6.9e3
	Factor of Safety	0.78

Table 9.3.6_3 Summary of the results obtained from the three methods.

Table 9.3.6_3. Comparative pillar stresses for grid and barrier pillars

Geometry	Grid m	*aps* MPa
TAT	12*4	185
Texan model	12x4	159
SPEC	12*4	165
	Barrier	
TEXAN	12*36	63
SPEC	12*36	59

9.3.7 Grodner and Malan (2006) monitoring at 14 Shaft Pillar Mining Site – Impala Platinum Mine.

During 2006, Grodner and Malan monitored pillar deformation at Impala Platinum Mine at a depth of 1132 m below surface by drilling horizontal boreholes into the pillars as shown in Figure 9.3.7_1.

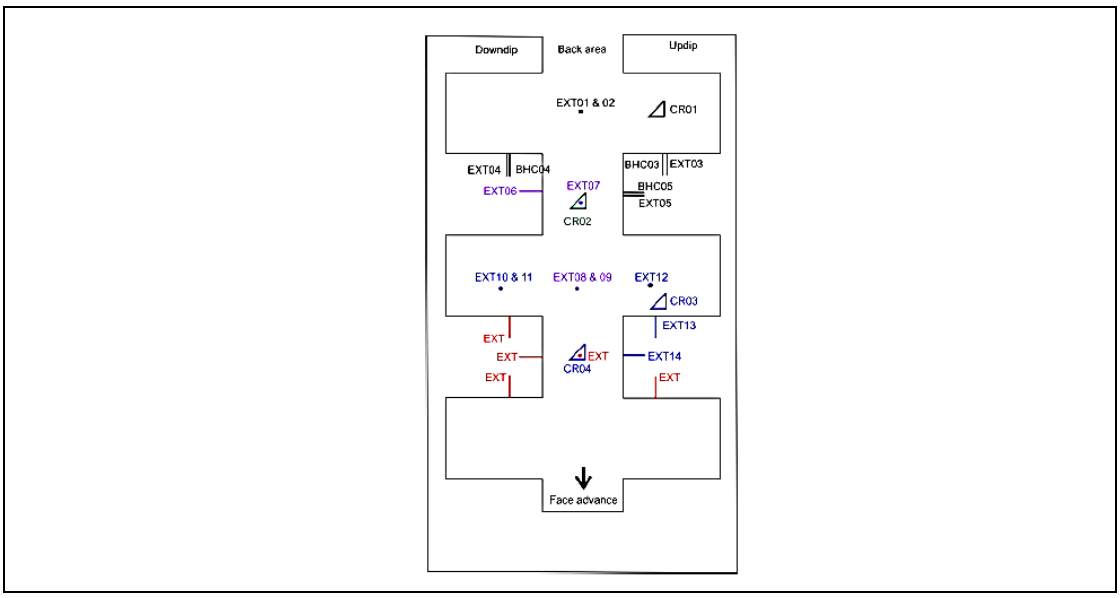

Figure 9.3.7_1 Experimental site at 14 Shaft, Impala Platinum Mine - (Grodner and Malan 2006)

No actual mine plan was available and the design dimensions were used.

The extensometer readings were taken from borehole collar to a depth of 3 m. The actual extensions are shown in Figure 9.3.7_2 for the extensometers EXT03, 04 and 05. Two sets of data were obtained, one set EXT03 and EXT06 gave a maximum value of approximately 35 mm, with EXT04 and EXT05 final values were of the order of 70 to 80 mm.

A circular pillar of 10 m was modelled using the *FLAC2D*/Hoek-Brown model to determine the pillar strength and its average pillar stress at the equilibrium point. The pillar strength and the convergence were then introduced in the relevant SPEC input in Table 9.3.7_1.

With the pillar strength of 222 MPa, the average pillar stress at the equilibrium point was 163 MPa, table 9.3.7_2, the stress to which the pillar was subjected at that stage.

Horizontal displacement profile for the equilibrium average pillar stress is shown in Figure 9.3.7_3, at a safety factor of 1.34

For the equilibrium point (safety factor of 1.34) the total modelled horizontal dilation was 15 mm. (Figure 9.3.7_3).

For a period of 80 days all curves lie in the range of 10 to 20 mm. EXT 03 reached a maximum of 35 mm while the remaining two, EXT05 and EXT04 recorded 70 mm. which was reached after a period of 300 days. It is proposed here that the initial 80 days is a reflection of the elastic convergence while the increase to 70 mm is due to time dependant effects.

The above comparison indicated that the *FLAC2D*/Hoek-Brown model in conjunction with the SPEC method could be used to approximate pillar dilation at a depth of 1132 m below surface.

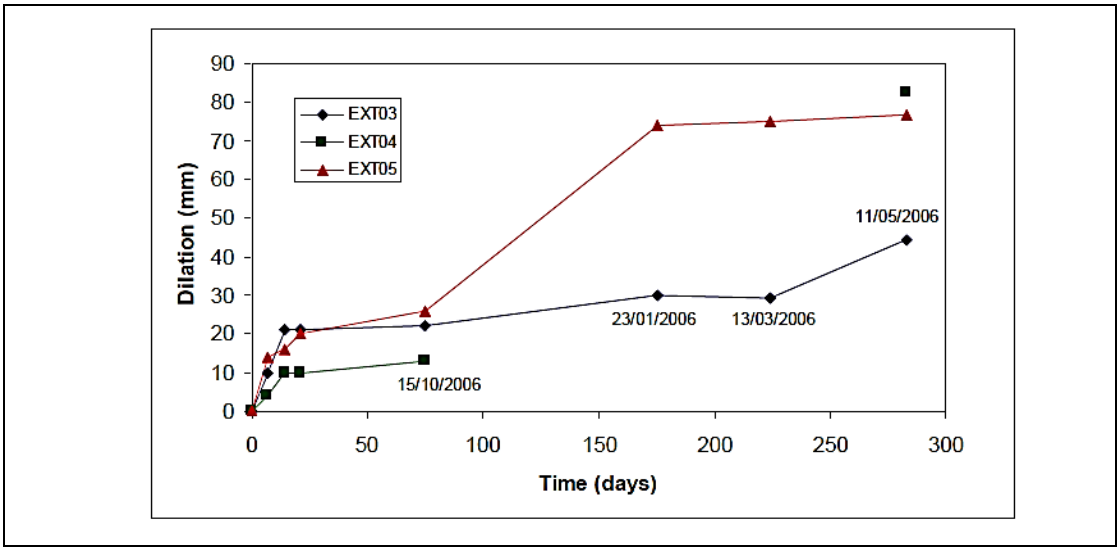

Figure 9.3.7_2 Extensometer readings in 3 m long horizontal boreholes in positions shown in Figure 9.3.7_1. (Grodner and Malan, 2006) (EXT04 was not recorded between 15/10/2006 to 11/05/2006)

Table 9.3.7_1: SPEC Input

Properties	Young's Modulus GPa		68
	Poisson's Ratio		0.29
	Density kg/m^3		2800
Geometry	Pillar	Strike m	10
		Dip m	10
	Bord	Strike m	14
		Dip m	14
	Halfspan m		60
	Stope width m		2
	% Extraction		82.6
	Overburden m		1132
Pillar Stress and convergence	Strength MPa		222
	Convergence m		11.35e-3

Table 9.3.7_2: SPEC Output

FLAC2D/H-B	
Average Pillar Stress MPa	163
Convergence m	5.6e-3
Factor of Safety	**1.34**

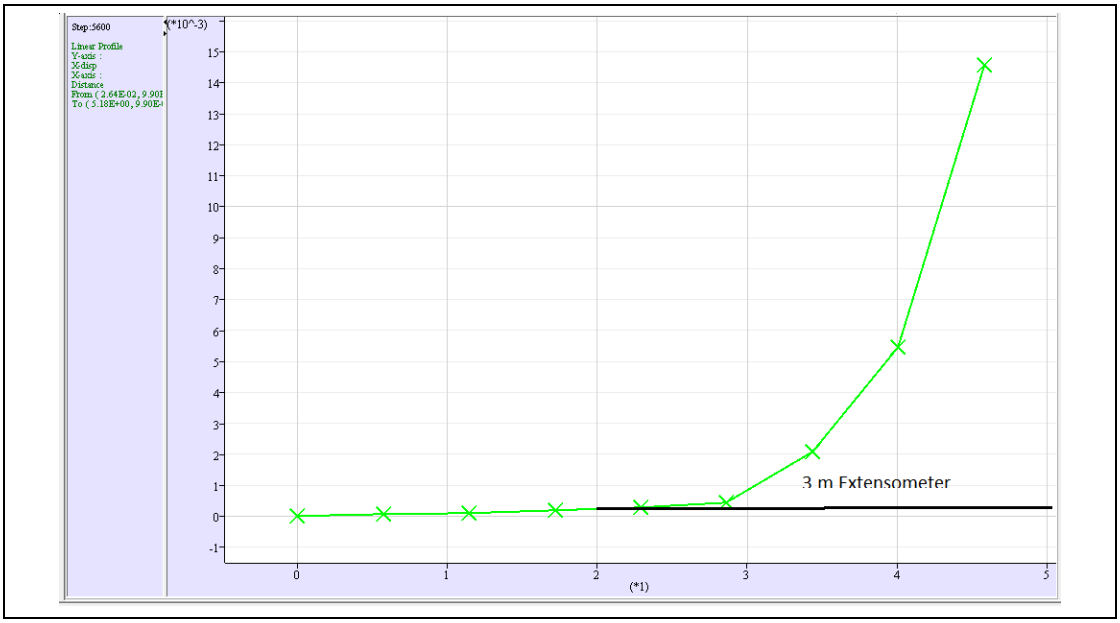

Figure 9.3.7_3 Horizontal displacement profile at a factor of safety of 1.34.

9.3.8 Ryder and Malan (2009) results.

The geometry was also investigated by Malan and Ryder in 2009 who obtained the stress profile shown in Figure 9.3.7_4. The average pillar stress obtained using the TEXAN code was 161 MPa.

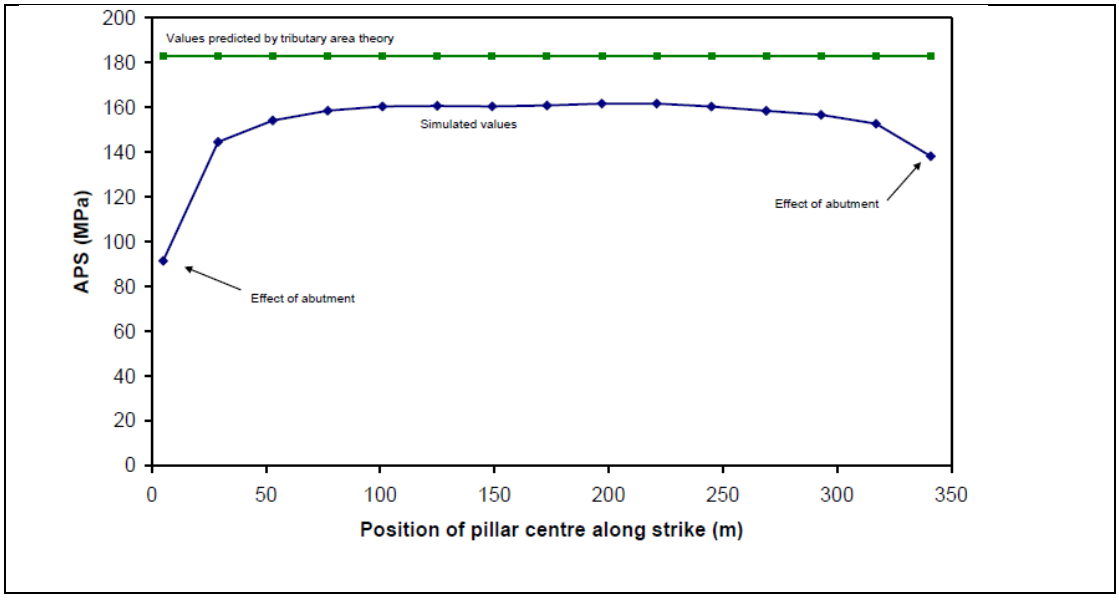

Figure 9.3.7_4 Average pillar stress according to Malan and Ryder (2009).

According to the SPEC method, the equilibrium average pillar stress was 163 MPa. It appeared to be a good correlation with a value of 161 MPa.

9.4 Summary of conclusions for Impala Platinum Mine data comparison.

- The volumetric strain increment value of 1e-2 to 3e-2 can be used to define the failure zone in a grid pillars.
- The stress at failure at the boundary between the dog-earing and fractured zone is inconsistent, ranging between 20 and 120 MPa.
- The rate of convergence can be predicted for different stope spans.
- The dilation predicted for a pillar at a depth of 1132 m below surface falls within the observed range.
- Pillar stresses calculated using the SPEC method compare well with those obtained from the TEXAN code at 822 and 1132 m below surface.

Overall, the extent of the fracture zone was predicted reasonably accurately using the volumetric strain increment criterion, and the average pillar stresses agree with the TEXAN method of calculation, the combination of the *FLAC2D*/Hoek-Brown model and the SPEC method could be used to obtain realistic values for the average pillar stress.

10 TWO RIVERS PLATINUM MINE

Two Rivers Platinum Mine was selected for verification purposes for the following reasons:-

- Unique sets of uniaxial compressive strengths test results across the ore body were available.
- The appearance of stress induced fractures on some of the pillars.
- A mining geometry apparently very close to design parameters.

10.1 Geology.

Two Rivers Platinum Mine is situated on the eastern limb of the Bushveld sequence, Figure 10.1_1.

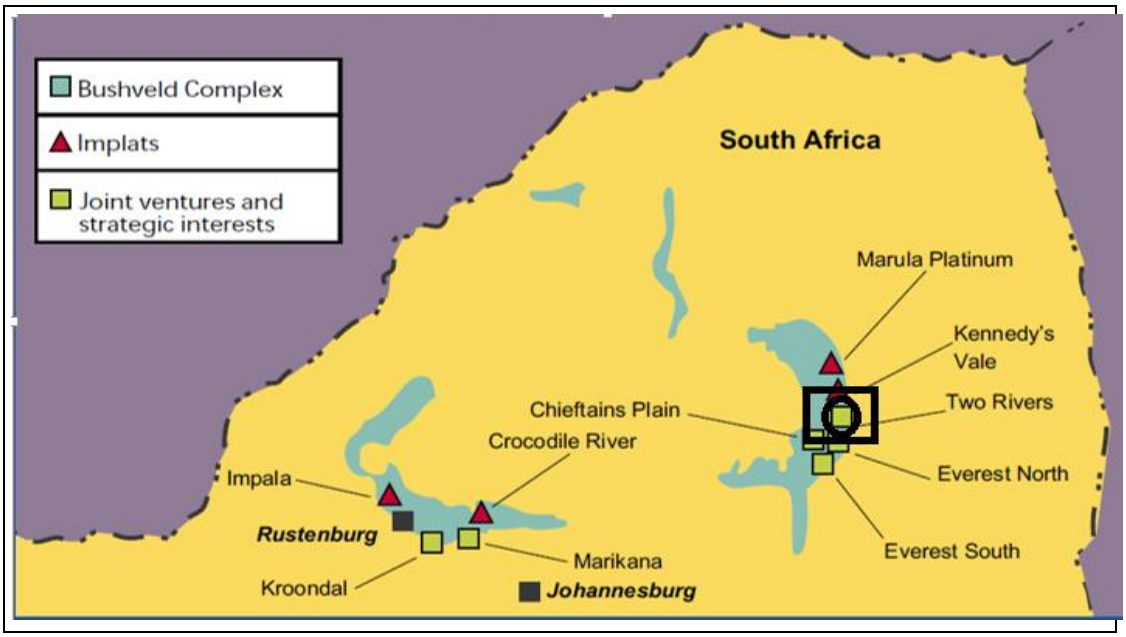

Figure 10.1_1 General setting of Two Rivers Platinum Mine in relation to other platinum producers in the eastern Bushveld (Implats Web site 2012)

Two Rivers Platinum Mine exploits the UG2 reef.

The UG2, including the pyroxenite parting and the leader horizon, ranges from surface to a depth of 650 m, with an average thickness of 2.1 to 2.3 m. The hanging wall and footwall consists of pyroxenite. Figure 10.1_2 shows detail of the geology in the immediate hanging wall of the UG2 horizon.

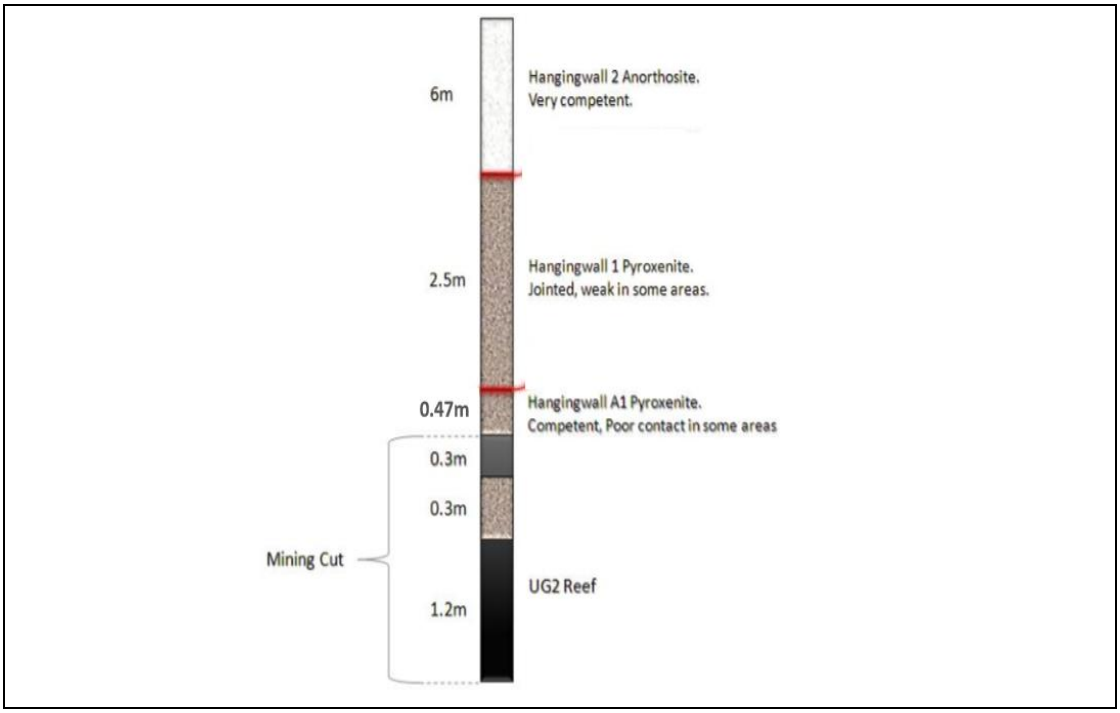

Figure 10.1_2 Geological section through the ore body and the immediate hanging wall (Code of practice, Two Rivers Platinum Mine, 2007)

The pillar design dimensions are 6 by 6 m with 6 by 6 m bords.

10.2 Rock mass data

Detail of the uniaxial compressive strength data set was discussed in in section 5.1.1 while the parameters as used for the Hoek-Brown failure criterion are given below.

Figure 10.2_1 is a repetition plot from section 5.1.1, showing the result of Kriging in the area where the specific boreholes were drilled (van der Merwe, 2013). The average value of the uniaxial compressive strength must lie between 100 and 140 MPa. Table 10.2_1 gives an arithmetic mean of one intersection of 129 MPa.

Note: the variation within this intersection also lay between 100 and 173 MPa with the majority of values falling in the 100 to 140 MPa range. It appeared that the variation within the intersection mirrored the variation over a wider area in plan.

For the calibration run the mean of the data set as given Tables 10.2_1 was used.

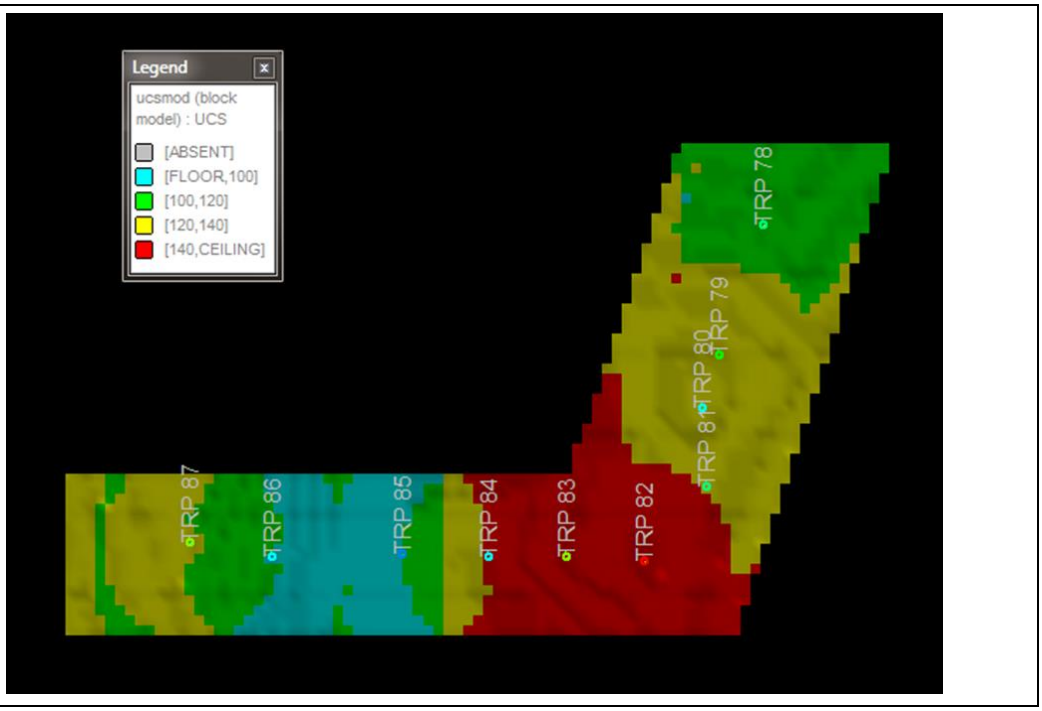

Figure 10.2_1 Borehole data distribution, van der Merwe, (2013) (Repeat of Figure 5.1.1_5 for convenience).

Table 10.2_1, contains the laboratory results for individual samples, including the pyroxenite, and the calculated shear and bulk moduli for an intersection of the UG2 reef. The mean for the entire pillar is given in the bottom line. Note: the tangent moduli were used since it was the deformation at "failure" that was important in the present context. Also included is the $sigc$ obtained using the RocLab programme at a constant GSI value of 80, m_i value of 22, and$s$, and s_r values of 0.1084 and 0.054 for a GSI of 80.

Table 10.2_1: Variation of rock properties over the width of an intersection of the UG2 (Data base at Two Rivers Platinum Mine)

	Distance		UCS	Etang		bu	sh	$sigc$
	From m	To m	MPa	GPa	v Tang	GPa	GPa	MPa
Leader			102	119	0.31	55	41	33.5
Pyroxenite			173	138	0.23	33	34	56.9
Chromitite	48.41	48.50	85	99	0.20	60	30	28.0
Chromitite	48.83	48.92	149	76	0.11	86	27	49.0
Chromitite	48.92	49.01	106	42	0.26	14	46	35.0
Chromitite	49.20	49.29	132	73	0.36	96	47	43.0
Chromitite	49.29	49.38	139	125	0.35	51	24	45.6
Chromitite	49.42	49.51	120	121	0.29	131	34	39.5
Chromitite	49.51	49.60	159	62	0.30	20	15	52.3
Chromitite	49.60	49.68	131	94	0.38	104	45	43.1
Mean			**129.6**	**94.9**	**0.279**	**70**	**30**	**42.6**

10.3 Previous work

The Initial design of the mine used the standard Hedley-Grant/Tributary Area Theory methodology as detailed in the standard Code of Practice for Two Rivers Platinum Mine.

The function of the pillars were as follows:

- Acting as systematic non-yield pillars.
- Designed for a factor of safety of at least 1.6.
- Designed to remain stable and intact.
- Supporting the full over-burden to surface.

The pillars have the following characteristics:

- Pillar size increased with increasing depth, from outcrop to 670 m.
- Surface topography had been taken into consideration.
- The Hedley Grant/ Tributary Area Theory method was used to determine the pillar sizes.
- No regional pillars were planned, but it was estimated that approximately 30% of reserve was classified as geological losses.
- As far as possible, these structures were left unmined and formed regional pillars. (Esterhuizen, 2011).
- From a perusal of the plans of the mined-out area, it was estimated that the average distance between potholes was 220 m.

For the initial mine design the k value was estimated to be 0.5 of the uniaxial compressive strength, 66 MPa.

As the depth of mining increased, the design factor of safety was maintained at 1.6 and pillar sizes adjusted accordingly.

10.4 Pillar observations

Stoping Section 9, 7N stoping was selected for calibration since it was the deepest section on the mine, 650 m below surface, and designed according to the standard procedure.

No distinctive fracture zones were present in the pillar sidewalls. Only occasional slight curvature of the hanging wall/ sidewall intersection was observed, Figure 10.4_1, while in instances, where a “remnant” was created just before holing into the upper drive, curved stress induced fractures in the pillar before holing could clearly be seen, (Figure 10.4_2).



Figure 10.4_1 Edge of pillar in 7N panel, slight curvature at top of pillar and initial spalling, note distinct fractures, on sidewall

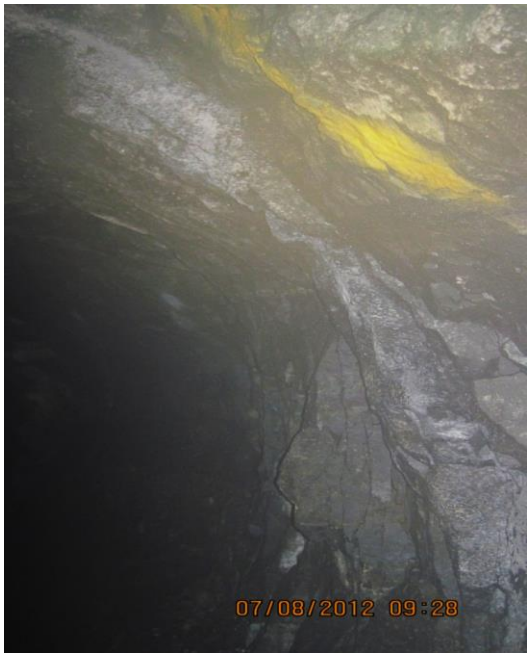

Figure 10.4_2 Face of up dip split before holing showing stress induced curvature over the whole face

10.5 Calibration

7N Stoping.

The actual width, length and stoping width of individual pillars in the section were measured on a plan of 1:500 scale and individually listed in a spreadsheet Figure 10.5_1 shows a portion of the selected area.

The surface topography was included in calculating the vertical stress component. Figure 10.5_2 gives the result of a *FLAC2D* simulation showing a dip section with the 7N line situated at a depth of 650 m below surface. The vertical stress contours shows the influence of the mountain side with the vertical stress component at 7N stope of 18 MPa and, in this instance, the same as that obtained by using the depth of 650 m multiplied by the density of 2800 kg/m^3.

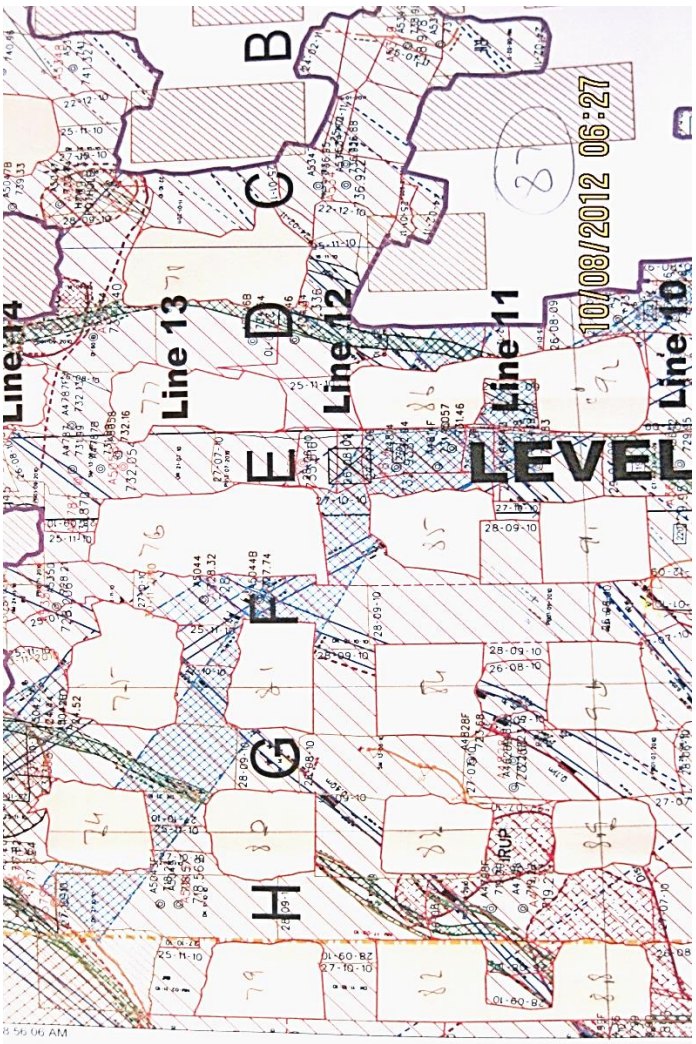

Figure 10.5_1 Stoping outline of portion of 7N panel

Calibration at this mine was based on the onset of pillar scaling/stress induced fracturing. Underground observations were that the scaling of pillars was in the initial stages.

Average stoping width in the section was 2.6 m.

The mine staff ascribed these fractures to the effect of blasting but the author decided the following:

- Blast damage did not produce the observed sidewall parallel fractures
- They were totally absent at shallower depth where the blasting method was the same.

- They also did not exhibit the typical blast fracture properties as defined by Saiang. (2008) the main criterion being that blast induced fractures propagated from drill holes while stress induced fractures did not.

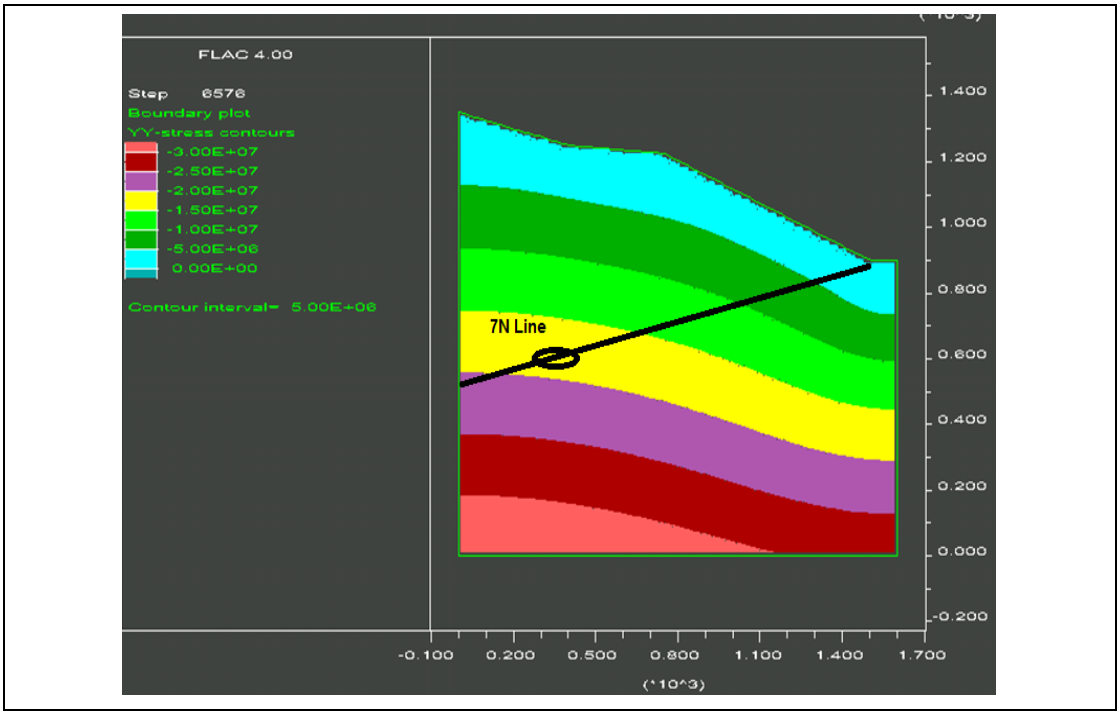

Figure 10.5_2 Stress distribution along a section parallel to the main decline on the UG2 reef at Two Rivers Platinum Mine, showing position of 7N panel

10.6 *FLAC2D* models and simulations

The basic *FLAC2D*/Hoek-Brown programme was the same as for the previous calibration runs with the mean rock mass values given in Table 10.6_1.

Two geometries are modelled:

- Using the design dimensions
- Actual mean dimensions.

The input parameters for the SPEC analysis used were based on the planned design values for the pillar strength and convergence calculated using the composite *FLAC2D* model incorporating a pyroxenite layer in the chromitite seam.

Table 10.6_1: SPEC Input and Output, planned layout.

100

Properties	Young's Modulus GPa		68
	Poisson's Ratio		0.29
	Density kg/m^3		2800
Geometry	Pillar	Strike m	6
		Dip m	6
	Bord	Strike m	6
		Dip m	6
	Halfspan m		110
	Stope width m		2
	% Extraction		75
	Overburden m		650
Pillar Stress and convergence	Strength MPa		114
	Convergence m		7.12e-3

FLAC2D/H-B	
Average Pillar Stress MPa	71
Convergence m	3.28e-3
Factor of Safety	**1.61**

Using the design dimensions the factor of safety is well within the accepted range for the Bushveld mines.

Using the actual dimensions obtained from the plan, portion of which is shown in Figure 10.5_1, would give a more realistic picture of the actual situation.

Table 10.6_3 shows the safety factors calculated using the SPEC model for half spans of 20 to 200 m. With increase in the half span, the factor of safety calculated by the SPEC method approaches a value of 1.67 for wide spans. The weakening effect of the increase in stope width from 2 to 2.6 m was off-set by the reduction in the percentage extraction, resulting in an acceptable factor of safety.

Table 10.6_2. : SPEC input and output for actual geometry.

Properties	Young's Modulus GPa		68
	Poisson's Ratio		0.29
	Density kg/m^3		2800
Geometry	Pillar	Strike m	6.8
		Dip m	5.87
	Bord	Strike m	3.9
		Dip m	4.4
	Stope width m		2.6
	Halfspan m		100
	% Extraction		63.7
	Depth m		650
Pillar Stress and convergence	Strength MPa		83
	Convergence m		6.6e-3

FLAC2D/H-B	
Average Pillar Stress MPa	49
Convergence m	2.4e-3
Factor of Safety	**1.69**

Table 10.6_3: Factor of safety and pillar stresses for various half spans using design parameters for the pillars and bords

Half Span m	Factor of safety
40	1.75
60	1.72
80	1.70
100	1.69
200	1.67

Figure 10.6_1 is the contour diagram of the volumetric strain increment of a 2.6 high with effective width of 6.2 m pillar in the 7N stoping setting for a halfspan of 100 m based on the average pothole spacing of 220 m.

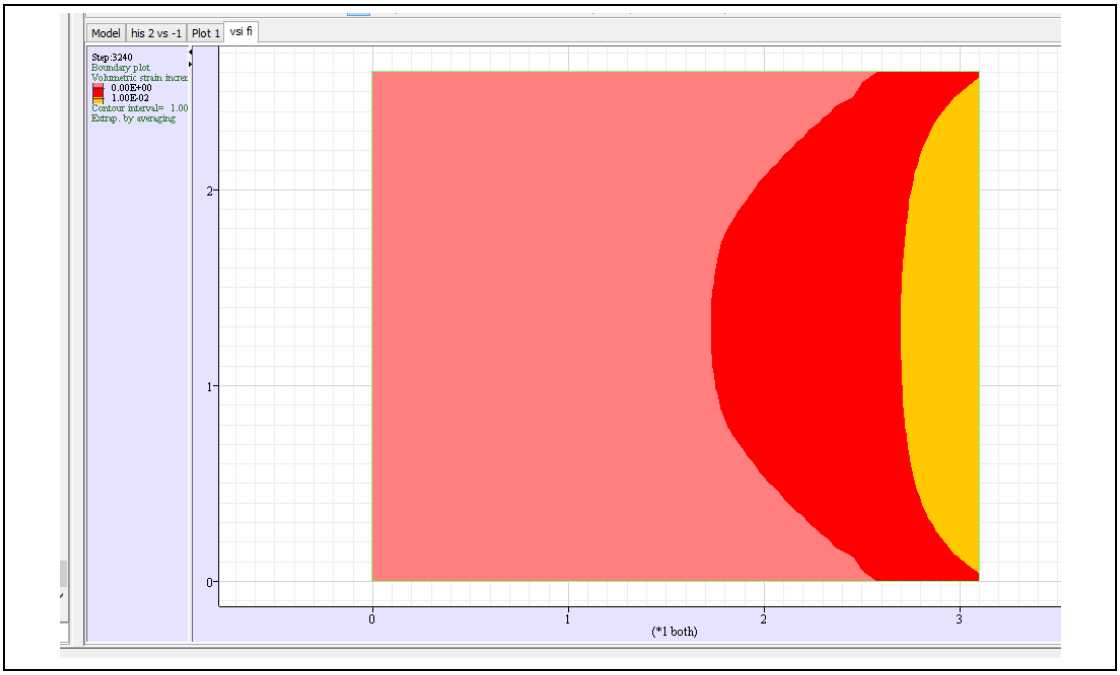

Figure 10.6_1 Volumetric strain increment contours for a 2.6 high by 6.2 m pillar at a half span of 100 m

The volumetric strain increment of 1e-2 is situated 0.4 m from the edge of the pillar boundary. The induced fracturing does not mean that the pillar has "failed", the factor of safety is still in excess of 1, progressive fracturing, i.e. the portion that has failed, vsi>1e-2, remains constant for the system equilibrium condition. This was borne out by underground observations.

10.7 Conclusion

Chromitite pillars started showing signs of scaling at a critical volumetric strain increment value between 1e-2 to 2e-2.

11 GENERAL CONCLUSION FROM THE CALIBRATION.

A summary of the conclusions of the calibration runs/back analysis is given below.

- The volumetric strain increment value for failure initiation lay between 1e-2 to 3e-2 for the extent of the fracture zone.
- The stress at failure at the boundary between the dog-earing and fractured rock ranges between 20 and 120 MPa, not a reliable method.
- Pillar stresses calculated using the SPEC method compared well with those obtained from the TEXAN code at 822 m and 1132 m below surface.
- The dilation predicted for a pillar at a depth of 1132 m below surface fell within the observed range for limited time spans

The general conclusion is that there is a good correlation between measured underground data and the results obtained from the modelling methodology used.

PART IV

The previous three sections dealt with defining deficiencies of the current design method, followed by proposals for an alternative pillar strength and loading design. The alternative system was subjected to a calibration process where it was found that the proposed method could be used to predict the onset and extent of fracturing as well as the stresses acting on the pillar.

It was found that the FLAC2D modelling can be used to derive pillar strength as well as pillar behaviour using an apparently lengthy process. In order to facilitate the process in practice a simpler procedure for obtaining pillar strength would be advantageous.

Part IV deals with the simplification of the pillar strength determinations in order to be able to subject it to sensitivity analysis using the Monte Carlo simulation as well as simplifying the prediction of pillar behaviour for various sections of a mine.

12 DERIVING A SIMPLE STRENGTH EQUATION.

12.1 Derivation of a simple pillar strength equation.

FLAC2D simulations are not routinely done on the mines and it would be an advantage if a simple equation could be derived for the pillar strength for given pillar dimensions, which would be able to handle the number of variables to investigate probability of failure.

In addition to the above, a simplified equation including the system stiffness could be incorporated in a Monte Carlo method simulating the effect of the high variability of the input parameters on the factor of safety and probability of failure.

To obtain a simplified strength equation it was decided to select a representative set of values that would cover the general ranges of values discussed previously. The results of the data set was then used to obtain regression curves representing the pillar strength as obtained from *FLAC2D*/Hoek-Brown simulations.

- The pillar width-to-height ratios ranged from 1 to 5 for a stoping width of 2m.
- Since the thesis deals with mechanised bord and pillar workings, a 2m mining height was used.
- The material properties are shown in Table 12.1_1.
    - The uniaxial compressive strengths = 60, 80, 100 and 120 MPa
    - Geological Strength Indexes = 60, 70, 80 and 90
    - m_i = 22.
- The GSI was set at 80 for the initial data set.
- The *FLAC2D*/Hoek-Brown model used is shown in Appendix IV.

Assumptions made with regard to them_i, m_b and $m_r$values

- The m_i value was kept constant in all the calculations with the GSI influence incorporated in the m_b values.
- The residual value, m_r strongly influences the pillar strength as well as its post-failure behaviour. Since little was known about the m_r value it was kept at 50% of the m_b value.

The *FLAC2D*/Hoek-Brown model used in all the runs was discussed in detail in Section 4.6. The programme models a 2 m high circular pillar with a variable radius. The required input parameters for the Hoek-Brown/*FLAC2D* programme were expressed in terms of the bulk and

shear moduli and the density of the rock mass. The failure criterion was defined by the Roclab parametersm_i, *s* and $sigc$ with their respective residual values. (Table 12.1_1).

Table 12.1_1: Properties data set at GSI 80

UCS MPa	bu GPa	sh GPa	m_b	m_r	s	s_r	$sigc$ MPa
120	80	38	11.28	5.14	0.1084	0.054	39.5

The Hoek-Brown criterion was given by the FISH function, hoek2.fis.

A series of runs were done using the above programme to establish the effect of a change in the pillar geometry, GSI changes as well as uniaxial compressive strength. Table 12.1_2 gives some of the results obtained in terms of the geometrical changes.

The data shown in the table 12.1_2 was extended to obtain the pillar strength for 80 different configurations, Appendix V:

- GSI values of 60, 70, 80 and 90
- Uniaxial compression for 60, 80, 100 and 120 MPa
- Width-to-height ratios 1, 2, 3, 4 and 5.
- The stoping width was kept constant at 2 m
- The $m_i$value was kept constant at 22.

Table12.1_2: Example of selected pillar strength values for different sized pillars at variable GSI and UCS values. Constant pillar height of 2 m.

UCS MPa	GSI	Diameter (m)	Pillar w/h	Pillar strength MPa
60	60	2	1	6.2
60	60	4	2	8.6
60	60	6	3	12.6
60	60	8	4	17.1
60	60	10	5	21.5
80	80	2	1	18.5
80	80	4	2	42
80	80	6	3	71
80	80	8	4	107
80	80	10	5	146
100	60	2	1	7.6
100	60	4	2	11.2
100	60	6	3	17
100	60	8	4	24.3
100	60	10	5	31.4
100	80	2	1	23
100	80	4	2	51
100	80	6	3	89
100	80	8	4	131
100	80	10	5	178

Note: The remainder of the strength data is given in Appendix V.

The values in Table 12.1_2 are plotted in 12.1_1.

Curves were fitted to the data in Figure 12.1_1 and it was found that they can be represented by a power equation, 12.1.

$$\sigma_{str} = \delta(\frac{w}{h})^{\beta} \qquad 12.1,$$

Where δ and β = Constants dependent on GSI and UCS.

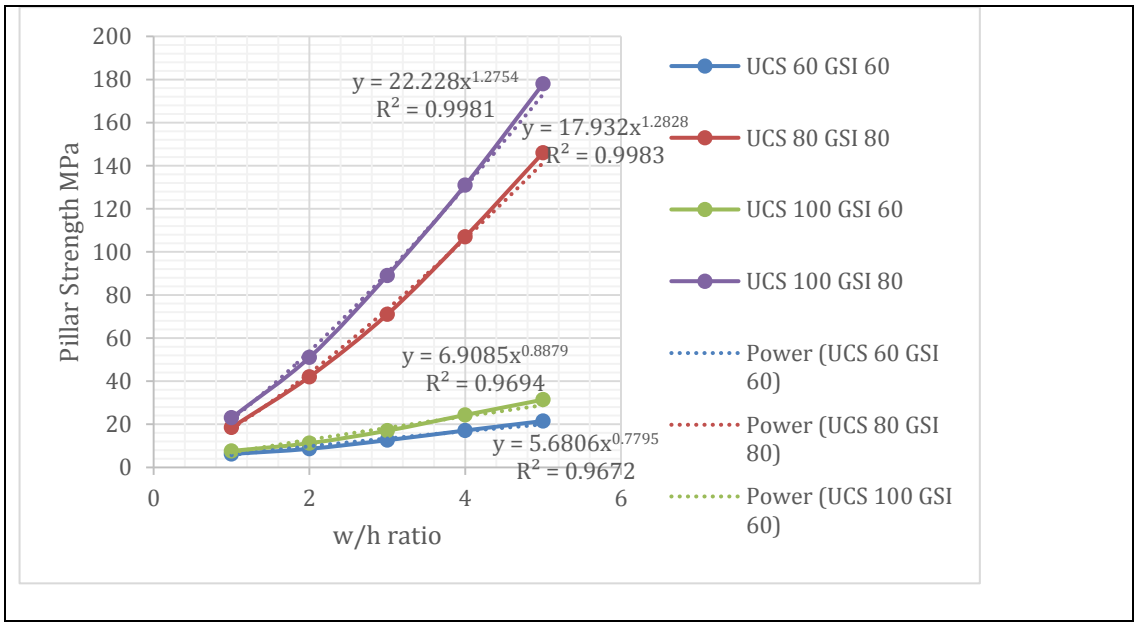

Figure 12.1_1 Example of pillar strength for GSI values of 60 to 90 and a UCS values of 60, 80 and 100 MPa.

The pillar strength values for the combinations of UCS of 60, 80, 100 and 120 MPa and GSI values of 60, 70, 80 and 90 are given in Appendix V. Also shown in Appendix V are the values for the individual values for Delta, Beta as well as the correlation coefficients.

For instance, the Delta value in Figure 12.1_1 for a UCS of 100 MPa and a GSI value of 80 are 22.22 and 1.2754 with a correlation coefficient of 0.9981.

By curve fitting it was established that the Delta (δ) and the Beta (β) values could be defined in terms of known Hoek-Brown parameters.

According to the Hoek-Brown criterion the GSI value has the greatest effect on the rock mass properties, see equations 5.1 to 5.4, in Section 5. It must, therefore, be assumed that using *FLAC2D*/H-B criterion combination that the effect of the GSI value will be significant.

By curve fitting, it was found that the Delta value can be expressed as a function of the GSI values. The equations, 12.2 to 12.5, were obtained for UCS values of 60 to 120 MPa and GSI values for 60 to 90, Figure 12.1_2.

$$\delta = 0.0999e^{0.0704GSI} \qquad 120 \text{ MPa} \qquad 12.2$$

$$\delta = .1089e^{0.0674GSI} \qquad 100 \text{ MPa} \qquad 12.3$$

$$\delta = .1675e^{0.06GSI} \qquad 80 \text{ MPa} \qquad 12.4$$

$$\delta = 0.1652e^{0.0574GSI} \qquad 60 \text{ MPa} \qquad 12.5$$

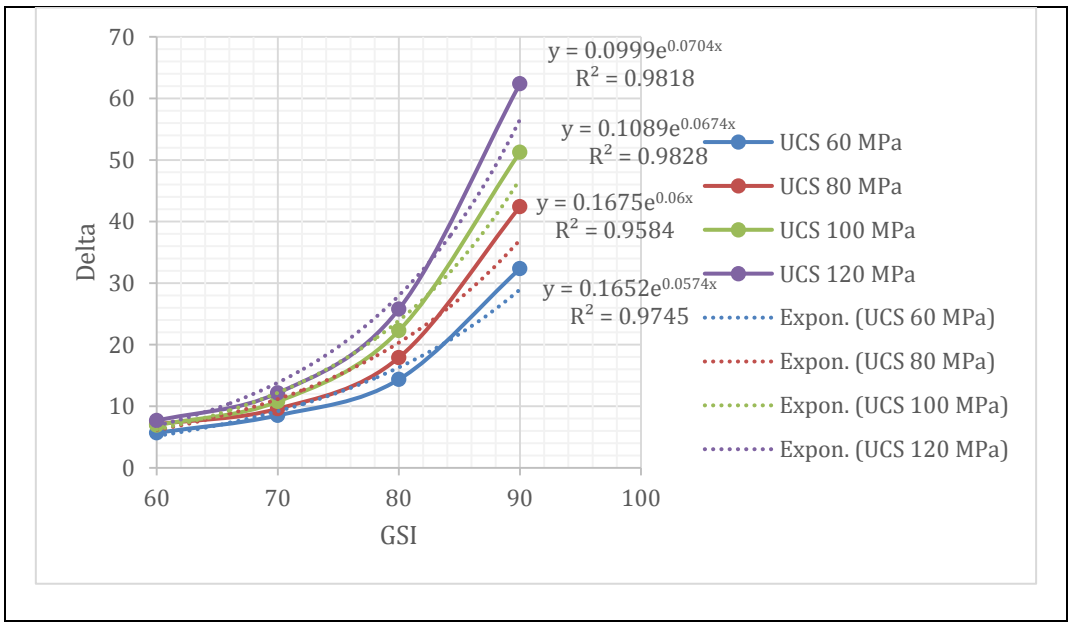

Figure 12.1_2. Correlation between the Delta value and GSI.

A similar plot of the Beta values in terms of the GSI values, Figure 12.1_3, shows an increasing trend for the Beta values for low GSI values and then flatten off beyond 80. The trend, appears to be erratic but by plotting the individual values, ignoring the UCS values, Figure 12.1_4, a function of TANH, equation 12.6, was developed by Mathey (2015) for all the Beta values, shown in Figure 12.1_4.

.

$$\beta = TANH\left[\left(\frac{GSI-a}{b}\right)\right]c \qquad 12.6$$

Where a = 46.866

b = 16.916

c = 1.2906

The conclusion drawn from the above is that the Beta value represents the influence of the GSI on the overall pillar strength while the Delta value is a combination of the UCS as well as the GSI.

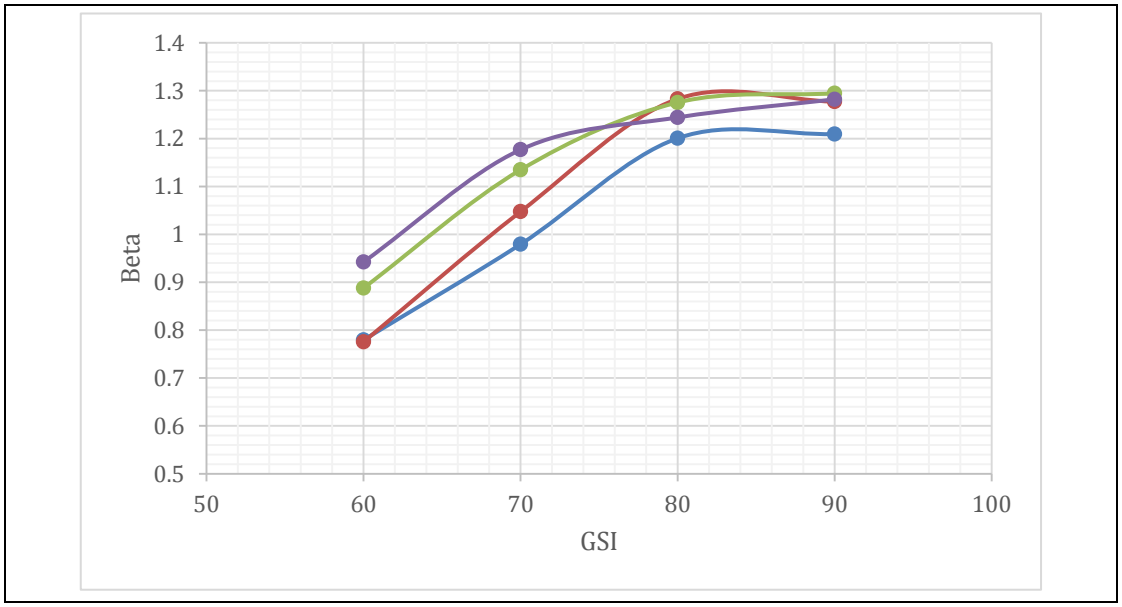

Figure 12.1_3 Beta value curves for GSI values of 60, 70, 80 and 90 for different UCS values.

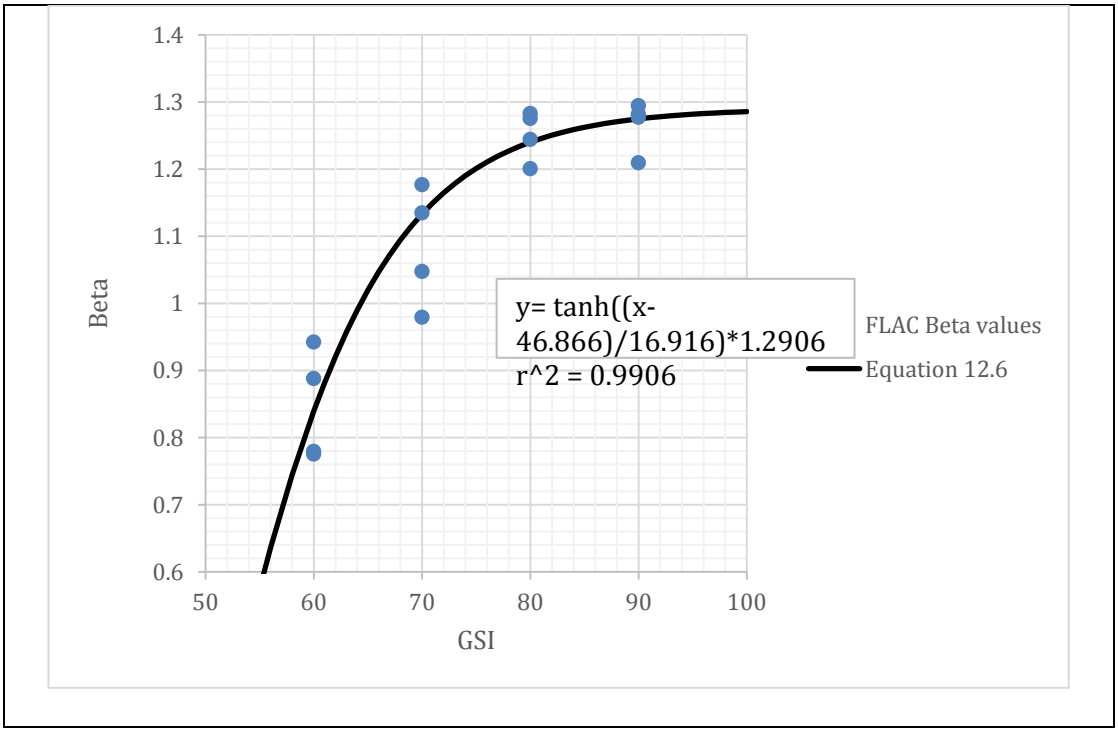

Figure 12.1_4. Beta values using equation 12.11 compared to all beta values obtained from FLAC2D modelling, Appendix VI.

With a reasonable definition for the Delta and Beta values, the generic equation can be used to calculate the strength of pillars using the values given in Tables 12.1_3 and 12.1_4

Table 12.1_3 Delta values for a given range of GSI and UCS values.

	GSI	UCS 60 MPa	UCS 80 MPa	UCS 100 MPa	UCS 120 MPa
	60	5.1727	6.1302	6.2132	9.7623
	70	9.1834	11.1700	12.1907	13.6722
	80	16.3039	20.3530	23.9190	27.6428
	90	28.9451	37.0856	46.9308	55.8888

Table 12.1_4 Beta obtained using the equation 12.11.

GSI	60	70	80	90
Beta	0.8397	1.1333	1.2402	1.2749

For the range 60<UCS<120

60<GSI<90

1< w/h <5

m_i = 22

h = 2 m

To determine what the effect of the assumptions made in the above correlations, a comparison was made between the *FLAC2D*/Hoek-Brown curves and those predicted using equation 12.1. The result is shown in Figure 12.1_ 5. It is concluded that the generic equation can be used to predict pillar strengths for the given ranges of UCS and GSI values.

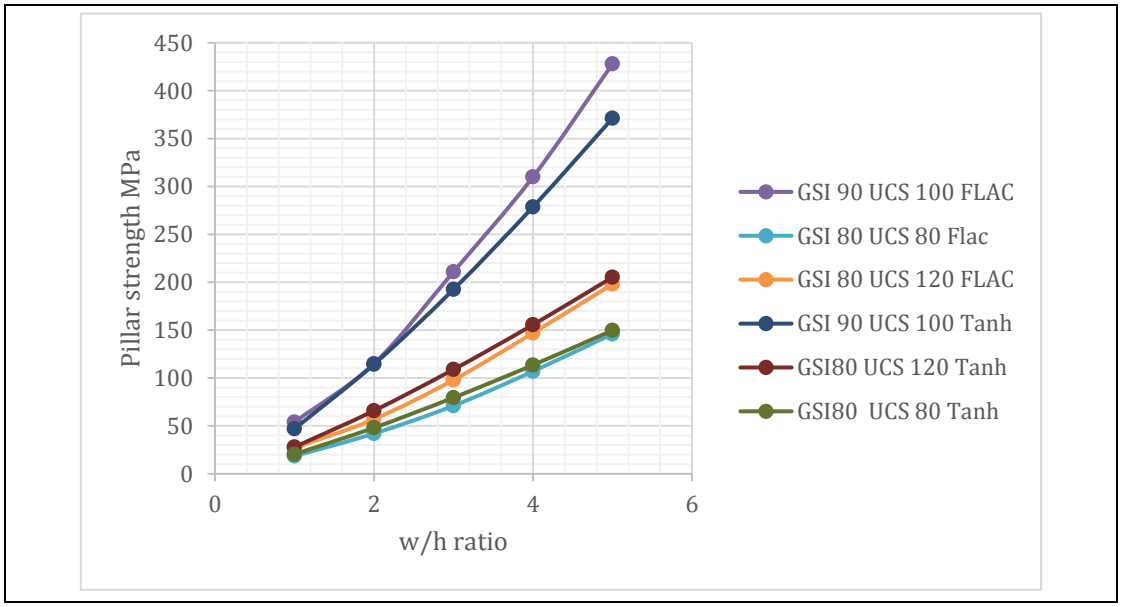

Figure 12.1_5 Comparison between the calculated pillar strength *FLAC2D*/Hoek-Brown simulations and the generic equation 12.1.

To check the validity of the generic equation for different stoping widths, check runs were made using stoping width of 1.5 m for the relevant w/h ratio. It was found that for the UCS of 100 MPa and a GSI of 90, the pillar strength values were 310 MPa (2 m) and 306 MPa (1.5 m). Similarly for a UCS of 120 MPa and a GSI of 80, the strength values were again comparable at 155 and 147 MPa.

12.2 Properties of the proposed equation.

Equation 12.1 includes the effects of the rock mass properties consisting of the uniaxial compressive strength, GSI, m_i as well as the geometric component of the pillar.

A comparative study was made for a UCS of 120 MPa, GSI 85 with the δ value held constant at 52.12 MPa but varying the β value of 0.8, 1.0 and 1.2 with results shown in Figure 12.2_1.

Figure 12.2_1 shows that for β values less than 1, the pillar strength rate of increase decreases with an increase for the w/h ratio. The opposite occurs when the β value is in excess of 1 while it is linear for a β value of 1.0, which is obtained at a GSI of 64.35.

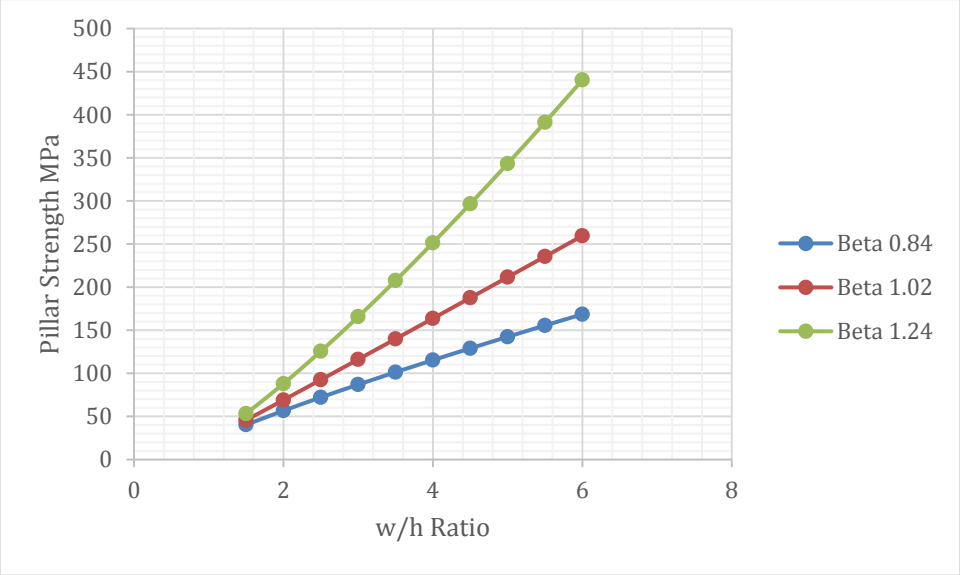

Figure 12.2_1. Various curves for the strength w/h ratios and β values.

The shape of the strength curves for 1.0 > β > 0.8 simulates the Hedley-Grant and derivatives of the Salamon strength curves. For β = 1, the linear Ryder and Ozbay (1990) equation is valid while the shape for β > 1 is described in this thesis.

The conclusion is that for rock masses with GSI < 64.35, the shape of the pillar strength curve is the same as those obtained using the Hedley-Grant and the Salamon-Munro (1967) equation. This demonstrates the power of the proposed new equation – for lower quality rock types, i.e. with GSI < 64, it indicates a decreasing strength increment while for higher quality rock types it predicts an increasing strength increment for increasing w/h ratio.

For lower strength material with a GSI < 60, the newly derived Overlap Reduction equation for coal mines (van der Merwe and Mathey, 2013) can be used as a reality check.

The empirically derived Overlap Reduction equation for coal pillar strength is given below:

$$\sigma_{str} = k\left(\frac{w^{0.8}}{h}\right) \qquad 12.7$$

Where k = Strength value

= 5.47 MPa for Witbank coal.

Using the proposed generic equation with estimated constants for low quality rock with UCS=40 and GSI= 60; a realistic comparison with coal, gives δ= 4.3 and β = 0.8397.

Figure 12.2_2 gives the strength of coal pillars using the Overlap Reduction equation as well as the generic equation. Similar values are obtained.

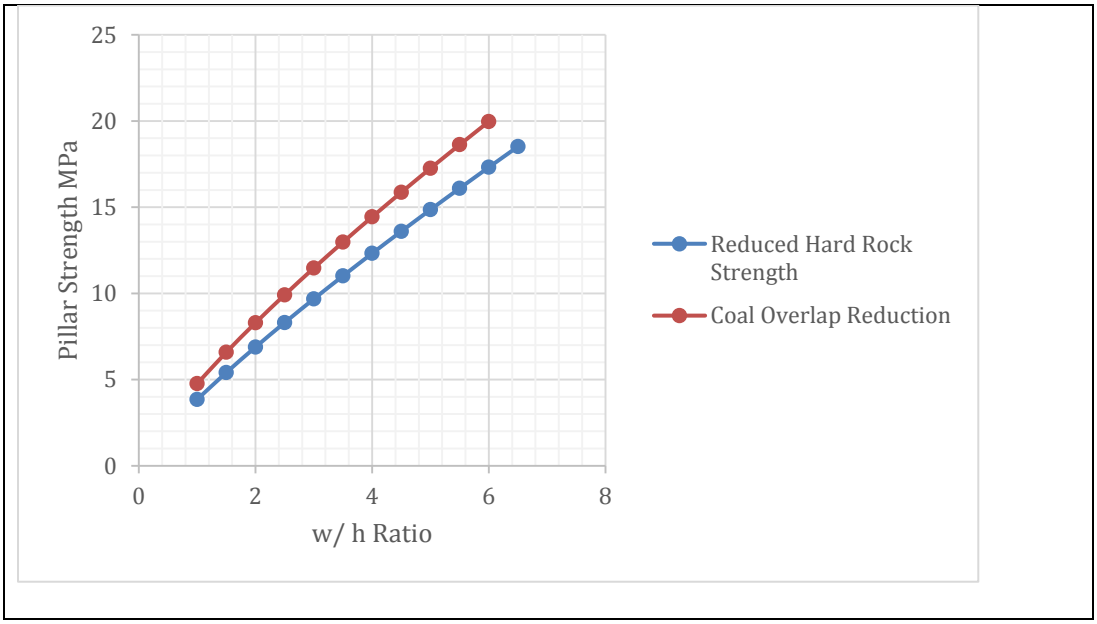

Figure 12.2_2. The Overlap Reduction Equation curves for coal and a low strength hard rock.

12.3 Comparison with pillar equations derived by Watson (2010) for the Merensky reef.

Watson (2010) conducted a detailed examination of crush pillars on the Merensky reef. The geometries of the experimental sites differed from a bord and pillar configuration with pillars spaced 30 m on dip and a stope width generally of the order of 1.5. The presence of footwall gullies increased the geometrical complexities of the pillar simulation but it was concluded that the results obtained could be used to compare the pillar strengths obtained by Watson with those obtained in this thesis.

The equations as used by Watson with their relevant properties are shown in Tables 12.3_1 and 12.3_2.

Table 12.3_1. Copy of data input from Watson (2010) Thesis, linear equation 5.10.

$$PS = K_i\left[b + (1-b)\frac{w_e}{h_e}\right] \qquad \textit{5-10}$$

Only two parameters are required in Equation 5-10 and the back-fit values are provided in Table 5-5.

Table 5-5 Back-fit values for Equation 5-10

Parameter	Value
K_i (*In situ* cube strength)	147 MPa
b (Linear w/h_e parameter)	0.70
s	0.075

Table 12.3_2. Copy of data input from Watson (2010) Thesis, power equation 5.11.

$$PS = K w_e^{\alpha} h_e^{\beta} \qquad \textit{5-11}$$

Table 5-6 Back-fit values for Equation 5-11

Parameter	Value
K	86 MPa
α (Effective width parameter)	0.76
β (Effective height parameter)	-0.36
s	0.080

The pillar strengths obtained using equations 5-10 and 5-11 (Tables 12.1_1 and 2) _are plotted in Figure 12.3_1 in conjunction with pillar strength values obtained using the *FLAC2D*/H-B model for a UCS of 120 MPa and GSI values of 90 and 80.

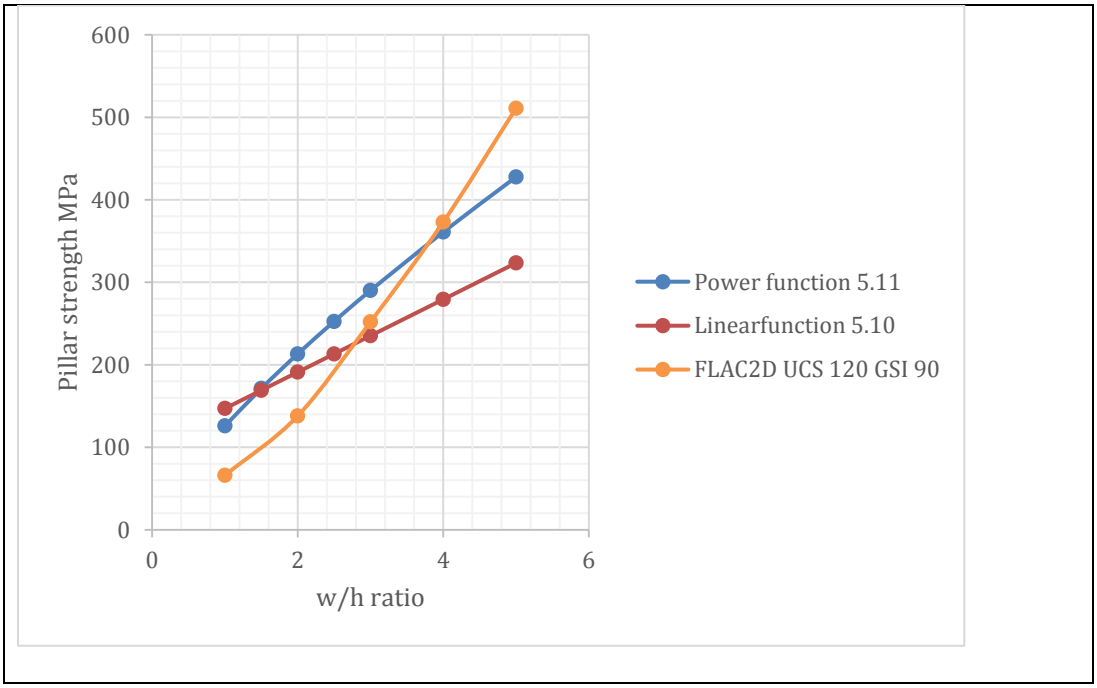

Figure 12.3_1. Comparison between Hedley-Grant, power equation 5.11 and 5.10 linear equation with the *FLAC2D*/H-B simulations.

Both equations, 5.10 and 5.11, give very high strength values for pillars at low w/h ratios; a pillar strength of 150 MPa for a w/h ratio of 1 is more than double that obtained by the Hedley-Grant equation, k value of approximately 60 MPa, used to date in some of the Bushveld mines.(See Table 2.1.5_1.)

The pillar strength values derived by Watson used k values of 86 and 147 MPa, Tables 12.3_1 and _2. To date the empirical back-analysis internationally have shown that the derived k value ranges from 0.69 to 0.31, Table 3.5_1, Section 3.5, as well as those obtained for pyroxenites in the Bushveld. The k values used by Watson are in excess of these ranges. The possible explanation could be found in the determination of the Average Pillar Stress, APS, obtained as described in the quote from Watson (2010):

"APS was estimated from stress measurements conducted in the hangingwall above the instrumented pillars. Appropriate conversion factors were determined from MinSim models and Boussinesq evaluations ……. Comparisons between the measurements and elastic models showed that stress-change measurements had to be evaluated using the "matrix' modulus of the host rock. However, the field measurements that were affected by microfracturing were evaluated using the methodology shown in Section 3.8. Peak pillar strengths were checked using detailed MinSim models of the stopes and the linear peak pillar strength formula".

The process was complicated and in conjunction with complex geometry of the pillars could explain the high values.

The generic *FLAC2D*/H-B equation, UCS 120 MPa and GSI 90, tends to agree with the standard Hedley-Grant equation below w/h ratios of 3 while value range corresponds more with the results obtained by Watson at a width-to-height ratio 4 to 5, Figure 12.3_1.

The calibration using data from Watson (2010) is not conclusive and additional data from underground is required for a final conclusion. It is predicted that the determination of the failure strength of a pillar underground will require more observation than just pillar scaling as done to date, especially at w/h ratios in excess of 3. The extent of the fracture zone into the pillar is thought to be a definitive criterion.

12.4 Incremental increase in strength with increase in w/h ratio

In addition to the discussion and conclusions in Section 12.2, recent experimental work by Mathey (2015) has shown that incrementally strength increase occurs in sandstone and granite test specimens. He conducted 42 tests each on granite and sandstone specimen and found that for both, a bi-linear strength/width-to-height ratio curve was obtained, Figure 12.4_1, for granite, similar in shape to that of the generic/*FLAC2D*/H-B equation.

The change in slope occurs at w/h ratios of 3.5 to 4 an incrementally increase in strength with increase in the w/h ratio.

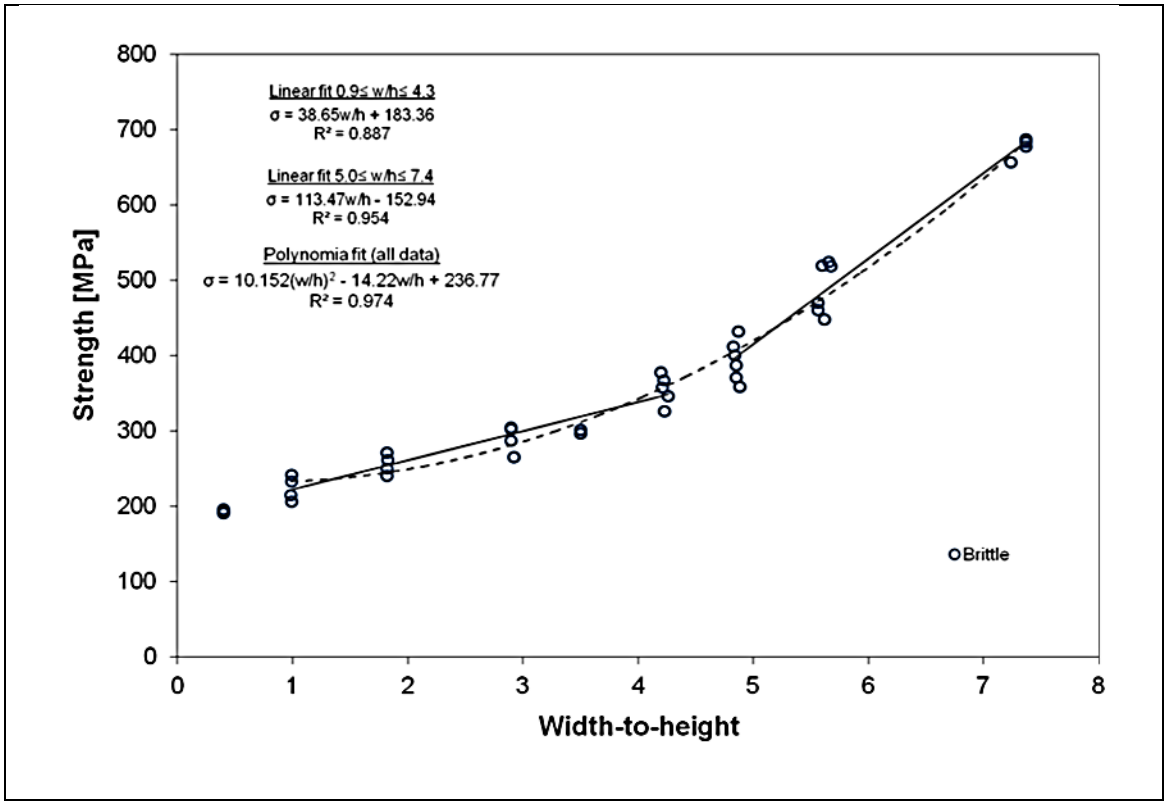

Figure 12.4_1. Bi-linear strength curve for granite obtained by Mathey (2015)

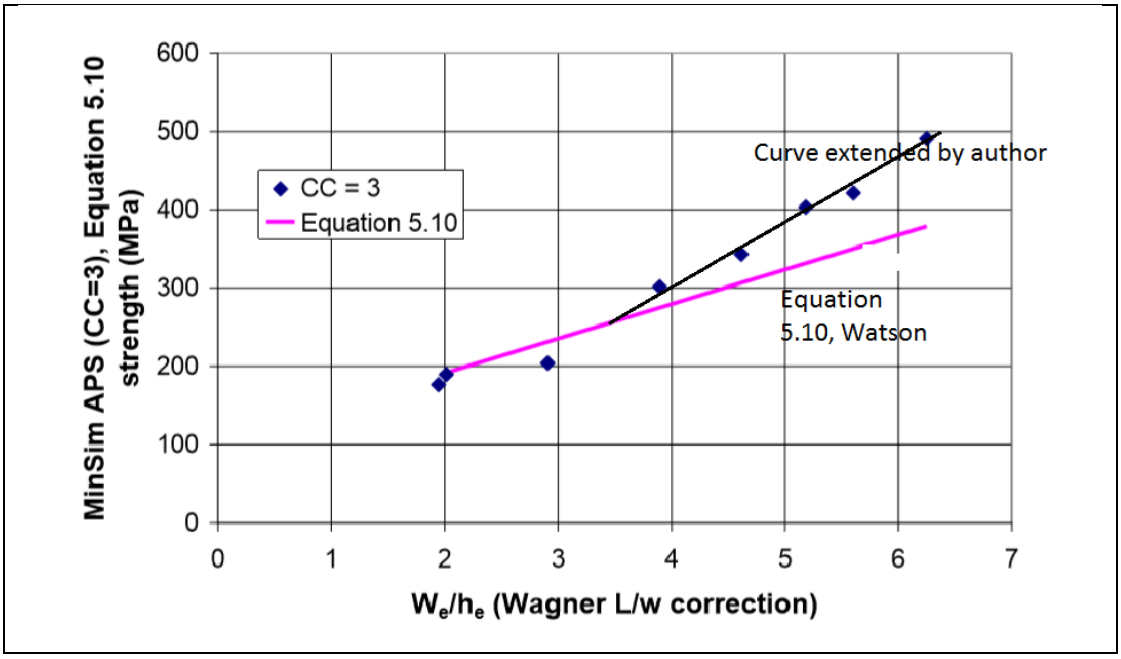

Figure 12.4_2. Possible bi-linear behaviour, Watson (2010)

Additional confirmation of the existence of such a trend is deduced from Figure 12.4_2 which is a strength curve copied from Watson (2010), showing the increase in pillar strength with increase in the w/h ratio using the linear equation. The lower linear curve was inserted by Watson, Equation 5.10.

It appears that the strength values derived from underground observations increase incrementally beyond a w/h ratio of 3.5. A line drawn by the author through the data points shows that the resulting change in slope is similar to the bi-linear curve obtained by Mathey and also shown in the *FLAC2D*/H-B models.

12.5 Summary.

- It was established that the pillar strength curves for different width-to-height ratios, uniaxial compressive strengths could be expressed by a simple power function.
- The proposed simplified equation incorporates the uniaxial compressive strength and the GSI value representing the rock mass variation apparently effectively.
- The equation makes it possible to include variation of rock mass properties over individual areas of a mine and adjusted accordingly.
- The generic/*FLAC2D*/H-B equations appears to simulate a range of empirical derived curves for the full range of width-to-height ratios, 1 to 5.
- The strength values obtained in this manner could be used in the SPEC methodology by using the rock mass Young's modulus to calculate the pillar convergence.

- The observed change in the slope of the pillar strength curve appears to be valid and needs further investigation.

- The generic equation 12.1 deals with homogeneous pillars under certain boundary conditions. Any changes from these pre-requisites makes it necessary to make use of more of the facilities available in the *FLAC2D* program.

12.6 Variability of input data and its influence on pillar design

According to van der Merwe (2014) the Monte Carlo simulation calculates the probability of pillars having a factor of safety less than a specified number, based on the variability of the input such as bord width, depth, *et cetera*. In essence, it repeated the calculation of the safety factor several hundred thousand times, each time selecting random input based on the specified distribution of the different input parameters. The distribution of the outcomes of the calculations was then used to determine which proportion of the outcomes was less than the specified number.

If it were postulated that a safety factor of 1.0 was the boundary between failure and stability, that is, that pillars with factors of safety less than 1.0 would fail while those with a factor greater than 1.0 would be stable, then the proportion of outcomes less than 1.0 would be the probability of failure.

If there were no variability in the input, that is, all the inputs were perfectly constant, then the variability of the outcomes would be zero and all the pillars would have a factor of safety equal to the deterministic value. The greater the variability of the input, the greater the spread of the outcomes would be and, consequently, the greater the probability of failure for any given deterministic factor of safety.

In practice, the real limit at which failure would occur is not as easy to determine as for instance with manufactured materials. In the case of coal mining in South Africa, the pillar strength had been determined by statistical back analysis of cases of failed and stable pillar lay-outs. There was, therefore, considerable variability in the output as there were so many variables that could not be incorporated into the back analysis. Some scope for variability had to be incorporated in the safety factor limits that were commonly applied.

In hard rock mining, statistical back analysis is not possible because there are simply not enough failed cases to allow reliable back analysis to be done. In this document, an analytical procedure was followed to determine the pillar strength and the important variables in the input to determine the strength had been identified.

We require the distribution of the inputs into the strength calculation ($sigc$, GSI, etc), but at that stage, these were not known.

In the remainder of this section, the influence of the variability of the controllable input parameters, such as bord width, pillar height, panel width*, et cetera*, on the probability of the

factor of safety being less than 1.0 was examined. For brevity, the probability of the safety factor being less than 1.0 would be termed the “Probability of Failure”.

The influence of the variability of the strength inputs was also shown for demonstration purposes. At this stage, it could not be used in practice as it required that the distribution of those variables, that is, type of distribution, mean and standard deviations, had to be known.

The variability of the controllable input parameters could be determined easily underground by simple measurement, and these could, therefore, be used in the practical situation.

Van der Merwe (2014) derived a simplified Monte Carlo simulation using an Excel spreadsheet. The simulation introduced all the relevant variables plus the standard deviation of the pillar width, height and depth. In essence it incorporates the pillar strength based on the simplified equation 12.1 in conjunction with the SPEC methodology, introducing the convergence component in pillar design.

The variables included in the simplified Monte Carlo simulations are:

- Geometrical parameters
    - Pillar centres
    - Pillar width
    - Pillar height
    - Depth below surface
- Rock mass properties
    - δ
    - Rock mass modulus
    - Pillar modulus
    - β

Each of these parameters was assigned a mean value with an associated standard deviation.

Individual simulations were done by varying one variable, based on the standard deviation, while maintaining constant values for the rest of the variables. For instance, the mean of the pillar distance is 10.5 m. The distances were then varied for a range between 9.79 and 11.25 and the factor of safety calculated maintaining the mean values for the rest of the variables.

This procedure is adopted for consecutive variables plotted in Figure 12.6_1 giving the average factor of safety and how it is influenced by the variations of the input parameters.

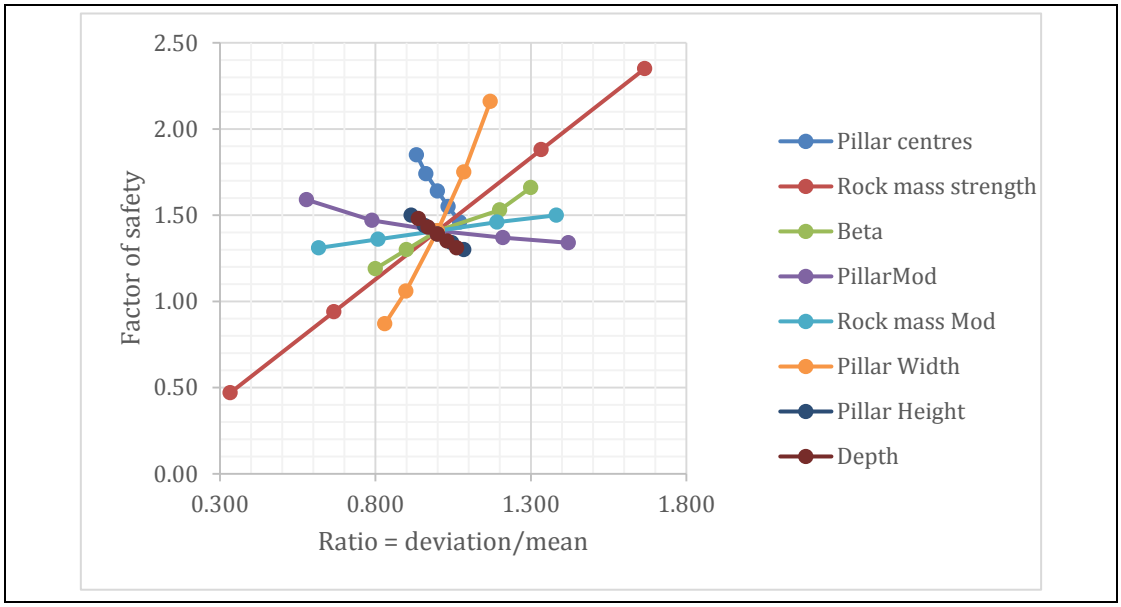

Figure 12.6_1 Sensitivities for the listed input parameters

The most important factors that influenced the result were rock strength, Delta, Pillar width, and Pillar centres.

In order of sensitivity on the Probability of Failure ranging from high to low are:

1. Rock strength- Delta
2. Pillar width
3. Pillar centres
4. Beta
5. Rock modulus
6. Pillar modulus
7. Pillar height
8. Depth

The sensitivity analysis shows that the pillar geometry and the rock mass properties need to be determined as accurately as possible.

12.7 Illustrative examples using the SPEC, the generic equation, Hedley-Grant and Tributary Area Theory.

To illustrate the difference of the results obtained using the *FLAC2D*/SPEC, the generic equation as well as the Hedley-Grant/TAT method, a typical mining situation was used input data given in Table 12.7_1.

12.7.1 Hedley-Grant/TAT methodology.

Table 12.7.1_1: Material properties and geometry of the mining layout.

Properties	Young's Modulus	GPa	68
	Poisson's Ratio		0.29
	Density kg/m^3		2800
	UCS	MPa	120
	Bulk Modulus	GPa	54
	Shear Modulus	GPa	26
	GSI		80
	m_i		22
	m_b		10.8
	m_r		5.4
	s		0.1084
	s_r		0.054
	$sigc$	MPa	39.5
	Hedley-Grant k	MPa	69
Geometry	Pillar	Strike m	8
		Dip m	8
	Bord	Strike m	6
		Dip m	6
	Stope width	m	2
	Halfspan	m	100
	Extraction	%	67.3
	Depth below surface	m	900

Using the standard TAT/H-G design method the pillar strength is 120 MPa with a pillar stress of 77 MPa giving a factor of safety of 1.55 at an extraction ratio of 67.3%

12.7.2 *FLAC2D*/Hoek-Brown with SPEC methodology.

Using the *FLAC2D*/Hoek-Brown model listed in Section 4.3.2, the pillar strength was calculated as 155 MPa for an 8 by 8 m pillar at a convergence of 7.85e-3 m.

Table 12.7.2_1. Input data required

Geometry	Depth h m	900
	Pillar width m	8
	Bord width m	6
	Span L m	200
	Stope width m	2
	Bord +pillar width X m	14
Properties	Young's modulus E GPa	68
	Shear modulus G GPa	26
	Poisson's ratio ν	0.29
8 by 8 m Pillar	Pillar strength σ_{pm} MPa	155
	Gravity acceleration g cm/sec^2	10
	Density ρ kg/m3	2800

Note: Rock properties as in Table 12.7.1_1.

The procedure for calculating the factor of safety equations is given in Table 12.7.2_1 are given in a format which can be transferred directly into an Excel spreadsheet.

Table 12.7.2_2: Equations and numerical values, *FLAC2D*/Hoek-Brown.

Equation		8*8 m pillar
	$\alpha = 2l/h$	2,22E-01
	$f(\alpha) = 1 + 0.41\alpha + 0.149\alpha^2 + 0.008\alpha^3$	1,10
6.3	$d_i = \left(\frac{2(1-\nu)\sigma_y l}{G}\right) f(\alpha)$	0,149
6.9	$C_g = XLg\rho H$	7.06e+10
6.10	$m_g = -\frac{c_g}{d_i}$	-4.67e+11

6.14	$d_p = \frac{\sigma_{pm}}{E}.h$	4.68e-03
6.15	$F_p = \sigma_{pm}.w^2$	1.02e10
6.16	$F_{pt} = F_p L/X$	1.45e11
6.17	$m_p = F_{pt}/d_p$	3.11e13
6.11	$F = \sigma_v A_m m_p / \left(m_p + \frac{\sigma_v A_m}{d_i}\right)$	6.95e10
6.18	FOS=F_{pt}/F	2.09

Where F_g = System force

m_g= Slope of the ground reaction curve

d_g = system convergence

F_p = Force on pillar

m_p = pillar stiffness

d_p = pillar convergence

c_g= total overburden weight

The factor of safety calculated using the *FLAC2D/*H-B methodology for a span of 200 m is 2.09. The FOS can be decreased by using 7 b7 m pillars and 6 m bords. The strength of the 7 b7 m pillar is 136 MPa and calculating the loading as given in Table 12.7.2_2 results in a FOS of 1.60; a generally acceptable design value. The percentage extraction increases to 71% as against 67.3 %.

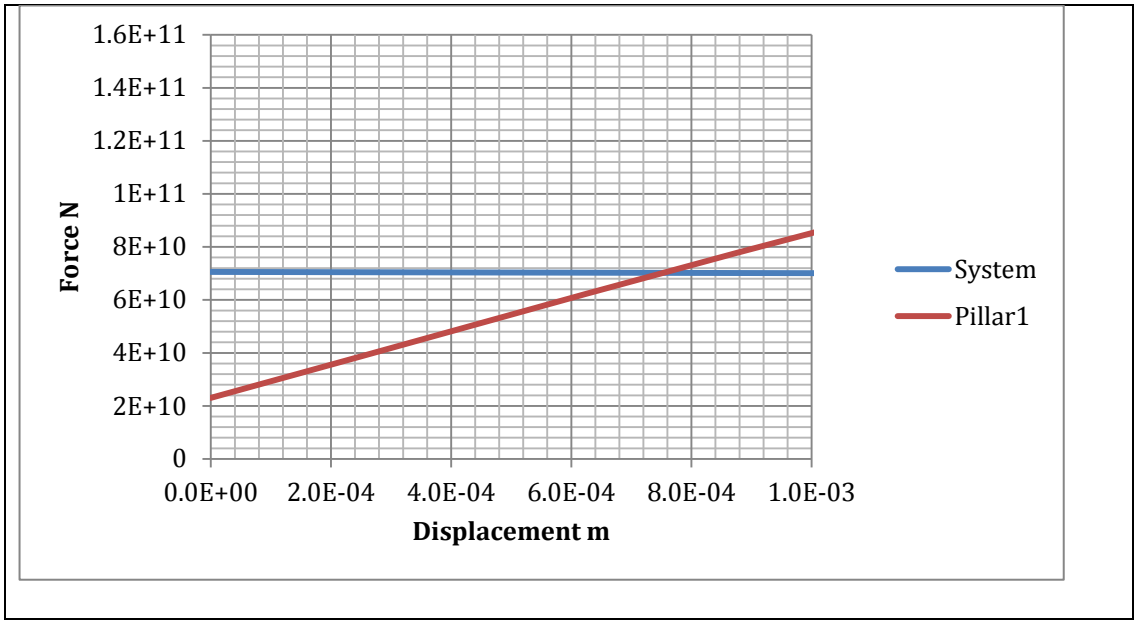

Figure 12.7.2_1. Pillar strength and system stiffness for the 8 by 8 m pillar example design

12.7.3 Generic equation and Tributary Area Theory.

The generic equation derived in Section 12.1 can be used in conjunction with the tributary area theory as well as the SPEC methodology.

The advantage of the generic equation over the Hedley-Grant equation is that the influence of the local geology/tectonic influence on the rock strength can be incorporated using known quantities such as the GSI and the rock mass strength factor. Equation 12.1 can be used to calculate the pillar strength for the rock mass properties listed in Table 12.7.1_1.

$$\sigma_{str=\delta(\frac{w}{h})^{\beta}} \qquad 12.1$$

The Delta and Beta values for a GSI of 80 and 120 MPa for the UCS can be obtained from Equations 12.2 to 12.6

$$\delta = 27.64$$

$$\beta = 1.2402$$

Using equation 12.1, strength of the 8 by 8 m pillar, 2 m high is 154 MPa.

Pillar stress is given by TAT as 25.2/0.327 = 77 MPa, resulting in factor of safety of 2.00.

12.7.4 Generic and SPEC

Table 12.7.4_1 summarises the input data for the SPEC model with the pillar strength given as 155 MPa and a convergence of 2.2e-3 m derived using the Young's modulus of 68 GPa.

Table 12.7.4_1: SPEC Input and Output.

100

Properties	Young's Modulus GPa		68
	Poisson's Ratio		0.29
	Density kg/m^3		2800
Geometry	Pillar	Strike m	8
		Dip m	8
	Bord	Strike m	6
		Dip m	6
	Halfspan m		100
	Stope width m		2
	% Extraction		63.7
	Overburden m		900
Pillar Stress and convergence	Strength MPa		155
	Convergence m		2.28e-3

FLAC2D/H-B	
Average Pillar Stress MPa	77
Convergence m	7.59e-3
Factor of Safety	**2.02**

The factor of safety for the Generic equation and SPEC method is 2.02.

12.7.5 Summary of illustrative examples.

The data in Table 12.7.4_2 is a combination of the various possible strength/stress combinations.

Table 12.7.4_2: Comparison of safety factors for the methodologies used

Method	8 by 8 m Pillar Strength/Stress	FOS 8 by 8 m
H/G-TAT	120/77	1.55
FLAC2D/SPEC	159/77	2.09
Generic/TAT	154/77	2.00
Generic/SPEC	154/77	2.02

Discussion and conclusions:

- The FOS is lowest for the TAT/H-G model due to the lower strength predicted by the Hedley-Grant equation
- The main difference in the results is due to the higher pillar strength obtained using the *FLAC2D*/H-B methodology.
- The percentage extraction can be increased to 71% by using 7 by 7 m pillars reducing the FOS to 1.60.
- Decreasing the span of the excavation to 100 m results in a higher FOS of 1.63. The SPEC method for determining the pillar stress is recommended for close spacing of losses of ground, say less than 200 m
- In conclusion, the TAT/H-G method is dependent mainly on an empirical estimate of the k value while the proposed *FLAC2D*/H-B/SPEC method can incorporate the changes in mining geometry and rock mass properties.

13 SUMMARY AND CONCLUSIONS.

13.1 Brief summary of objective and procedures adopted.

Figure 13.1_1 is a graph by Gale (1999) showing the wide range of likely pillar strengths for a change in the width-to-height ratio for confinement and changes from “strong to weak” geology. To obtain such distribution of strength using the Hedley-Grant/TAT method, the k value needs to cover a wide range instead of the limited ranges used to date. It was the objective of this thesis to propose a method that could give quantitative pillar strength values for “Strong/Normal and Weak geology”

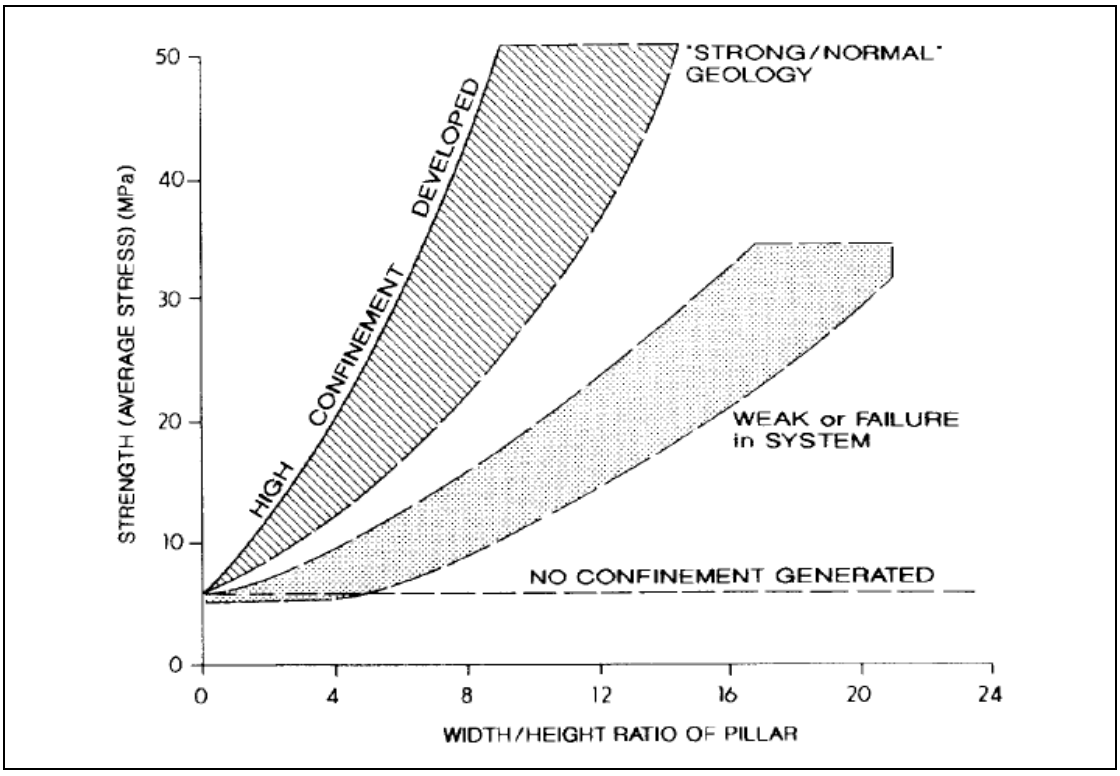

Figure 13.1_1 Generalized grouping of pillar strength with strong, medium and weak geology, after Gale (1999)

To achieve this objective the thesis was structured along the following framework:

- Examine the pillar design method currently in use for its strengths and weaknesses.
- Investigate alternative methods in use, actual and suggested.
- Propose an improvedd method for calculating the pillar strength and pillar loading.
- Compare the improvedd method with underground observations.
- Propose a simplified pillar strength equation based on the improvedd method.
- Present main conclusions and recommendations.

The current pillar design relies on the Hedley/Grant pillar strength equation and the tributary area theory for calculating the pillar load. The ratio between the two provided the factor of safety for the design. The selection of the k value was taken as a ratio of the UCS determined from a limited selected number of laboratory specimens generally with the GSI = 100.

Further investigation pointed to shortcomings in both the pillar strength equation as well as the loading system. These shortcomings could result in gross over design of the mines with a resultant loss in ore reserves.

A new design procedure was, therefore, required and the objective of this research was to develop a pillar strength and loading system that was closer to reality but still relied on known rock mass parameters and maintained a certain degree of simplicity in everyday application.

Detailed study of the shortcomings of the existing method was done where the literature survey also did not produce a method that addressed all the shortcomings of the current design.

An alternative pillar strength determination and loading system was investigated that did not suffer from the same shortcomings

An alternative pillar strength and loading and methodology was proposed which was used for calculating pillar deformation and pillar fracturing for comparison with underground data available in the literature. The comparison led to the conclusion that the System Pillar Equilibrium Concept (SPEC) in conjunction with the *FLAC2D*/Hoek-Brown method could be used to predict pillar behaviour better than the existing system.

Obtaining a simple pillar equation, based on known rock mass properties, was developed from the *FLAC2D/*Hoek-Brown model and a sensitivity analysis was done that highlighted the input parameters that had the maximum influence on the design procedure.

In the process of reducing the number of weaknesses/limitations existing in the current system, other shortcomings were identified which requires additional research.

The individual components of the research are summarized in sub sections for greater clarity:

13.2 Examine the pillar design method currently in use for its strengths and weaknesses.

The current design method was critically reviewed and the following main deficiencies were identified.

- Empirical pillar strength equation needed to be improved/augmented by analytical procedures.
- The influence of the variation in input parameters had to be incorporated.
- For rectangular pillars, the definition of effective width had to be refined.

- Strata stiffness needed to be incorporated.
- Pillar/hanging wall/footwall interaction required to be quantified.

The literature survey on pillar design procedures proposed by other authors produced the following results:

- None of the methods considered the interaction between hanging wall and/or footwall and its effect on the pillar strength.
- Three methods considered composite pillars
- Three methods discussed the strata stiffness concept but dealt with the post-failure implications.
- The variability of the mining dimensions and the rock mass properties were dealt with quantitatively in parts by four methods.

In summary, the following aspects had to be addressed:-

- Empirical equations should be replaced by analytical procedures.
- A rock mass classification that can assist in developing a simple equation for a specific set of conditions.
- The effect of planes of weakness needs to be incorporated
- Simulation of composite pillars such as found in the chrome mines
- Pillar hanging wall/footwall interaction.
- The ability to cope with the influence of the variation in input parameters; rock mass properties as well as mining geometry.
- The inclusion of strata stiffness.

An attempt had been made to include all the components in the proposed design methodology. The pillar strength determination and pillar loading were discussed in separate chapters and combined thereafter.

(The interaction between hanging and footwall with the pillar was not addressed and requires a separate investigation by expanding the *FLAC2D*/Hoek-Brown model incorporating the hanging and footwall in the model.)

13.3 Propose an improved method for calculating the pillar strengths.

The Hoek-Brown failure criterion was selected and used in conjunction with *FLAC2D* for determining the pillar stress and deformation variations under loading. To simplify the procedure, the *FLAC2D* axial symmetry function was used to simulate the average square pillar as a circular pillar, thereby excluding the necessity to use *FLAC3D* modelling.

The essential properties required for modelling were the following:-

- The uniaxial compressive strength.
- The m_i and the m_r values.
- The Geological Strength Index, GSI.

The general stress distribution in the pillar played a significant role in the elucidation of pillar behaviour and design:

- Pillar failure is a progressive process.
- The volumetric strain increment could be a possible measure of the depth of fracturing in, and eventual failure of a pillar.
- Homogeneous pillars as well as the influence of planes of weakness, could be modelled and analysed using the *FLAC2D*/Hoek-Brown model.
- The vertical stress at the core of the pillar generally exceeded the uniaxial strength of the rock.
- The model fixes the x and y displacements on the bottom and top loading surfaces, simulating a "frozen" contact, which creates high horizontal stresses in the pillar.
- The vertical stress was lowest at the pillar edge.

13.4 Re-define pillar loading.

The Tributary Area Theory is used extensively in pillar design. It was thought that the approach can lead to errors in pillar design and should be improved upon.

The research dealt with the pre-failure portion of pillar design. Therefore, the theory of elasticity could be used to the point of pillar failure allowing accurate calculation of pillar stresses and deformations. To date, the concept of the system stiffness was generally used for the post failure region in pillar and support design but is also well suited to model the pre-failure region.

Pillar loading is a function of the strata stiffness and the areal extent of the mining geometry. By including the effect of span of the mining geometry, the influence due to geological losses could be simulated using the load line of the system. A requirement was a knowledge of the Poisson's ratios, Young's Modulus and depth for calculating the load line. The required deformation or convergence was calculated using the equation for a finite depth model.

13.5 Combining the proposed pillar strength and the pillar loading.

The load deformation relationship of pillars prior to failure was generally assumed to be a linear. Similarly, the load line of the system could be approximated by a linear equation. The pillar and

load system had to be in equilibrium for a safe pillar design and is given by the intersection point of the two linear equations.

The factor of safety was determined by the ratio of the average pillar stress at equilibrium and the pillar strength.

The overall design methodology is summarised In Figure 13.5_1.

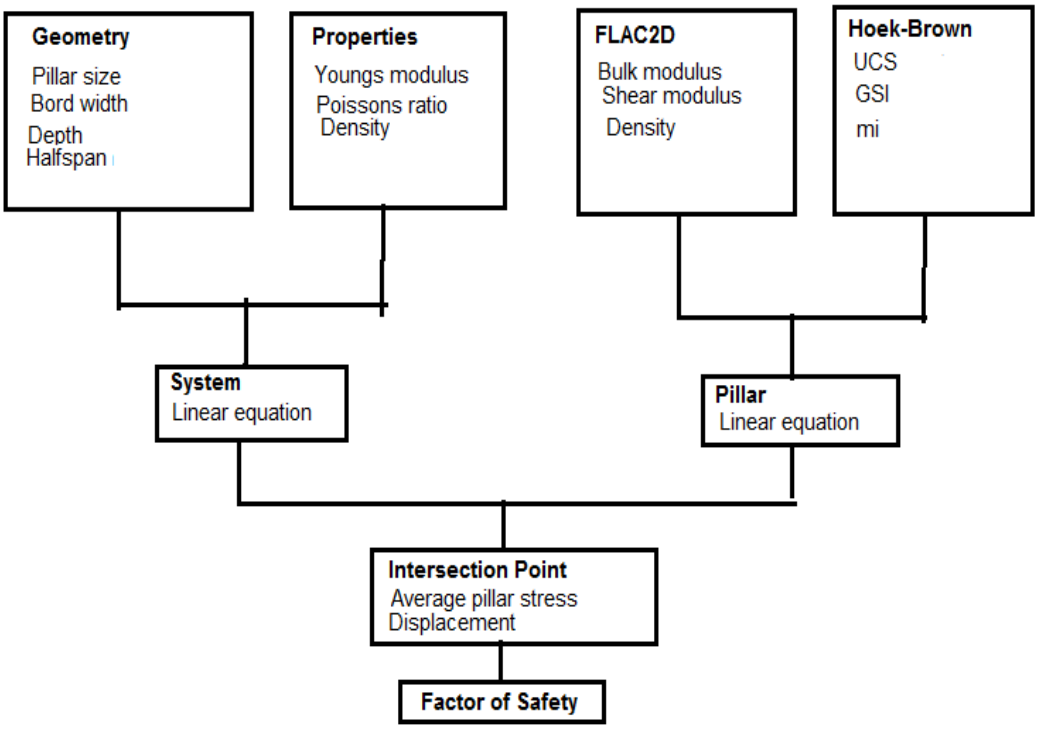

Figure 13.5_1. Design methodology summary.

The two main components were the loading system and the pillar strength. These two were combined and the equilibrium point was defined from which the factor of safety was then calculated.

13.6 Compare the improved method with underground observations.

To test the proposed method, calibrations were done using underground observations made in two platinum mines where the following was found.

- From the comparative volumetric strain increment values with the extent of fracturing, it appeared as if the *FLAC2D*/Hoek-Brown model in conjunction with the SPEC method approximated the real underground situation.
- The volumetric strain increment value for failure initiation was 1e-2 to 3e-2 for the extent of the fracture zone for both pyroxenite and chromitite pillars.

- The stress at failure at the boundary between the dog-earing and fracture varied between 20 and 120 MPa.
- The same order of magnitude for the average pillar stress for grid and barrier pillars were obtained using the SPEC method as those obtained by Malan and Napier (2007), using the Texan method,

The results obtained from a combination of the *FLAC2D*/Hoek-Brown and the SPEC model showed encouraging results and could be used to do the following:-

- Calculate a realistic pillar strength for a variety of rock mass conditions.
- Predict the extent of the fracture zones for alternative mining geometries.
- Predict most likely failure of pillars at greater depth. Alternative pillar mining methods could be investigated.
- With both the force and convergence values known, the concept could be extended into incorporating the energy balance of the system.
- The influence of the variability of the input parameters could be quantified using sensitivity analysis and Monte Carlo simulations.

13.7 Propose a simplified pillar strength equation based on the improved method.

It had been established that the pillar strength curves for different width-to-height ratios, uniaxial compressive strength and different heights, using *FLAC2D*/Hoek-Brown failure criterion for the current set of data, could be expressed by a simple generic power function:

$$\sigma_{str} = \delta(\frac{w}{h})^{\beta} \qquad 12.1$$

Where $\delta = de^{pGSI}$

$$\delta = 0.0999e^{0.0704GSI} \quad \text{120 MPa} \qquad 12.2$$

$$\delta = .1089e^{0.0674GSI} \quad \text{100 MPa} \qquad 12.3$$

$$\delta = .1675e^{0.06GSI} \quad \text{80 MPa} \qquad 12.4$$

$$\delta = 0.1652e^{0.0574GSI} \quad \text{60 MPa} \qquad 12.5$$

$$\beta = TANH\left[\left(\frac{GSI-a}{b}\right)\right]c \qquad 12.6$$

Where a = 46.866

b = 16.916

C = 1.2906

For the ranges 60<UCS<120

60<GSI<90

1< w/h <5

m_i = 22 h = 2 m

The generic pillar strength equation satisfied the requirement of simplicity in the design procedure. It also enabled its incorporation in a practical Monte Carlo simulation for sensitivity analysis.

13.8 Incremental increase in strength with increase in w/h ratio.

To date the general pillar strength curve has shown a decreasing trend in strength with increase in the width to height ratio. The generic equation on the other hand showed an increase in pillar strength with the increase in the width to height ratio. A detailed study of the generic equation showed that the trend of the strength increase appears to be a function of the Beta/GSI value. For GSI values below 64 the trend of the strength curve replicates the conventional shape but for GSI > 64, the positive trend predominates.

Latest research findings tend to support the findings above.

13.9 Incorporating the variability of the input data.

A Monte Carlo simulation of the combined generic equation and SPEC system indicated, in order of importance/influence on the factor of safety are mainly 2 values:

- The pillar geometry, width of pillar and roadway, pillar height were the most critical parameters.
- The rock mass strength,δ function of the GSI, was the second most important.

14 FUTURE RESEARCH.

Five major areas of concern were identified:

- In the light of the substantial variability in uniaxial compressive strength data that has been observed, it is doubtful whether obtaining just a few values, typical less than 10, is sufficient.

- The proposed design procedure is deemed an improvement of the current system but it should be viewed as the start of a system that can be improved in future. In particular the effect of the hanging- and footwall contacts should be incorporated.

- Pillar failure is a progressive process and the term pillar strength needs closer definition for the determination of the factor of safety. This is of particular importance for pillars displaying incremental strengthening.

- Statistical procedures need to be incorporated to accommodate the variation in geometrical and property values.

- The slope of the pillar strength h/w ratio curve needs special attention as it will affect the design of pillars significantly, especially the “squat” pillar region.

The use of the Hoek-Brown failure criterion depends on three parameters, the UCS, GSI and the m_i value. On closer inspection, it was found that all three input parameters were not clearly defined and that future research should concentrate on a better determination of input parameters, not dealt with in the thesis.

Suggestions for future research identified in the process of writing the thesis are summarised below.

- It appeared that the properties determined from laboratory specimens were influenced by the stress levels at which the samples were obtained in the prospecting diamond drilling process. The stress-strain curves for specimens taken at depths in excess of 800 m below surface showed an apparent progressive reduction in strength with increase in strain and exhibited positive volumetric strain before the peak strength was reached. The uniaxial compressive strength, Young’s modulus and Poisson’s ratio became less clearly defined. The influence of the sample collection underground and on diamond drill core requires further research.

- The m_i, and the residual m_r, value for rocks strongly influenced its pre- and post-failure behaviour of pillars. This change in value had a significant effect on the prediction of the mode of pillar failure. For Bushveld rocks, the m_i and m_r values were such that using *FLAC2D*/Hoek-Brown criterion, at width-to-height ratios in excess of 2, no pillar bursting should occur. A progressive reduction in the m_r value with increase in induced fracturing could lead to a situation where a negative stress/strain curve could result with the possibility of creating a seismic event. These findings require serious attention since it would clarify the definition between yielding and bursting pillars. The determination of the Geological Strength Index as well as its progressive change as pillar failure progressed with an increase in stress needed to

be quantified. This effect would go hand-in-hand with the observations on the m_i and m_r values.

- The hanging and footwall above and below the pillar has a significant influence, one that increased with an increase in the differences in rock mass properties. Ample observational data should be used for back analysis using available simulation models and input parameters.

- The stiffness of the rock mass is a function of the mining spans. In the platinum mines, numerous un-pay areas, such as potholes, iron enriched zones and structurally complex areas, are left *in situ*. A general rule is that these "geological losses" occupied up to 30% of the mined out region. The resultant "pillars" are of such a size that failure of these is highly improbable. The effect of this on the stiffness was that a local stiffness and a regional stiffness could be considered depending on the nature of the frequency and spacing of the "geological pillars" allowing for the percentage extraction in the isolated areas be increased. This concept would facilitate localised high grade extraction, even in old areas of the mine.

REFERENCES

Babcock C. (1994) Critique of Pillar Design Equations from 1833 to 1990. U S Department of the Interior, Bureau of Mines. IC 9398.

Barczak T.M. Esterhuizen G. S. Ellenberger J. L. and Zhang P. (2009) a first step in developing standing roof support design criteria based on the ground reaction data for Pittsburgh longwall tailgate support. NIOSH publication.

Bieniawski, Z.T. and Van Heerden, W.L. (1975). The significance of in situ tests on large rock specimens, Int. J. Rock Mech. Min. Sci. and Geomech. Abstr., Vol. 12 no.4, pp. 101-113.

Budavari, S (1983). Stresses and displacements induced by mining – in *Rock Mechanics in Mining Practice*, South Afr. Inst. Min. and Metall. Monograph Series 5.

Canbulat M. Grodner N. Lightfoot J., Ryder F. Essrich, T., Dlokeni A., Wilkinson C. Krog and Prohaska G. (2006) The determination of loading conditions for crush pillars and the performance of crush pillars under dynamic loading *Final report SIMRAC 40302*, March 2006

Detournay, E. (2012) Personal communication

Detournay E. and Fairhurst C.(1982) Generalization of the Ground Reaction Curve Concept. Chapter 92, p1. 1982 *Am Inst. Mining Engineering*.

Dolinar D. and Esterhuizen G. (2007) Evaluation of the Effects of Length on Strength of Slender Pillars in Limestone Mines Using Numerical Modelling. *26th International Conference on Ground Control in Mining,* Morgantown.

Du Plessis M., Malan D.F. and Napier J.A.L. (2011) Evaluation of limit equilibrium model to simulate crush pillar behaviour. *J.S.Afr. Inst.Min&Metall*., Volume 11, no 12, December 2011.

Esterhuisen A. (2011) Two Rivers, Bord and pillar practices. *Best Practice Industry Workshop on Rock Engineering in Hard-Rock Room & Pillar Mining,* February 2011. Polokwane.

Esterhuizen G.S. (2003). Variability considerations in hard rock pillar design. Proceedings: Rock engineering problems related to hard rock mining at shallow to intermediate depth, SANGORM, Rustenburg, pp 48-54

FLAC Fast Lagrangian Analysis of Continua. On-line version, FLAC version 4.

Gale W. J. (1999) Experience of field measurements and computer simulation methods for pillar design**.** *Proceedings of the Second International Workshop on Coal Pillar Mechanics and Design. Information Circular 9448 U.S. Dept of Health and Human reserves*, June 1999.

Godden S. J. (2012) Pillar design for Bushveld mines. 2012.

Godden S J. Pillar design and cutting at Everest Mine. *Consulting report by S.Godden and Associates* April 2009.

Grodner M. W. and Malan D.F. (2006) Pillar monitoring during the formation of 10 by 10 m pillars at 14 shaft. *Contract report, Impala Platinum Mines, CR254/03022/IMP009.*

Hart R. (2012) Personal communication 2012

Hedley D.G.F. and Grant F. (1972). Stope pillar design for the Elliot Lake uranium mines, *Bull. Can. Inst. Min. Metal.*, Vol. 65, pp. 37-44.

Hoek E. and Bieniawski Z. T. (1968) Brittle Rock Fracture Propagation In Rock Under Compression . *South African Council for Scientific and Industrial Research* Pretoria, 1968.

Hoek E. (2012) Notes on estimation of GSI and Hoek-Brown parameters. Private communication, 6 July 2012.

Hoek E. (1968) Brittle fracture in rock. Chapter 4, *Rock Mechanics In Engineering practice*. Edited Stagg and Zienkiewicz, Wiley press, 1968.

Hoek E. (1983) Strength of jointed rock masses. *23rd Rankine lecture to the Geological Society* 1983. Geotechnique, vol 23, no 3.

Hoek E, and Marinos P. (2000) GSI: A Geologically Friendly Tool for Rock Mass Strength Estimation. *Proc Geo Eng 2000 Conference*, Melbourne.

Hoek E. Caranza-Torres C. and Corkum B. (2002) Hoek-Brown failure criterion-2002 Edition. Proceedings NARMS-TAC Conference, Toronto.

Holt R.M., Brignoli M. and Kenter C.J. (2000). Core quality: quantification of core-induced rock alteration, *Int. J. Rock Mech. Min. Sc.,* Vol. 37, pp. 889-907.

Implats Web Site, www.implats.co.za Issue 1,(2015)

Implats Data Bank (2012) Composite data bank of rock properties.

Itasca Consulting Goup, inc. (1993). Fast Lagrangian Analysis of Continua (FLAC), Vers. 3.2. Minneapolis Minnesota, USA.

ITASCA. FLAC; (2011) Fast Lagrangian Analysis of Continua, Online manual and users guide, ITASCA 2011

Joughin N.C. (2011) Engineering considerations in the tolerability of risk. Mine Occupational Health and safety 2010. *J.S.Afr. Inst.Min&Metall*.Vol 111 August 2011.

Joughin W.C., Swart A.H. **and Wesseloo J** (2000) Risk based chromitite pillar design – Part II. SANIRE 2000, *Keeping up in the Bushveld and advances in support technology*, 2000.

Kersten R.W.O. and Leach A. R. (1996) The calibration of material models in FLAC for deep level gold mines. Eurock 96, *ISRM International Symposium, Torino*. Balkema 1996.

Kersten R.W.O. (1992) Pillar stability at Lavino Chrome Mine. Internal report, Anglovaal 1992.

Kersten, R.W.O., and A. R. Leach. "The Calibration of Material Models in FLAC for Deep-Gold Mine Problems," in *Prediction and Performance in Rock Mechanics & Rock Engineering (Proceedings of ISRM International Symposium EUROCK '96, Turin, September 1996)*, Vol. 2, pp.1179-1084. G. Barla, Ed. Rotterdam: Balkema, 1996.

Kersten R.W.O. (2009) Review of proposed mining layout at Kamoto Mines Report to management, April 2009.

Kersten R.W.O.(1984) The design of pillars in the shrinkage stopes of a South African gold mine. *J.S.Afr. Inst.Min&Metall*. vol 84, no 11, 1984 pp365-368.

Kersten R.W.O (2001) Backfill strength requirements. Report to Nkomati Management, November 2001.

Kersten R.W.O (2009) Black Rock Mines; comments on the rock engineering requirements. Associate Manganese Mines report.

Kersten R.W.O (2002) Support requirements for centre and rim drives. Report to Nkomati Management, June 2002.

Kersten R.W.O (2013) Pillar and bord dimensions of section 6, Two Rivers Platinum Mines.

Kersten R.W.O. (2009) Comments on the rock engineering aspects of Black Rock Mining Operations. Contact report to the Associated Manganese mines.

Leach A.R. (2011) A comparative study between circular and square pillars. Contract report to R W O Kersten

Leach A R. (2008) Summary Report; Assessment of Stability of Proposed Room and Pillar Workings for Nkomati Mine. Itasca Africa (Pty) Ltd May 2008

Lougher D.R and Ozbay M.U. (1995) In-situ measurements of pillars and rock mass behaviour in a moderately deep hard-rock mine. *J.S.Afr. Inst.Min&Metall*., February 1995.

Malan D. F. (2006) Numerical modelling of the bord and pillar layout at Kroondal mine. Groundworks report TN1/0209/XE003 2006.

Malan D. F., and Napier J. A. L. (2006) a. Practical application of the TEXAN code to solve pillar design problems in tabular excavations. *SANIRE 2006, Facing the challenges in Rock mechanics*, pp 1-20.

Malan D. F. (2011) Pillar design in hard rock mines: can we do this with confidence? *2nd Australasian Ground Control in Mining Conference, Sydne*y, NSW, 23 - 24 November 2010.

Malan D. F. and Napier J.A.L..(2007) b. Numerical Modelling of the Bord and Pillar Layout at Impala no 12 Shaft. *Contract report CR269/0307/IMP021* March 2007.

Malan D. F, and Napier J.A. L. (2011) c. The design of stable pillars in the Bushveld Complex mines: a problem solved? *J.S.Afr. Inst.Min&Metall*., Volume 11, no 12 December 2011.

Malan D.F. and Ryder J. (2009) Numerical modelling of the current and revised lay-out in the mechanised section at 14 Shaft*. Groundworks report TN622/1009/IP044*. 2009

Mathey, M.(2015): Investigation into the mechanism of strength and failure in squat coal pillars in South Africa. PhD Thesis, University of the Witwatersrand, 2015.

Mathey, M.(2015): Personal communication, 2015.

Mandatory code of practice to combat rock fall and rock burst accidents in tabular metalliferous mines. Two Rivers Platinum Mine, revision December 2012

Mark C. and Chase E.E.(1997) Analysis of Retreat Mining Pillar Stability (ARMPS). Proceedings of the New Technology for Ground Control in Retreat mining. U S Department of Heal and Human Services, National Institute for Occupational Safety and Health (NIOSH), IC 9448.

Mark, C. (1999) Empirical Methods for Coal Pillar design. Proceedings of the Second International Workshop on Coal Pillar Design. U S Department of Heal and Human Services, National Institute for Occupational Safety and Health (NIOSH), IC 9446.

Martin C. D. and Maybee W. G. (2000) The strength of hard rock pillars. *International Journal of Rock Mechanics and Mining Science* 37, 2000.

Mitchell A. A. and Scoon R. N. (2007) The Merensky Reef at Winnaarshoek, Eastern Bushveld Complex:A Primary Magmatic Hypothesis Based on a Wide Reef Facies. 2007. *Society of Economic Geologists, Inc. Economic Geology,* v. 102, pp. 971–1009

Napier J. A. L., and Malan D. F. (2011) d. Numerical modelling of average pillar stress and implications for pillar design. *J.S.Afr. Inst.Min&Metall*. . Volume 11, no 12, December 2011.

Özbay M.U., Ryder, J.A. and Jager A.J. (1995). The design of pillar systems as practised in shallow hard-rock tabular mines in South Africa, *J.S.Afr. Inst.Min&Metall*., Jan/Feb 1995, pp. 7-18.

Piper P.S., and Flanagan F. W., (2005) The In-Situ Performance of Yielding Pillars at Impala 12 Shaft. *J.S.Afr. Inst.Min&Metall*. *3rd Southern African Rock Engineering Symposium*, 2005.

Qi Zhang, Hehua Zhu, Lianyang Zhang and Xiaobin Ding.(2012) Effect of micro-parameters on the Hoek-Brown strength parameter *mi* for intact rock using particle flow modelling. *American Rock Mechanics Assoc.* Chicago 2012.

Roberts M.K.C., Grave D.M.H., Jager A.J. and Klokow J. (1997). Rock mass behaviour of the Merensky Reef at Northam Platinum Mine, *Proc. 1st Southern African Rock Eng. Symp.*, Johannesburg, pp. 467-474.

Roberts D.P., Ryder J.A. and van der Merwe J.N. (2005). Development of Design Procedures for Long Slender Pillars. *Final Report Task 2.14, Coaltech 2020*, March11, 65 pp.

Ryder J.A., (2005) Personal communication.

Ryder, J.A. and Özbay, M.U. (1990). A methodology for designing pillar layouts for shallow mining, Int. Symp. on Static and Dynamic considerations in Rock Eng., Swaziland, ISRM, pp. 273-286.

Roberts D.P. (2003) Numerical modelling for design of pillars at Impala platinum mines. *Contract report, Impala Platinum Mines*, No 2003-0107, 2003.

SAIMM. (2011)Best Practice Industry Workshop on RockEngineering in Hard-Rock Room & Pillar Mining presented by Samancor, Eastern Chrome, at the *Best Practice Workshop in Polokwane*, January 2011. 16 to 18 February 2011.

Salamon M.D.G and Munro A.H. (1967). A study of the strength of coal pillars. *J.S.Afr. Inst.Min&Metall*.68.

Saiang D. (2008) Behaviour of Blast-Induced Damaged Zone Around Underground Excavations in Hard Rock Mass, Luleå *University of Technology Department of Civil, Mining and Environmental Engineering Division of Rock Mechanics*, 2008.

Salamon M.D.G. and Oravecz, K.I. (1976) Rock Mechanics in Coal Mining. Johannesburg
Chamber of Mines of SA. 1976 (ISBN 0-620-00232-8 [HB]).

Salamon M.D.G. (1993). The Role of Pillars in Mining. The South African Institute of Mining and Metallurgy, Monograph Series No 5, Rock Mechanics in Mining practice.

Spencer D. (2012) Personal communication, 2012.

Stacey I.R. and Page C.H (1986) Practical handbook for Underground Rock mechanics"' Series on Rock and Soil Mechanics, Vol.12 *Trans Tech Publications*, 1986, pp.53-63.

Swart A. H., Stacey T. R., Wesseloo J, ,Joughin W. C., le Roux K., Walker D. and Butcher R. (2000) Investigation of factors governing the stability/instability of stope panels in order to define a suitable design methodology for near surface and shallow mining operations. Final report SIMRAC OTH 5011, SRK Consulting. July 2000.

Two Rivers Platinum Mine Code of Practice for the prevention of Falls of Ground 2007, Two Rivers Platinum Mine standard procedures.

van der Merwe P. (2013) African Rainbow Minerals. Kriging of values of rock strength data. 2013.

van der Merwe, J. N, Ph.D. (1999) The role of overburden integrity in pillar failure. Information Circular 9448 *U S Department of Health and Human services*, June 1999.

van der Merwe J.N. (2011) Monte Carlo Simulations. Workshop on the use of statistical methods in mining, Wits University.

van der Merwe J.N. and Mathey M. (2013) Update of coal pillar strength formulae for South African coal using two methods of analysis. *J.S.Afr. Inst.Min&Metall*. Volume 113 November 2013..

van der Merwe J.N. (**2014**) Personal communication

Wagner, H. (1974). Determination of the complete load-deformation characteristics of coal pillars, Proc. 3rd Int. Cong. on Rock Mech., ISRM, Denver, USA, Vol. 2B, pp. 1076-1082.

Wagner H. (1980) Pillar design in coal mines. *J.S.Afr. Inst.Min&Metall*. February 1980.

Watson B. P. (2010) Rock behaviour of the Bushveld Merensky reef and the design of crush pillars. PhD thesis Wits University, 2010

Watson B.P, Roberts M.K.C, Nkwana M.M. Kuijpers J., and van Aswegen L. (2007) The stress-strain behaviour of in-stope pillars in the Bushveld Platinum deposits in South Africa. *J.S.Afr. Inst.Min&Metall*. Volume 107 March 2007.

Watson B.P., Ryder J.A., Kataka M.O., Kuijpers J.S. and Leteane F.P. (2008). Merensky pillar strength formulae based on back-analysis of pillar failures at Impala Platinum, *J.S.Afr. Inst.Min&Metall*. Vol.108, pp. 449-461.

Wilson A H, Jermy C A., Ridgeway M., and Chunnett G. (2005) Rock-strength and physical properties of Norites of the Merensky and Bastard Units, western Bushveld Complex. *South African Journal of Geology,* 2005, Volume 108 Page 525-540

Yilmaz H. (2012) Module 9: Stresses and convergences induced by tabular excavations. 3rd Year lecture notes, department of mining, Wits University.

Zipf K. (1998) Using a post-failure stability criterion in pillar design Dept Mining engineering, University Missouri-Rolla. *DHHS (NIOSH) Publication* No. 99-114

June 1998

APPENDICES

Appendix I

Report by A. R. Leach on the comparative study between circular and square pillars.

Comparative modelling of circular and square pillars.

Models have been run using the three dimensional program FLAC3D. Each represents a quarter of a three-dimensional pillar with reflective fixed boundaries on the centre line of the pillar to account for the full pillar geometry.

Models have been run that represent the following:-

- Square pillar, 6 m x 6 m.
- Square pillar, 4 m x4 m.
- Square pillar, 2 m x 2 m.
- Circular pillar, 6 m diameter.
- Circular pillar , 4 m diameter.
- Circular pillar, 2 m diameter.

In all cases, the ore body was taken as being horizontal and 1.8m thick. In all models, stope of half-span 5m was excavated around each pillar, and sufficient rock mass (20m) was included in hanging wall and footwall for punching to occur, if this becomes the dominant failure mechanism with wider pillars. Model geometry is shown in Figure A_1.

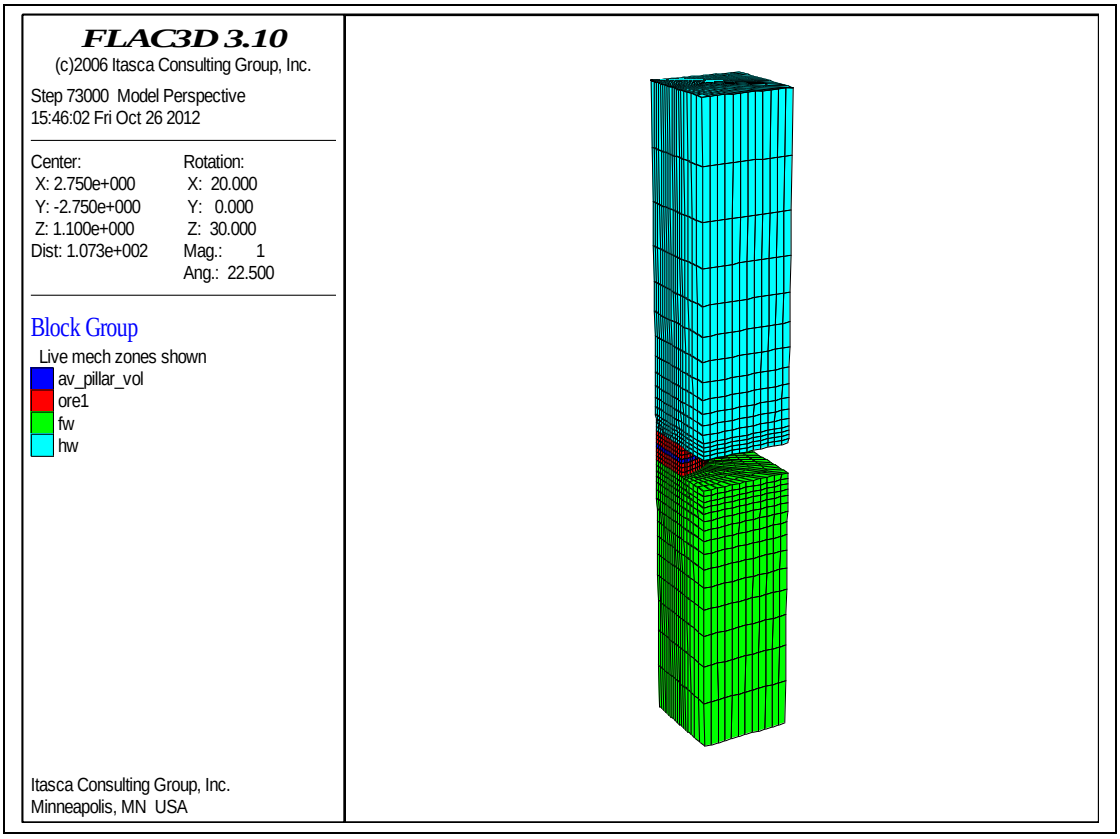

Figure A_1 Example model geometry

Convergence in models

All models were first brought to an equilibrium state with a hydrostatic stress of 3 MPa, to provide a limited confinement in the hanging wall and footwall, and then were loaded with a vertical compressive velocity of 2.5 x 10^6 metres per time step. This provides a steady and ongoing compression to the model, progressively increasing the stress within the pillar.

While compression to the top of the model may be constant, the compression across the pillar, between hanging wall and footwall, is influenced by the stiffness and degree of damage in the pillar. A comparison between typical compression across the pillar (black line), versus that between top and base of model (linear red line) is shown in Figure A_2.

Subsequent assessments of pillar load versus convergence are based on the compression between hanging wall and footwall across the pillar.

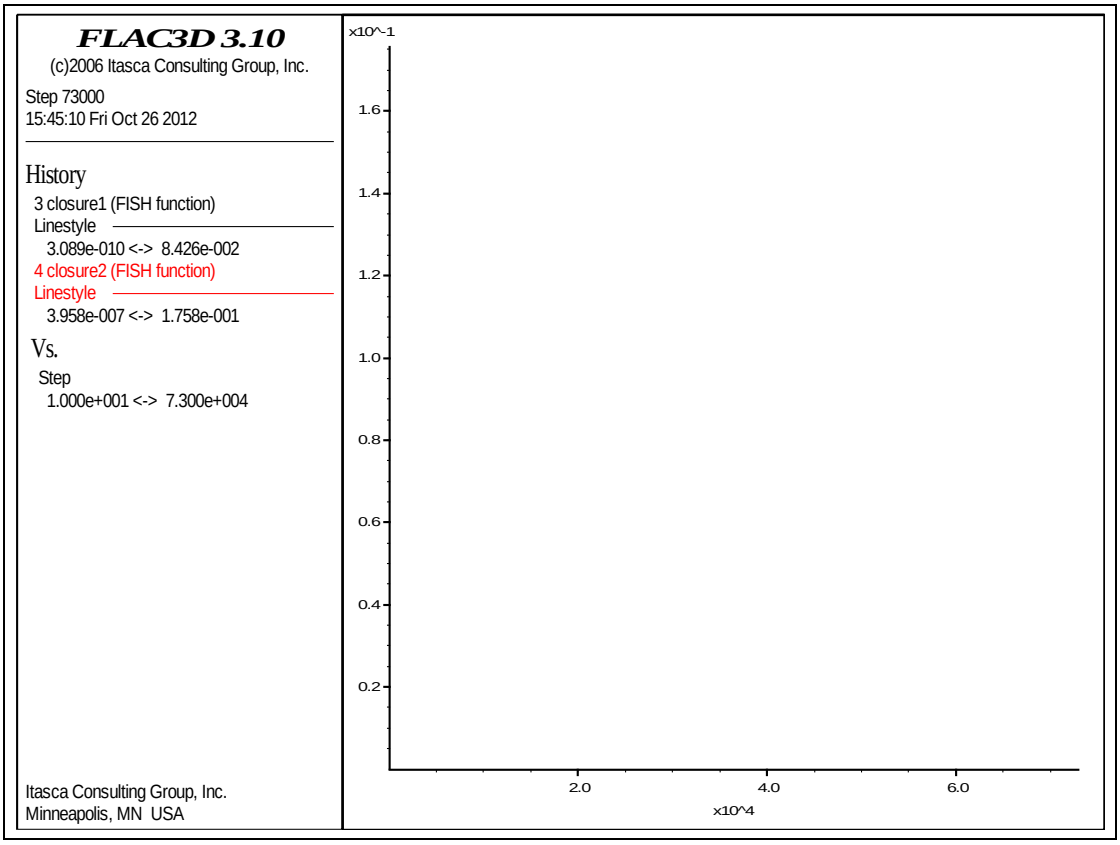

Figure A_2 Comparison of compression in model between top and bottom of model (red line) and between footwall and hangingwall of pillar (black line)

This example is from a 6m diameter circular pillar model.

Rock properties

Apart from an elastic layer at the top of the model to ensure even loading, the rock mass in the model was represented with a Hoek-Brown failure criterion and uniform properties throughout (i.e. all one rock material).

Properties were as follows:-

- Bulk Modulus 12.7 GPa
- Shear Modulus 13.0 GPa
- Density 2900 kg/m^3
- Hoek-Brown peak m 23.8
- Hoek-Brown residual m 5
- Hoek-Brown peak s 0.329

- Hoek-Brown residual s 0.005
- Strain (peak to residual) 0.01
- UCS 52 MPa

Model results

The following series of plots provide a quick comparison of results. There is one plot per model. The plots show the following:-

- Final state of damage in the model on a plane through the centre of the pillar.
- Graph of average pillar stress versus pillar compression (black line).
- Graph of a history of the stress in a zone in the centre, at mid-height, in the pillar versus pillar compression (red line).

The final state of damage is not that useful, as it merely indicates failure through the pillar in the final residual state, with quite extensive damage in hanging wall and footwall too. The other graphs are more revealing and for all pillar sizes show and increase in strength, and loss of strength post-peak.

A comparison of the peak average pillar stresses in each model is given below:-

Pillar size	Circular pillar – peak APS	Square pillar – peak APS
6 m	150.3 MPa	149.9 MPa
4 m	98.1 MPa	98.7 MPa
2 m	61.7 MPa	56.1 MPa

Despite the fact that the square pillars have a larger total area and volume that the circular pillars, the results are almost identical – there is some concern that the smaller zones in the core of the circular pillars, compared to identical zone sizes throughout the square pillars may be making the circular pillars stiffer than they should be (i.e. there is a numerical artifact in play), though the difference in area was accounted for in the ‘averaging’ calculation.

There is also a possibility that the velocity loading rate should be lower, and would produce more consistent results particularly in the smallest sized pillars, where the circular pillar ends up being stronger than the square one – these results seem particularly unlikely.

However the models would tend to indicate that the results from a two dimensional axi-symmetric model can be taken as being very similar to the equivalent 3-dimensional square pillar.

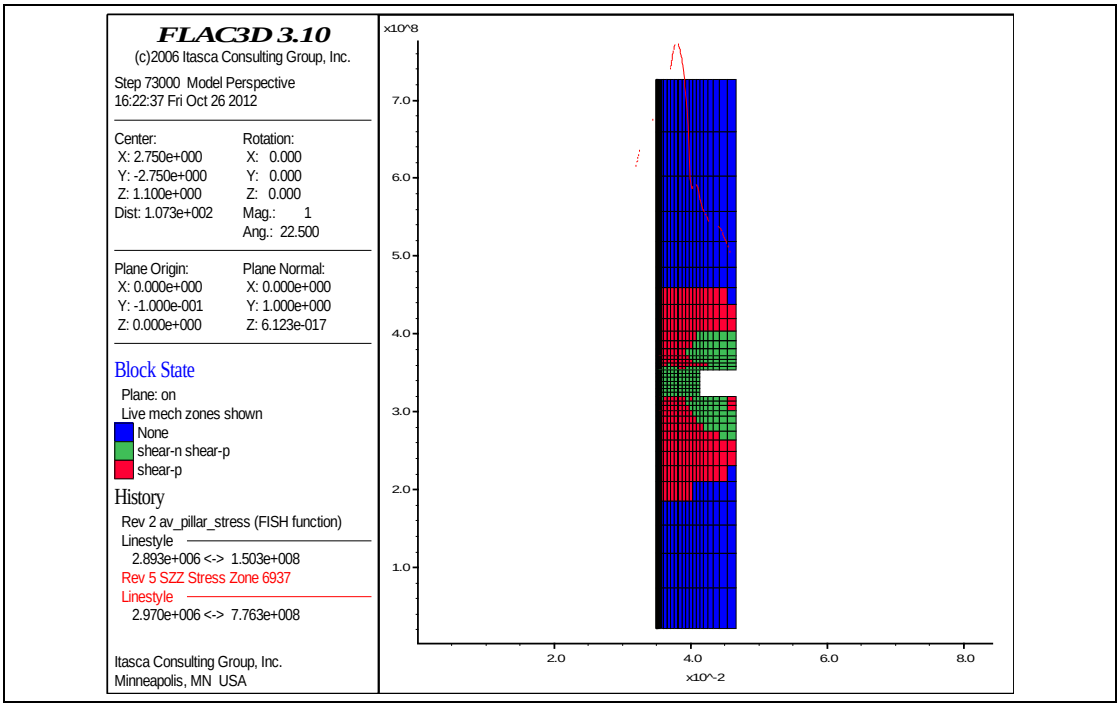

Figure A_3 Circular pillar, 6 m in diameter

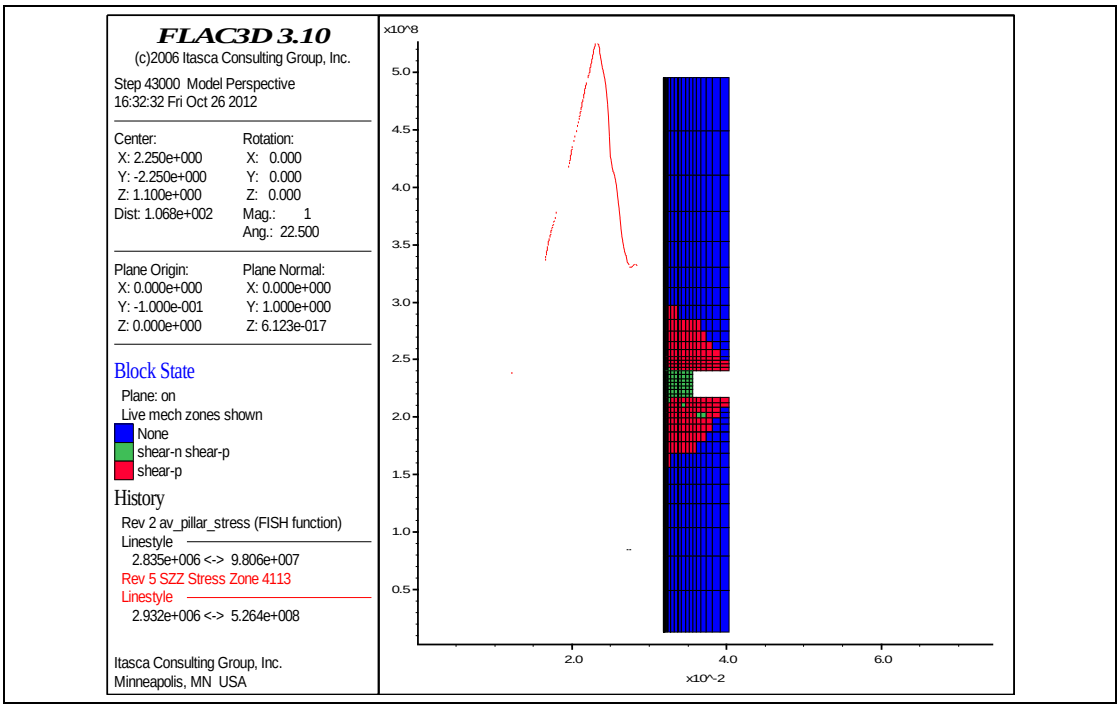

Figure A_4 Circular pillar, 4 m in diameter

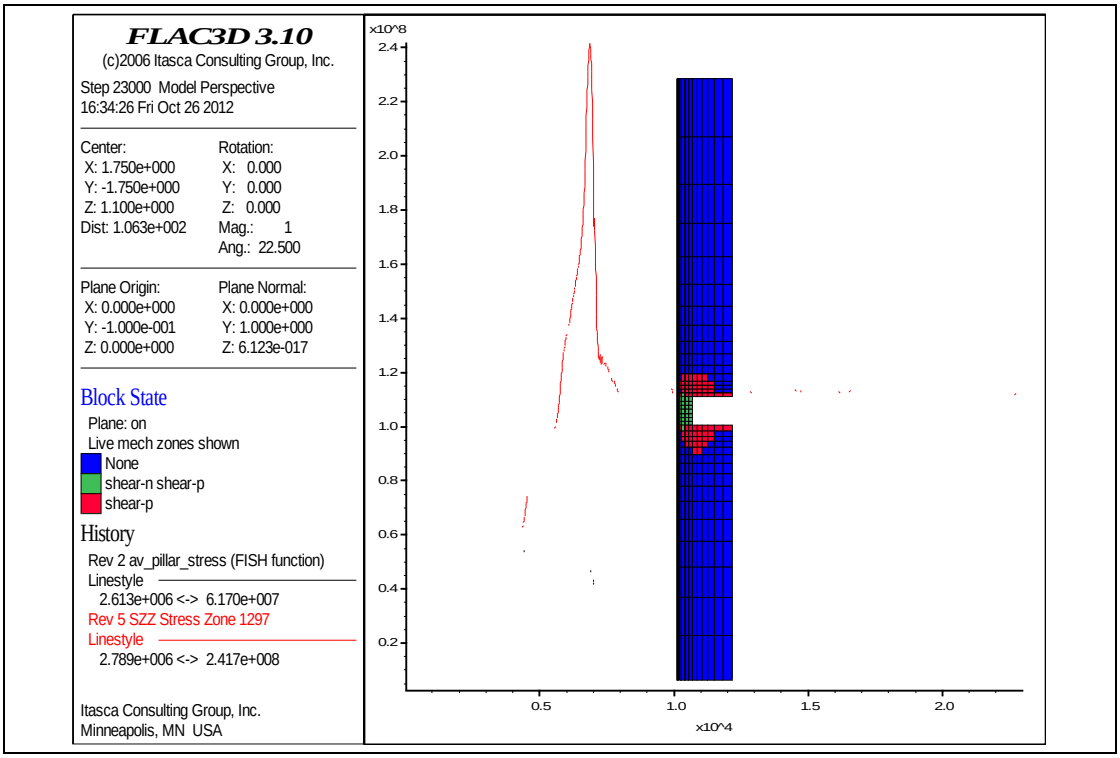

Figure A_5 Circular pillar, 2 m in diameter

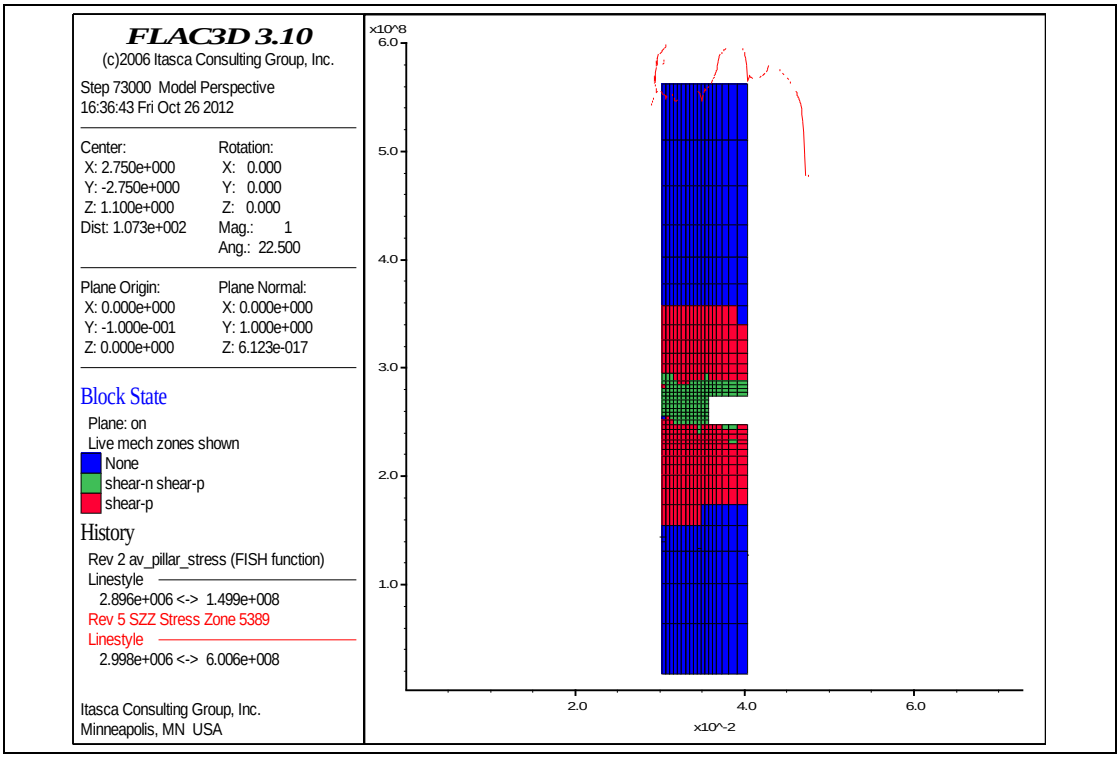

Figure A_6 Square pillar, 6 x 6 m in size

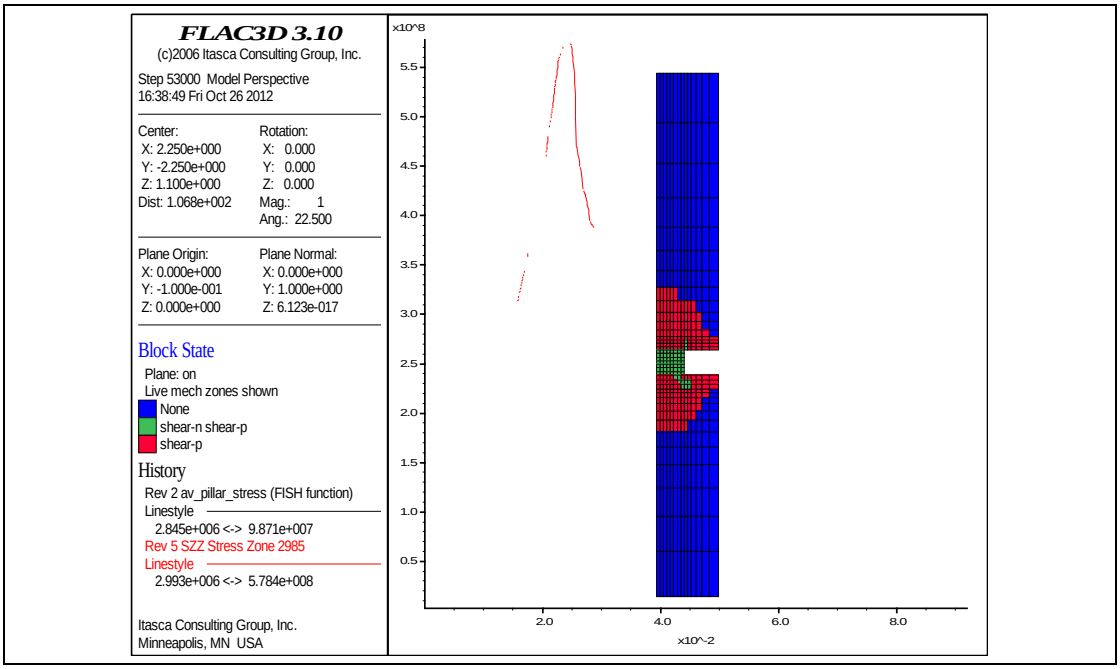

Figure A_7 Square pillar, 4 x 4 m in size

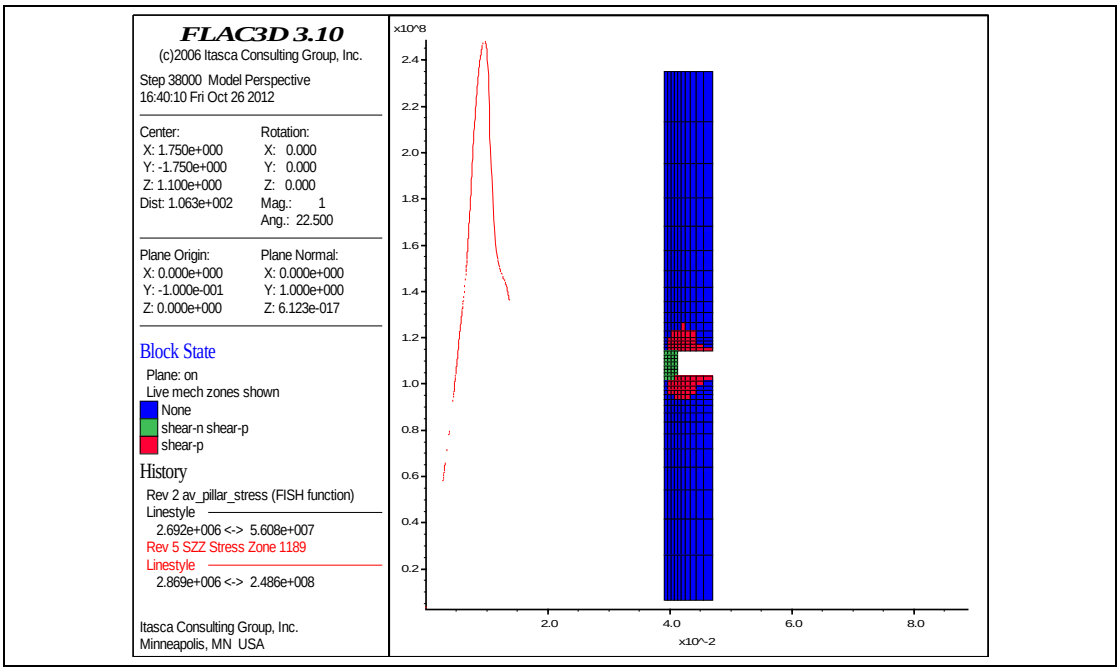

Figure A_8 Square pillar, 2 x 2 m in size

A R Leach - 2012.

Appendix II.

```
new
ti
Hoek Brown Composite model for 2 layers
config axi
gr 24,20
gen 0,0 0,2 2.5,2 2.5,0
mod mo
;Chromitite
prop bu=54e9 sh=26e9 d=3900 *c=12.94e6 fric=45.7
call hoek3.fis                    ;<--(updated fish function - meant to work
                                  ;    with 2 different sets of properties)
set hb_mmi=11.6  hb_mmr=5.5
set hb_ssi=.1084 hb_ssr=.0542
set hb_sc=42.7e6
;Pyroxenite
prop bu=3e9 sh=1.5e9 d=2900  i=1,24 j=17,18
set j1=17 j2=18
set  hb_mmi2=2.35   hb_mmr2=1.67       ;     <--(use  new  property  name  for
j=17,18)
set hb_ssi2=.0013 hb_ssr2=0.0007
set hb_sc2=4.3e6
; Circular pillar FISH function for calculating the total force
def load
  sum2=yforce(1,jgp)*x(2,jgp)*0.25
  loop i (2,igp)
    sum2=sum2+yforce(i,jgp)*x(i,jgp)
  end_loop
  ftot = 2.*pi*sum2
; (Total area of strip pillar - axi-symmetric mode)
  _area = pi*x(igp,jgp)*x(igp,jgp)
  load  = ftot
  aps   = ftot/_area
end
his yd i=1 j=21
hist load
his aps
fix x y j=1
fix x y j=21
ini yv -1e-6 j=21
set nsup=9000 ns=10 ; note, FLAC will cycle nsup*ns times
supsolve
```

Appendix III

```
new
ti
Mohr Coulomb multilayer model.
config axi
gr 24,20
mod mo
; Pillar radius and height
gen 0,0 0,2 6,2 6,0
*prop fric=21 dil=10                                        ;<--(associated)
 prop  bu=4.1e10  sh=10.8e10  d=3900  coh=10.8e6  fri=19.5  i=1,24  j=19,20
;chromitite leader                                                    ;<--
(look)
prop  bu=3.3e10  sh=3.3e10  d=2900  coh=16.6e6  fri=17  i=1,24  j=16,18
;Pyroxenite
prop  bu=7.5e10  sh=2.8e10  d=3900  coh=9e6  fri=19.6  i=1,24  j=1,18
;chromitite UG2
prop bu=2.9e10 sh=1.7e10 d=3900 coh=15.4e6 fri=19.2 i=1,24 j=13,15
prop bu=8.7e10 sh=2.7e10 d=3900 coh=11.2e6 fri=19.6 i=1,24 j=14,16
prop bu=14e10 sh=4.6e10 d=3900 coh=13.5e6 fri=18.8 i=1,24 j=11,12
prop bu=9.6e10 sh=4.7e10 d=3900 coh=14.3e6 fri=19 i=1,24 j=11,13
prop bu=5.2e10 sh=2.4e10 d=3900 coh=11.9e6 fri=18.1 i=1,24 j=7,8
prop bu=13e10 sh=3.4e10 d=3900 coh=14.3e6 fri=14.8 i=1,24 j=5,10
prop bu=8.5e10 sh=5.6e10 d=3900 coh=12.4e6 fri=17.1 i=1,24 j=3,4
prop bu=10e10 sh=4.5e10 d=3900 coh=12.9e6 fri=18.1 i=1,24 j=1,4
; Circular pillar FISH function for calculating the total force and avergae
pillar stress.
 def load
  sum2=yforce(1,jgp)*x(2,jgp)*0.25
  loop i (2,igp) sum2=sum2+yforce(i,jgp)*x(i,jgp end_loop ftot = 2.*pi*sum2
(Total area of strip pillar - axi-symmetric mode)
 _area = pi*x(igp,jgp)*x(igp,jgp)                                ;<--(look)
```

```
  load  = ftot
  aps   = ftot/_area
end
hist load
his  aps
fix x y j=1
fix x y j=21
ini yv -1e-7 j=21
step 100000
```

Appendix IV

```
new
ti
Hoek Brown Model for calibration
config axi
gr 24,20
gen 0,0 0,2 2.5,2 2.5,0
mod mo
;Pyroxenite
prop bu=54e9 sh=26.4e9 d=2800 *coh=14e6 ten=1e20 fric=46
call hoek2.fis                                    ;<--(associated rule)
set hb_mmi=12.876 hb_mmr=6.4;.51
set hb_ssi=.1889 hb_ssr=.094 ;0.0010
set hb_sc=52.1e6
; Circular pillar FISH function for calculating the total force
def load
  sum2=yforce(1,jgp)*x(2,jgp)*0.25
  loop i (2,igp)
    sum2=sum2+yforce(i,jgp)*x(i,jgp)
  end_loop
  ftot = 2.*pi*sum2
; (Total area of strip pillar - axi-symmetric mode)
  _area = pi*x(igp,jgp)*x(igp,jgp)
  load  = ftot
  aps   = ftot/_area
end
his yd i=1 j=20
fix x y j=1
*fix y j=11
fix x y j=21
fix x i=1
*ini yv  1e-7 j=1
ini yv -1e-6 j=21
his aps
his load
his xd i=19 j=10
set nsup=3000 ns=10 ; note, FLAC will cycle nsup*ns times
supsolve
pause
```

Also included is the subroutine hoek2.fis Hoek-Brown failure criterion to be used in all the simulations of homogeneous pillars.

```
FISH routine for Hoek-Brown failure surface
; the dilation angle is specified using hoek_psi
; (hoek_psi = fi for an associated flow rule)
;
def cfi
  loop i (1,izones)
    loop j (1,jzones)
       if state(i,j) > 0 then
           h_mm=hb_mmr
           h_ss=hb_ssr
       else
           h_mm=hb_mmi
           h_ss=hb_ssi
       end_if
       effsxx = sxx(i,j)  + pp(i,j)
       effsyy = syy(i,j)  + pp(i,j)
       effszz = szz(i,j)  + pp(i,j)
       tension(i,j)=0.5*hb_sc*(sqrt(h_mm^2+4*h_ss)-h_mm)
       temp1=-0.5*(effsxx+effsyy)
       temp2=sqrt(sxy(i,j)^2+0.25*(effsxx-effsyy)^2)
       s3=min(temp1-temp2,-effszz)
       if s3<0.0 then
         s3=0.  end_if
  if s3<0.0 then
         s3=0.
 end_if
```

Appendix V

Summary tables of pillar strength for all GSI UCS w/h ratios

UCS MPa	GSI	w/h	Strength MPa	δ	β	r^2
60	60	1	6.2	5.68	.7795	0.9672
60	60	2	8.6			
60	60	3	12.6			
60	60	4	17.1			
60	60	5	21.5			
60	70	1	9.4	8.51	.9793	0.9716
60	70	2	14.7			
60	70	3	22.8			
60	70	4	33.9			
60	70	5	45.3			
60	80	1	15.1	14.35	1.2007	0.9951
60	80	2	30.8			
60	80	3	51.4			
60	80	4	77			
60	80	5	103.8			
60	90	1	33.4	32.34	1.2095	0.9980
60	90	2	71			
60	90	3	121			
60	90	4	173			
60	90	5	233			

UCS MPa	GSI	w/h	Strength MPa	δ	Beta	r^2
80	60	1	7.8	7.07	.7753	0.9579
80	60	2	10.6			
80	60	3	15.2			
80	60	4	21.5			
80	60	5	26.8			
80	70	1	10.5	9.59	1.0745	0.9800
80	70	2	17.4			

80	70	3	28.4			
80	70	4	42			
80	70	5	56			
80	80	1	18.5	17.9	1.2828	0.9983
80	80	2	42			
80	80	3	71			
80	80	4	107			
80	80	5	146			
80	90	1	44	42.41	1.2772	0.9978
80	90	2	97			
80	90	3	170			
80	90	4	251			
80	90	5	341			

UCS MPa	**GSI**	**w/h**	**Strength MPa**	δ	**Beta**	**r^2**
100	60	1	7.6	6.91	0.8879	0.9694
100	60	2	11.2			
100	60	3	17			
100	60	4	24.3			
100	60	5	31.4			
100	70	1	11.7	10.76	1.1348	0.9855
100	70	2	21			
100	70	3	35.2			
100	70	4	53			
100	70	5	72			
100	80	1	23	22.28	1.2754	0.9981
100	80	2	51			
100	80	3	89			
100	80	4	131			
100	80	5	178			
100	90	1	54	51.25	1.2946	0.9955
100	90	2	115			
100	90	3	211			
100	90	4	310			

100	90	5	428			

UCS MPa	**GSI**	**w/h**	**Strength MPa**	δ	**Beta**	**r^2**
120	60	1	8.4	7.66	0.9423	0.9745
120	60	2	13			
120	60	3	20			
120	60	4	29			
120	60	5	38			
120	70	1	13	12.15	1.1768	0.9910
120	70	2	25			
120	70	3	42			
120	70	4	63			
120	70	5	86			
120	80	1	27	25.77	1.2442	0.9960
120	80	2	57			
120	80	3	98			
120	80	4	147			
120	80	5	198			
120	90	1	66	62.39	1.282	0.9948
120	90	2	138			
120	90	3	252			
120	90	4	373			
120	90	5	511			